A New and Efficient Method of Designing Low Noise Microwave Oscillators

By

Ulrich L. Rohde

Chairman

Synergy Microwave Corporation

Table of Contents

1 Introduction

The need for oscillators has been in existence for a long time. The first time it became an important issue was when Maxwell's Equations were to be experimentally proven. Heinrich Hertz made the first known oscillator. He used a dipole as the resonator and a spark gap generator as the oscillator circuit as shown in Figure 1-1.

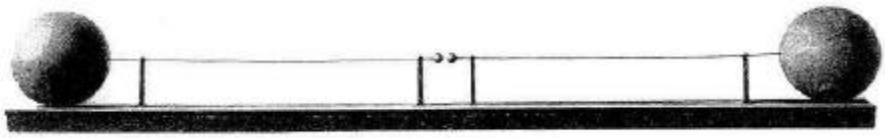

Figure 1-1 Original dipole made by Heinrich Hertz in 1887 using balls at the end to form a capacitive load (Deutsches Museum, Munich).

The spark gap oscillator changes AC or DC power into a spark which is energy rich and wide band. The dipole then takes the energy at the resonant frequency, radiated it and caused an electromagnetic field. Other discharges such as lightning with short pulse duration generates RF power from a few tens of KHz to hundreds of MHz.

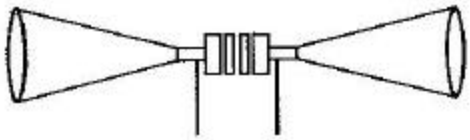

Figure 1-2 Dipole formed by two conical resonators with spark gap (1914).

Figure 1-3 Dipole oscillator after Ludenia placed in a parabolic mirror to increase efficiency (1929).

Figures 1-2 and 1-3 show additional examples of early oscillators. The pictures in this section are taken from [1].

Today, oscillators are used in test and measurement equipment and communication equipment. Given the large number of two-way radios and handies (cellphones) in use, they are the largest group of users. In this paper high performance and high volume applications are considered, but not the mass-market applications. I will consider

external resonators rather than monolithic resonators because high-quality phase noise requirements have only been met using external resonators thus far.

In these applications, the oscillators have to meet a variety of specifications, which affect the quality of operation of the system. An important feature is the cleanliness of the oscillator (low phase noise) and its freedom of spurious signals and noise. While the oscillator is almost always used as a voltage-controlled oscillator (VCO) in a frequency synthesizer system, its free-running noise performance outside the loop is still extremely important and solely determined by the oscillator.

An oscillator is a circuit that consists of an amplifier and a resonator. The feedback circuit takes a portion of the energy from the output of the amplifier and feeds it into the resonator to compensate its losses. The amplitude of the oscillator depends on the DC input power and the circuit itself. A small portion of the energy is used to sustain oscillation. Most of the RF power is available to be withdrawn at the output to be further amplified and used depending on the application. The frequency of the oscillator is largely determined by the resonator.

The classic papers deal with the maximum output power and noise properties of an oscillator as they were first measured and then optimized by trial and error. Even this did not always provide the best possible answer. The purpose of this work is to give, for the first time, a new, simple, complete, but efficient way to "synthesize" the design of a high performance, low noise oscillator. A general solution will be discussed and validation for the popular Colpitts/Clapp oscillator will be found. This approach will be valid for all types of oscillators [2-9].

An intensive literature search has been done to cover all the relevant previously published discussions.

The first approach to understand the noise properties of an oscillator, was done by Leeson [70] in 1966. This classic paper is still an extraordinarily good design guide. The advantage of this approach is the fact that it is easy to understand and leads to a good approximation of the phase noise. The drawback of this approach is the fact that the values for the flicker noise contribution, which is a necessary input to the equation, the RF output power, the loaded Q, and the noise factor of the amplifier under large-signal conditions, are not known. Other classic papers, such as Kurokawa [82], indicate where the operating point for best phase noise lies, but the value of the phase noise as such is not known [17]. The next breakthrough in oscillator noise analysis was developed by Rizzoli [77-79]. It is based on a noise correlation matrix and incorporates the various noise sources from the active device. Commercial simulation programs use a fixed topology for the transistor models. Available are the Gummel-Poon bipolar transistor model, an HBT model, the various gallium arsenide FET-based models, as well as MOS

and JFET models. The implementation of the noise sources for these semiconductors are shown in the user's manual of the simulator, specifically the model library.

The latest approach is a general noise theory for arbitrary circuits as shown by Lee and Hajimiri [64-67]. Their noise model is based on the time varying properties of the current waveform of the oscillator and the phase noise analysis is based on the effect of noise impulse on a periodic signal.

If an impulse is injected into the tuned circuit at the peak of the signal, it will cause maximum amplitude modulation and no phase modulation. If an impulse is injected at the zero crossing of the signal, there will be no amplitude modulation but maximum phase modulation. If noise impulses are injected between zero crossing and the peak, there will be components of both phase and amplitude modulation. Based on this theory and the intention to obtain the best phase noise, a special technique has to be adopted to make sure that any noise impulse occurs at the peak of the output voltage rather than any other point. Lee and Hajimiri introduced an impulse sensitivity function (ISF), which is different for each oscillator topology. This ISF is a dimensionless function periodic in 2π. It has its largest value when the most phase modulation occurs and has the smallest value when only amplitude modulation occurs.

This approach appears to be purely mathematical. It lacks practicality. The calculation of the ISF is tedious and depends upon the oscillator topology. The flicker noise conversion is not clearly defined. Also, there is no general mathematical equation that can be written about the phase noise in terms of components of the circuit, which can be differentiated to obtain both maximum power and best noise performance. Recent publications by Tom Lee have shown that the noise analysis for a given topology can be expressed and give good results once all the data is known, but does not lead to exact design rules [107]. Similar to the Leeson equation, it suffers from the fact that the actual noise performance of the device, the loaded Q and the output power, are not known a priori. As a matter of fact, some of the published oscillators by Lee and Hajimiri could be "optimized." This means that the published oscillator circuit did not have the best possible phase noise. By using the optimizer of a commercial harmonic-balance program, the phase noise could be improved significantly. Of course, a good direct synthesis procedure would have given the correct answer immediately.

The oscillators considered in this work are based on commercially available silicon bipolar transistors and silicon germanium transistors. As most designers and companies do not have elaborate and expensive equipment for parameter extraction (to obtain accurate nonlinear models), this concept of synthesis is based on using available data from the manufacturer as well as measurements of large-signal S-parameters using a network analyzer. Modern microwave transistors are very well characterized by the manufacturer up to approximately 6 GHz. Noise data, as well as a SPICE-type Gummel-Poon model data set are available.

There are several oscillator topologies. For the purpose of validating the general synthesis procedure, initially, a simple transistor circuit (Colpitts/Clapp oscillator) is used as the basis of discussion [2-8]. The oscillator itself can be described as a one-port device supplying a negative resistance to the tuned circuit, which is ideal to determine the best feedback network. Alternatively, it can be described as a two-port device using a resonator and an amplifier and allows us to calculate the complete noise analysis. It will be shown that both cases provide the same answer. The second case gives more insight into the phase noise calculation. For the first time, this new mathematical approach will show a step-by-step procedure using large-signal conditions on how to design an oscillator with good output power (high efficiency) and phase noise. As a third case, the values for P_{out}, Q_l, and F required for the Leeson equation will be numerically determined. All three cases will give an excellent agreement with the oscillator built under these test conditions and its measurements starting from the simple oscillator. A more complex circuit, including all the parasitics, will be used to show the general validity of this approach (Appendix C).

Any successful design for microwave oscillators mandates, besides building and measuring it, the use and validation with a microwave harmonic-balance simulator. In the harmonic-balance analysis method, there are two techniques in use to convert between the time-domain nonlinear model and the frequency-domain evaluation of the harmonic currents of the linear network. One technique is the Almost Periodic Discrete Fourier Transform technique (APDFT) and the other is the Multi-Dimensional Fast Fourier Transform technique (MFFT) using quasi-analytic or analytic derivatives to evaluate the Jacobian matrix. The first one, which has a somewhat random sampling approach, has a typical dynamic range of 75 to 80 dB, while the second one offers greater than 180 dB dynamic range.

In mixer designs and intermodulation analysis, which includes the calculation of noise in oscillator circuits, it is important to be able to accurately predict a small signal in the presence of a large signal. To reliably predict this, the dynamic range (the ratio of a large signal to a minimally detectable small signal) needs to be more than 175 dB. The APDFT technique was found to have a dynamic range of 75 dB, while the MFFT, and with analytically calculated derivatives, was found to have a dynamic final dynamic range of 190 dB. Given the fact that in noise calculations for oscillators, a noise floor of –174 dBm is the lower reference and the reference level can be as high as +20 dBm up to 190 dB dynamic range is required. Such a numerically stable approach is definitely required [10-13].

Organization

This work is organized in 14 Sections.

Section 1 – the Introduction, describes the purpose of the work and defines the problem.

Section 2 – defines the oscillator, its application, and parameters. In addition, the history of microwave oscillators is briefly discussed and various types of oscillators are introduced.

Section 3 – describes the various transistor models and gives insight into their parameters and their presentation. For better understanding, some current examples are shown.

Section 4 – develops the concept of "large-signal *S* parameters". The transistor models shown in Section 3 are mostly provided in linear form; the large-signal conditions have to be determined from the SPICE-type time-domain signal parameters. A good way of describing a transistor under large-signal conditions is the use of "large-signal *S*-parameters" which are introduced here. Examples of measured *S*-parameters are shown [18-53].

Section 5 – discusses resonators used for the frequency selective circuit of the oscillator. The popular resonators are shown and resulting Q factors are discussed.

Section 6 – develops a comprehensive treatment of the oscillator. Initially, the linear theory is shown, which explains the design strategy. There are two types of oscillator configurations that are relevant. One is the parallel type and the other is the series type. For both cases, a numerical design is shown. The more precise design method of an oscillator is an approach which considers large-signal conditions. Therefore, the start-up conditions are described, then the steady-state behavior. Under large-signal conditions, the time-domain behavior has to be considered, as the collector (or drain) current now consists of a DC component and harmonically related RF currents. In order to describe this, a normalized drive level is introduced which determines the conducting angle. As the conducting angle becomes narrower, the efficiency increases and the noise improves. However, there is a wide range over which the output power is constant, but the noise varies widely. Finding this optimum condition is the objective of Section 8. This section is supported by Appendix A.

Section 7 – is a detailed discussion of noise in oscillators, both linear and nonlinear. The linear section shows how the Leeson model is derived, which is used as the best case model. It contains the loaded Q, the noise factor, and the output power. These three variables determine the phase noise of an oscillator. The linear example is now useful because these three values were practically unknown. An accurate calculation based on large-signal S-parameters, specifically S_{21}, is possible for the first time. Finally, a phase noise test setup is shown which is used to validate this large-signal noise theory. This section is supported by Appendix B.

Section 8 –is the key contribution of this work. Section 6 gave a good insight into the large-signal operation of the oscillator, including its optimization for power, and discussed some phase noise results under these conditions. As mentioned, the normalized drive level *x* can vary over a broad range with output powers only changing a few dB's, while the phase noise changes drastically. A change in a few dB of output power drastically changes the efficiency, but the goal here is to find the best phase noise condition. After showing that reducing the conducting angle and proving that the phase noise gets better, the actual noise calculation and termination of the feedback capacitance is shown. There are three cases:

1. First is the Leeson equation, which contains a need for output power, operating noise figure, and loaded Q is tested for its validity. To do this, the exact calculations for the output power, the loaded Q, and the resulting noise factor are presented. An example shows the accuracy of this approach is limited, however, since an ideal transistor without parasitics is assumed.
2. The second approach calculates the noise contribution of a time varying negative resistance that cancels the losses. It will be shown that this is a time average value, that the noise calculations can be further improved, and the optimum feedback conditions are found.
3. The third and final approach is based on the loop approach and considers all noise contributions. Therefore it is the most accurate way to determine the oscillator's performance. A graphical differentiation of the phase noise equation shows a region to obtain the best phase noise. The phase noise increases on either side of this optimal point.

Appendix C shows a complete approach to the design.

Section 9 – shows three selected microwave oscillators for validation purposes which provide state-of-the-art phase noise. Their design was built upon the optimization shown in Section 8. Bipolar transistors and GaAs FETs are used. Measured data was available for the 1000 and 4100 MHz oscillators with bipolar transistors, as well as the 2000 MHz GaAs FET oscillator. The ceramic resonator-based oscillator shows a measured phase noise of 125 dBc/Hz at 10 kHz, 145 dBc/Hz at 100 kHz, and 160 dBc/Hz or better at 1 MHz. The 4.1 GHz oscillator shows a phase noise above 89 dBc/Hz at 10 kHz, 113 dBc/Hz at 100 kHz, and 130 dBc/Hz at 1 MHz, which is in excellent agreement with the prediction. The 2 GHz GaAs FET oscillator at 100 kHz offset is 2 dB too pessimistic and at 1 MHz 2 dB too optimistic. Because of the high flicker corner frequency of the GaAs FET, this may be due to modeling problems.

Section 10 – contains conclusions and recommendations for future work. The derivations in this work were based on oscillator circuits with simple parasitics. At frequencies above 4000 MHz, the circuit analysis becomes more complicated as more parasitics have to be identified. A good example of this is shown in Appendix C.

Another conclusion is that regular push/pull CMOS oscillators where $n = 2$ or $C_1/C_2 = 1$ do not have the best phase noise [99-107]. This does not apply for a push/pull Colpitts oscillator. It will be an interesting task to design an asymmetrical oscillator with a symmetrical output. This work has concentrated on oscillators and the next important task is to find design guides for voltage controlled oscillators. Recent publications have shown a differentially tuned oscillator which is quite promising [114]. As an extension of this work, an effort is currently being undertaken to design very wideband oscillators based on the push/push principal. As a result of this work, a patent disclosure has been submitted for an international patent covering the United States, Asia, and Europe [97-107].

Section 11 – explains the various symbols and abbreviations. To follow the established literature, some of the abbreviations can have more than one meaning.

Section 12 – shows a list of all relevant references used throughout this work.

Section 13 – contains Appendices A, B, and C. This section contains three oscillator designs. The Appendices are very important because they apply all the new design rules that have been established in this work. These circuits were also used for verification purposes.

The first design, Appendix A, is based on large-signal S-parameters for optimum power. The unique approach here also shows that an inductor, instead of a feedback capacitor may be needed to make the design for a given transistor possible. This has not been shown in the literature before.

The second design, Appendix B, is based on Bessel functions and on a large-signal design for best output power. Consistent with Appendix A, a detailed numerical approach is given to easily follow the step-by-step procedure. Again, the design is a typical application for a high performance oscillator. In this case, the output power was the priority and the phase noise was allowed to degrade.

The third design, Appendix C, combines all the technologies discussed in this work. It starts with the specific requirements for output power and phase noise. It further assumes a real transistor with its parasitics considered. It shows the schematic first, which is the optimum choice for this application. The Bessel function approach is used to determine the operating point and the bias point. The design calculation shows that the key equation, Eq. (8-94) in Section 8, despite its simplification, gives an accurate answer for the phase noise at 10 kHz. The result is consistent with the predicted phase noise and the measured phase noise.

2 General Comments on Oscillators

An oscillator consists of an amplifier and a resonant element, as well as a feedback circuit. In many cases the intention is to build a selective amplifier, but an oscillator ends up being built because of internal or external feedback either in the active device or as part of the external circuit. An amplifier is an electrical circuit with a defined input and output impedance which increases the level of the input signal to a predetermined value at the output. The energy required for this is taken from the DC power supply connected to the amplifier. The amplifier impedances can vary from several ohms to several Meg ohms, but for high frequency application, it is standard to build amplifiers with 50Ω real input and output impedance. The active circuit responsible for the gain can be a bipolar transistor, a field-effect transistor, or a combination of both, or a gain block like a wideband amplifier offered by several companies. These are typically a combination of Darlington stages with RF feedback. Wideband amplifiers can cover frequencies such as a few hundred kHz to over ten thousand MHz. An oscillator built with an amplifier and a tuned circuit is a device which transforms DC energy into RF energy. It does this at a desired frequency at an acceptable efficiency. The efficiency of a low noise oscillator varies depending upon frequencies and configurations between 10% and 70%. In most cases, the efficiency is a secondary problem, while the primary task is to have a signal frequency output which is stable, free of spurious signals (clean), low phase noise, and of sufficient level [12].

The term "stability" refers to both short-term and long-term stability, and the oscillator should be clean in the sense it does not pick up unwanted signals and noise in the circuit. There are various noise sources which contribute to the oscillator noise. Some examples are: the loss of the resonator, the noise sources inside the transistor, noise (hum) modulated on the power supply, and noise contributions from the tuning diode(s).

This work will focus on phase noise optimization at a given and reasonable DC efficiency. These type of oscillators, which can be voltage-controlled oscillators by adding a tuning diode, are required to have a sinusoidal voltage output. Most systems cannot tolerate high harmonics from the oscillator, as these will cause unwanted mixing products.

Sinusoidal Oscillators

All amplifier-based oscillators are inherently nonlinear. Although the nonlinearity results in some distortion of the signal, linear analysis techniques can normally be used for the initial analysis and design of oscillators. Figure 2-1 shows, in block diagram form, the necessary components of an oscillator. It contains an amplifier with frequency-dependent forward loop gain $G(jw)$ and a frequency-dependent feedback network $H(jw)$.

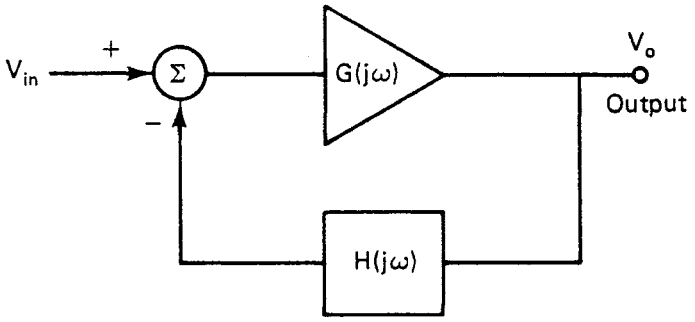

Figure 2-1 Block diagram of an oscillator showing forward and feedback loop components.

The output voltage is given by

$$V_o = \frac{V_{\text{in}} G(jw)}{1 + G(jw)H(jw)} \tag{2-1}$$

For an oscillator, the output V_o is nonzero even if the input signal $V_{in} = 0$. This can only be possible if the forward loop gain is infinite (which is not practical), or if the denominator

$$1 + G(jw)H(jw) = 0 \tag{2-2}$$

at some frequency w_o. This leads to the well-known condition for oscillation (the *Nyquist criterion*), where at some frequency w_o

$$G(jw_o)H(jw_o) = -1 \tag{2-3}$$

That is, the magnitude of the open-loop transfer function is equal to 1:

$$|G(jw_o)H(jw_o)| = 1 \tag{2-4}$$

and the phase shift is 180°:

$$\arg[G(jw_o)H(jw_o)] = 180° \tag{2-5}$$

This can be more simply expressed as follows: If in a negative-feedback system, the open-loop gain has a total phase shift of 180° at some frequency w_o, the system will oscillate at that frequency provided that the open-loop gain is unity. If the gain is less than unity at the frequency where the phase shift is 180°, the system will be stable, whereas if the gain is greater than unity, the system will be unstable.

This statement is not correct for some complicated systems, but it is correct for those transfer functions normally encountered in oscillator design. The conditions for stability are also known as the *Barkhausen criterion*, which states that if the closed-loop transfer function is

$$\frac{V_o}{V_{in}} = \frac{m}{1 - mb} \tag{2-6}$$

where m is the forward voltage gain and b is the feedback voltage gain, the system will oscillate provided that $mb = 1$. This is equivalent to the Nyquist criterion, the difference being that the transfer function is written for a loop with positive feedback. Both versions state that the total phase shift around the loop must be 360° at the frequency of oscillation and the magnitude of the open-loop gain must be unity at that frequency.

2.1 Phase Noise Effects

A noisy oscillator causes interference at adjacent channels, a phenomenon which is called blocking or reciprocal mixing. Figure 2-2 shows how phase noise affects the signal of an ideal oscillator.

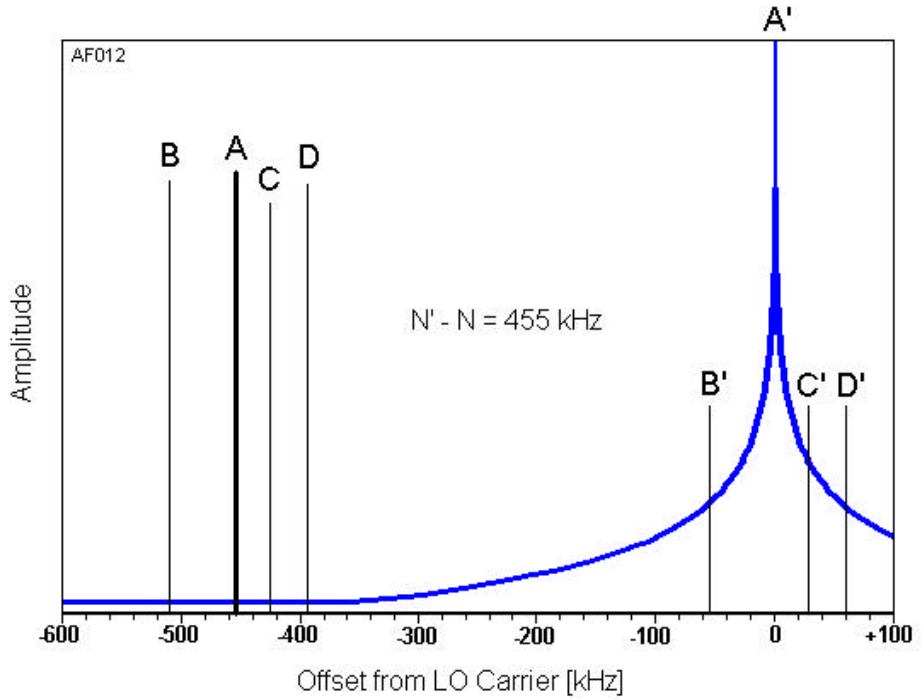

Figure 2-2 Reciprocal mixing occurs when incoming signals mix energy from an oscillator's sidebands to the IF. In this example, the oscillator is tuned so that its carrier, at A', heterodynes the desired signal, A, to the 455 kHz as intended. At the same time, the undesired signals B, C and D mix with the oscillator noise-sideband energy at B', C' and D', respectively, to the IF. Depending on the levels of the interfering signals and the noise-sideband energy, the result may be a significant rise in the receiver noise floor.

The spectral density, or phase noise, is measured in dBc (dB below the carrier) in a bandwidth of 1 Hz at an offset frequency f_n. The phase noise, therefore, is related to the output power. The noise power and the curve shown in Figure 2-3 can have different shapes based on the noise sources, as seen in Figure 2-8.

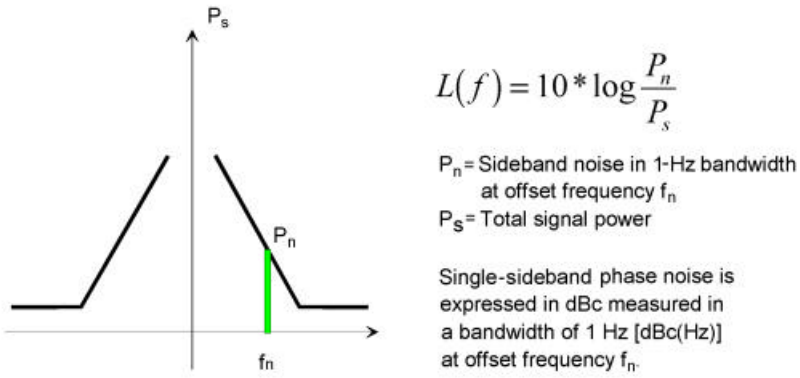

Figure 2-3 Phase noise calculation.

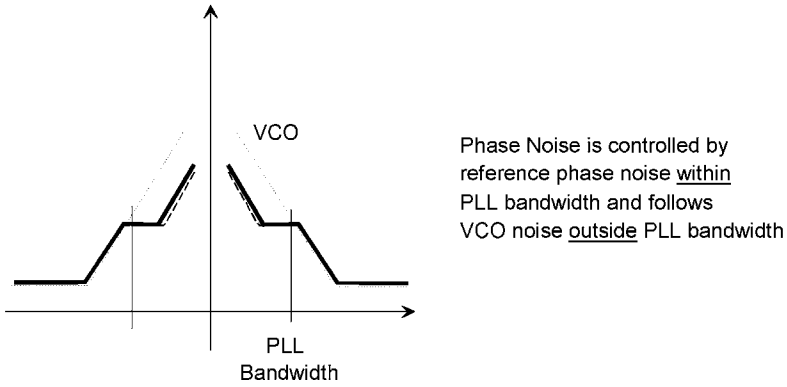

Figure 2-4 Phase noise of an oscillator controlled by a phase-locked loop.

If the oscillator is configured to be a VCO (voltage-controlled oscillator), the phase noise inside the loop bandwidth (hopefully) improves. Outside the loop bandwidth, the phase noise is determined solely by the resonator of the oscillator as seen in Figure 2-4.

Maximum condition, or the best phase noise number, is $10 \times \log (P_{output}/kT)$ at room temperature calculating from kT (-174 dBm/Hz) to the output power typically between 0 dBm and 30 dBm. The tuned circuit is responsible for most of the filtering. This phenomenon was first observed by Leeson in 1966 [70] and has been the basis of all linear-based assumptions. Later, it will be shown that his approach, with some additional terms, forms a useful but not always scientifically accurate, method of characterizing the oscillator.

Again, if a strong signal is fed to the receiving system, it will mix with the noise bands of the oscillator and produce a noise signal at one or more adjacent channels. This effect desensitizes or blocks the channel or one or more adjacent channels. Reciprocal mixing is a descriptive term as it shows that the phase noise of the oscillator at a given space is being mixed as an unwanted effect to the desired channel. Figures 2-5 and 2-6 show the mechanism of reciprocal mixing for both an analog and a digital receiver. In the case of the analog receiver, the phase noise of the oscillator and its spurious signals create interfering signals, while in the case of the digital receiver a desensitization occurs [14].

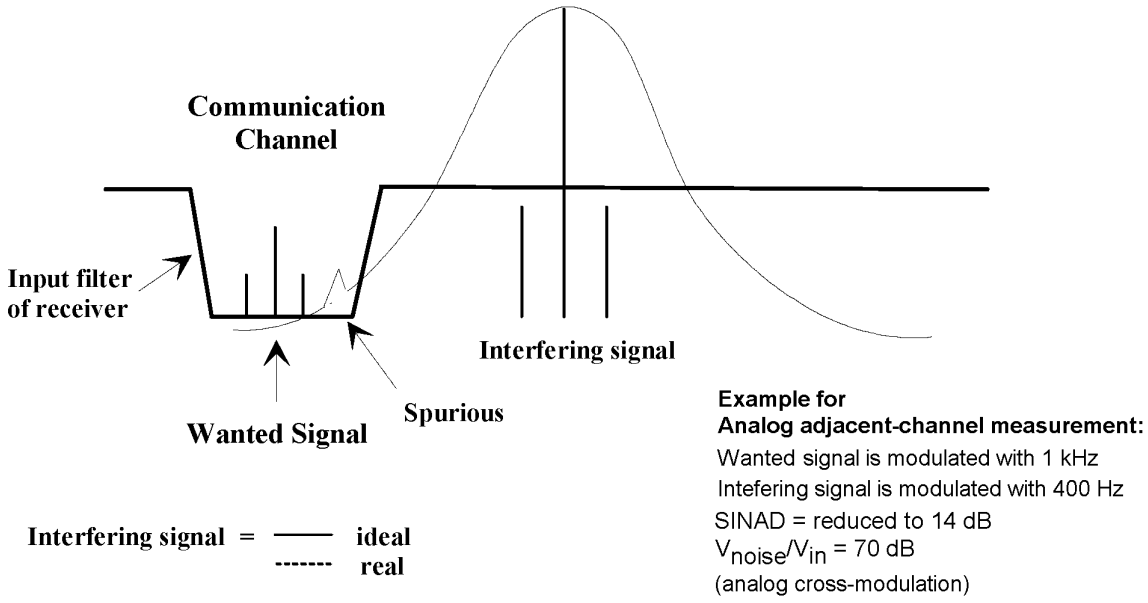

Figure 2-5 Principle of selectivity measurement for analog receivers.

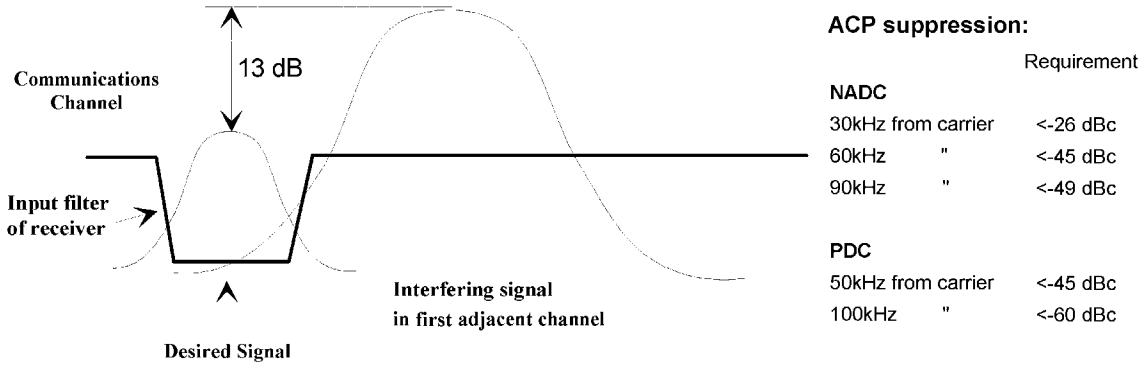

Figure 2-6 Principle of selectivity measurement for digital receivers.

2.2 Specifications of Oscillators and VCOs

The properties of an oscillator can be described in a set of parameters. The following is a list of the important and relevant parameters as they need to be discussed with oscillators.

Frequency Range

The output frequency of a VCO can vary over a wide range. The frequency range is determined by the architecture of the oscillator. A standard VCO has a frequency range typically less than 2:1, as an example, 925-1650 MHz.

Phase Noise

Unfortunately, oscillators do not generate perfect signals. The various noise sources in and outside of the transistor modulate the VCO, resulting in energy or spectral distribution on both sides of the carrier. This occurs via modulation and frequency conversion. The noise, or better, AM and FM noise is expressed as the ratio of output power divided by the noise power relative to 1 Hz bandwidth measured at an offset of the carrier. Figure 2-7 shows a typical measured phase noise plot of a high Q oscillator using a ceramic resonator.

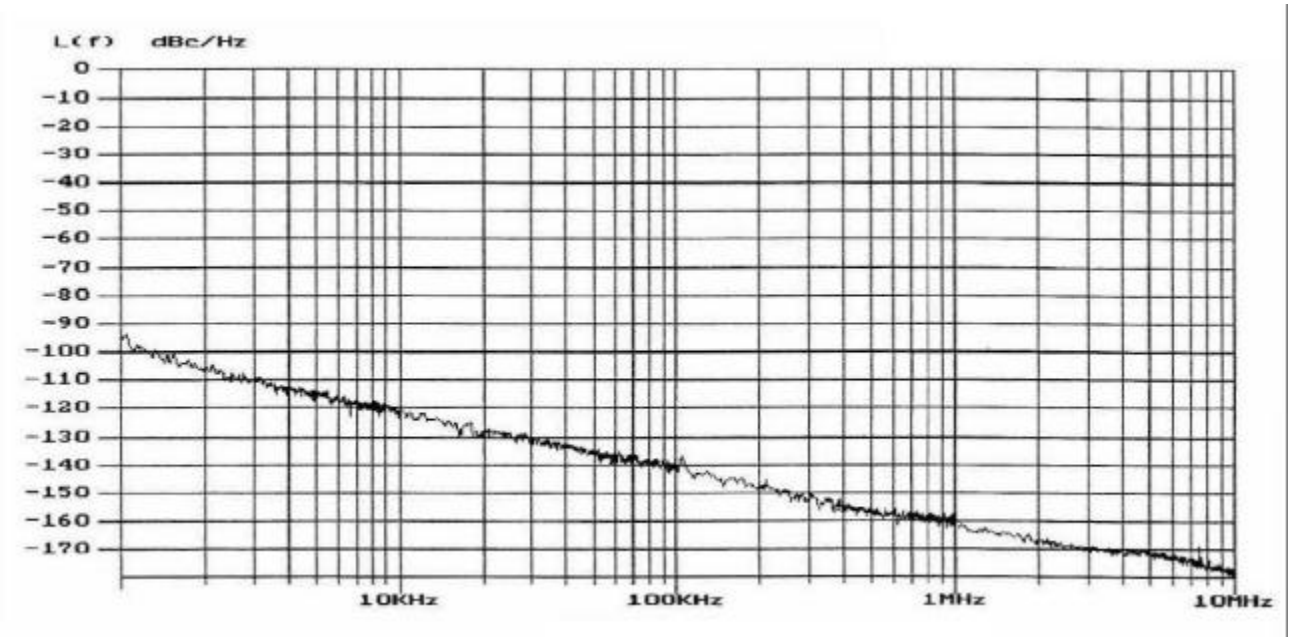

Figure 2-7 Measured phase noise of an 880-MHz resonator-based oscillator with a small tuning range.

The stability or phase noise of an oscillator can be determined in the time and frequency domain. Phase noise is a short-term phenomenon and has various components. Figure 2-8a shows the stability in the time domain. For an oscillator or VCO, this is rarely

relevant because the oscillator is used in a PLL system. The phase noise characteristics are more important and Figure 2-8b shows the various contributions. These contributions will be analyzed in the next section.

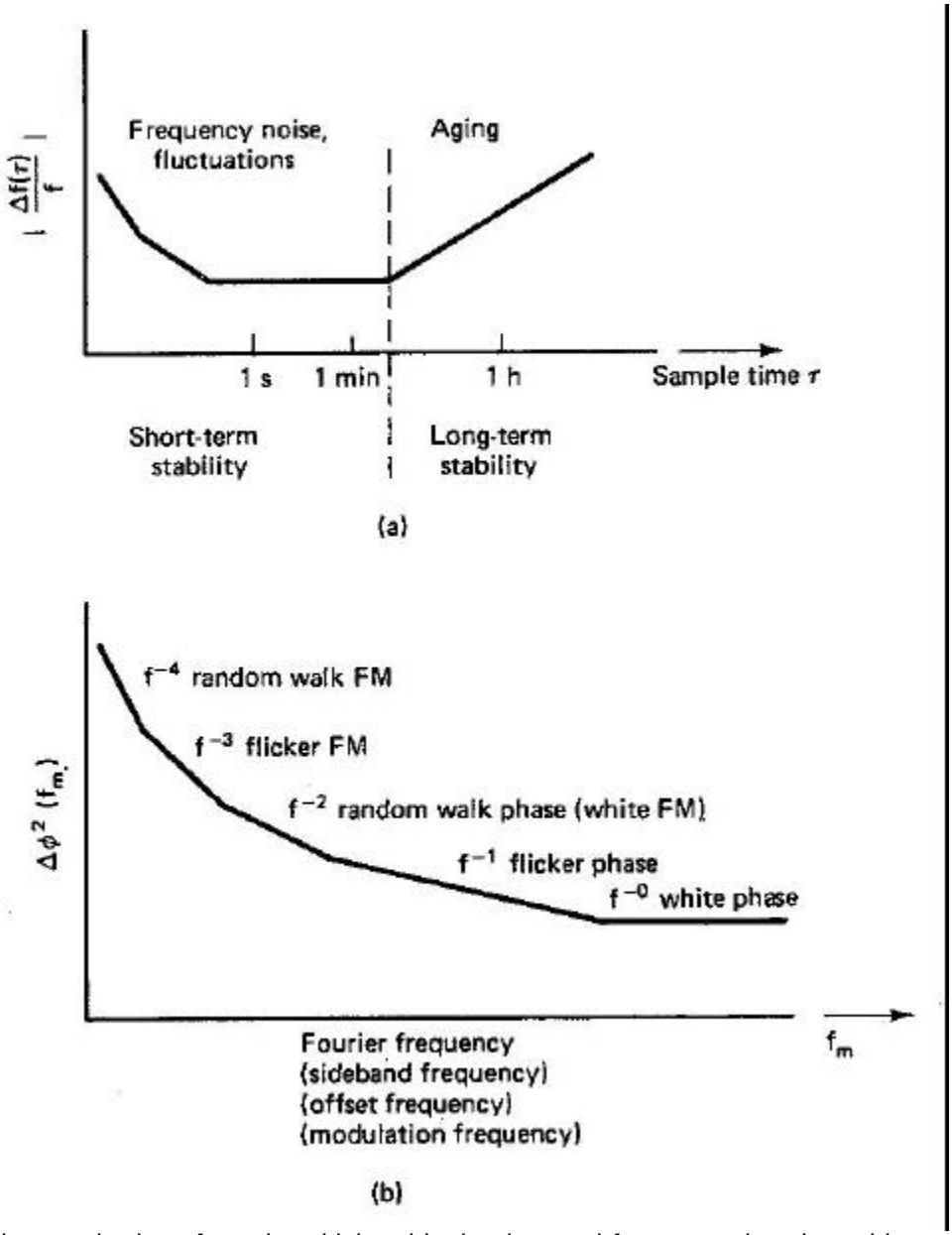

Figure 2-8 Characterization of a noise sideband in the time and frequency domain and its contributions: (a) time domain and (b) frequency domain. Note that two different effects are considered, such as aging in (a) and phase noise in (b).

Output Power

The output power is measured at the designated output port of the frequency synthesizer. Practical designs require one or more isolation stages between the oscillator and the output. The VCO output power can vary as much as ±2 dB over the tuning range. A typical output level is 0 to +10 dBm.

Harmonic Suppression

The oscillator/VCO has a typical harmonic suppression of better than 15 dB. For high performance applications, a low pass filter at the output will reduce the harmonic contents to a desired level. Figure 2-9 shows a typical output power plot of a VCO.

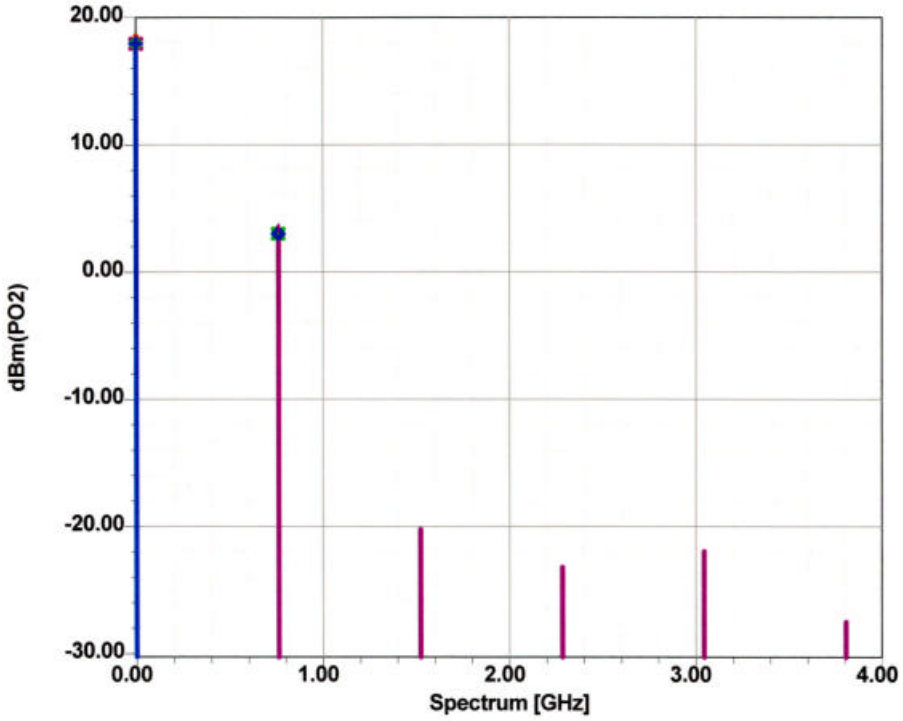

Figure 2-9 Predicted harmonics at the output of a microwave oscillator.

Output Power as a Function of Temperature

All active circuits vary in performance as a function of temperature. The output power of an oscillator over a temperature range should vary less than a specified value, such as 1 dB.

Spurious Response

Spurious outputs are signals found around the carrier of an oscillator which are not harmonically related. A good, clean oscillator needs to have a spurious-free range of 90 dB, but these requirements make it expensive. Oscillators typically have no spurious frequencies besides possibly 60 Hz and 120 Hz pick-up. The digital electronics in a synthesizer generates a lot of signals, and when modulated on the VCO, are responsible for these unwanted output products.

Frequency Pushing

Frequency pushing characterizes the degree to which an oscillator's frequency is affected by its supply voltage. For example, a sudden current surge caused by activating a transceiver's RF power amplifier may produce a spike on the VCOs DC power supply and a consequent frequency jump. Frequency pushing is specified in frequency/voltage form and is tested by varying the VCOs DC supply voltage (typically ± 1V) with its tuning voltage held constant. Frequency pushing must be minimized, especially in cases where power stages are close to the VCO unit and short pulses may affect the output frequency. Poor isolation can make phase locking impossible.

Sensitivity to Load Changes

To keep manufacturing costs down, many wireless applications use a VCO alone, without the buffering action of a high reverse-isolation amplifier stage. In such applications, frequency pulling, the change of frequency resulting from partially reactive loads, is an important oscillator characteristic. Pulling is commonly specified in terms of the frequency shift that occurs when the oscillator is connected to a load that exhibits a non-unity VSWR (such as 1.75, usually referenced to 50Ω), compared to the frequency that results with unity-VSWR load (usually 50Ω).

Post-tuning Drift

After a voltage step is applied to the tuning diode input, the oscillator frequency may continue to change until it settles to a final value. The post-tuning drift is one of the parameters that limits the bandwidth of the VCO input and the tuning speed.

Tuning Characteristic

This specification shows the relationship, depicted as a graph, between the VCO operating frequency and the tuning voltage applied. Ideally, the correspondence between operating frequency and tuning voltage is linear.

Tuning Linearity

For stable synthesizers, a linear deviation of frequency versus tuning voltage is desirable. It is also important to make sure that there are no breaks in tuning range, for example, that the oscillator does not stop operating with a tuning voltage of 0V.

Tuning Sensitivity, Tuning Performance

This datum, typically expressed in megahertz per volt (MHz/V), characterizes how much the frequency of a VCO changes per unit of tuning voltage change.

Tuning Speed

This characteristic is defined as the time necessary for the VCO to reach 90% of its final frequency upon the application of a tuning voltage step. Tuning speed depends on the internal components between the input pin and the tuning diode, including, among other things, the capacitance present at the input port. The input port's parasitic elements, as well as the tuning diode, determine the VCOs maximum possible modulation bandwidth.

Power Consumption

This characteristic conveys the DC power, usually specified in milliwatts and sometimes qualified by operating voltage, required by the oscillator to function properly.

2.3 History of Microwave Oscillators

Early microwave oscillators were built around electron tubes and great efforts were made to obtain gain and power at high frequencies. Starting from simple glass triodes (lighthouse tubes) and coaxial ceramic triodes, a large number of circuits designed to obtain reasonable performance were built. After using the Lecher lines (quarter-wave length U-shaped parallel wires, shorted at the end, with a few centimeters spacing), the next step was the use of coaxial systems, which became mechanically very difficult and expensive. At higher frequencies, cavities dominated the application and a lot of publications dealt with the various resonant modes. For special applications such as microwave ovens and radar applications, magnetrons and reflex klystrons were developed.

Today, the good understanding of the planar structures, such as microstrip, stripline, and coplanar waveguide have been instrumental in extending the practical frequency range up to 100 GHz and higher.

Early transistors followed the same trend. Siemens at one time produced a coaxial microwave transistor, Model TV44 and Motorola offered similar devices. Today, microwave transistors, when packaged, are also in microstrip form or are sold as bare die, which can be connected via bond wires to the circuit. These bond wires exhibit parasitic effects and can be utilized as part of the actual circuit. The highest form of integration is RFICs, either in gallium arsenide (GaAs) or in silicon germanium (SiGe) technology.

The SiGe circuits are typically more broadband because of lower impedances and GaAs FETs are fairly high impedance at the input. From an application point of view, in oscillators, SiGe seems to be winning. From a practical design, both transistor types can be considered a black box with a set of *S* parameters, which are bias and frequency dependent.

We will see that the transistor operates in large-signal condition, and historically, people have used FETs to demonstrate that there is little change in parameters from small to large-signal operation. Bipolar transistors have much more pronounced changes.

Early pioneers have invented a variety of oscillator circuits which are named after them. The following picture, Figure 2-10, shows a set of schematics, applicable for both bipolar and field-effect transistors. The ones using magnetic coupling are not useful for microwave applications.

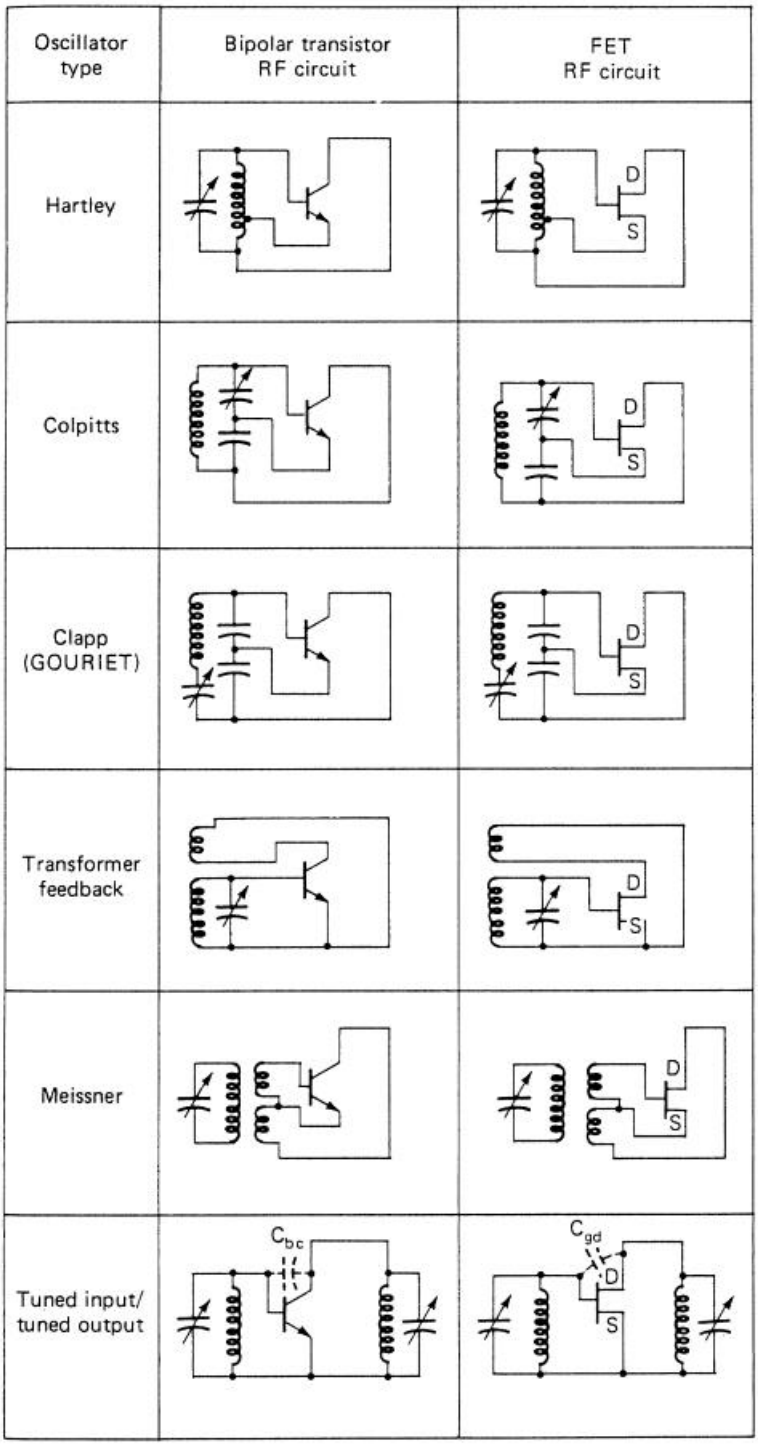

Figure 2-10 Six different configurations which can be built either around bipolar transistors or FETs. Some of the modern microwave oscillators are built around the Colpitts and Clapp oscillator circuits [15].

The Colpitts and Clapp oscillator configurations show an air variable capacitor as a tuning element. As the technology progressed, they were replaced by tuning diodes.

2.4 Three Types of Microwave Oscillators

The oscillator types shown in the previous section where shown for historical reasons. As mentioned, the Colpitts oscillator and its cousin, the Clapp oscillator, have found their way into modern microwave applications. The basic concept is that the capacitive feedback arrangement generates a negative resistance across the tuned circuit which compensates the losses of the tuned circuit.

These types of oscillators are called one-port oscillators because the transistor and the feedback circuit can be substituted with a negative resistance. For stable operation, the feedback capacitance values have to be carefully selected, as will be shown in the next section. As the gain varies with frequency, it limits the tuning range, which also affects the phase noise and the output power. Figure 2-11 shows the Colpitts-type oscillator. Tuning this circuit will alter these conditions for optimal phase noise and requires additional tunable elements to achieve optimal performance.

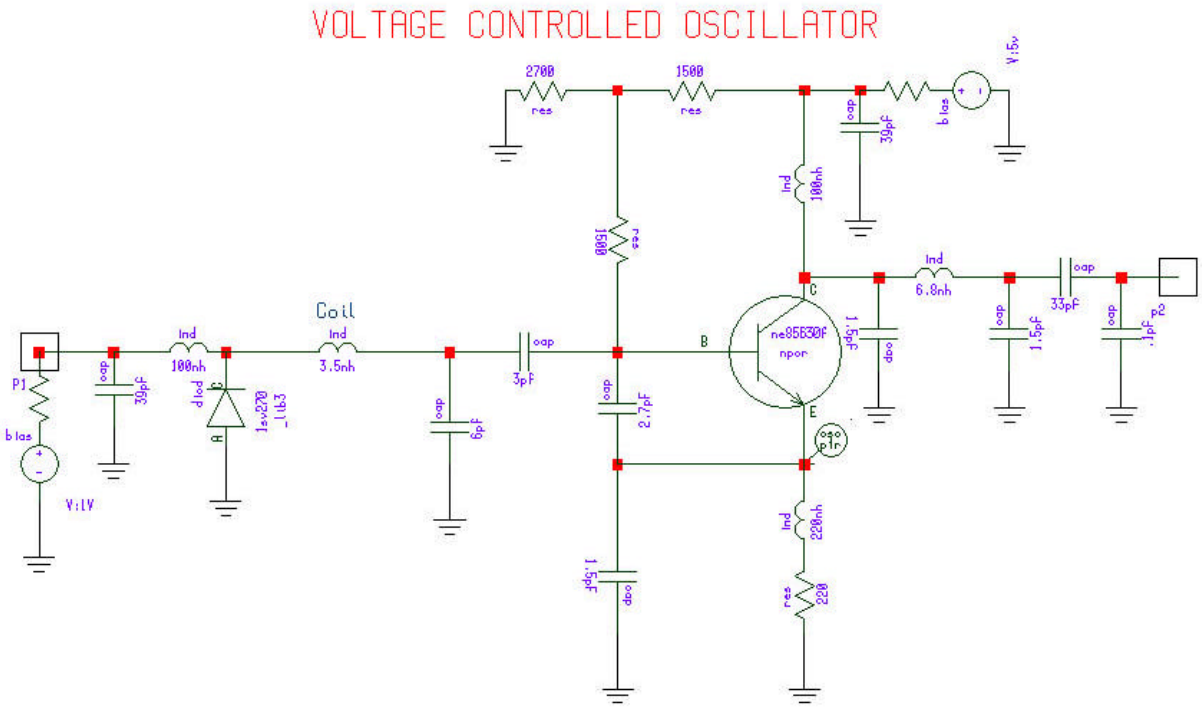

Figure 2-11 Schematic of a voltage-controlled Colpitts-type oscillator. The Colpitts circuit is recognized by the capacitive feedback network comprised of the capacitors connected between base and emitter and emitter to ground. This will be further explained in the appropriate section.

A second type of oscillator is the two-port oscillator. The transistor is used as a two-terminal device, with the third terminal at ground and its tuned circuit as a feedback element determines the frequency as shown in Figure 2-12.

As the transistor, or black box in question, has a frequency dependent Y_{21} (or S_{21}), one needs an additional element to compensate the phase shift generated inside the black box. These types of oscillators, therefore, have a gain block, a phase shift/matching circuit, and a resonator. In this configuration, the resonators are typically used in a Π configuration and in series resonant mode. A typical candidate for this is a SAW resonator (Surface Acoustical Wave). This is shown in Figure 2-12. The resonator is used in series resonant mode.

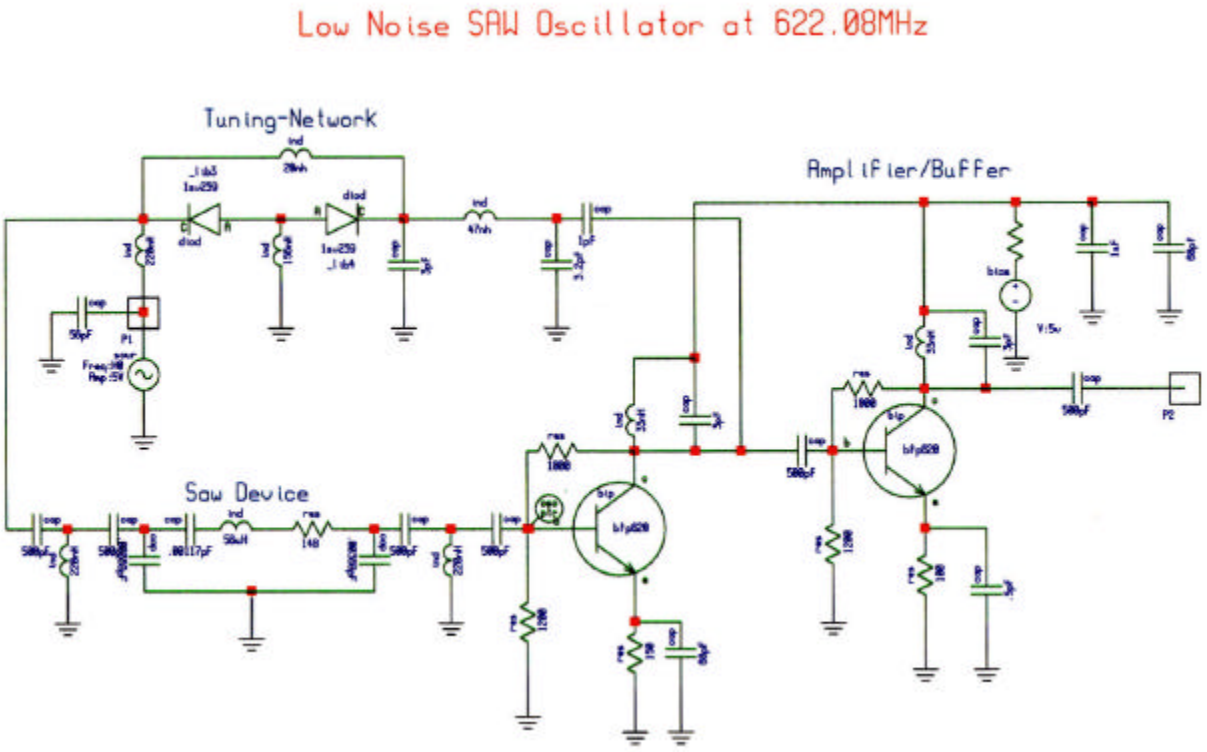

Figure 2-12 Circuit diagram of a 2-port SAW oscillator.

The third type of oscillator, which is typically used for microwave frequencies greater than 4 GHz, is shown in Figure 2-13. The base of the device (3-port, 3-terminal device) is floating above ground via a base (or gate) inductor. The feedback occurs due to the inductor and the capacitive portion of Y_{22} (or S_{22}). This circuit type was first explained by [2]. This type of feedback generates a negative input and output resistance for the circuit, which as an example, can match the 50Ω load [16, 17].

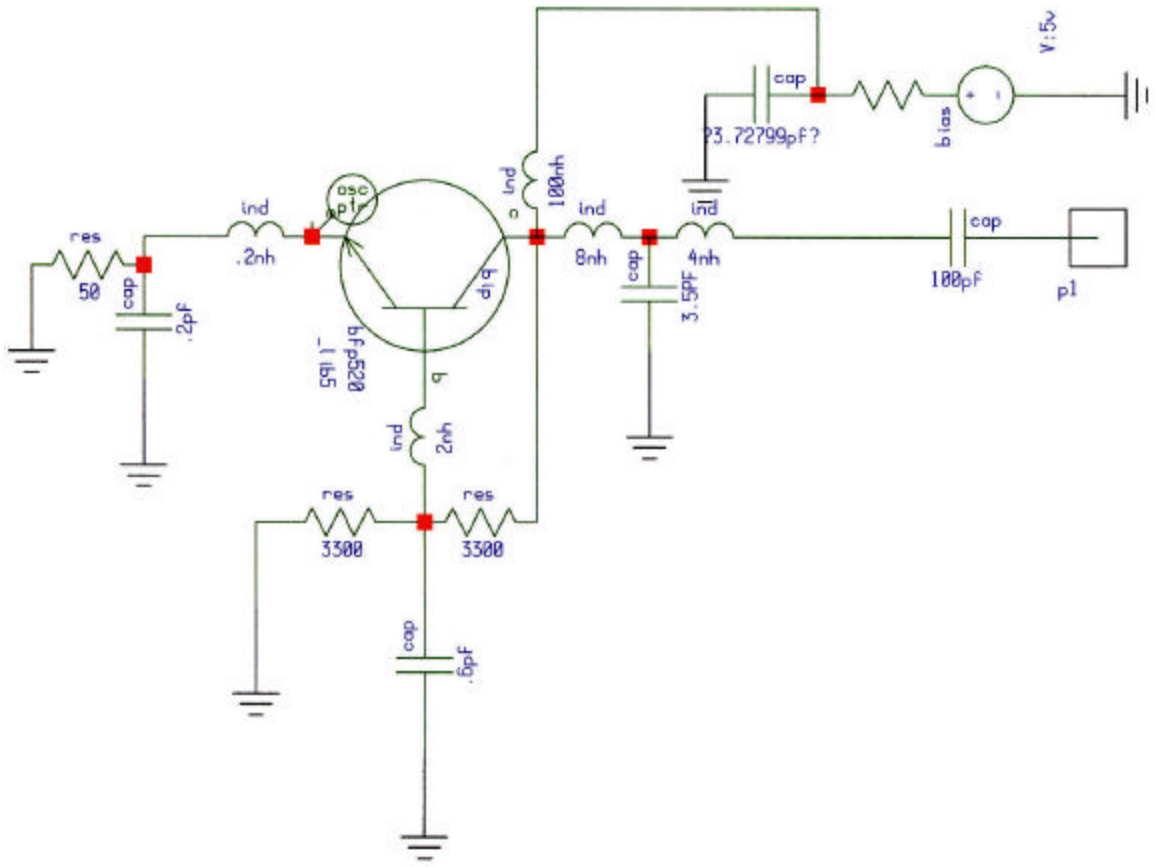

Figure 2-13 Circuit diagram of a 4 GHz oscillator using series feedback with the Infineon transistor BFP520.

Three-Reactance Oscillators Using *Y*-Parameters, An Introduction

Although the block-diagram formulation of the stability criteria shown earlier is the easiest to express mathematically, it is frequently not the easiest to apply since it is often difficult to identify the forward loop gain $G(jw)$ and the feedback ratio $H(jw)$ in electronic systems. A direct analysis of the circuit equations is frequently simpler than the block diagram interpretation (particularly for single-stage amplifiers). Figure 2-14 shows a generalized circuit for an electronic amplifier. This approach here uses *Y*- parameters. In the next section, a complete, complex analysis with *Y* and *S* parameters will follow. First, the concept of oscillator analysis will be introduced.

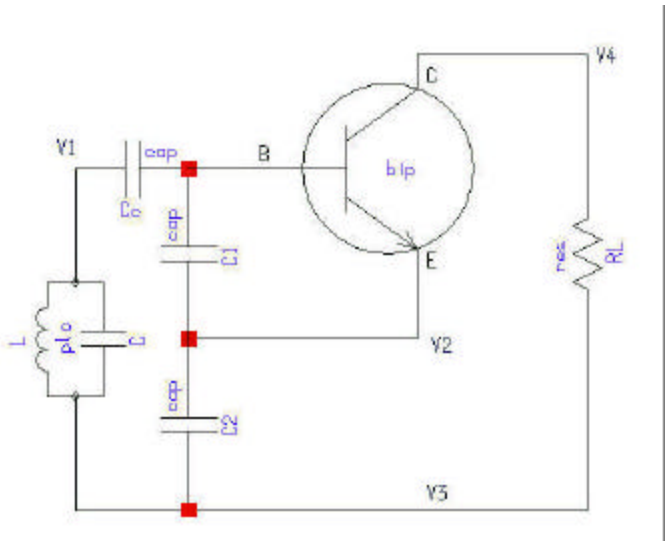

Figure 2-14 General topology of the Colpitts oscillator.

Figure 2-14 shows a simplified Colpitts oscillator, which is derived from Figure 2-11. It has a capacitive feedback network, C_1 and C_2, and a tuned circuit, which is built from the inductor L and the capacitor C and coupled to the transistor circuit via a coupling capacitor C_C. Figure 2-14 can be redrawn by putting the tuned circuit with its coupling capacitor between base and collector. The feedback capacitor C_1 now is in parallel to the base emitter junction, and the feedback capacitor C_2 is in parallel to the collector emitter connection. We also assume a load resistor marked R_L in parallel with C_2. This is shown in Figure 2-15.

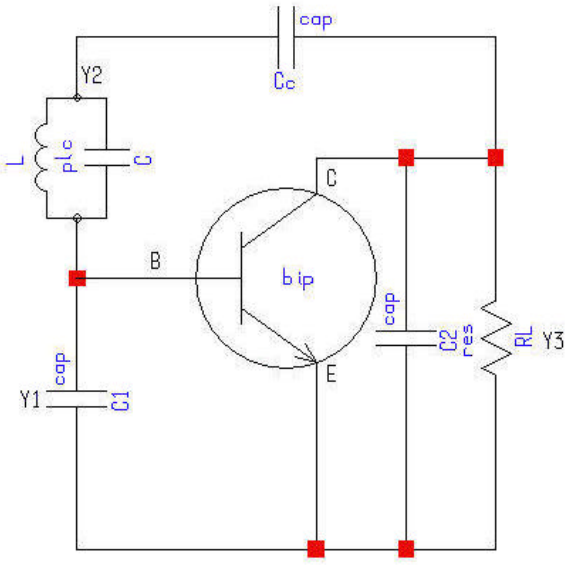

Figure 2-15 Modified Colpitts oscillator.

For the purpose of having a general arrangement, we are now introducing the admittance Y_1, Y_2, and Y_3. For this early introduction, we also assume that the transistor is ideal, meaning that we are assuming that $Y_{12} = 0$, and in $\mathrm{Im}(Y_{11}, Y_{22}) = 0$. Later we will reformulate without this assumption.

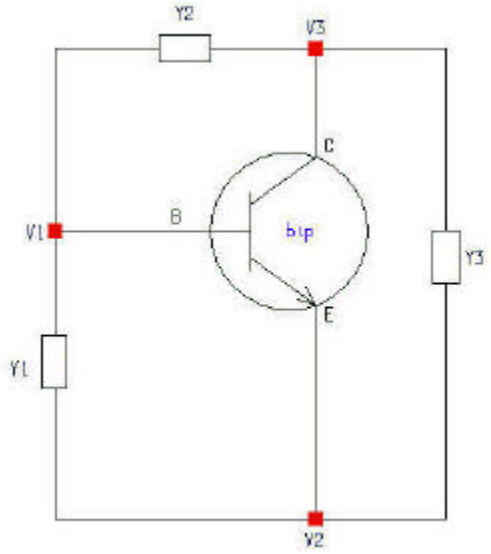

Figure 2-16 Equivalent circuit of the feedback oscillator.

Figure 2-16 shows the feedback circuit with three parallel admittances. Y_2 can either be a reactance or a more complex circuit such as a resonance circuit with a capacitance in series. In the case of a crystal oscillator, Y_2 is a series resonant circuit with a parallel capacitor, which comes from the crystal holder. The voltages V_1, V_2, and V_3 are measured relative to ground. The circuit is assumed floating.

It can be shown that:

$$\begin{bmatrix} (Y_1 + Y_3 + Y_i) & -Y_3 \\ -(Y_3 - Y_{21}) & (Y_2 + Y_3) \end{bmatrix} \begin{bmatrix} V_1 \\ V_2 \end{bmatrix} = 0 \tag{2-7}$$

In this equation $Y_i = Y_{11}$ and Y_{21} are the Y-parameters of the transistor.

In order for this circuit to oscillate, it must satisfy the matrix condition [Y][V] = 0 for a non-zero value of [V] (output power). Assuming the feedback circuit has lossless components, then

$$\begin{aligned} &(Y_2 + Y_3)(Y_1 + Y_3 + Y_i) - Y_3(Y_3 - Y_{21}) = 0 \\ &Y_1Y_2 + Y_1Y_3 + Y_2Y_3 + Y_iY_2 + Y_iY_3 + Y_3Y_{21} = 0 \end{aligned} \tag{2-8}$$

If the feedback network has ideal reactive components and Y_{11} = real, then

$$Y_i = G_i, Y_1 = jB_1, Y_2 = jB_2, Y_3 = jB_3 \tag{2-9}$$

and the equation above is further simplified to:

$$\begin{aligned} &-B_1B_2 - B_1B_3 - B_2B_3 + jB_2G_i + jB_3G_i + jB_3Y_{21} = 0 \\ &-(B_1B_2 + B_2B_3 + B_1B_3) + j(B_2G_i + B_3G_i + B_3Y_{21}) = 0 \end{aligned} \tag{2-10}$$

From the equation above, the real and imaginary part will need to be zero separately to satisfy det[Y]=0.

$$\begin{aligned} &B_1B_2 + B_2B_3 + B_1B_3 = 0 \Rightarrow \frac{1}{B_1} + \frac{1}{B_2} + \frac{1}{B_3} = 0 \\ &Y_{21}B_3 + G_iB_3 + G_iB_2 = 0 \Rightarrow \frac{1}{B_3} + \left(1 + \frac{Y_{21}}{G_i}\right)\frac{1}{B_2} = 0 \end{aligned} \tag{2-11}$$

If we convert susceptance to reactance, and let

$$X_1 = \frac{1}{B_1}, X_2 = \frac{1}{B_2}; X_3 = \frac{1}{B_3} \quad \text{and} \tag{2-12}$$

$$X_1 + X_2 + X_3 = 0 \Rightarrow X_3 + \left(1 + \frac{Y_{21}}{G_i}\right)X_2 = 0 \tag{2-13}$$

then $$\frac{Y_{21}}{G_i} = \frac{X_1}{X_2} \Rightarrow \frac{Y_{21}}{Y_{11}} \tag{2-14}$$

Feedback conditions: $$\frac{C_2}{C_1} = \frac{Y_{21}}{Y_{11}} \tag{2-15}$$

If Y_{21} and G_i are positive (simplified transistor model), it is implied that X_1 and X_2 have the same sign, and therefore, either capacitors or inductors. $X_1 + X_2 + X_3 = 0$, implies that X_3 must be opposite in sign from X_1 and X_2, and therefore, the opposite type of component.

$$X_1 + X_2 + X_3 \Rightarrow \frac{1}{wC_1} + \frac{1}{wC_2} - wL_3 = 0 \rightarrow Colpitts\,oscillator$$
$$w = \sqrt{\frac{1}{L_3}\left(\frac{1}{C_1} + \frac{1}{C_2}\right)}\, angular\ \ frequency, resonant\ \ condition \tag{2-16}$$

For complex value of Y_3 (Lossy Inductor):

$$Y_3 = G_3 + jB_3 \Rightarrow Y_3 = \frac{1}{Z_3}$$
$$Z_3 = R + jwL_3$$
$$\frac{1}{jwC_1} + \frac{1}{jwC_2} + \frac{G_i R}{jwC_1} + jwL_3 = 0 \tag{2-17}$$
$$w = \sqrt{\frac{1}{L_3}\left(\frac{1}{C_1} + \frac{1}{C_2} + \frac{G_i R}{C_1}\right)} \Rightarrow w = \sqrt{\frac{1}{L_3}\left(\frac{1}{C_1^{'}} + \frac{1}{C_2}\right)}$$

where

$$C_1^{'} = \frac{C_1}{1 + G_i R} \qquad \text{and} \tag{2-18}$$
$$\frac{R}{G_i} = \left(\frac{(1 + \frac{Y_{21}}{G_i})}{w^2 C_1 C_2}\right) - \frac{L_3}{C_1} \bullet \tag{2-19}$$

For steady oscillation the following condition has to be satisfied:

$$R_{Loss} < G_i \left[\frac{(1 + \frac{Y_{21}}{G_i})}{w^2 C_1 C_2} - \frac{L_3}{C_1}\right] \tag{2-20}$$

Since $\frac{Y_{21}}{G_i}$ is the frequency dependent current gain b:

$$R_{Loss} < \left| real\left(Y_{11}\left[\frac{(1+b)}{w^2 C_1 C_2} - \frac{L_3}{C_1}\right]\right)\right| \tag{2-21}$$

A similar approach is found in [15].

3 Transistor Models

Introduction

For the design of oscillators we are looking at members of bipolar and field-effect transistor families. In the case of the bipolar transistor, conventional microwave silicon transistors are manufactured with an f_T up to 25 GHz, while the more advanced SiGe transistors take over from this frequency range. Today, SiGe transistors are available up to 100 GHz if used as part of an RFIC. Their cousins, the heterojunction bipolar transistors (HBTs), based on GaAs technology, can achieve similar cut-off frequencies, but this technology is much more expensive for medium to large integrated circuits. HBTs also have a higher flicker noise corner frequency. SiGe transistors have a much lower flicker noise corner frequency and lower breakdown voltages (typically 2-3V). However, because of the losses of the transmission line in practical circuits, there is not much difference between HBT and SiGe oscillator noise as f_T is the same.

There is a similar competing situation between Bi-CMOS transistors implemented in a 0.12 micron technology and with GaAs FETs, specifically p-HEMTs. The GaAs FETs have well-established performance with good models, and the Bi-CMOS transistors are currently being investigated as to what models are the best. Also, there is the $1/f$ noise problem, specifically, with GaAs FETs more than with MOS transistors. The 0.12mm technology is somewhat impractical because of poor modeling. This means that most CAD predictions do not translate in a good design.

For the purpose of this discussion, it should be assumed that the designer has the ability to do their own parameter extraction to obtain an accurate model, or receive this data from the transistor manufacturer, or as part of the foundry service.

While the bipolar transistor models tend to be more physics-based, the FET models are mostly based on analytic equations, which are generated using curve-fitting techniques.

There are two types of models:

1) The models which describe DC and RF behavior are SPICE-type models, which means they can be incorporated in a frequency/time domain simulator and give reasonable agreement with measured data, both in the DC and RF areas.
2) Linear RF microwave models based on equivalent circuits.

In the bipolar modeling world, the Ebers-Moll equations have been used to generate the Gummel-Poon model (transport model) and its various subtle, modified (sometimes) proprietary implementations. Only in SPICE, particularly in Berkley-SPICE and H-SPICE, do we find these models to which the industry has agreed upon [18, 19]. Two other important and popular SPICE programs are P-SPICE and RF Spectre from CADENCE Design Systems [20, 21]. As an extension to this modeling effort, the

University of Delft/Philips has introduced a complex model consisting of a NPN and a complimentary PNP transistor for better RF modeling [22-24]. This model claims better simulation results for intermodulation distortion products under large-signal conditions. For the purpose of noise calculation of oscillators, one needs to know that the modulation indices are so small and the resulting noise currents and voltages are so small compared to the RF currents/voltages. The standard models, which are continuous and the third derivative to voltage and current exists, are sufficient.

For members of the FET family, the development of models was based on junction-FETs and MOS-transistors as implemented in early forms of SPICE. Junction-FETs are available only up to 1000 MHz and have lost importance in the RF and microwave area.

The first models for GaAs transistors were the Curtice-Ettenberg models, particularly the quadratic and cubic models. They were developed from the MOS model by adding a diode at the gate and removing the MOS capacitor at the input. Today, there is a long list of GaAs models where the individual researchers believe their model has big advantages.

These models are used to describe the behavior of the transistors over a wide frequency, temperature and bias range. Their accuracy varies by model. The most important factors are the input parameters. They are obtained from a process called parameter extraction. Having used CAD tools for a long time, it appears that a majority of discrepancies between measured and modeled results can be explained by a lack of accuracy stemming from parameter extraction. There is very little software available for reliable parameter extraction. Many companies have written their own software and assembled the necessary test equipment to obtain those parameters. The most popular software tools are from Silvaco and Agilent.

A successful path for generating model parameters has been the extraction of DC and RF parameters using DC I-V data and *S*-parameter data sets under various bias and frequency conditions. The model equations are curve fit to the data. To more accurately extract parameters that affect the noise characteristics of the model, it has also been proposed to include noise data as part of the parameter extraction procedure [25, 26].

When experimenting with these parameter extraction programs, it will be noticed that under certain conditions, input parameters for the nonlinear models are generated, which no longer have any practical meaning. This means that they are not realizable in the manufacturing process, but in a given frequency range, may give the right *S*-parameters. The inclusion of noise parameters cures this problem to a large extent [27, 28].

The following shows the information obtained for bipolar transistors and their modeling. The synthesis approach is applicable to all three terminal devices, which includes not only bipolar transistors, but all FETs such as JFETs, GaAs FETs, and MOSFET transistors.

Bipolar Transistors

The bipolar transistor has been known and used for many decades. Many scientists have explained its behavior, and probably the best analysis in the DC/RF area is summarized in [29]. This summary is based largely on the Infineon transistor BFP520 as an example, but is applicable to other transistors also.

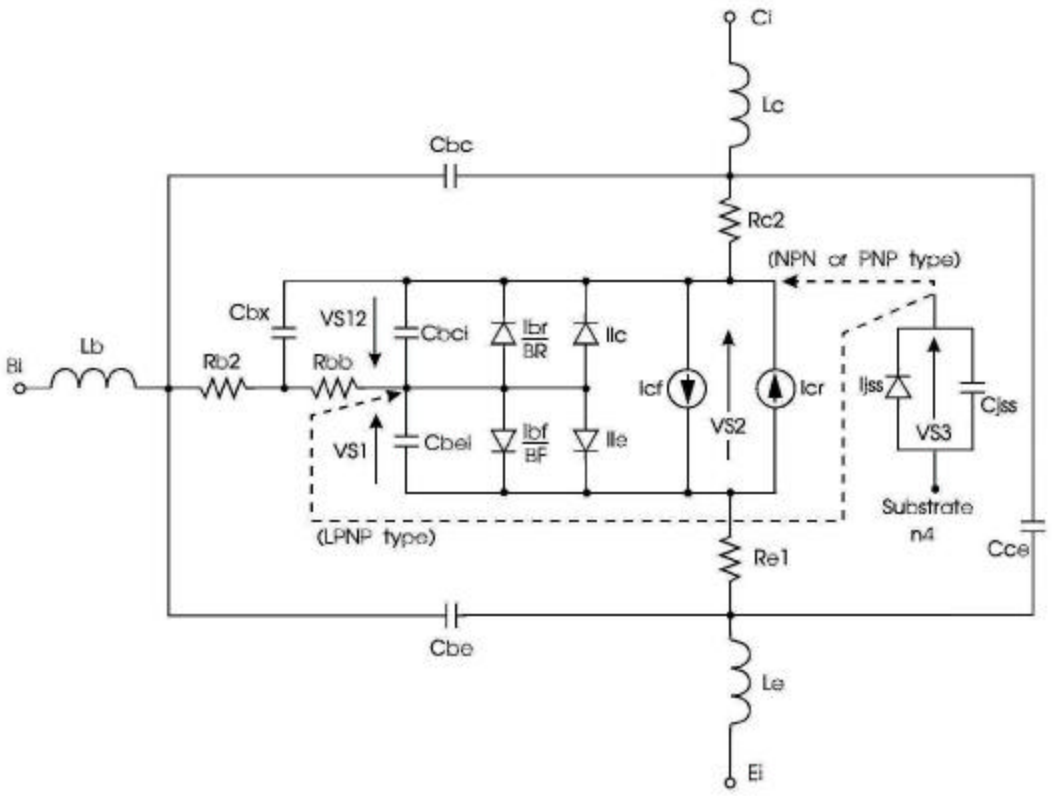

Figure 3-1 Shows an equivalent circuit for a microwave bipolar transistor. It deviates from the SPICE implementation by having two base-spreading resistors.

The first thing we need to do is look at the model used to calculate the DC and RF performance of a microwave transistor. There are subtle differences between the standard SPICE implementation and the one suited for higher frequencies. Figure 3-1 shows a modification that was necessary for greater accuracy by introducing an additional base-spreading resistor, R_{b2}.

Obtaining the input parameters is a major issue. For the purpose of this work, the Infineon transistor, model BFP520, was chosen. It is well documented and has a high enough operating frequency. Figures 3-2 to 3-5 and Table 3-1 reproduce the manufacturers data.

BFP520
NPN Silicon RF Transistor

- For highest gain low noise amplifier at 1.8 GHz and 2 mA/2V
  Outstanding G_{ms} = 23 dB
  Noise Figure F = 0.95 dB
- For oscillators up to 15 GHz
- Transition frequency f_T = 45 GHz
- Gold metalization for high reliability
- SIEGET® 45-Line
  45 GHZ f_T – Line

Figure 3-2 shows measured data provided from Infineon to further characterize the transistor.

SPICE Parameters (Gummel-Poon Model, Berkley-SPICE 2G.6 Syntax) :

Transistor Chip Data

IS =	15	aA	BF =	235	-	NF =	1	-
VAF =	25	V	IKF =	0.4	A	ISE =	25	fA
NE =	2	-	BR =	1.5	-	NR =	1	-
VAR =	2	V	IKR =	0.01	A	ISC =	20	fA
NC =	2	-	RB =	11	Ω	IRB =	-	A
RBM =	7.5	Ω	RE =	0.6		RC =	7.6	Ω
CJE =	235	fF	VJE =	0.958	V	MJE =	0.335	-
TF =	1.7	ps	XTF =	10	-	VTF =	5	V
ITF =	0.7	A	PTF =	50	deg	CJC =	93	fF
VJC =	0.661	V	MJC =	0.236	-	XCJC =	1	-
TR =	50	ns	CJS =	0	fF	VJS =	0.75	V
MJS =	0.333	-	XTB =	-0.25	-	EG =	1.11	eV
XTI =	0.035	-	FC =	0.5	-	TNOM	298	K

Package Equivalent Circuit:

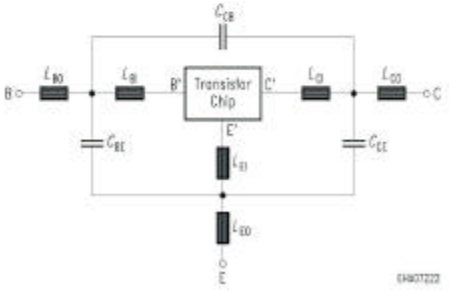

L_{BI} =	0.47	nH
L_{BO} =	0.53	nH
L_{EI} =	0.23	nH
L_{EO} =	0.05	nH
L_{CI} =	0.56	nH
L_{CO} =	0.58	nH
C_{BE} =	136	fF
C_{CB} =	6.9	fF
C_{CE} =	134	fF

Valid up to 6GHz

Figure 3-2 SPICE parameters and package equivalent circuit of the Infineon transistor BFP520.

These parameters are fit to the Berkley-SPICE 2G.6 syntax. In case of the base-spreading resistor, it is recommend that it be separated into two equal terms to fit the improved model shown above. Likewise, the feedback capacitor should also be split into two terms. The equivalent circuit of the package is valid up to 6 GHz and assumes that the two emitter leads are tied together.

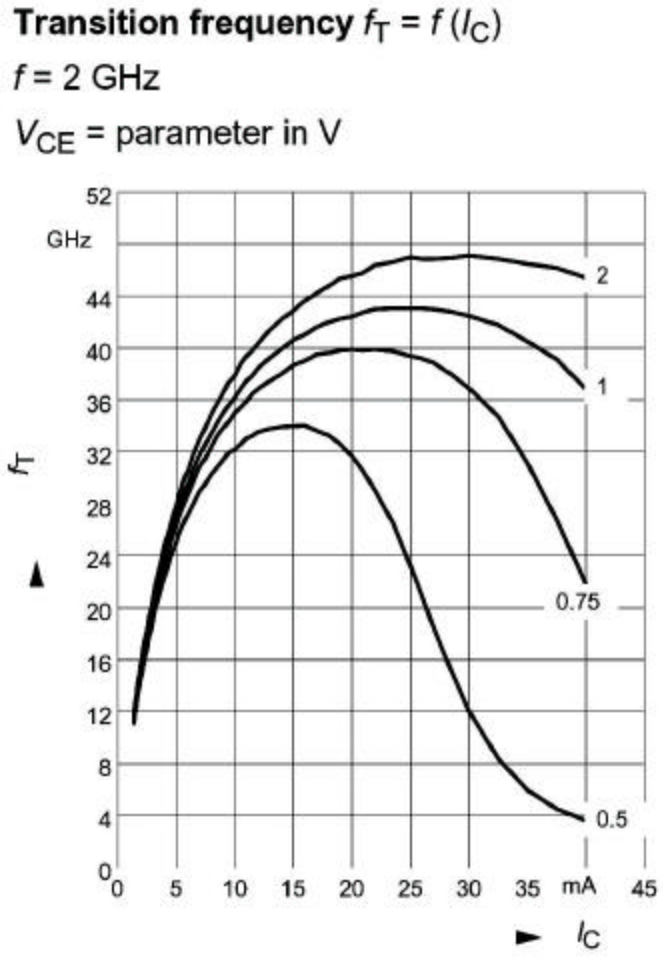

Figure 3-3 Transition frequency as a function of voltage and current.

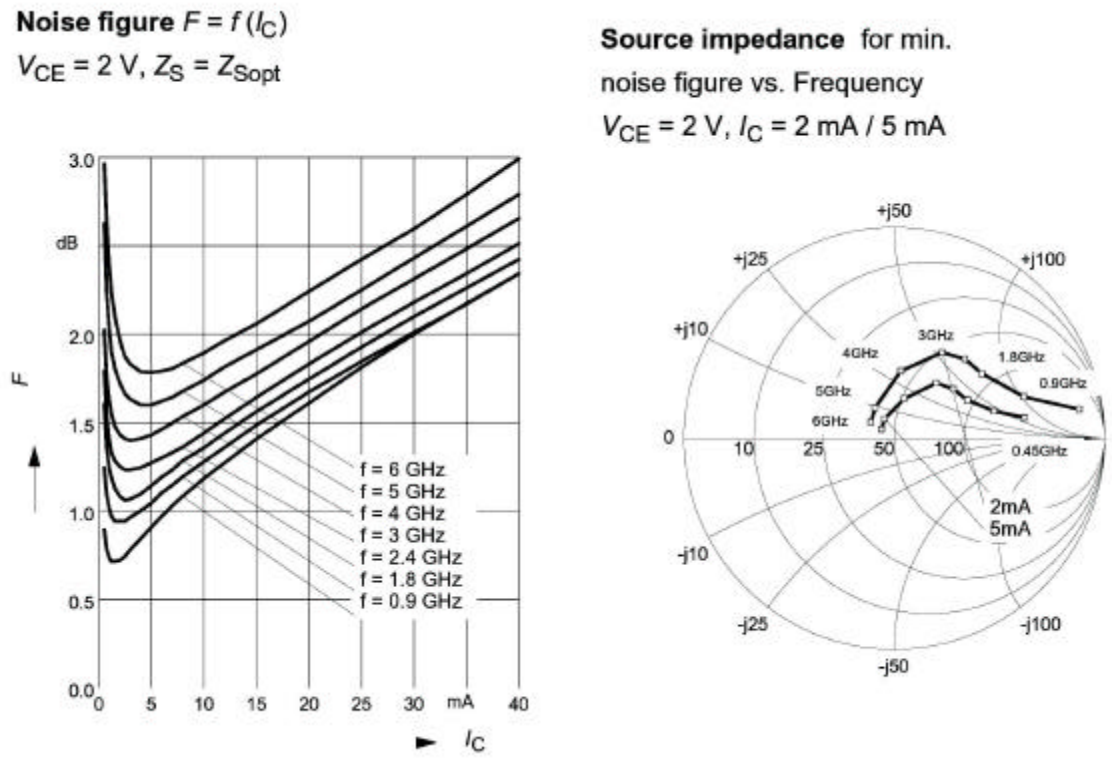

Figure 3-4 Noise figure and source impedance for best noise figure as a function of current and frequency of the Infineon transistor BFP520.

Electrical Characteristics at T_A = 25°C, unless otherwise specified.

Parameter	Symbol	Values			Unit
		min.	typ.	max.	
AC characteristics (verified by random sampling)					
Transition frequency I_C = 30 mA, V_{CE} = 2 V, f = 2 GHz	f_T	-	45	-	GHz
Collector-base capacitance V_{CB} = 2 V, f = 1 MHz	C_{cb}	-	0.06	-	pF
Collector-emitter capacitance V_{CE} = 2 V, f = 1 MHz	C_{ce}	-	0.3	-	
Emitter-base capacitance V_{EB} = 0.5 V, f = 1 MHz	C_{eb}	-	0.35	-	
Noise figure I_C = 2 mA, V_{CE} = 2 V, Z_S = Z_{Sopt} , f = 1.8 GHz	F	-	0.95	-	dB
Power gain, maximum stable [1)] I_C = 20 mA, V_{CE} = 2 V, Z_S = Z_{Sopt}, Z_L = Z_{Lopt} , f = 1.8 GHz	G_{ms}	-	23	-	
Insertion power gain I_C = 20 mA, V_{CE} = 2 V, f = 1.8 GHz, Z_S = Z_L = 50Ω	$\lvert S_{21}\rvert^2$	-	21	-	dB
Third order intercept point at output V_{CE} = 2 V, f = 1.8 GHz, Z_S=Z_{Sopt}, Z_L=Z_{Lopt} , I_C = 20 mA I_C = 7 mA	IP_3	 - -	 25 17	 - -	dBm
1dB compression point V_{CE} = 2 V, f = 1.8 GHz, Z_S=Z_{Sopt}, Z_L=Z_{Lopt} , I_C = 20 mA I_C = 7 mA	P_{-1dB}	 - -	 12 5	 - -	

[1] $G_{ms} = \lvert S_{21} / S_{12}\rvert$

Figure 3-5 Some technical data of the Infineon transistor BFP520.

Table 3-1

Common Emitter S-Parameters

f	S_{11}		S_{21}		S_{12}		S_{22}	
GHz	MAG	ANG	MAG	ANG	MAG	ANG	MAG	ANG
V_{CE} = 2 V, I_C = 20 mA								
0.01	0.7244	-0.7	32.273	178.6	0.0007	69.4	0.9052	1.2
0.1	0.7251	-8.4	31.637	171.4	0.0041	92.8	0.9363	-4.4
0.5	0.6368	-40.7	27.293	140.7	0.0194	75.9	0.8523	-26.7
1	0.4768	-73.6	19.601	113.5	0.0351	66.5	0.6496	-46.1
2	0.2816	-123.8	11.021	84.9	0.0057	56.3	0.3818	-64.6
3	0.2251	-166.1	7.481	67.6	0.0788	49.2	0.2407	-73.6
4	0.2552	156.2	5.636	53.1	0.0994	41.5	0.1544	-95.3
5	0.3207	133.6	4.488	39.7	0.1177	32.9	0.0951	-128.9
6	0.3675	118.7	3.683	27.5	0.1343	24.7	0.0545	177.6

The Infineon data set also contains noise parameters and *S*-parameters (see Table 1), however, these are less relevant because the large-signal conditions will modulate the intrinsic nonlinear capacitances and other elements so a large-signal noise model is needed. The following equivalent circuit in Figure 3-6 can be used to calculate the noise performance. Noise is mostly assumed to be derived in a linear mode, specifically, the flicker corner frequency under a large-signal condition will change significantly [30]. Information about SiGe transistors with much higher operating frequencies is well shown in [89-98].

Noise Model

Let Δf be the bandwidth (usually normalized to a 1Hz bandwidth). The noise generators introduced in the intrinsic device are shown below, and have mean-square values of:

$$\left\langle i_{bn}^2 \right\rangle = 2qI_B\ \Delta f + \mathrm{KF}\frac{I_B^{\mathrm{AF}}}{f^{\mathrm{FCP}}}\Delta f$$

$$\left\langle i_{cn}^2 \right\rangle = 2qI_C\ \Delta f$$

$$\left\langle i_{Rbb}^2 \right\rangle = \frac{4kT}{R_{bb}}\Delta f$$

$$\left\langle i_{Re1}^2 \right\rangle = \frac{4kT}{RE1}\Delta f$$

$$\left\langle i_{Rc2}^2 \right\rangle = \frac{4kT}{RC2}\Delta f$$

$$I_B = \frac{I_{bf}}{BF} + I_{le}$$

$$I_C = I_{cf} - I_{cr}$$

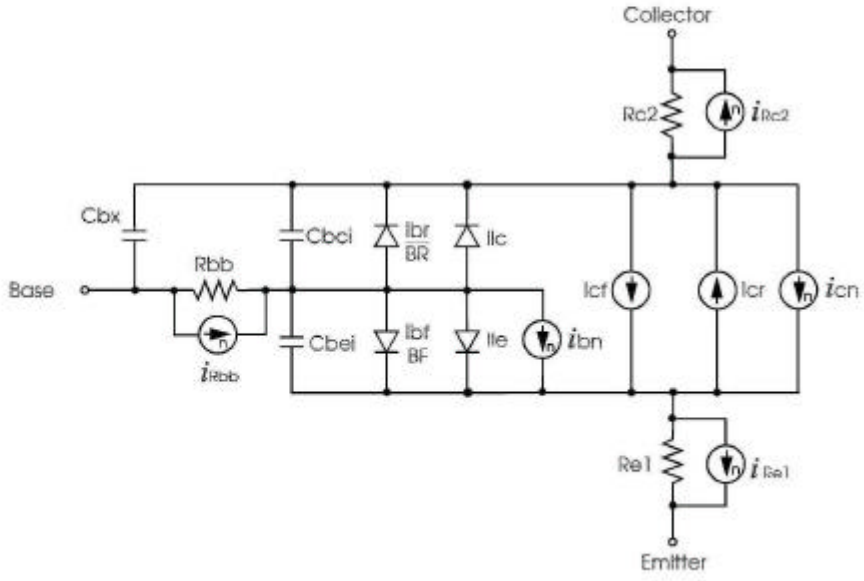

Figure 3-6 Noise model of the bipolar transistor (not showing extrinsic parasitics). Current sources with "n" are noise sources.

4 Large Signal *S*-Parameters

The description of linear, active or passive two-ports, can be explained in various forms. In the early days *Z*-parameters were commonly used which then were replaced by the *Y*-parameters. *Z*-parameters are assumed open-ended measurements and *Y*-parameters are short circuit measurements relative to the output or input depending on the parameter. In reality, however, the open circuit condition does not work at high frequencies because it becomes capacitive and results in erroneous measurements. The short-circuit measurements also suffer from non-ideal conditions as most "shorts" become inductive. Most RF and microwave circuits, because of the availability of 50Ω coaxial cables, are now using 50Ω impedances. Component manufacturers are able to produce 50Ω termination resistors which maintain their 50Ω real impedance up to tens of GHz (40 GHz). The 50Ω system has become a defacto standard. While the *Z*- and *Y*-parameter measurements were based on voltage and currents at the input and output, the *S*-parameters refer to forward and reflected power.

4.1 Definition

For low frequency applications, one can safely assume that the connecting cable from the source to the device under test or the device under test to the load plays no significant role. The wavelength of the signal at the input and output is very large compared to the physical length of the cable. At higher frequencies, such as microwave frequencies, this is no longer true. Therefore, a measuring principle was founded which would look at the incoming and the outgoing power at the input and output. The following is a mathematical explanation of the *S*-parameters. This follows the definitions of [14] as outlined by Hewlett-Packard.

$$b_1 = S_{11}a_1 + S_{12}a_2 \tag{4-1}$$

$$b_2 = S_{21}a_1 + S_{22}a_2 \tag{4-2}$$

or, in matrix form,

$$\begin{bmatrix} b_1 \\ b_2 \end{bmatrix} = \begin{bmatrix} S_{11} & S_{12} \\ S_{21} & S_{22} \end{bmatrix} \begin{bmatrix} a_1 \\ a_2 \end{bmatrix} \tag{4-3}$$

where, referring to Figure 2-78:

a_1 = (incoming power at Port 1)^{½}
b_1 = (outgoing power at Port 1)^{½}
a_2 = (incoming power at Port 2)^{½}
b_2 = (outgoing power at Port 2)^{½}
E_1, E_2 = electrical stimuli at Port 1, Port 2

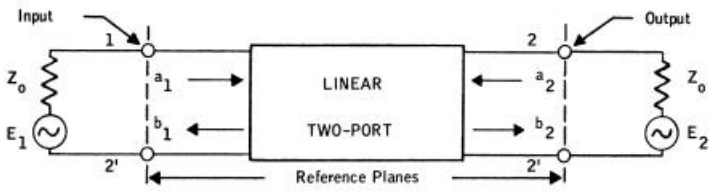

Figure 4-1 Two-port *S*-parameter definition.

From Figure 4-1 and defining linear equations, For $E_2 = 0$, then $a_2 = 0$, and (skipping through numerous rigorous steps):

$$\begin{aligned} S_{11} &= \frac{b_1}{a_1} \\ &= \left[\frac{\text{Outgoing Input Power}}{\text{Incoming Input Power}}\right]^{1/2} \\ &= \frac{\text{Reflected Voltage}}{\text{Incident Voltage}} \\ &= \text{Input Reflection Coefficient} \end{aligned} \tag{4-4}$$

$$\begin{aligned} S_{21} &= \frac{b_2}{a_1} \\ &= \left[\frac{\text{Outgoing Output Power}}{\text{Incoming Input Power}}\right]^{1/2} \\ &= \left[\frac{\text{Output Power}}{\text{Available Input Power}}\right]^{1/2} \\ &= \left[\text{Foward Transducer Gain}\right]^{1/2} \end{aligned} \tag{4-5}$$

or, more precisely in the case of S_{21}:

$$\text{Forward Transducer Gain} = G_{TF} = |S_{21}|^2 \tag{4-6}$$

$$Z_i = Z_o \tag{4-7}$$

Similarly at Port 2 for E_1=0, then a_1=0, and

$$S_{22} = \frac{b_2}{a_2} = \text{Output Reflection Coefficient} \tag{4-8}$$

$$S_{12} = \frac{b_1}{a_2} = [\text{Reverse Transducer Gain}]^{1/2} \tag{4-9}$$

$$G_{\text{TR}} = |S_{12}|^2 \tag{4-10}$$

Since many measurement systems display *S*-parameter magnitudes in decibels, the following relationships are particularly useful [54-57]:

$$\begin{aligned} |S_{11}|_{\text{dB}} &= 10\log|S_{11}|^2 \\ &= 20\log|S_{11}| \end{aligned} \tag{4-11}$$

$$|S_{22}|_{\text{dB}} = 20\log|S_{22}| \tag{4-12}$$

$$\begin{aligned} |S_{21}|_{\text{dB}} &= 10\log|S_{21}|^2 \\ &= 20\log|S_{21}| \\ &= 10\log|G_{\text{TF}}| = |G_{\text{TF}}|_{\text{dB}} \end{aligned} \tag{4-13}$$

$$\begin{aligned} |S_{12}|_{\text{dB}} &= 10\log|S_{12}|^2 \\ &= 20\log|S_{12}| \\ &= 10\log|G_{\text{TR}}| = |G_{\text{TR}}|_{\text{dB}} \end{aligned} \tag{4-14}$$

4.1 Large Signal *S*-Parameter Measurements

Assume S_{11} and S_{21} are functions only of incident power at port 1 and S_{22} and S_{12} are functions only of incident power at port 2. Note: the plus (+) sign indicates the forward wave (voltage) and the minus (-) sign would be the reflected wave (voltage).

$$S_{11} = S_{11}\left(\left|V_1^+\right|\right) \qquad S_{12} = S_{12}\left(\left|V_2^+\right|\right) \tag{4-15}$$

$$S_{21} = S_{21}\left(\left|V_1^+\right|\right) \qquad S_{22} = S_{22}\left(\left|V_2^+\right|\right) \tag{4-16}$$

The relationship between the travelling waves now becomes

$$V_1^- = S_{11}(V_1^+)V_1^+ + S_{12}(V_2^+)V_2^+ \tag{4-17}$$

$$V_2^- = S_{21}(V_1^+)V_1^+ + S_{22}(V_2^+)V_2^+ \tag{4-18}$$

Measurement is possible if V_1^+ is set to zero,

$$S_{12}(V_2^+) = \frac{V_1^-(V_2^+)}{V_2^+} \tag{4-19}$$

Check the assumption by simultaneous application of V_1^+ and V_2^+

$$\begin{bmatrix} V_1^- \\ V_2^- \end{bmatrix} = \begin{bmatrix} F_1(V_1^+, V_2^+) \\ F_2(V_1^+, V_2^+) \end{bmatrix} \tag{4-20}$$

If harmonics are neglected, a general decomposition is

$$\begin{bmatrix} V_1^-(V_1^+, V_2^+) \\ V_2^-(V_1^+, V_2^+) \end{bmatrix} = \begin{bmatrix} S_{11}(V_1^+, V_2^+) & S_{12}(V_1^+, V_2^+) \\ S_{21}(V_1^+, V_2^+) & S_{22}(V_1^+, V_2^+) \end{bmatrix} \begin{bmatrix} V_1^+ \\ V_2 + \end{bmatrix} \tag{4-21}$$

As mentioned before, these measurements are initially done under small-signal conditions with the RF power increasing up to 0 dBm or larger as needed. Small-signal conditions mean power levels of the vicinity of –40 dBm. The network analyzers which are used to measure these *S*-parameters have bias tees built-in and have 90 dB dynamic range. For the measurement of *S*-parameters of transistors, a much smaller dynamic range is sufficient.

If the output signal from the signal generator is increased in power, it essentially has no impact on passive devices until a level of several hundred watts is reached where intermodulation distortion products can be created due to dissimilar alloys. However, active devices, depending on the DC bias point, can only tolerate relatively low RF levels to remain in the linear region.

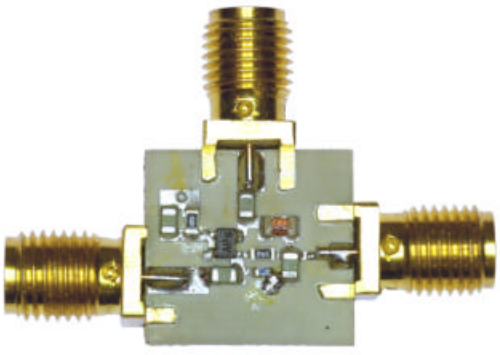

Figure 4-2 Test fixture to measure large signal *S*-parameters. A proper de-embedding has been done [27].

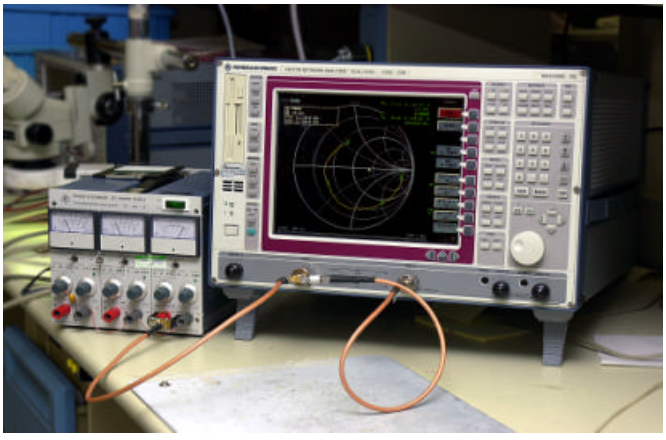

Figure 4-3 Rohde & Schwarz 3 GHz network analyzer to measure the large-signal *S*-parameters at different drive levels.

In the case of the oscillator, there is a large RF signal, voltage and current, imposed on the DC voltage/current. Assuming an RF output power from 0 dBm to 10 dBm, and assuming 10-15 dB gain in the transistor, the RF power level driving the emitter/source or base/gate terminal is somewhere in the vicinity of –15 dBm.

An RF drive of –15 dBm will change the input and output impedance of the transistor, even if the transistor operates at fairly large DC currents.

It is important to note that the input and output impedances of field-effect transistors are much less RF voltage-dependent or power-dependent than the bipolar transistor. The generation of "large signal *S*-parameters" for bipolar transistors is, therefore, much more important than for FETs.

Figure 4-2 shows the test fixture which was used to measure the large-signal *S*-parameters for the device under test (DUT). The test fixture was calibrated to provide 50Ω to the transistor leads. The test set-up shown in Figure 4-3 consists of a DC power supply and a network analyzer for combined *S*-parameter measurements. The R&S ZVR network analyzer, as shown in Figure 4-3, was chosen because its output can be changed from +10 dBm to –60 dBm. This feature is necessary to perform these measurements. The picture shows that the actual test system is very simple, but unfortunately, very expensive.

Currents and voltages follow Kirchof's law in a linear system. A linear system implies that there is a linear relationship between currents and voltages. All transistors, when driven at larger levels, show nonlinear characteristics. The FET shows a square law characteristic, while the bipolar transistor has an exponential transfer characteristic. The definition of *S*-parameters in large-signal environment is ambiguous compared to small-signal *S*-parameters. When driving an active device with an increasingly higher level, the output current consists of a DC current and RF currents, the fundamental frequency and its harmonics. When increasing the drive level, the harmonic contents rapidly increases. S_{12}, mostly defined by the feedback capacitance, now reflects harmonics back to the input. If these measurements are done in a 50Ω system, which has no reactive components, then we have an ideal system for termination. In practical applications, however, the output is a tuned circuit or matching network which is frequency selective. Depending on the type of circuit, it typically presents either a short circuit or an open circuit for the harmonic. For example, say the matching network has a resonant condition at the fundamental and second harmonic frequency or at the fundamental and third harmonic freuquency (quarterwave resonator). Then a high voltage occurs at the third harmonic, which affects the input impedance, and therefore, S_{11} (Miller effect).

This indicates that *S*-parameters measured under large-signal conditions in an ideal 50Ω system may not correctly predict device behavior when used in a non-50Ω environment.

A method called load pulling, which includes fundamental harmonics, has been developed to deal with this issue [58-62].

In the case of an oscillator, however, there is only one high Q resonator which suppresses the harmonics of the fundamental frequency (short circuit). In this limited case, the *S*-parameters, stemming from a 50Ω system, are useful. The following tables show two sets of measurements generated from the Infineon transistor BFP520 under different drive levels.

Since the oscillator will be in quasi-large-signal operation, we will need the large-signal *S*-parameters as a starting condition for the large-signal design (output power, harmonics, and others). The *S*-parameters generated from this will be converted into *Y*-parameters, defined under large-signal conditions and then used for calculating the large-signal behavior. We will use the symbol Y^+ to designate large-signal *Y*-parameters. Tables 4-1 and 4-2 show the large-signal *S*-parameters for –20 dBm and –10 dBm. However, in some cases the analysis starts at small-signal conditions. All derivations have been verified with MATHCAD and the original text input has been used. Therefore, in some cases the Y^+ marker has <u>not</u> been used. The use of the MATHCAD equation set allows for error free reuse of the equations.

Table 4-1

Frequency Dependent S-Parameters

LSignal 1	100MHz		3000MHz		*S*-Parameters at "-20dBm"			
	S_{11}		S_{21}		S_{12}		S_{22}	
1.000E+08	0.78	-17.15	29.57	-160.6	0.01	69.66	0.96	-7.63
1.500E+08	0.74	-19.95	30.87	-175.17	0.01	73.05	0.94	-10.27
2.000E+08	0.71	-23.01	30.87	174.87	0.01	73.61	0.92	-12.8
2.500E+08	0.69	-26.34	30.43	167.17	0.01	73.11	0.9	-15.25
3.000E+08	0.66	-29.8	29.8	160.76	0.01	72.13	0.87	-17.61
3.500E+08	0.64	-33.28	29.08	155.2	0.01	70.91	0.85	-19.92
4.000E+08	0.61	-36.73	28.3	150.22	0.01	69.59	0.83	-22.16
4.500E+08	0.59	-40.1	27.5	145.68	0.02	68.24	0.81	-24.33
5.000E+08	0.56	-43.36	26.68	141.5	0.02	66.91	0.78	-26.44
5.500E+08	0.53	-46.47	25.85	137.62	0.02	65.66	0.76	-28.44
6.000E+08	0.51	-49.42	25.02	134	0.02	64.51	0.73	-30.33
6.500E+08	0.48	-52.19	24.18	130.62	0.02	63.5	0.7	-32.07
7.000E+08	0.46	-54.78	23.35	127.46	0.02	62.63	0.68	-33.64
7.500E+08	0.44	-57.2	22.54	124.52	0.02	61.9	0.65	-35.04
8.000E+08	0.42	-59.44	21.74	121.76	0.02	61.3	0.63	-36.26
8.500E+08	0.39	-61.53	20.98	119.19	0.02	60.82	0.6	-37.31
9.000E+08	0.38	-63.48	20.24	116.77	0.03	60.43	0.58	-38.2
9.500E+08	0.36	-65.29	19.53	114.51	0.03	60.13	0.56	-38.95
1.000E+09	0.34	-66.99	18.85	112.38	0.03	59.88	0.54	-39.57
1.500E+09	0.22	-80.06	13.7	96.21	0.04	58.66	0.41	-41.5
2.000E+09	0.14	-91.02	10.61	85.03	0.04	57.04	0.33	-40.51
2.500E+09	0.09	-105.04	8.64	76	0.05	54.51	0.29	-39.1
3.000E+09	0.06	-129.69	7.27	68.07	0.06	51.33	0.25	-37.7

Table 4-2

Frequency Dependent S-Parameters

LSignal 3	**100MHz**		**3000MHz**		***S*-Parameters at "-10dBm"**			
	S_{11}		**S_{21}**		**S_{12}**		**S_{22}**	
1.00E+08	0.81	-12.8	14.53	179.18	0.02	39.17	0.55	-20.62
1.50E+08	0.79	-14.26	14.51	170.01	0.02	51.38	0.6	-24.42
2.00E+08	0.77	-16.05	14.46	163.78	0.02	57.11	0.65	-27.11
2.50E+08	0.76	-17.94	14.4	158.86	0.03	60.47	0.67	-28.33
3.00E+08	0.74	-19.85	14.31	154.78	0.03	62.9	0.69	-28.28
3.50E+08	0.73	-21.74	14.21	151.32	0.03	64.83	0.7	-27.33
4.00E+08	0.72	-23.62	14.1	148.32	0.03	66.46	0.71	-25.99
4.50E+08	0.71	-25.51	13.99	145.65	0.03	67.72	0.73	-24.6
5.00E+08	0.7	-27.42	13.88	143.19	0.03	68.57	0.74	-23.39
5.50E+08	0.68	-29.37	13.76	140.87	0.03	68.99	0.76	-22.5
6.00E+08	0.67	-31.38	13.65	138.62	0.04	68.98	0.77	-21.93
6.50E+08	0.66	-33.45	13.54	136.4	0.04	68.59	0.77	-21.68
7.00E+08	0.64	-35.56	13.42	134.2	0.04	67.95	0.78	-21.68
7.50E+08	0.63	-37.71	13.31	132	0.04	67.2	0.78	-21.89
8.00E+08	0.61	-39.88	13.19	129.83	0.04	66.31	0.77	-22.25
8.50E+08	0.59	-42.06	13.07	127.7	0.04	65.37	0.77	-22.62
9.00E+08	0.58	-44.23	12.95	125.6	0.04	64.48	0.76	-23.26
9.50E+08	0.56	-46.4	12.82	123.57	0.04	63.69	0.76	-24.04
1.00E+09	0.54	-48.55	12.69	121.6	0.04	62.82	0.75	-24.71
1.50E+09	0.37	-70.76	11.35	104.37	0.05	52.76	0.67	-33.77
2.00E+09	0.21	-91.19	9.99	88.64	0.05	46.68	0.48	-43.79
2.50E+09	0.12	-107.22	8.43	77.36	0.06	49.37	0.33	-43.13
3.00E+09	0.07	-130.38	7.18	68.7	0.06	48.69	0.27	-40.46

The following four plots, Figures 4-4, 4-5, 4-6, 4-7, show S_{11}, S_{12}, S_{21}, and S_{22} measured from 50 MHz to 3000 MHz with driving levels from –20 dBm to 5 dBm. The DC operation conditions were 2V and 20mA.

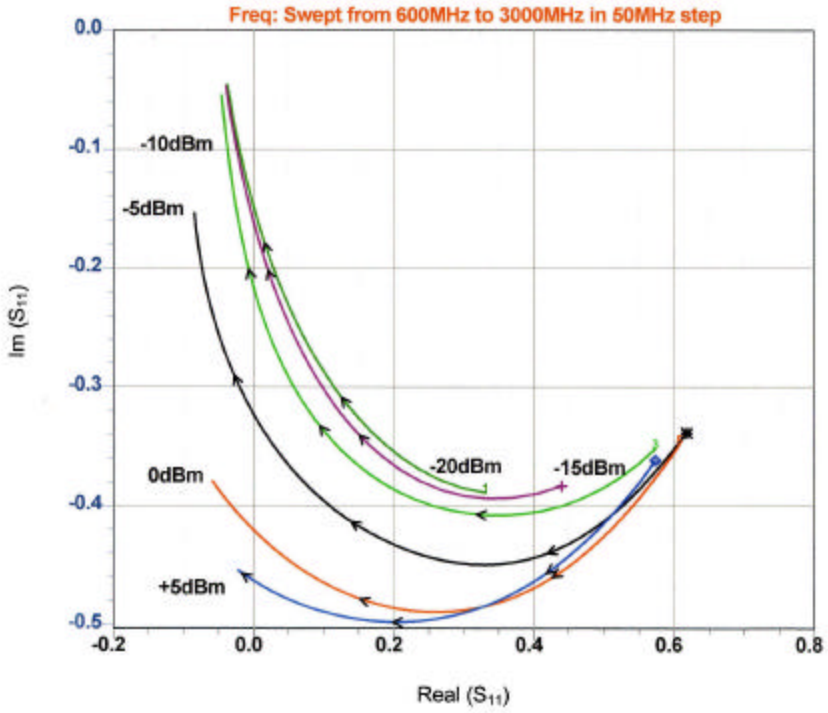

Figure 4-4 Measured large-signal S_{11} of the BFP520.

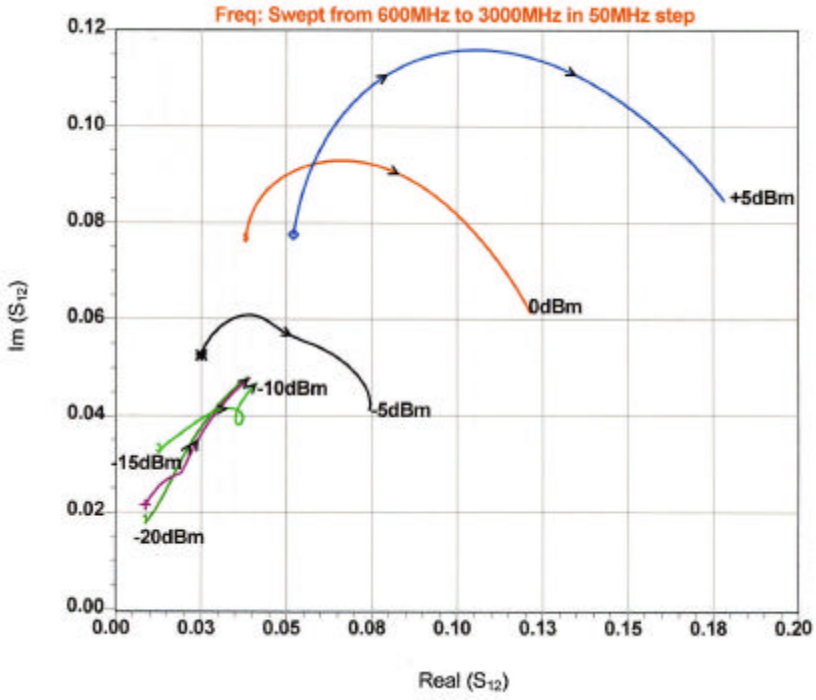

Figure 4-5 Measured large-signal S_{12} of the BFP520.

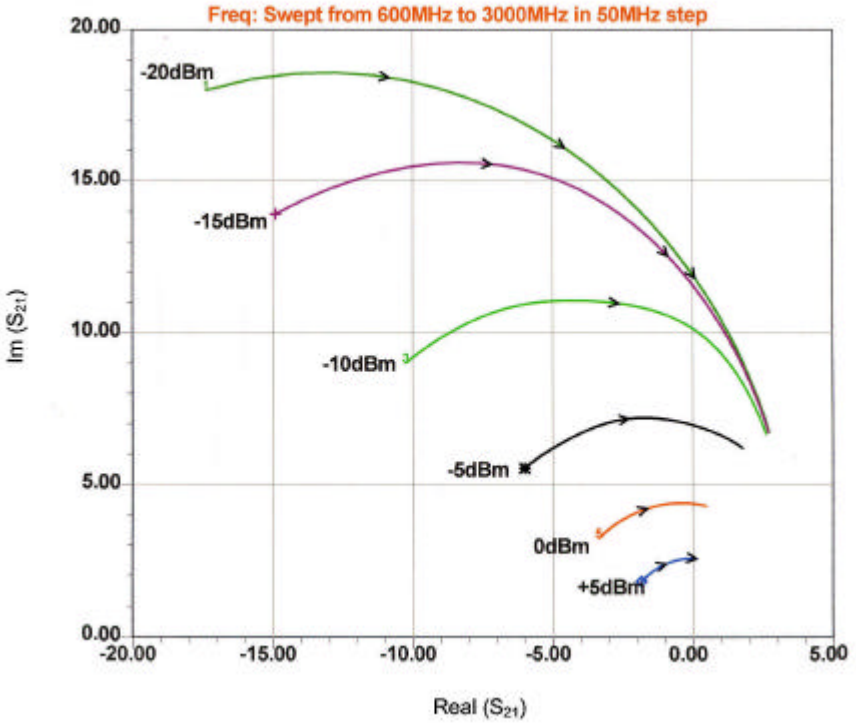

Figure 4-6 Measured large-signal S_{21} of the BFP520.

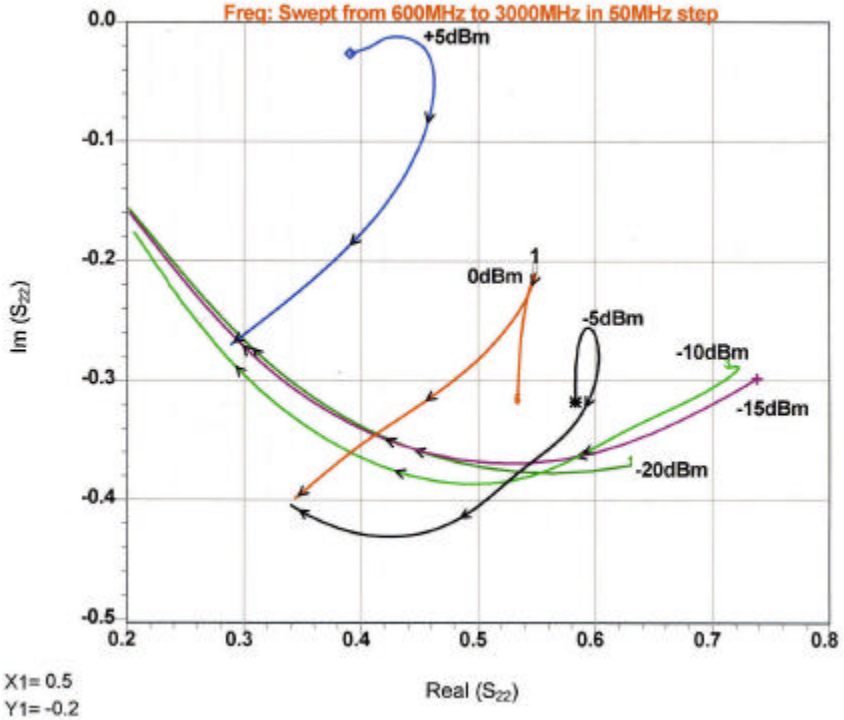

Figure 4-7 Measured large-signal S_{22} of the BFP520.

5 Resonator Choices

5.1 LC Resonators

The following resonators are found in various microwave oscillators. The lumped resonator consists of a lossy 2pF capacitor and a lossy 1.76nH inductor with a 0.2pF parasitic capacitor. The capacitor has a lead inductor of 0.2nH and 0.2Ω loss. Likewise, the inductor has the same loss resistor. To measure the operating Q, this combination is attached to a network analyzer, which determines S_{11}. The operating Q is calculated by dividing the center frequency by the 3 dB bandwidth of S_{11}. The quality factor Q is defined as stored energy/dissipated energy. If there is no energy loss, the Q is infinite. Figure 5-1 shows the circuit diagram of the resonator and the coupling.

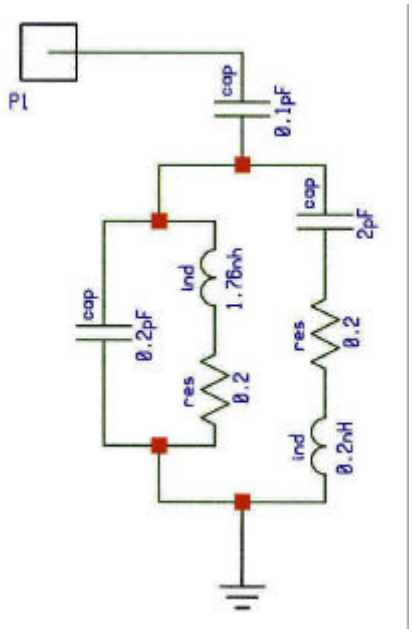

Figure 5-1 Shows the circuit diagram of a parallel tuned circuit with lossy components and parasitics loosely coupled to the input.

To determine the operating Q of the circuit, let us calculate the Q of the individual branches. The total Q of the circuit can be calculated by combining the two individual Q values following the equation.

$$Q = \frac{Q_1 \times Q_2}{Q_1 + Q_2} \tag{5-1}$$

$Q_1 = 2 \times \pi \times 2.4\ \text{GHz} \times 1.76nH/0.2\Omega = 133$, $Q_2 = 165$

$$Q = 73$$

The reason for the low Q is due to the 0.2Ω loss resistor. It should be possible to reduce this by more than a factor of 2.

5.2 Microstrip Resonators

Distributed/Lumped Resonators

The same parallel tuned circuit can be generated by using a printed transmission line instead of the lumped inductor and maintain the same capacitance. This is shown in Figure 5-2. Since the transmission line has losses due to the material, they need to be considered. It is not practical to calculate these by hand, but rather use a CAD program which does this accurately [115, 116]. These references describe how to get the Q factor from S_{11} measurements.

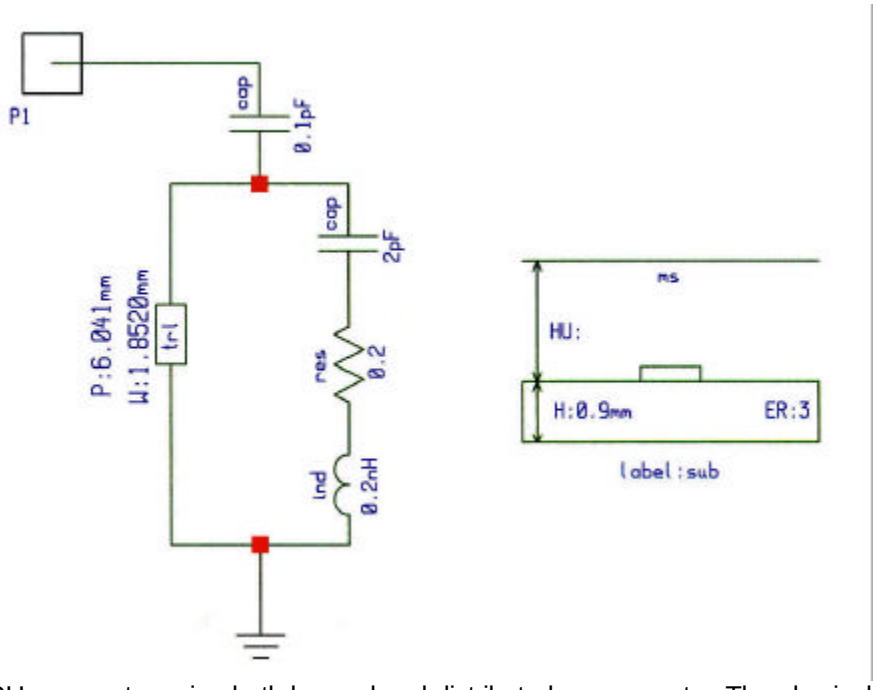

Figure 5-2 2.4 GHz resonator using both lumped and distributed components. The physical dimensions are given.

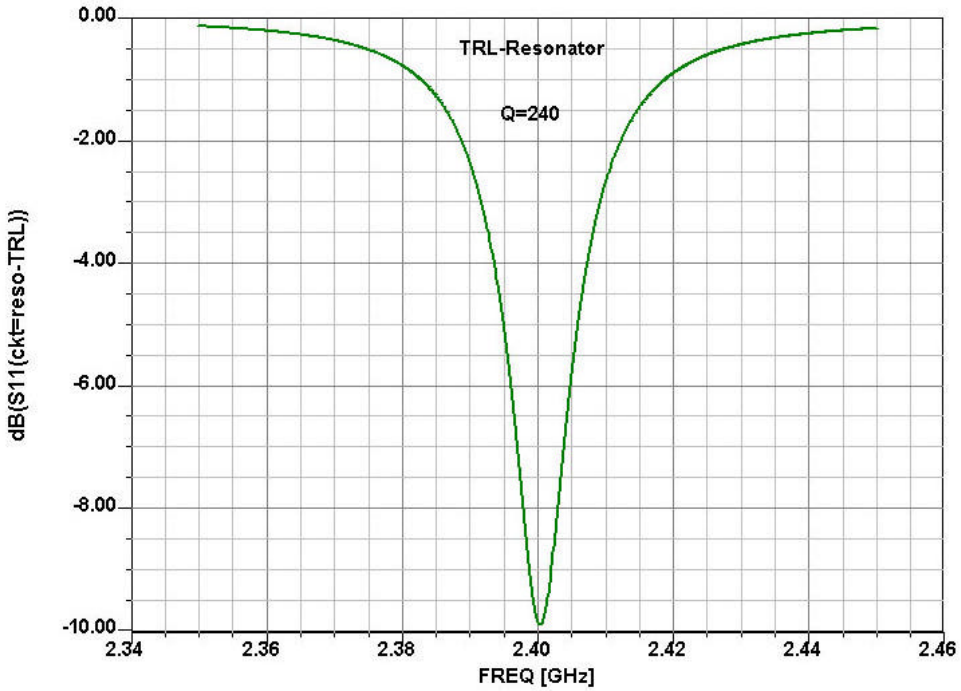

Figure 5-3 Simulated reflection coefficient S_{11} to determine the operating Q. Since this material has fairly high losses, an operating Q of only 240 was achieved.

The Q can be determined from the 3 dB bandwidth shown in Figure 5-3 and was determined to be 240. This is also valid if the Y or Z parameters are used. This is a typical value for a microstrip resonator. Values up to 300 are possible if the appropriate layout and material is used.

Integrated Resonators

The same circuit can be generated not only using printed circuit board material, but also in GaAs or in silicon. Figure 5-4 shows the schematic of a parallel tuned circuit using a rectangular inductor and an interdigital capacitor. The ground connection is achieved using a via. At 2.4 GHz, the number of turns and size of the inductor would be significant. The same applies to the capacitor. This arrangement should be reserved for much higher frequencies, above 5 GHz. The inductor losses, both in GaAs and silicon are substantial and this case is only shown for completeness. Where possible an external resonator should be used.

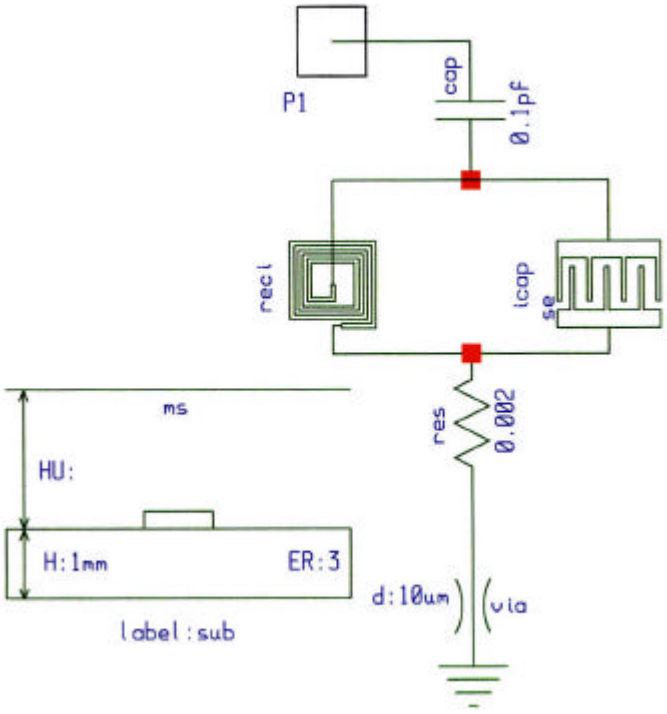

Figure 5-4 Parallel tuned circuit using a rectangular inductor (spiral could also be used) and an interdigital capacitor. If implemented on GaAs or silicon, it exhibits low Q.

5.3 Ceramic Resonators

A very popular resonator is the ceramic resonator, which is based on a quarter-wavelength arrangement. The ceramic is silver plated and can be modeled as a cable with a high relative dielectric constant ranging from 33 to 88. The two 1pF capacitors shown in Figure 5-5 load the resonator to achieve a resonance frequency of 2.4 GHz. This resonator has an operating Q of about 400, which is much higher than the previous cases. By varying the capacitors, the frequency can be altered. These are commercial parts, which are made by a variety of companies. Most of the high performance 800 MHz to 2.4 GHz oscillators use these resonators.

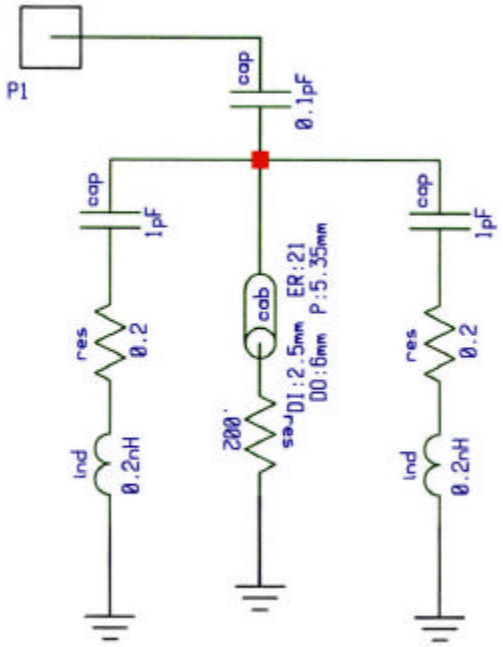

Figure 5-5 Shows a high Q resonator based on a quarter-wavelength ceramic resonator (CRO). Operating Q's of up to 500 are easily achievable.

5.4 Dielectric Resonators

One of the highest-Q resonators is the dielectric resonator. This is a resonant structure which is coupled to a transmission line. Its physical dimensions and dielectric constant determine the operating frequency. These resonators can have a Q of several thousand. By using the dielectric resonator/transmission line combination as part of an oscillator, very low phase noise oscillators can be obtained. The drawback of this device is its temperature coefficient and the fact that it is tuned by using a mechanical post, which is a few millimeters above the resonator. This is used for coarse tuning. Its equivalent circuit is a high-Q parallel circuit replacing the resonator. It is used as a stop-band filter as shown in Figure 5-6.

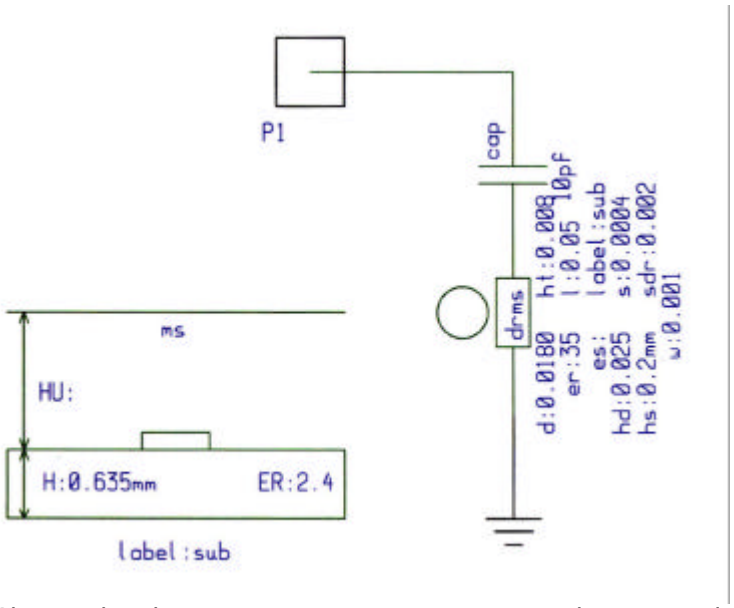

Figure 5-6 Shows a band-stop type resonant arrangement using a ceramic resonator.

Figure 5-7 shows the simulated 3 dB bandwidth based on the S_{11}. The Q, of course, depends on the coupling to the transmission line and other factors such as the ratio of diameter to height of the resonator. These types of resonators can be used to 20 GHz and above and have become quite popular as a point of reference for low-noise designs.

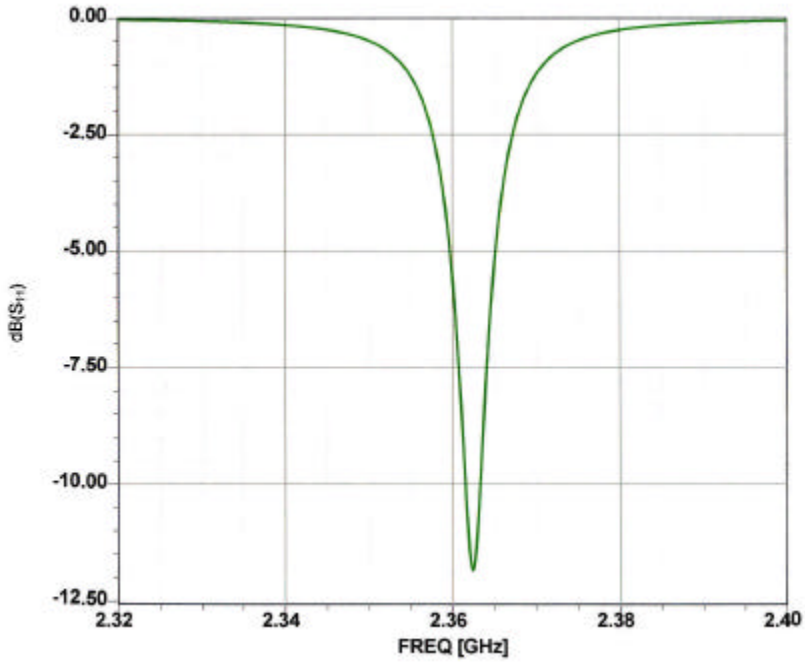

Figure 5-7 Simulated S_{11} in dB for a dielectric resonator. This can be used to determine the 3 dB bandwidth and the Q, if translated to Y or Z parameters.

6 General Theory of Oscillators

6.1 Oscillator Equations

The following section describes the linear theory of understanding and designing oscillators to be optimized for a specific frequency of oscillation and output power. This is followed by analyzing the oscillator as a nonlinear system using a set of nonlinear equations, after the start-up conditions in the time-domain have been explored.

Linear Theory

The following is a general Y matrix approach to describe the feedback requirements for an oscillator. Deviating from the standard approach, this will be done by *S*-parameters, which will then be converted into *Y*-parameters for easy calculations. In the nonlinear analysis, Section 6.2, we will have to distinguish between the start-up condition and the sustaining condition. The linear theory does not allow us to do this. For the final calculation in the linear theory, the large-signal *S*-parameters converted to *Y*-parameters will be used rather than the small-signal values.

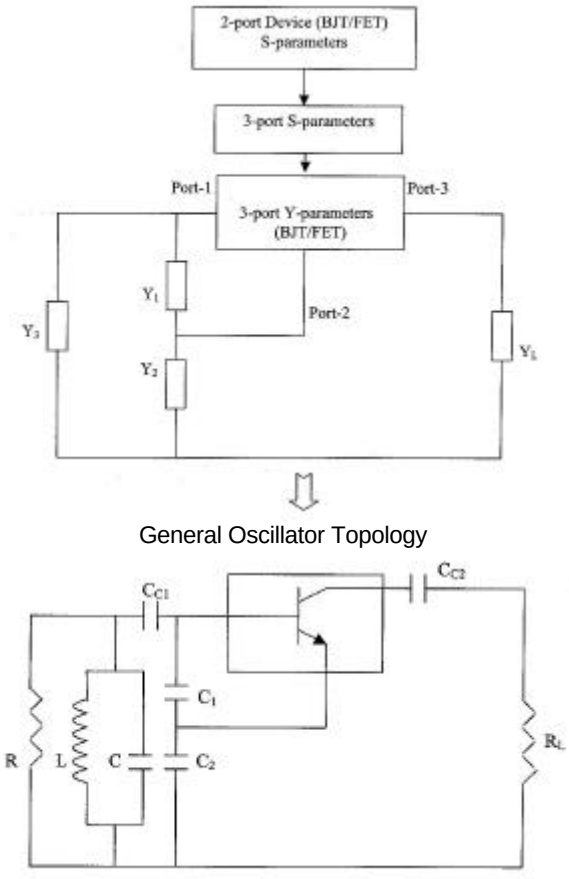

Figure 6-1 Shows a flow diagram on how to convert *S*-parameters of the measured device to a 3-port configuration for the transistor. The elements for the Colpitts oscillator, as an example, are then added.

6.1.1 The Calculation of the Oscillating Condition

Considering Parasitics

In the practical case, the device parasitics and loss resistance of the resonator will play an important role in the oscillator design. Figure 6-2 incorporates the base lead-inductance L_p and the package-capacitance C_p.

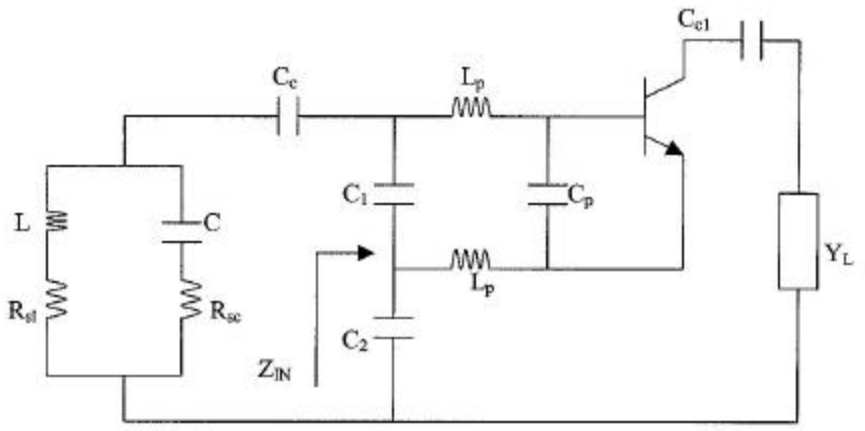

Figure 6-2 Colpitts oscillator with base-lead inductances and package capacitance. C_C is neglected. The equivalent circuit of the intrinsic transistor is shown in Figure 8-12.

The expression of input impedance is given as

$$Z_{IN}\big|_{pacakage} = -\left[\frac{Y_{21}}{w^2(C_1+C_p)C_2}\frac{1}{(1+w^2Y_{21}^2L_p^2)}\right] - j\left[\frac{(C_1+C_P+C_2)}{w(C_1+C_P)C_2} - \frac{wY_{21}L_P}{(1+w^2Y_{21}^2L_p^2)}\frac{Y_{21}}{w(C_1+C_P)C_2}\right] \quad (6\text{-}1)$$

$$Z_{IN}\big|_{without-pacakage} = -\left[\frac{Y_{21}}{w^2C_1C_2}\right] - j\left[\frac{(C_1+C_2)}{wC_1C_2}\right] \quad (6\text{-}2)$$

where L_p is the base-lead inductance of the bipolar transistor and C_p is base-emitter package capacitance. All further circuits are based on this model.

From the expression above, it is obvious that the base lead-inductance makes the input capacitance appear larger and the negative resistance appear smaller. The equivalent negative resistance and capacitance can be defined as

$$R_{NEQ} = \frac{R_N}{(1+w^2Y_{21}^2L_p^2)} \quad (6\text{-}3)$$

$$\frac{1}{C_{EQ}} = \left\{ \left[\frac{1}{\frac{(C_1 + C_P)C_2}{(C_1 + C_2 + C_P)}} \right] - \left[\frac{w^2 Y_{21} L_P}{(1 + w^2 Y_{21}^2 L_P^2)} \right] \left[\frac{Y_{21}}{w(C_1 + C_P)C_2} \right] \right\} \tag{6-4}$$

$$R_N = -\frac{Y_{21}}{w^2 C_1 C_2} \tag{6-5}$$

where

R_N: Negative resistance without lead inductance and package capacitance.
R_{NEQ}: Negative resistance with base-lead inductance and package capacitance.
C_{EQ}: Equivalent capacitance with base-lead inductance and package capacitance

At resonance:

$$j\left[\frac{wL}{1 - w^2 LC} - \frac{1}{wC_C} \right] - j\left[\frac{(C_1 + C_P + C_2)}{w(C_1 + C_P)C_2} - \frac{wY_{21} L_P}{(1 + w^2 Y_{21}^2 L_p^2)} \frac{Y_{21}}{w(C_1 + C_P)C_2} \right] = 0 \tag{6-6}$$

$$\Rightarrow \left[\frac{wL}{1 - w^2 LC} - \frac{1}{wC_C} \right] = \left[\frac{(C_1 + C_P + C_2)}{w(C_1 + C_P)C_2} - \frac{Y_{21}}{w(C_1 + C_P)C_2} \frac{wY_{21} L_P}{(1 + w^2 Y_{21}^2 L_p^2)} \right] \tag{6-7}$$

$$\Rightarrow \left[\frac{w^2 LC_C - (1 - w^2 LC)}{wC_C (1 - w^2 LC)} \right] = \left[\frac{(1 + w^2 Y_{21}^2 L_p^2)(C_1 + C_P + C_2) - wL_P Y_{21}^2}{w(C_1 + C_P)C_2 (1 + w^2 Y_{21}^2 L_p^2)} \right] \tag{6-8}$$

The expression above can be rewritten in terms of a determinant as

$$\text{Det} \begin{vmatrix} [w^2 LC_C - (1 - w^2 LC] & [(1 + w^2 Y_{21}^2 L_p^2)(C_1 + C_P + C_2) - wL_P Y_{21}^2] \\ [wC_C (1 - w^2 LC)] & [w(C_1 + C_P)C_2 (1 + w^2 Y_{21}^2 L_p^2)] \end{vmatrix} = 0 \tag{6-9}$$

and the resonance condition is given as $K_1 - K_2 \to 0$

where

$$K_1 = [w^2 LC_C - (1 - w^2 LC)][w(C_1 + C_P)C_2 (1 + w^2 Y_{21}^2 L_p^2)] \tag{6-10}$$

$$K_2 = [wC_C (1 - w^2 LC)][(1 + w^2 Y_{21}^2 L_p^2)(C_1 + C_P + C_2) - wL_P Y_{21}^2] \tag{6-11}$$

K_1 and K_2 are expressed in terms of the polynomial as

$$K_1 = K_{11}w^5 + K_{12}w^4 + K_{13}w^3 + K_{14}w^2 + K_{15}w \tag{6-12}$$

$$K_2 = K_{21}w^5 + K_{22}w^4 + K_{23}w^3 + K_{24}w^2 + K_{25}w \tag{6-13}$$

where the coefficients of the polynomial K_1 are

$$K_{11} = [Y_{21}^2 LL_p^2 C_2 (C_1 C_c + C_c C_P + CC_1 + CC_P)] \tag{6-14}$$

$$K_{12} = 0 \tag{6-15}$$

$$K_{13} = [LC_2 (C_1 C_C + C_P C_C + C_1 C + CC_P) - Y_{21}^2 L_p^2 C_2 (C_1 + C_P)] \tag{6-16}$$

$$K_{14} = 0 \tag{6-17}$$

$$K_{15} = -[C_2 (C_1 + C_P)] \tag{6-18}$$

and the coefficients of the polynomial K_2 are

$$K_{21} = -[(C_1 + C_P + C_2) Y_{21}^2 L_p^2 LCC_C] \tag{6-19}$$

$$K_{22} = [L_P Y_{21}^2 LCC_C] \tag{6-20}$$

$$K_{23} = [(C_1 + C_P + C_2) C_C (Y_{21}^2 L_p^2 - LC)] \tag{6-21}$$

$$K_{24} = -[L_P Y_{21}^2 C_C] \tag{6-22}$$

$$K_{25} = [(C_1 + C_P + C_2) C_C] \tag{6-23}$$

Now $K_1 - K_2$ can be further simplified as

$$[K_{11}w^5 + K_{13}w^3 + K_{15}w] - [K_{21}w^5 + K_{22}w^4 + K_{23}w^3 + K_{24}w^2 + K_{25}w] = 0 \tag{6-24}$$

$$[(K_{11} - K_{21})w^5 - K_{22}w^4 + (K_{13} - K_{23})w^3 - K_{24}w^2 + (K_{15} - K_{25})w] = 0 \tag{6-25}$$

$$K_1 - K_2 \Rightarrow A_{11}w^5 + A_{12}w^4 + A_{13}w^3 + A_{14}w^2 + A_{15}w \tag{6-26}$$

$$f(w, A_{11}, A_{12}, A_{13}, A_{14}, A_{15}) = A_{11}w^5 + A_{12}w^4 + A_{13}w^3 + A_{14}w^2 + A_{15}w = 0 \quad (6\text{-}27)$$

where

$$A_{11} = (K_{11} - K_{21}) = [Y_{21}^2 LL_p^2 C_2 (C_1 C_c + C_c C_P + CC_1 + CC_P)] + [Y_{21}^2 L_p^2 LCC_C (C_1 + C_P + C_2)] \quad (6\text{-}28)$$

$$A_{12} = (K_{12} - K_{22}) = [0 - L_P Y_{21}^2 LCC_C] \quad (6\text{-}29)$$

$$A_{13} = (K_{13} - K_{23})$$
$$= [LC_2 (C_1 C_C + C_P C_C + C_1 C + CC_P) - Y_{21}^2 L_p^2 C_2 (C_1 + C_P)] - [(C_1 + C_P + C_2) C_C (Y_{21}^2 L_p^2 - LC)] \quad (6\text{-}30)$$

$$A_{14} = (K_{14} - K_{24}) = L_P Y_{21}^2 C_C \quad (6\text{-}31)$$

$$A_{15} = (K_{15} - K_{25}) = -[C_2 (C_1 + C_P) + (C_1 + C_P + C_2) C_C] \quad (6\text{-}32)$$

The function $f(w, A_{11}, A_{12}, A_{13}, A_{14}, A_{15}, A_{16})$ will have five possible solutions, which can be solved with the help of MathCAD.

For $L_p \to 0$

$$w_0 = \sqrt{\frac{[C_2 C_1 + C_1 C_C + C_2 C_C]}{L[C_1 C_2 C_C + C_1 C_2 C + C_1 C C_C + C_2 C C_C]}} \quad (6\text{-}33)$$

$$w_0 = \sqrt{\frac{1}{L\left[C + \frac{C_1 C_2 C_C}{C_1 C_2 + C_1 C_C + C_2 C_C}\right]}} \quad (6\text{-}34)$$

C_C is a coupling capacitor used for separating the bias circuit, and its value is normally small, but similar to C_1 and C_2, typically 0.2pF to 2pF.

Rewriting the polynomial equation without considering C_C,

$$w = \sqrt{\frac{1}{L\left[\frac{C_1 C_2}{C_1 + C_2} + C\right]}} \tag{6-35}$$

6.1.2 Parallel Feedback Oscillator

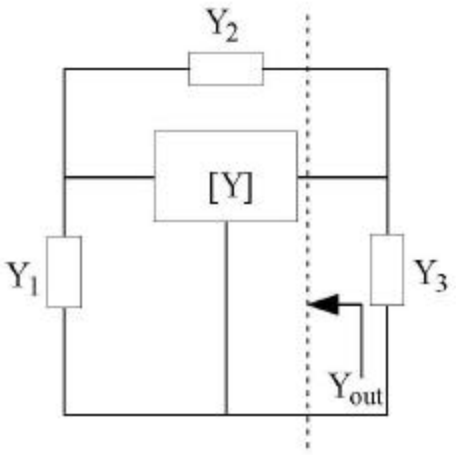

Figure 6-3 Parallel feedback oscillator topology.

This example uses the large-signal *Y*-parameters derived from the large-signal *S*-parameters (measured or simulated).

The steady state oscillation condition for the parallel feedback oscillators given in Figure 6-3 is shown as

$$Y_{out} + Y_3 \Rightarrow 0 \tag{6-36}$$

The steady-state stationary condition can be expressed as

$$Det\begin{bmatrix} Y_{11} + Y_1 + Y_2 & Y_{12} - Y_2 \\ Y_{21} - Y_2 & Y_{22} + Y_2 + Y_3 \end{bmatrix} = 0 \tag{6-37}$$

$$Y_3 = -[Y_{22} + Y_2] + \frac{[Y_{12} - Y_2][Y_{21} - Y_2]}{[Y_{11} + Y_1 + Y_2]} \tag{6-38}$$

where Y_{ij} (i,j=1,2) are *Y*-parameters of the hybrid bipolar/FET-transistor model.

As shown in Figure 6-3, the active 2-port network, together with the feedback elements Y_1 and Y_2, are considered as a one-port negative resistance oscillator circuit. The output admittance Y_{out} can be given as

$$Y_{out} = -Y_3 \Rightarrow [Y_{22} + Y_2] - \frac{[Y_{12} - Y_2][Y_{21} - Y_2]}{[Y_{11} + Y_1 + Y_2]} \tag{6-39}$$

According to optimum criterion, the optimum values of feedback susceptance B_1 and B_2, at which the negative value of $\mathrm{Re}[Y_{\mathrm{out}}]$ is maximum, are determined by solving the following differential condition:

$$\frac{\partial \mathrm{Re}[Y_{out}]}{\partial B_1} = 0 \; and \; \frac{\partial \mathrm{Re}[Y_{out}]}{\partial B_2} = 0 \tag{6-40}$$

and the solution of the above differential condition will give the optimum values of output admittance Y_{out}^* and feedback susceptance B_1^* and B_2^*, which can be expressed in terms of the two-port *Y*-parameters of the active device (BJT/FET) as

$$B_1^* = -\left\{ B_{11} + \left[\frac{B_{12} + B_{21}}{2} \right] + \left[\frac{G_{21} - G_{12}}{B_{21} - B_{12}} \right] \left[\frac{G_{12} + G_{21}}{2} + G_{11} \right] \right\} \tag{6-41}$$

$$B_2^* = \left[\frac{B_{12} + B_{21}}{2} \right] + \left[\frac{(G_{12} + G_{21})(G_{21} - G_{12})}{2(B_{21} - B_{12})} \right] \tag{6-42}$$

The optimum values of the real and imaginary part of the output admittance are

$$Y_{out}^* = [G_{out}^* + jB_{out}^*] \tag{6-43}$$

where G_{out}^* and B_{out}^* is given as

$$G_{out}^* = G_{22} - \left[\frac{(G_{12} + G_{21})^2 (B_{21} - B_{12})^2}{4G_{11}} \right] \tag{6-44}$$

$$B_{out}^* = B_{22} + \left[\frac{G_{21} - G_{12}}{B_{21} - B_{12}} \right] - \left[\frac{(G_{12} + G_{21})}{2} + G_{22} - G_{out}^* \right] + \left[\frac{B_{21} + B_{12}}{2} \right] \tag{6-45}$$

Thus, in the steady-state stationary oscillation mode, the general condition for oscillation is given as:

$$\left| Y_{out}^* + Y_3 \right| \Rightarrow 0; \; and \; [G_{out}^* + G_L] + [B_{out}^* + B_3^*], \; and \; finally \; we \; get \; G_{out}^* + G_L = 0 \; and \; B_{out}^* + B_3^* = 0 \tag{6-46}$$

where $Y_3 = [G_L + jB_3]$, $G_L = 1/R_L$, R_L is the load resistance.

The output power for the given load $Y_3 = [G_L + jB_3]$ is given as $P_{out} = \frac{1}{2} V_{out}^2 G_L$, where V_{out} is the voltage across the load. We can now introduce the voltage feedback factor *m* and phase Φ_n, which can be expressed in terms of the transistor *Y*-parameters as

$$m = \frac{\sqrt{(G_{12} + G_{21} - 2G_2)^2 + (B_{21} - B_{12})^2}}{2(G_{12} + G_{21} - G_2)} \tag{6-47}$$

$$\Phi_n = \tan^{-1} \frac{B_{21} - B_{12}}{G_{12} + G_{21} - 2G_2} \tag{6-48}$$

An example is shown in Appendix A and explains the use of the two terms.

6.2 Large-Signal Oscillator Design

Traditionally, oscillators have been designed using small-signal parameters and establishing a negative resistance using a feedback network to compensate the losses. This approach allows for the determination of the start-up condition, but not for the time it takes to reach steady-state oscillation, nor the steady-state operating conditions, nor the output power. Using a nonlinear approach described here, a design rule for maximum power will be given. Some applications impose higher priority on the DC efficiency rather than the best phase noise and the following steps will demonstrate a procedure to accomplish this. The question of noise in oscillators and the optimization of oscillators for best noise will be shown in Section 7.

6.2.1 Start-Up Condition

The oscillator is an autonomous circuit. The noise present in the active device or power supply turn-on transients leads to the initial oscillation build-up. Linear analysis is useful only for analyzing oscillation start-up. It is no longer valid as the oscillation amplitude continues to grow and the nonlinearity of the circuit becomes important. Nonlinear analysis needs to be used to predict the oscillation amplitude and the spectral purity of the oscillator output signal. As a basic requirement for producing a self-sustained near-sinusoidal oscillation, an oscillator must have a pair of complex-conjugate poles on the imaginary axis i.e. in the right half of s-plane with $\alpha>0$.

$$P(p_1, p_2) = a \pm jb \tag{6-49}$$

While this requirement does not guarantee an oscillation with a well-defined steady-state (squeaking), it is a necessary condition for any oscillator. When subjected to an excitation

due to power supply turn-on transient or noise associated with the oscillator circuit, the right half plane poles in the equation above produce a sinusoidal signal with an exponentially growing envelope given as

$$v(t) = V_0 \exp(a\,t)\cos(b\,t) \tag{6-50}$$

$$v(t)\big|_{t=0} \to V_0 \tag{6-51}$$

V_0 is determined by the initial conditions. $v(t)$ is eventually limited by the associated nonlinearity of the oscillator circuit.

Using either a feedback model approach or a negative resistance model, one can perform the analysis of the oscillator. Depending on the oscillator topology one approach is preferred over the other. The condition of oscillation build-up and steady-state oscillation will be discussed using both approaches.

Figure 6-4 shows, in block diagram form, the necessary components of an oscillator. It contains an amplifier with the frequency-dependent forward amplifier gain block, $G(jw)$, and a frequency-dependent feedback network, $H(jw)$.

When oscillation starts up, the signal level at the input of the amplifier is very small and the amplitude dependence of the forward amplifier gain can be initially neglected until it reaches saturation.

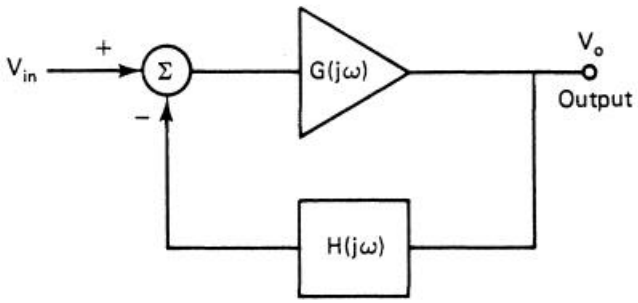

Figure 6-4 Block diagram of basic feedback model-oscillator.

The closed loop transfer function (T.F) and output voltage $V_o(w)$ are given by

$$T.F = \frac{V_o(w)}{V_{\text{in}}(w)} = \frac{G(jw)}{1 + G(jw)H(jw)} \tag{6-52}$$

$$V_o(w) = \left[\frac{G(jw)}{1 + G(jw)H(jw)}\right] V_{\text{in}}(w) \tag{6-53}$$

For an oscillator, the output voltage V_o is nonzero even if the input signal $V_i = 0$. This is only possible if the forward loop gain is infinite (which is not practical), or if the denominator $1 + G(jw)H(jw) = 0$ at some frequency w_o; that is, the loop gain is equal to unity for some values of the complex frequency $s=jw$.

This leads to the well-known condition for the *Barkhausen criterion*, and can be mathematically expressed

$$|G(jw_o)H(jw_o)| = 1 \tag{6-54}$$

and

$$Arg[G(jw_o)H(jw_o)] = 2np \quad where\ n = 0,1,2... \tag{6-55}$$

When the *Barkhausen criterion* are met, the two conjugate poles of the overall transfer function are located on the imaginary axis of the s-plane. Any departure from that position will lead to an increase or a decrease of the amplitude of the oscillator output signal in time domain, which is shown in Figure 6-5.

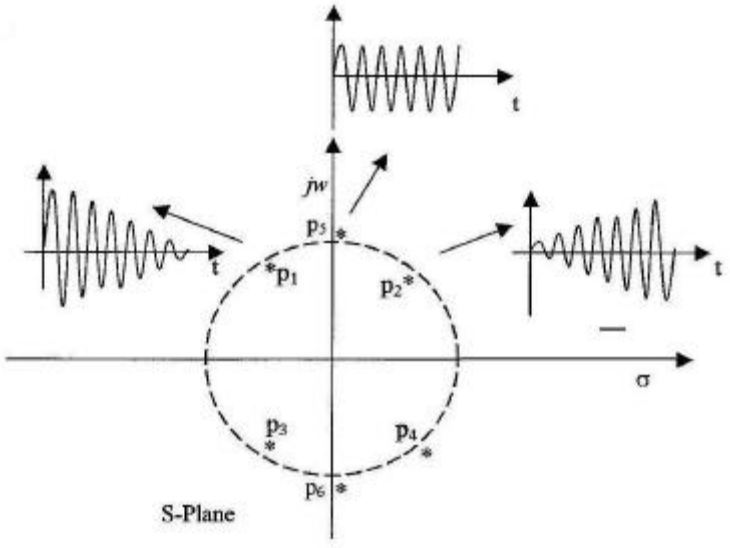

Figure 6-5 Frequency domain root locus and the corresponding time domain response.

In practice, the equilibrium point cannot be reached instantaneously without violating some physical laws. As an example, high-Q oscillators take longer than low-Q types to achieve full amplitude. The oscillator output sine wave cannot start at full amplitude instantaneously after the power supply is turned on. The design of the circuit must be

such that at start-up, the poles are located in the right half plane, but not too far from the *Y*-axis. However, the component tolerances and the nonlinearities of the amplifier will play a role. This oscillation is achievable with a small-signal loop gain greater than unity. As the output signal builds up, at least one parameter of the loop gain must change its value in such a way that the two complex-conjugate poles migrate in the direction of the *Y*-axis. The parameter must then reach that axis for the desired steady-state amplitude value at a given oscillator frequency.

Figure 6-6 shows the general schematic diagram of a one-port negative resistance model. The oscillator circuit is separated into a one-port active circuit which is nonlinear time variant (NLTV) and a one-port frequency-determining circuit, which is linear time invariant (LTIV).

The frequency determining circuit or resonator sets the oscillation frequency and is amplitude independent.

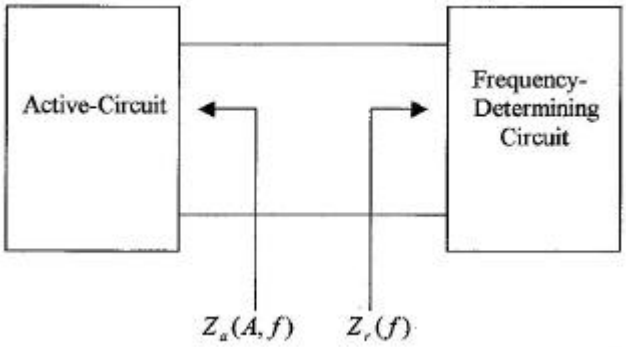

Figure 6-6 Schematic diagram of a one-port negative resistance model.

Assuming that the steady state current at the active circuit is almost sinusoidal, the input impedance $Z_a(A,f)$ can be expressed in terms of a negative resistance and reactance as

$$Z_a(A,f) = R_a(A,f) + jX_a(A,f) \tag{6-56}$$

A is the amplitude of the steady state current into the active oscillator circuit and *f* is the resonant frequency. $R_a(A,f)$ and $X_a(A,f)$ are the real and imaginary parts of the active circuit and depend on amplitude and frequency.

Since the frequency-determining circuit is amplitude independent, it can be represented as

$$Z_r(f) = R_r(f) + jX_r(f) \tag{6-57}$$

$Z_r(f)$ is the input impedance of the frequency-determining circuit. $R_r(f)$ and $X_r(f)$ are the loss resistance and reactance associated with the resonator/frequency-determining circuit.

To support the oscillator build-up, $R_a(A, f) < 0$ is required so that the total loss associated with the frequency-determining circuit can be compensated. Oscillation will start building up if the product of the input reflection coefficient, $\Gamma_r(f_0)$, looking into the frequency-determining circuit and the input reflection coefficient, $\Gamma_a(A_0, f_0)$, of the active part of the oscillator circuit is unity at $A = A_0$ and $f = f_0$.

The steady state oscillation condition can be expressed as

$$\Gamma_a(A, f)\Gamma_r(f)\big|_{f=f_0} \Rightarrow \Gamma_a(A_0, f_0)\Gamma_r(f_0) = 1 \tag{6-58}$$

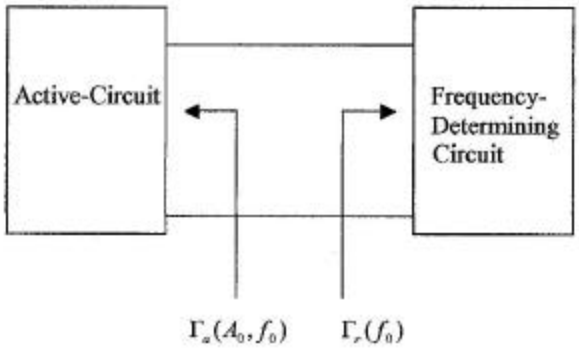

Figure 6-7 Schematic diagram of a one-port negative reflection model.

Figure 6-7 shows the input reflection coefficient $\Gamma_a(A_0, f_0)$ and $\Gamma_r(f_0)$, which can be represented in terms of the input impedance and the characteristic impedance Z_0 as

$$\Gamma_a(A_0, f_0) = \frac{Z_a(A_0, f_0) - Z_0}{Z_a(A_0, f_0) + Z_0} \tag{6-59}$$

$$\text{and} \qquad \Gamma_r(f_0) = \frac{Z_r(f_0) - Z_0}{Z_r(f_0) + Z_0} \tag{6-60}$$

$$\Gamma_a(A_0, f_0)\Gamma_r(f_0) = 1 \Rightarrow \left[\frac{Z_a(A_0, f_0) - Z_0}{Z_a(A_0, f_0) + Z_0}\right]\left[\frac{Z_r(f_0) - Z_0}{Z_r(f_0) + Z_0}\right] = 1 \tag{6-61}$$

$$[Z_a(A_0, f_0) - Z_0][Z_r(f_0) - Z_0] - [Z_a(A_0, f_0) + Z_0][Z_r(f_0) + Z_0] = 0 \tag{6-62}$$

$$\Rightarrow Z_a(A_0, f_0) + Z_r(f_0) = 0 \tag{6-63}$$

The characteristic equation $Z_a(A_0, f_0) + Z_r(f_0) = 0$ can be written as

$$R_a(A_0, f_0) + R_r(f_0) = 0 \tag{6-64}$$

and

$$X_a(A_0, f_0) + X_r(f_0) = 0 \tag{6-65}$$

To support the oscillator build-up, $R_a(A, f) < 0$ is required so that the total loss associated with $R_r(f_0)$ of the frequency-determining circuit can be compensated. This means that the one-port circuit is unstable for the frequency range $f_1 < f < f_2$ where $R_a(A, f)\big|_{f_1<f<f_2} < 0 \Rightarrow \big|R_a(A, f)\big|_{f_1<f<f_2} > \big|R_r(f)\big|$. At the start-up oscillation, when the signal amplitude is very small, the amplitude dependence of the $R_a(A, f)$ is negligible and the oscillation build-up conditions can be given as

$$\big[R_a(f) + R_r(f)\big]_{f=f_x} \Rightarrow R_a(f_x) + R_r(f_x) = \leq 0 \tag{6-66}$$

requires slight negative resistance

and

$$\big[X_a(f) + X_r(f)\big]_{f=f_x} \Rightarrow X_a(f_x) + X_r(f_x) = 0 \tag{6-67}$$

f_x denotes the resonance frequency at which the total reactive component equals zero. The conditions above are necessary, but not sufficient conditions for oscillation build-up, particularly in the case when multiple frequencies exist to support the above shown conditions.

To guarantee the oscillation build-up, the following condition at the given frequency needs to be met:

$$\frac{\partial}{\partial f}\big[X_a(f) + X_r(f)\big]_{f=f_x} > 0 \tag{6-68}$$

$$R_a(f_x) + R_r(f_x) < 0 \tag{6-69}$$

$$X_a(f_x) + X_r(f_x) = 0 \tag{6-70}$$

Alternatively, for a parallel admittance topology

$$Y_a(f_x) + Y_r(f_x) = 0 \tag{6-71}$$

$$G_a(f_x) + G_r(f_x) < 0 \tag{6-72}$$

$$B_a(f_x) + B_r(f_x) = 0 \tag{6-73}$$

$$\frac{\partial}{\partial f}\left[B_a(f) + B_r(f)\right]_{f=f_x} > 0 \tag{6-74}$$

Figure 6-8 below shows the start and steady-state oscillation conditions.

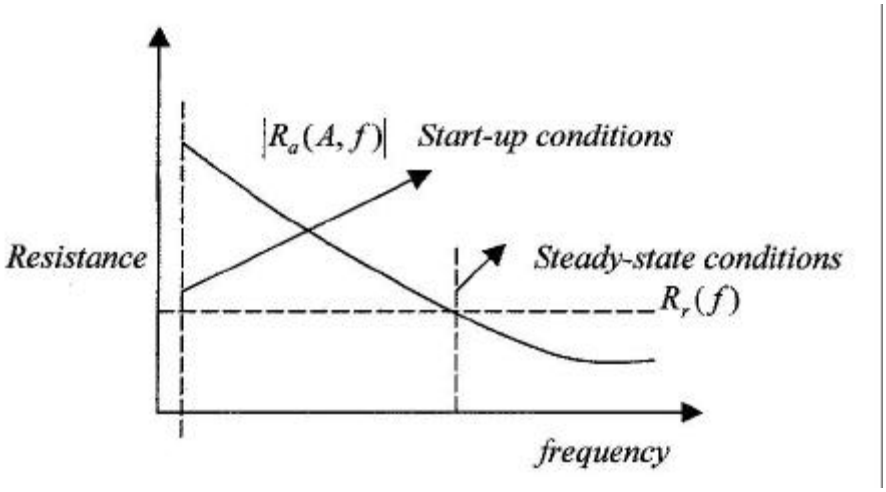

Figure 6-8 Plot of start and steady state oscillation conditions.

To demonstrate the transient behavior, a ceramic resonator-based oscillator was designed and simulated as shown in Figure 6-9. This transistor circuit, shown in Figure 9-2, is used several times in this work. The transient analysis function of *Ansoft Designer* was used to show the DC bias shift and the settling of the amplitude of the oscillation that occurs after 60 nS. The transient analysis of microwave circuits, because of the distributed elements, is a major problem for most CAD microwave simulators. The voltage shown is sampled at the emitter of the Colpitts oscillator.

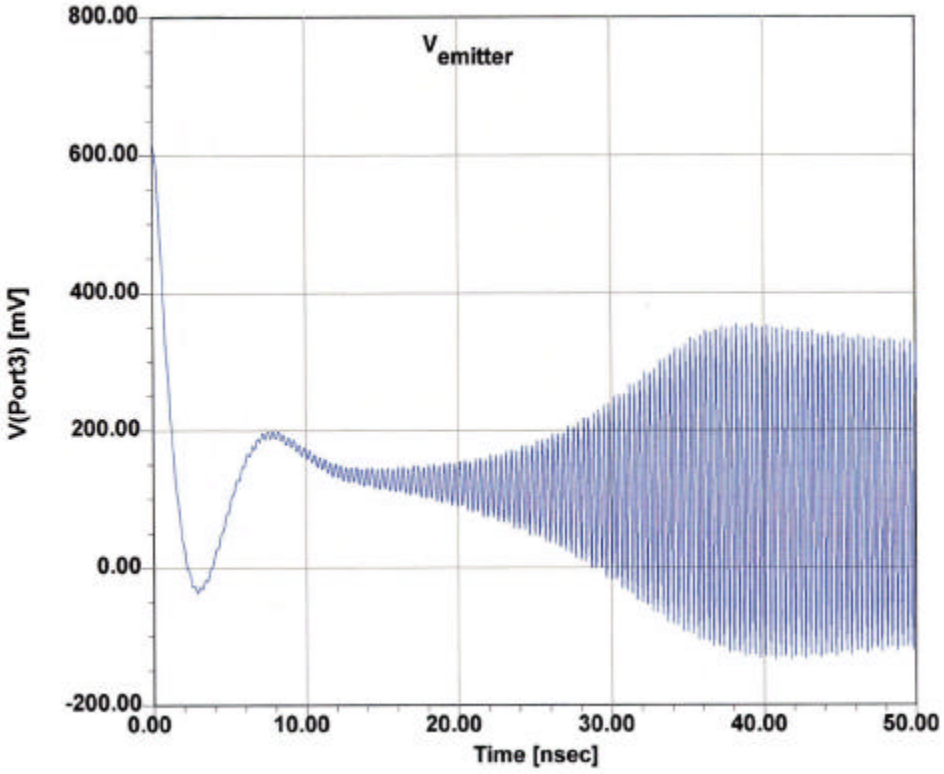

Figure 6-9 Transient simulation of the ceramic resonator-based high-Q oscillator shown in Figure 9-2. The voltage displayed is taken from the emitter.

6.2.2 Steady-State Behavior

As discussed earlier, if the closed-loop voltage gain has a pair of complex-conjugate poles in the right half of the s-plane, close to the imaginary axis, then due to an ever-present noise voltage generated in the circuit or power-on transient, a growing, near-sinusoidal voltage appears. As the oscillation amplitude grows, the amplitude-limiting capabilities, due to the change in transconductance from small-signal g_m to the large-signal G_m of the amplifier, produce a change in the location of the poles. The changes are such that the complex-conjugate poles move towards the imaginary axis and at some value of the oscillation amplitude, the poles reach the imaginary axis, giving the steady-state oscillation.

$$\left|G(jw_o)H(jw_o)\right| = 1 \tag{6-75}$$

In the case of the negative resistance model, the oscillation will continue to build up as long as $R_a(A, f)\big|_{f_1<f<f_2} < 0$; *active circuit or* $\Rightarrow \left|R_a(A, f)\right|_{f_1<f<f_2} > \left|R_r(f)\right|$, resonant circuit, see Figure 6-6.

The frequency of oscillation is determined by $R_a(A_0, f_0) + R_r(f_0) = 0$. $X_a(A_0, f_0) + X_r(f_0) = 0$ might not be stable because $Z_a(A, f)$ is frequency and amplitude-dependent. To guarantee stable oscillation, the following conditions are to be satisfied: The first term of Eq. 6-76 is larger than the second term because the derivative of the negative resistance must be larger than or equal to the derivative of the loss resistance. This can be rewritten in the form of Eq. 6-77.

$$\frac{\partial}{\partial A}\left[R_a(A)\big|_{A=A_0}\right] * \frac{\partial}{\partial w}\left[X_r(f)\big|_{f=f_0}\right] - \frac{\partial}{\partial A}\left[X_a(A)\big|_{A=A_0}\right] * \frac{\partial}{\partial w}\left[R_r(f)\big|_{f=f_0}\right] > 0 \tag{6-76}$$

$$\frac{\partial}{\partial A}\left[R_a(A)\big|_{A=A_0}\right] * \frac{\partial}{\partial w}\left[X_r(f)\big|_{f=f_0}\right] > \frac{\partial}{\partial A}\left[X_a(A)\big|_{A=A_0}\right] * \frac{\partial}{\partial w}\left[R_r(f)\big|_{f=f_0}\right] \tag{6-77}$$

In the case of an LC resonant circuit, $R_r(f)$ is constant and the equation above can be simplified to

$$\frac{\partial}{\partial A}\left[R_a(A)\big|_{A=A_0}\right] * \frac{\partial}{\partial w}\left[X_r(f)\big|_{f=f_0}\right] > 0 \tag{6-78}$$

Alternatively, for a parallel tuned circuit, the steady-state oscillation condition is given as

$$G_a(f_0) + G_r(f_0) = 0 \tag{6-79}$$

$$B_a(f_0) + B_r(f_0) = 0 \tag{6-80}$$

$$\frac{\partial}{\partial A}\left[G_a(A)\big|_{A=A_0}\right] * \frac{\partial}{\partial w}\left[B_r(f)\big|_{f=f_0}\right] > 0 \tag{6-81}$$

6.2.3 Time-Domain Behavior

The large-signal transfer characteristic affecting the current and voltage of an active device in an oscillator circuit is nonlinear. It limits the amplitude of the oscillation and produces harmonic content in the output signal. The resonant circuit and resulting phase shift sets the oscillation frequency. The nonlinear, exponential relationship between the voltage and current of a bipolar transistor is given as

$$i(t) = I_s e^{\frac{qv(t)}{kT}} \tag{6-82}$$

I_s is device saturation current, $v(t)$ is the voltage drive applied across the junction, k is Boltzman's constant, q is the electronic charge, and T is the temperature of the device in Kelvins. The bipolar case is mathematically more complex than the FET case. For the FET a similar set of equations exist which can be derived. Since most RFIC's now use SiGe bipolar transistors, the bipolar case has been selected.

The voltage $v(t)$ across the base-emitter junction consists of a DC component and a driven signal voltage $V_1\cos(wt)$. It can be expressed as

$$v(t) = V_{dc} + V_1\cos(wt) \tag{6-83}$$

As the driven voltage $V_1\cos(wt)$ increases and develops enough amplitude across the base-emitter junction, the resulting current is a periodic series of pulses whose amplitude depends on the nonlinear characteristics of the device and is given as

$$i_e(t) = I_s e^{\frac{qv(t)}{kT}} \tag{6-84}$$

$$i_e(t) = I_s e^{\frac{qV_{dc}}{kT}} e^{\frac{qV_1\cos(wt)}{kT}} \tag{6-85}$$

$$i_e(t) = I_s e^{\frac{qV_{dc}}{kT}} e^{x\cos(wt)} \tag{6-86}$$

assuming $I_c \approx I_e$ (b>10)

$$x = \frac{V_1}{(kT/q)} = \frac{qV_1}{kT} \tag{6-87}$$

$i_e(t)$ is the emitter current and x is the drive level which is normalized to kT/q.

From the Fourier series expansion, $e^{x\cos(wt)}$ is expressed as

$$e^{x\cos(wt)} = \sum_n a_n(x)\cos(nwt) \tag{6-88}$$

$a_n(x)$ is a Fourier coefficient and given as

$$a_0(x)\big|_{n=0} = \frac{1}{2p}\int_0^{2p} e^{x\cos(wt)}d(wt) = I_0(x) \tag{6-89}$$

$$a_n(x)\big|_{n>0} = \frac{1}{2p}\int_0^{2p} e^{x\cos(wt)}\cos(nwt)d(wt) = I_n(x) \tag{6-90}$$

$$e^{x\cos(wt)} = \sum_n a_n(x)\cos(nwt) = I_0(x) + \sum_1^{\infty} I_n(x)\cos(nwt) \tag{6-91}$$

$I_n(x)$ is the modified Bessel function.

$$\text{As } x \to 0 \Rightarrow I_n(x) \to \frac{(x/2)^n}{n!} \tag{6-92}$$

$I_0(x)$ are monotonic functions having positive values for x≥0 and n≥0; $I_0(0)$ is unity, whereas all higher order functions start at zero.

The short current pulses are generated from the growing large-signal drive level across the base-emitter junction, which leads to strong harmonic generation. The emitter current represented above can be expressed in terms of harmonics as

$$i_e(t) = I_s e^{\frac{qV_{dc}}{kT}} I_0(x)\left[1 + 2\sum_1^{\infty}\frac{I_n(x)}{I_0(x)}\cos(nwt)\right] \tag{6-93}$$

$$I_{dc} = I_s e^{\frac{qV_{dc}}{kT}} I_0(x) \tag{6-94}$$

$$V_{dc} = \frac{kT}{q}\ln\left[\frac{I_{dc}}{I_s I_0(x)}\right] \Rightarrow \frac{kT}{q}\ln\left[\frac{I_{dc}}{I_s}\right] + \frac{kT}{q}\ln\left[\frac{1}{I_0(x)}\right] \tag{6-95}$$

I_s = collector saturation current

$$V_{dc} = V_{dcQ} - \frac{kT}{q}\ln I_0(x) \tag{6-96}$$

$$i_e(t) = I_{dc}\left[1 + 2\sum_1^{\infty}\frac{I_n(x)}{I_0(x)}\cos(nwt)\right] \tag{6-97}$$

V_{dcQ} and I_{dc} are the operating DC bias voltage and the DC value of the emitter current. Furthermore, the Fourier transform of $i_e(t)$, a current pulse or series of pulses in the time domain yields a number of frequency harmonics common in oscillator circuit designs using nonlinear devices.

The peak amplitude of the output current, the harmonic content defined as $\left[\frac{I_N(x)}{I_1(x)}\right]$, and the DC offset voltage are calculated analytically in terms of the drive level, as shown in Table 6-1. It gives good insight of the nonlinearities involved in the oscillator design.

Table 6-1 For T=300 K, data are generated at a different drive–level.

Drive level [x]	Drive-Voltage $[\frac{kT}{q}$*x] mV	Offset-Coefficient ln[I_0(x)]	DC-Offset $\frac{kT}{q}[\ln I_0(x)]$ mV	Fundamental Current 2[I_1(x)/I_0(x)]	Second-Harmonic [I_2(x)/I_1(x)]
0.00	0.000	0.000	0.000	0.000	0.000
0.50	13.00	0.062	1.612	0.485	0.124
1.00	26.00	0.236	6.136	0.893	0.240
2.00	52.00	0.823	21.398	1.396	0.433
3.00	78.00	1.585	41.210	1.620	0.568
4.00	104.00	2.425	63.050	1.737	0.658
5.00	130.00	3.305	85.800	1.787	0.719
6.00	156.00	4.208	206.180	1.825	0.762
7.00	182.00	5.127	330.980	1.851	0.794
8.00	208.00	6.058	459.600	1.870	0.819
9.00	234.00	6.997	181.922	1.885	0.835
10.00	260.00	7.943	206.518	1.897	0.854
15.00	390.00	12.736	331.136	1.932	0.902
20.00	520.00	17.590	457.340	1.949	0.926

From the table above, the peak current 2[I_1(x)/I_0(x)] in column 5 approaches 1.897I_{dc} for a drive level ratio x=10.

$$\text{for T=300K, } \frac{kT}{q} = 26mV \tag{6-98}$$

$$\text{and } V_1 = 260mV \text{ for x=10} \tag{6-99}$$

The second harmonic-distortion [63] $\frac{I_2(x)}{I_1(x)}$ is 85% for a normalized drive level of x=10 and the corresponding DC offset is 205.518mV. When referring to the amplitude, x is always meant as normalized to $\frac{kT}{q}$. Figure 6-10 is generated with the help of Math-

CAD, and shows the plot of the normalized fundamental and second harmonic current with respect to the drive level.

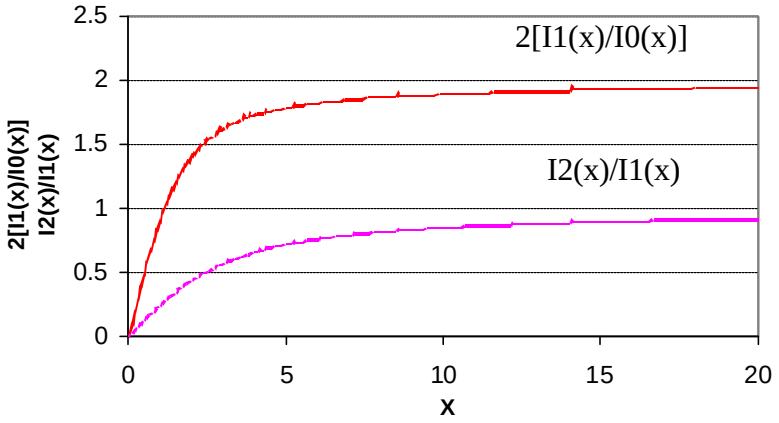

Figure 6-10 Plot of the normalized fundamental current $2I_1(x)/I_0(x)$ and second harmonic $I_2(x)/I_1(x)$ with respect to the drive level x.

One can notice that as the drive level x increases, the fundamental $2I_1(x)/I_0(x)$ and harmonic $I_2(x)/I_1(x)$ increases monotonically. Figure 6-11 shows the plot of the coefficient of offset $[\ln I_0(x)]$ with respect to drive level x so that the DC offset voltage can be calculated at different temperatures by simply multiplying the factor $\frac{kT}{q}$ [61].

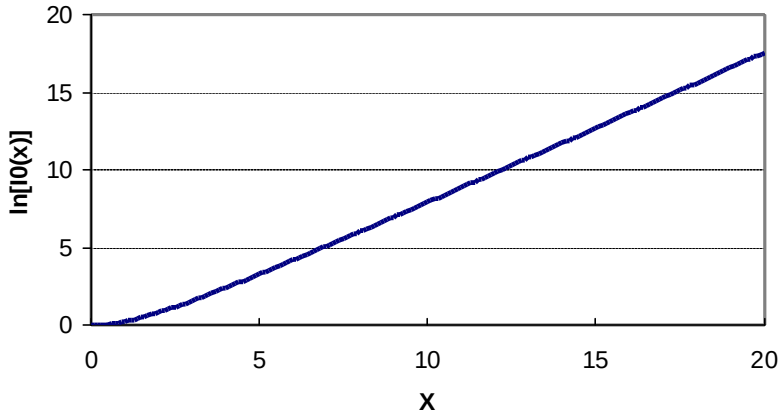

Figure 6-11 Plot of $[\ln I_0(x)]$ Vs drive level X.

At T= 300K the DC voltage shift is $-26[\ln I_0(x)]mV$

for x=10 (6-100)

$$V_{dc} = V_{dcQ} - \frac{kT}{q}\ln I_0(x) \tag{6-101}$$

$$V_{dc-offset} = \frac{kT}{q} \ln I_0(x) = 206mV \tag{6-102}$$

V_{dcQ} and $V_{dc-offset}$ are the operating bias points and DC offsets due to an increase in the drive level. The DC voltage shift at x=10 is 206mV. Figure 6-12 shows the shape of the output current with respect to the drive level and demonstrates that as the drive level increases, the output current pulse width becomes shorter and the peak current amplitude becomes greater.

$$i_e(t)\big|_{x=10} \to 0, \text{ For conduction angle } \geq 60^0 \tag{6-103}$$

$$i_e(t)\big|_{x=5} \to 0, \text{ For conduction angle } \geq 90^0 \tag{6-104}$$

$$i_e(t)\big|_{x=2} \to 0, \text{ For conduction angle } > 180^0 \tag{6-105}$$

The harmonic content trade-off is an important consideration in reducing the noise content by using shorter current pulses [64-67].

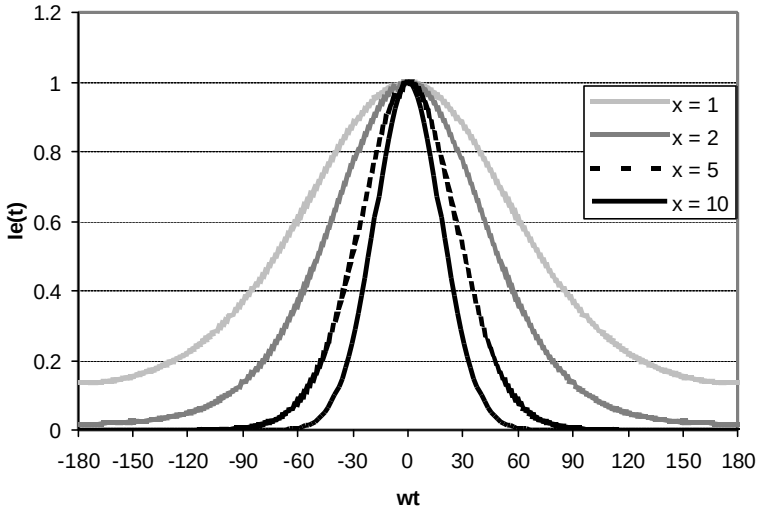

Figure 6-12 Plot of current with respect to conduction angle- (wt) and drive level X.

The designer has a limited control over the physical noise sources in a transistor. He can only control the device selection and the operating bias point. However, knowing the bias level, the designer is able to substantially improve the oscillator phase noise by reducing the duty cycle of the current pulses and in turn reducing the conduction angle of the current.

From the equation above, it can be seen that the emitter current $i_e(t) = I_s e^{\frac{qV_{dc}}{kT}} e^{x\cos(wt)}$ is proportional to $e^{x\cos(wt)}$ to any fixed drive value of x. The output current is normalized with respect to e^x for the purpose of plotting the graph. Figure 6-13 shows the dependence of the conduction angle with respect to the drive level over one cycle of the input drive signal $v_1 = V_1\cos(wt)$.

$$i_e(t) = I_s e^{\frac{qV_{dc}}{kT}} e^{\frac{qV_1\cos(wt)}{kT}} \tag{6-106}$$

$$v_1 = V_1\cos(wt), x = \frac{qV_1}{kT} \Rightarrow i_e(t) = I_s e^{\frac{qV_{dc}}{kT}} e^{x\cos(wt)} \tag{6-107}$$

$$i_e(t) \propto \frac{e^{x\cos(wt)}}{e^x} \tag{6-108}$$

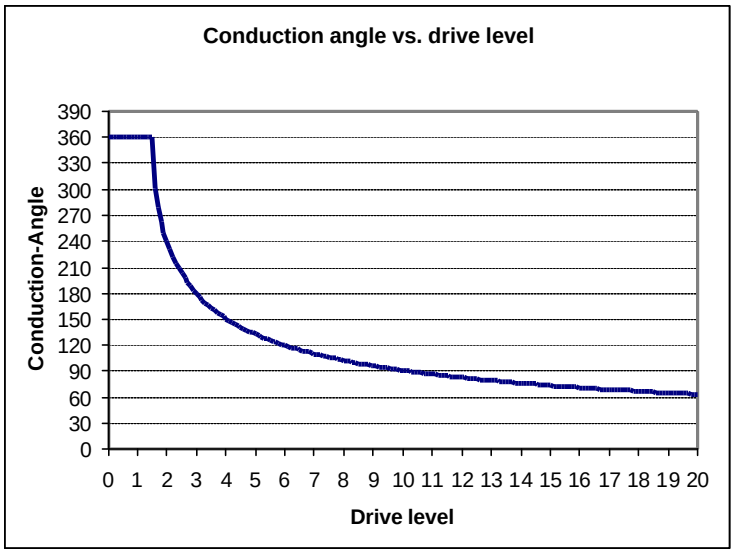

Figure 6-13 Plot of conduction angle vs. drive level

Note that for small values of x, the output current is almost a cosine function as expected. However, as the drive level x increases, the output current becomes pulse-like and most of the portion of the cycle is non-conducting; there will be only negligible current during the time between these current pulses. Therefore, aside from thermal noise, the noise sources that depend on the transistor on-current, such as shot noise, partition noise, and 1/f noise, exist only during the conducting angle of the output current pulses. The operation of the oscillator will cause the current pulse to be centered on the negative peak of the output voltage because of the 180° phase shift between base and collector. If the current pulse, and consequently the noise pulse, is wide, it will have a component which

contributes a substantial amount of phase noise. If the drive level is increased, the current/noise pulses will become narrower, and therefore, have less PM noise contribution than wider conduction angle-pulses. This is nicely seen in Figure 6-20.

Due to the exponential nature of $i_e(t)$, it is not possible to define a conduction angle for these pulses in a conventional sense, however, we may define a special conduction angle as the angular portion of the cycle for which $\frac{e^{x\cos(wt)}}{e^{x}} \geq 0.05$ for which a solution for φ is derived.

$$\frac{e^{x\cos(wt)}}{e^{x}} = 0.05 \tag{6-109}$$

$$f = wt \tag{6-110}$$

$$\frac{e^{x\cos j}}{e^{x}} = 0.05 \Rightarrow j = \cos^{-1}\left[1 + \frac{\ln(0.05)}{x}\right] \tag{6-111}$$

The plot of the conduction angle 2φ vs. drive level is shown in Figure 6-13. When the drive level increases above x = 2, the overall current wave shapes rapidly change from cosinusoidal to impulse-shaped and cause a DC bias shift. This effectively aids the signal by shutting the base-emitter junction off for a good portion of the cycle, and thereby makes the conduction angle of the output current narrower. This analysis is valid for the intrinsic transistor. In practice all parasitics need to be considered.

Figure 6-14 is the oscillator circuit for the calculation of start-up and sustained condition.

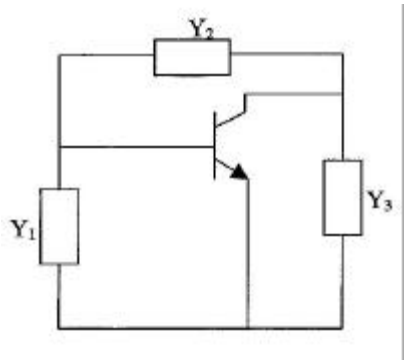

$$Y_1 = G_1 + jB_1$$
$$Y_2 = G_2 + jB_2$$
and $$Y_3 = G_3 + jB_3$$

Figure 6-14 General topology of oscillator.

The bipolar transistor is represented by a current source and an input conductance at the emitter for easier analysis of the reactance transformation. For easier calculation of the capacitive transformation factor n, the oscillator circuit is rearranged as shown in Figure 6-15 [68].

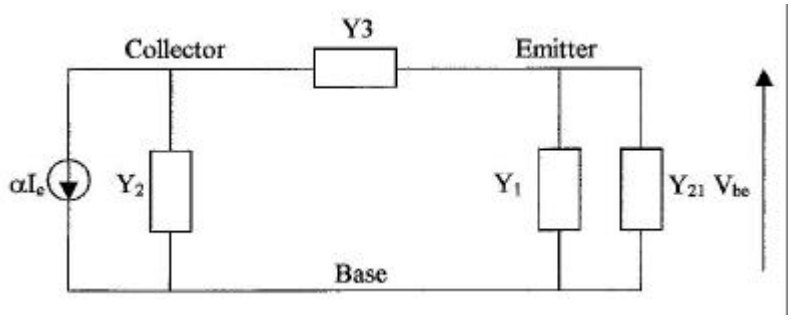

Figure 6-15 Equivalent oscillator circuit for the analysis of the transformed conductance seen by the current source.

αI_e and Y_{21} are the current source and large-signal transconductance of the device given by the ratio of the fundamental-frequency component of the current to the fundamental-frequency of the drive voltage.

$$Y_{21} = \left.\frac{I_{1peak}}{V_{1peak}}\right|_{fundamental-frequency} \tag{6-112}$$

$$I_1\big|_{n=1} = I_{dc}\left[1 + 2\sum_{1}^{\infty}\frac{I_1(x)}{I_0(x)}\cos(wt)\right] \Rightarrow I_{1peak} = 2I_{dc}\frac{I_1(x)}{I_0(x)} \tag{6-113}$$

x = normalized drive level from (6-87)

$$V_1\big|_{peak} = \frac{kT}{q}x \tag{6-114}$$

$$Y_{21}\big|_{large-signal} = G_m(x) \tag{6-115}$$

$$Y_{21}\big|_{small-signal} = \left.\frac{I_{dc}}{kT/q}\right| = g_m \tag{6-116}$$

$$Y_{21}\big|_{large-signal} = G_m(x) = \frac{qI_{dc}}{kTx}\left[\frac{2I_1(x)}{I_0(x)}\right]_{n=1} = \frac{g_m}{x}\left[\frac{2I_1(x)}{I_0(x)}\right]_{n=1} \tag{6-117}$$

$$\frac{[Y_{21}|_{large-signal}]_{n=1}}{[Y_{21}|_{small-signal}]_{n=1}} = \frac{G_m(x)}{g_m} \Rightarrow \frac{2I_1(x)}{xI_0(x)} \tag{6-118}$$

$$|Y_{21}|_{small-signal} > |Y_{21}|_{large-signal} \Rightarrow g_m > G_m(x) \tag{6-119}$$

The ratio of the large-signal and small-signal transconductance as a function of drive level is given in the Table 6-2, and its graph is plotted in Figure 6-16.

Table 6-2 Plot of $G_m(x)/g_m=2[I_1(x)/xI_0(x)]$ vs. the drive level=x.

Drive level :x	$G_m(x)/g_m=2[I_1(x)/xI_0(x)]$
0.00	1
0.50	0.970
1.00	0.893
2.00	0.698
3.00	0.540
4.00	0.432
5.00	0.357
6.00	0.304
7.00	0.264
8.00	0.233
9.00	0.209
10.00	0.190
15.00	0.129
20.00	0.0975

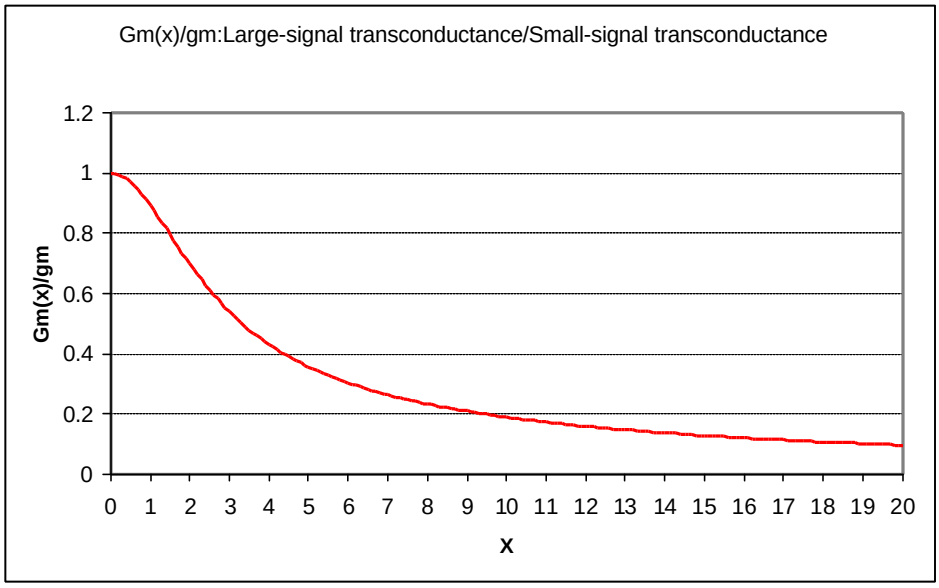

Figure 6-16 Plot of $G_m(x)/g_m=2[I_1(x)/xI_0(x)]$ vs. drive level =x.

The voltage division for transformation purpose is computed with respect to V_{cb} (voltage from collector to base) because the current source is connected from the collector to the base. The quality factor of the tuned circuit is assumed to be reasonably high for the calculation of the impedance transformation, and finally the current source, which is connected from collector to base, will see a total conductance G_{total}. The oscillator circuit with passive component parameters is shown in Figure 6-17.

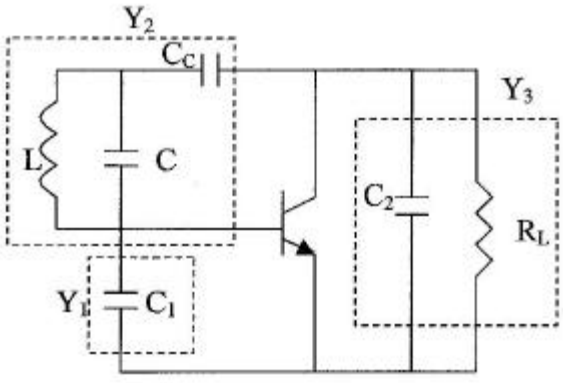

Figure 6-17 Oscillator circuit with the passive components Y_1, Y_2, and Y_3. The equivalent circuit is shown in Figure 8-12.

where

$$Y_1 = G_1 + jB_1 \Rightarrow jwC_1 \text{ For } G_1 = 0 \tag{6-120}$$

$$Y_2 = G_2 + jB_2 \Rightarrow G_2 + j\left[\frac{(w^2LC-1)wC_c}{w^2L(C_c+C)-1}\right];$$

G_2 = loss parameter/load conductance of the resonator connected parallel to the resonator component C_1, C_2 and L, respectively.

$$Y_3 = G_3 + jB_3 \Rightarrow G_3 + jwC_2;$$

G_3 = conductance of the bias resistor placed across C_2, $1/R_L$ in Figure 6-17.

The large-signal transconductances Y_{21} and G_1 are transformed to the current source through the voltage divider $\frac{V_{eb}}{V_{cb}}$. The voltage V_{eb} must be added to V_{ce} to calculate the transformation ratio, which can be written as

$$\frac{V_{eb}}{V_{cb}} = \frac{C_2}{C_1 + C_2} = \frac{1}{n} \tag{6-121}$$

and

$$\frac{V_{ce}}{V_{cb}} = \frac{C_1}{C_1 + C_2} = \frac{n-1}{n} \tag{6-122}$$

The conductance G_2 is already in parallel with the current source so it remains unchanged. The factor n represents the ratio of the collector-base voltage to the emitter-base voltage at the oscillator resonance frequency.

$$G_1 \rightarrow \frac{G_1}{n^2} \tag{6-123}$$

$$Y_{21} \rightarrow \frac{Y_{21}}{n^2} \Rightarrow \frac{G_m}{n^2} \tag{6-124}$$

$$G_3 \rightarrow \left[\frac{n-1}{n}\right]^2 G_3 \tag{6-125}$$

G_2 remains constant

The transformed conductance is proportional to the square of the voltage ratios given in Eq. 6-121 and Eq. 6-122, producing a total conductance as seen by the current source at resonance as

$$G_{total} = G_2 + \frac{G_m + G_1}{n^2} + \left[\frac{n-1}{n}\right]^2 G_3 \tag{6-126}$$

For sustained oscillation, the closed loop gain at resonance is given as

$$\left[\frac{\left(\frac{V_{be} Y_{21} a}{n G_{total}}\right)}{V_{be}}\right] = 1 \Rightarrow n G_{total} = Y_{21} a \tag{6-127}$$

$$\frac{Y_{21}}{n G_{total}} = \frac{1}{a} \Rightarrow \frac{Y_{21}}{n G_{total}} > 1 \tag{6-128}$$

a is assumed to be 0.98 and variation in the value of a, does not influence the expression above greatly. Rearranging the device conductance and circuit conductance, the general oscillator equation, after multiplying (6-126) with n on both sides, is written as

$$nG_{total} = n\left[G_2 + \frac{Y_{21} + G_1}{n^2} + \left(\frac{n-1}{n}\right)^2 G_3\right] \tag{6-129}$$

$$Y_{21}a = n\left[G_2 + \frac{Y_{21} + G_1}{n^2} + \left(\frac{n-1}{n}\right)^2 G_3\right] \Rightarrow \left[\frac{-(1-na)}{n^2}\right]Y_{21} = \left[G_2 + \frac{G_1}{n^2} + \left(\frac{n-1}{n}\right)^2 G_3\right] \tag{6-130}$$

$$n^2(G_2 + G_3) - n(2G_3 + Y_{21}a) + (G_1 + G_3 + Y_{21}) = 0 \tag{6-131}$$

$$n = \frac{(2G_3 + Y_{21}a) \pm \sqrt{(2G_3 + Y_{21}a)^2 - 4(G_2 + G_3)(G_1 + G_3 + Y_{21})}}{2(G_2 + G_3)} \tag{6-132}$$

$$n_1 = \frac{(2G_3 + Y_{21}a)}{2(G_2 + G_3)} + \frac{\sqrt{(2G_3 + Y_{21}a)^2 - 4(G_2 + G_3)(G_1 + G_3 + Y_{21})}}{2(G_2 + G_3)} \tag{6-133}$$

$$n_2 = \frac{(2G_3 + Y_{21}a)}{2(G_2 + G_3)} - \frac{\sqrt{(2G_3 + Y_{21}a)^2 - 4(G_2 + G_3)(G_1 + G_3 + Y_{21})}}{2(G_2 + G_3)} \tag{6-134}$$

From the quadratic equation above, the value of the factor n can be calculated, and thereby, an estimation of the capacitance can be done a priori. To ensure higher loop gain, n_1 is selected from n[n_1, n_2]**.**

Once the value of n is fixed, then the ratio of the capacitance is calculated as

$$\frac{C_2}{C_1 + C_2} = \frac{1}{n} \tag{6-135}$$

$$C_2 = \frac{C_1}{n-1} \Rightarrow \frac{C_1}{C_2} = n - 1 \tag{6-136}$$

If G_3 and G_1 are zero then the above quadratic equation is reduced to

$$n^2 G_2 - nY_{21}a + Y_{21} = 0 \tag{6-137}$$

$$Y_{21} \cong \frac{n^2}{1-n} G_2 \Rightarrow Y_{21} = \left[\frac{n^2}{1-n}\right]\frac{1}{R_P} \tag{6-138}$$

$$\frac{Y_{21}R_P}{n} = \frac{n}{1-n} \tag{6-139}$$

$$R_P = \frac{1}{G_2}$$

$$\frac{Y_{21}R_P}{n} \rightarrow Loop\ Gain \tag{6-140}$$

$$Loop\ Gain\ \ \frac{Y_{21}R_P}{n} \rightarrow 1 \tag{6-141}$$

From equation (6-135) and (6-138)

$$Y_{21} \Rightarrow G_m(x) = \frac{1}{R_P}\frac{[C_1 + C_2]^2}{C_1 C_2} \tag{6-142}$$

For a relatively optimum phase noise, the drive level has to be adjusted in such a way that the output current pulse is conducting for a short period without appreciably increasing the harmonic content. Section 8 will show the absolute best phase noise operating point.

From equation (6-117) follows

$$Y_{21}\Big|_{large-signal} = G_m(x) = \frac{qI_{dc}}{kTx}\left[\frac{2I_1(x)}{I_0(x)}\right]_{n=1} = \frac{g_m}{x}\left[\frac{2I_1(x)}{I_0(x)}\right]_{n=1} \tag{6-143}$$

From equation (6-142)

$$G_m(x) = \frac{1}{R_P}\frac{[C_1 + C_2]^2}{C_1 C_2} \tag{6-144}$$

From equation (6-143) and (6-144)

$$\frac{g_m}{x}\left[\frac{2I_1(x)}{I_0(x)}\right]_{n=1} = \frac{1}{R_P}\frac{[C_1 + C_2]^2}{C_1 C_2} = \frac{1}{R_P}\frac{C_1}{C_2}\left[1 + \frac{C_2}{C_1}\right]^2 \tag{6-145}$$

$$\frac{C_1}{C_2}\left[1 + \frac{C_2}{C_1}\right]^2 = \frac{R_P g_m}{x}\left[\frac{2I_1(x)}{I_0(x)}\right]_{n=1} \tag{6-146}$$

From equation (6-119)

$$\frac{R_P g_m}{x}\left[\frac{2I_1(x)}{I_0(x)}\right]_{n=1} \le \frac{C_1}{C_2}\left[1+\frac{C_2}{C_1}\right]^2 \le R_P g_m \tag{6-147}$$

$$x = \frac{g_m\left[\frac{2I_1(x)}{I_0(x)}\right]_{n=1}}{\left(\frac{1}{R_P}\frac{C_1}{C_2}\right)\left(1+\frac{C_2}{C_1}\right)^2} \tag{6-148}$$

The value of $\left[\frac{2I_1(x)}{I_0(x)}\right]_{n=1}$ increases monotonically as the drive level x increases, and for large values of x and $C_2 < C_1$, $n>1$, the dependency of x can be expressed as

$$x = \frac{R_P G_m C_2}{C_1} \tag{6-149}$$

For large drive level, $x \propto C_2$, and the corresponding conduction angle of output current is given as

$$j = \cos^{-1}\left[1+\frac{\ln(0.05)}{x}\right] \Rightarrow j \approx \cos^{-1}\left[1-\frac{3}{x}\right] \tag{6-150}$$

$$j = \cos^{-1}\left[1-\frac{C_1}{3R_P G_m C_2}\right] \tag{6-151}$$

$$j \propto \frac{1}{C_2} \tag{6-152}$$

$$x \propto C_2 \tag{6-153}$$

Normally, the value of C_1 is kept fixed to avoid loading by the transistor. By increasing the value of C_2, the conduction angle can be reduced, thereby shortening the output current pulse. Any change in designed frequency, due to the variation of C_2, can be compensated by changing the value of the resonator inductance without much change of the value of the drive level x.

The following shows an example for a 100 MHz and a 1 GHz oscillator circuit for different normalized drive levels x. This is provided to give some insight into the relationship between the drive level, the current pulse, and the phase noise.

Figure 6-18 shows the circuit diagram of a 100 MHz Colpitts oscillator with a load of 500Ω. The reason for selecting 100 MHz is because the transistor parasitics do not play a major role at such a low frequency. For this example, a NEC 85630 transistor has been selected. The emitter to ground capacitor determines the normalized drive level x. As the drive level x produces narrow pulses, the phase noise improves. This can be seen n Figure 6-19.

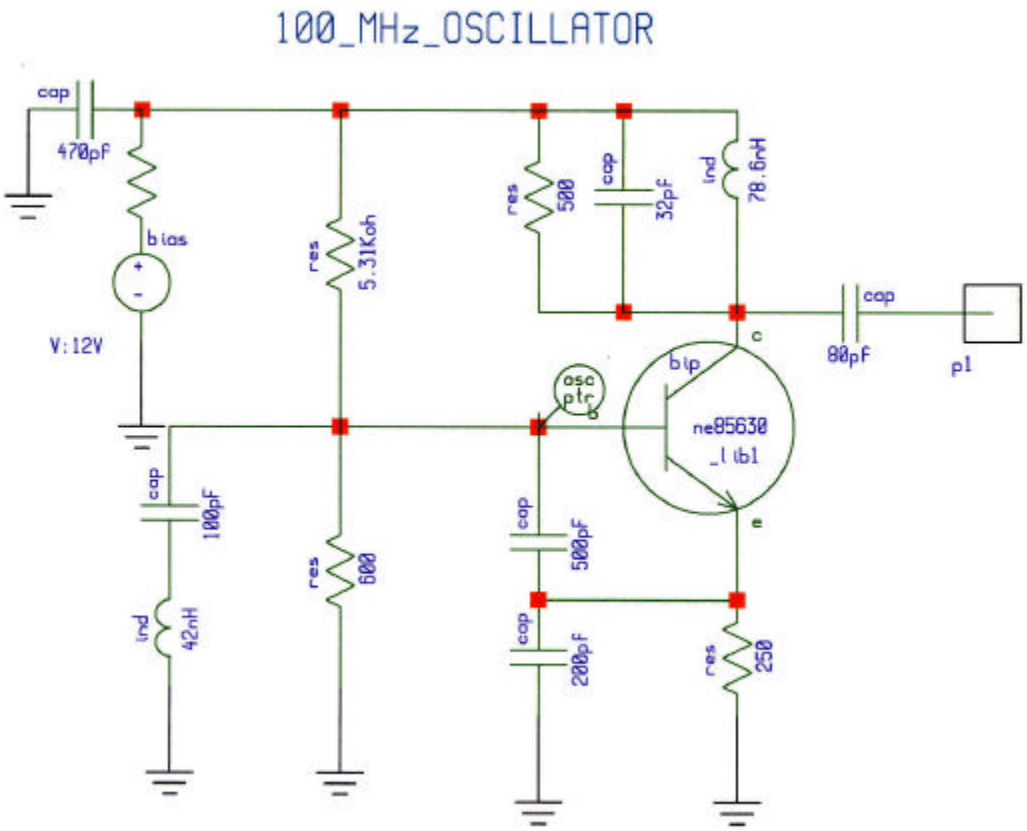

Figure 6-18 Schematic of a 100 MHz reference oscillator.

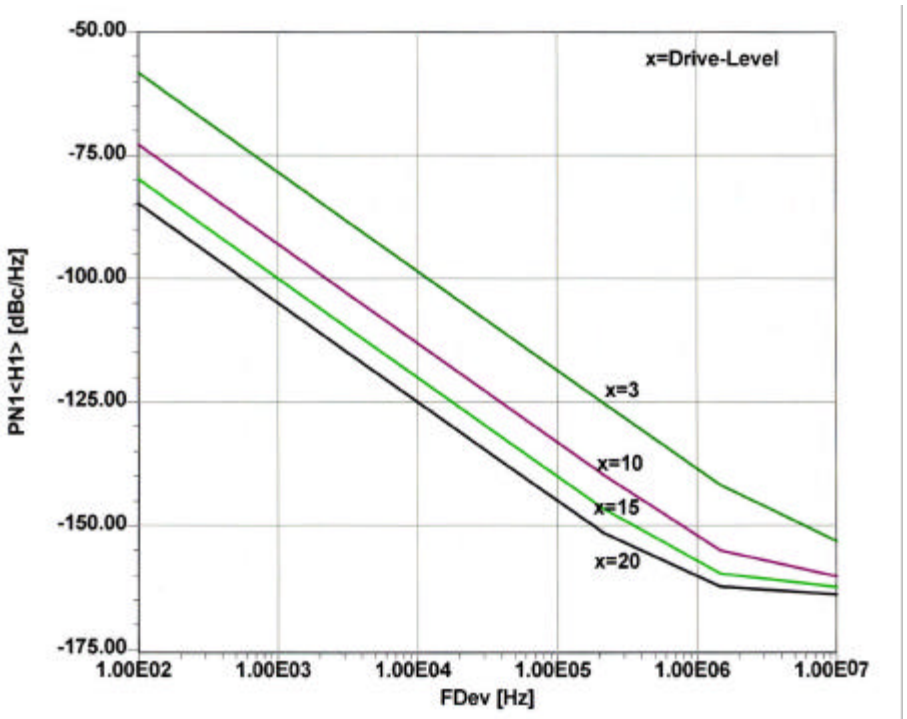

Figure 6-19 Single sideband phase noise as a function of the normalized drive level x.

The collector current plotted in Figure 20 becomes more narrow as the normalized drive level x moves towards x = 20. At the same time, the base-emitter voltage swing increases. This is plotted in Figure 6-21.

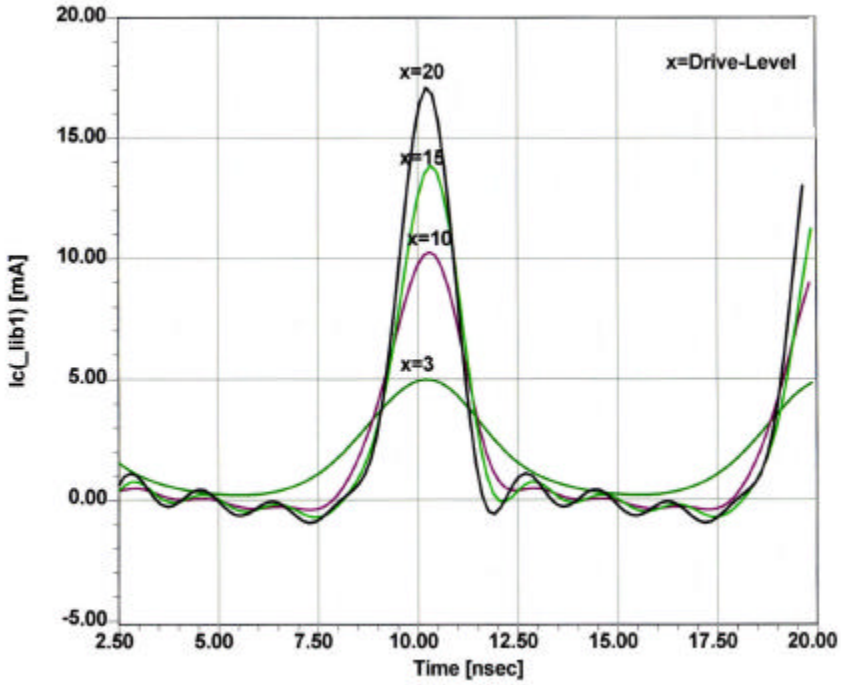

Figure 6-20 Shows the collector current pulses of the 100 MHz oscillator.

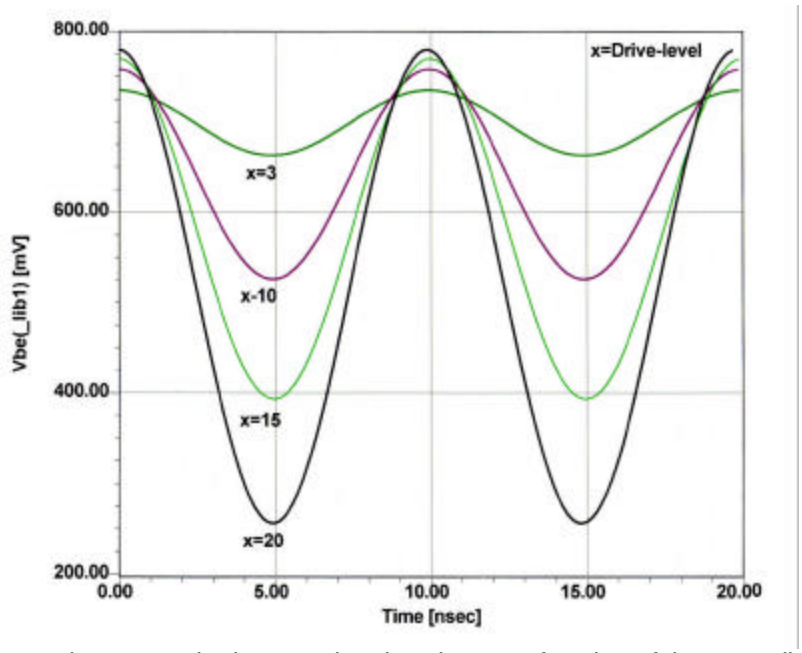

Figure 6-21 RF voltage Vbe across the base-emitter junction as a function of the normalized drive level x.

Now, moving to the 1000 MHz oscillator and using the BFP520, which has a much higher cut-off frequency, we will evaluate the same conditions. Figure 6-22 shows the 1000 MHz oscillator and Figure 6-23 shows the collector pulses as a function of the normalized drive.

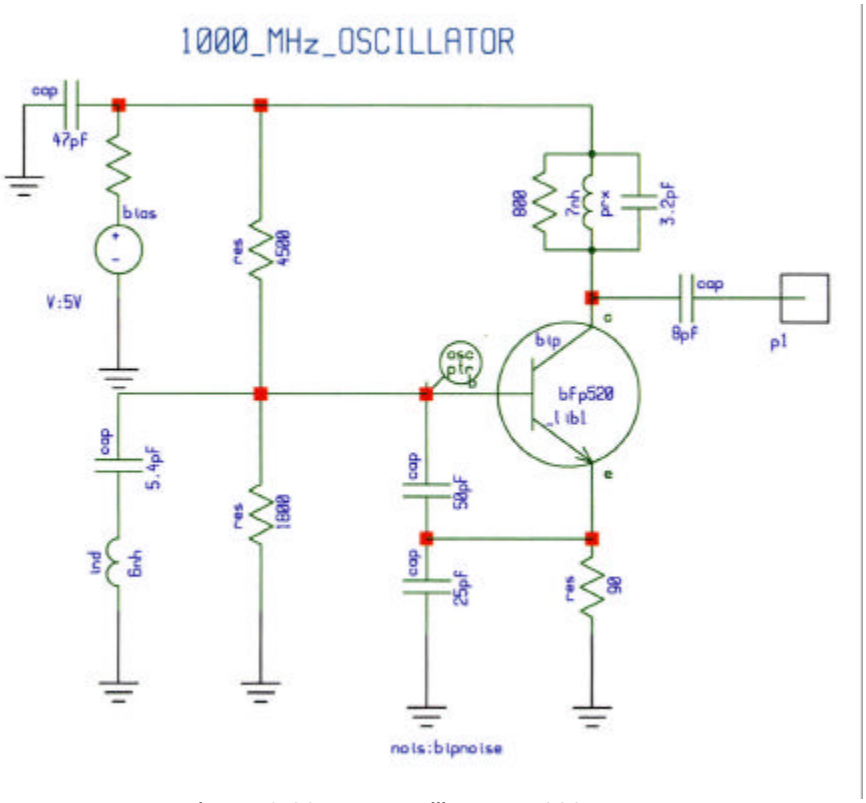

Figure 6-22 Test oscillator at 1000 MHz.

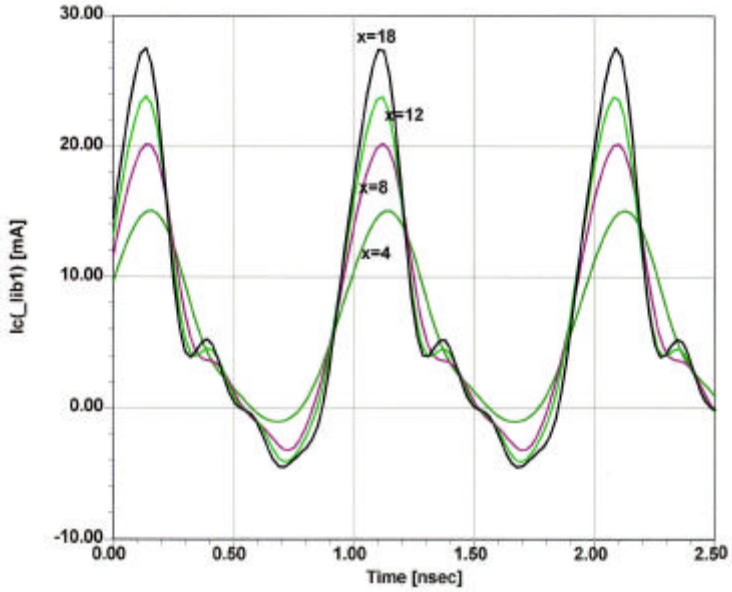

Figure 6-23 Collector current pulses as a function of the normalized drive level x.

There already is some ringing at the negative current of the collector. The base-emitter voltage, based on the tuned circuit, remains less distorted as shown in Figure 6-24. The change of phase noise in this case for close-in phase noise, is no longer that dramatic, but at frequencies above 100 kHz from the carrier, there is a big difference in the phase noise. This can be observed in Figure 6-25.

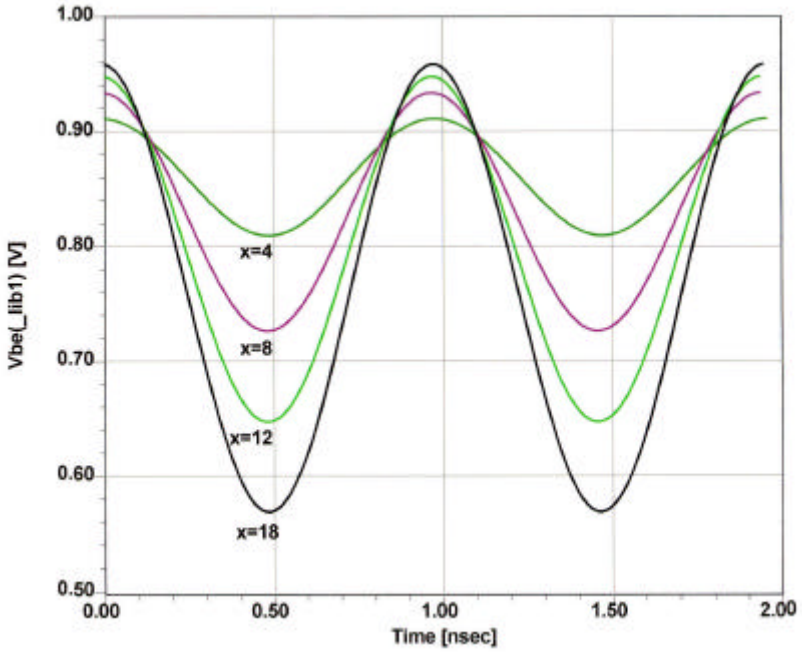

Figure 6-24 Shows the base emitter RF voltage of the normalized drive level x.

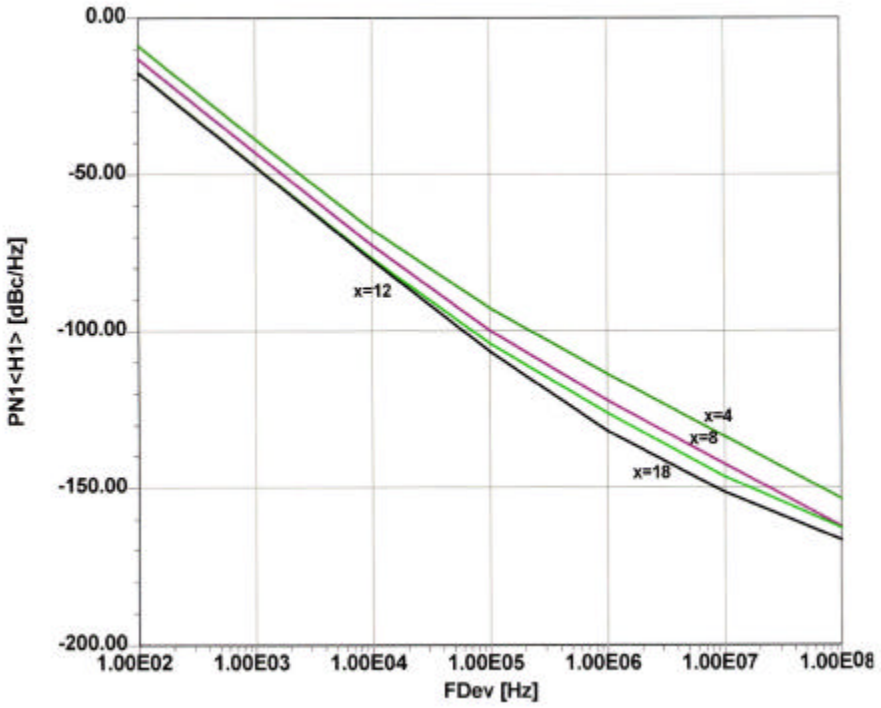

Figure 6-25 Simulated SSB phase noise as a function of the normalized drive level x.

Tables 6-3 and 6-4 show the drive level for different values of C_2 for a 100 MHz and 1000 MHz oscillator.

Table 6-3 Drive level for different values of C_2 for a 100MHz Oscillator.

Drive level: x	C_1	C_2	L	Phase Noise @10KHz offset	Frequency
3	500pF	50pF	80nH	-98dBc/Hz	100MHz
10	500pF	100pF	55nH	-113dBc/Hz	100MHz
15	500pF	150pF	47nH	-125dBc/Hz	100MHz
20	500pF	200pF	42nH	-125dBc/Hz	100MHz

Table 6-4 Drive level for different values of C_2 for a 1000 MHz Oscillator.

Drive level: x	C_1	C_2	C_c	L	Phase Noise @10KHz offset	Frequency
4	50pF	5pF	10pF	6nH	-68dBc/Hz	1000MHz
8	50pF	10pF	6.5pF	6nH	-72dBc/Hz	1000MHz
12	50pF	15pF	5.7pF	6nH	-75dBc/Hz	1000MHz
18	50pF	20pF	5.4pF	6nH	-77dBc/Hz	1000MHz

Now, a further look at the phase noise will be performed. Figure 6-26 shows the plot of the output current of the 100 MHz oscillator circuit for x=15. The ringing of the current at the off-portion of the device is due to the device parasitic.

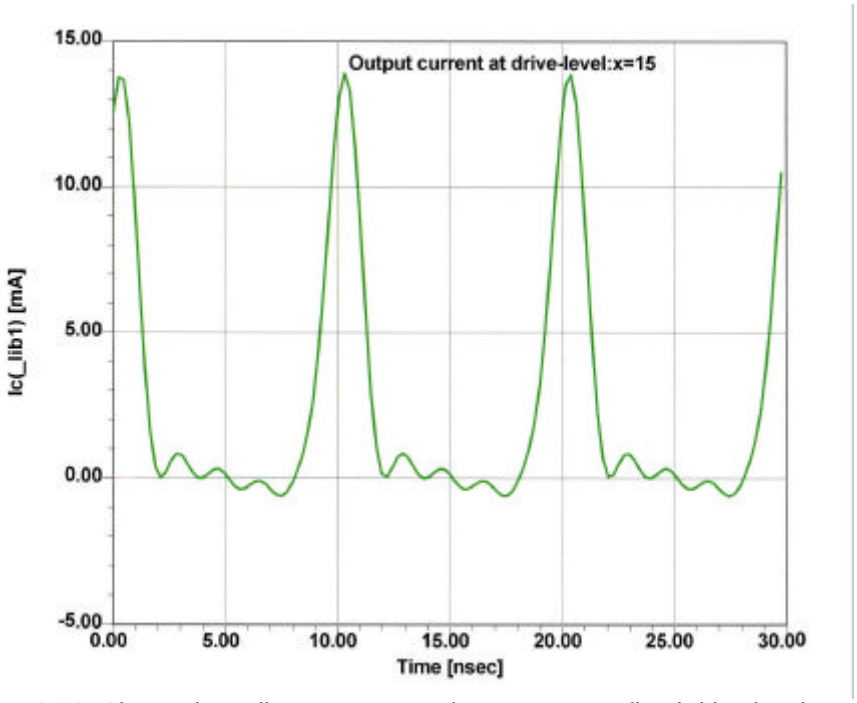

Figure 6-26 Shows the collector current pulses at a normalized drive level x=15.

Figure 6-27 shows the same oscillator circuit frequency scaled to 10 MHz and Figure 6-28 at 1000 MHz to verify the parasitic and packaging effect at higher frequency. At low frequencies, the device parasitics do not have much influence compared to higher frequencies. The noise current for the 10 MHz oscillator during off-cycle has little variation and more or less is the same throughout the off-window. The noise currents for the 100 MHz and 1000 MHz oscillators during the off cycle have a large variation in magnitude and the variation is more predominant at 1000 MHz. The root cause of the phase noise lies in the noise sources of the active device used in the oscillator. Shot noise, burst noise, thermal noise, and 1/f noise are the major transistor noise sources, and all of these noise sources, except thermal noise, exist only when there is current in the device. It can be controlled up to some extent by adjusting the duty cycle of the current. The basic process responsible for oscillation is due to feedback, and uses a resonant circuit in which a series of periodic current pulses charge the tuned circuit. Between each charging pulse, the bipolar transistor conducts zero current and is considered off. The phase noise is produced depending on the shape of the current pulse when the transistor is on. If the current is a relatively narrow pulse, existing for a very short time, there will be less phase noise produced than from a wider pulse.

The simulated results support Lee and Hajimiri's theory [64-67], which states that narrowing the current pulse width will decrease phase noise. It is important to understand

that the optimum drive level will generate higher harmonics and the device may go into saturation, which will degrade the phase noise performance. Lee and Hajimiri's theory [64-67] does not emphasize the optimum phase noise at a given power output which is a strong function of ratio and absolute value of the feedback capacitors at given drive level and resonator Q. Appendix B shows a numerical example.

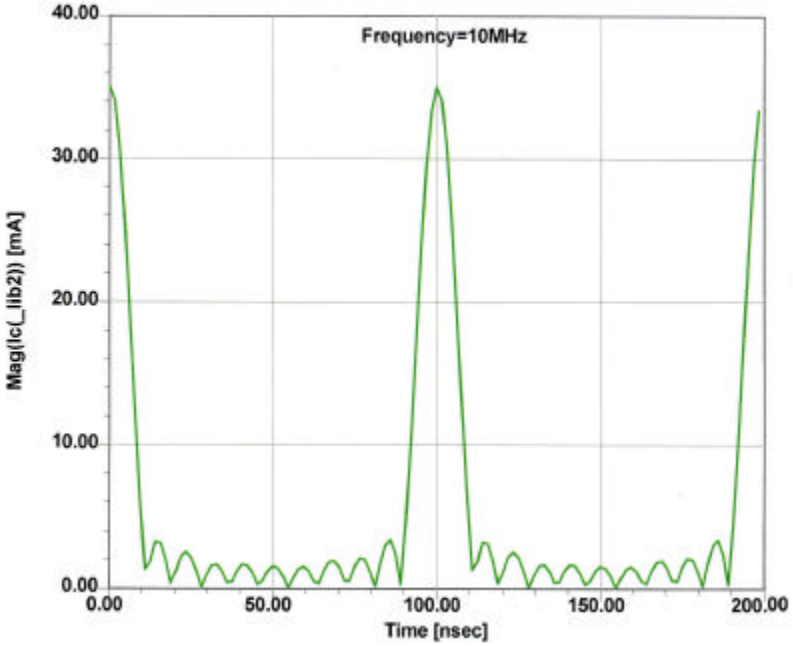

Figure 6-27 Collector current for a 10 MHz LC oscillator at a normalized drive level x=15. The ringing shown is due to the harmonic content.

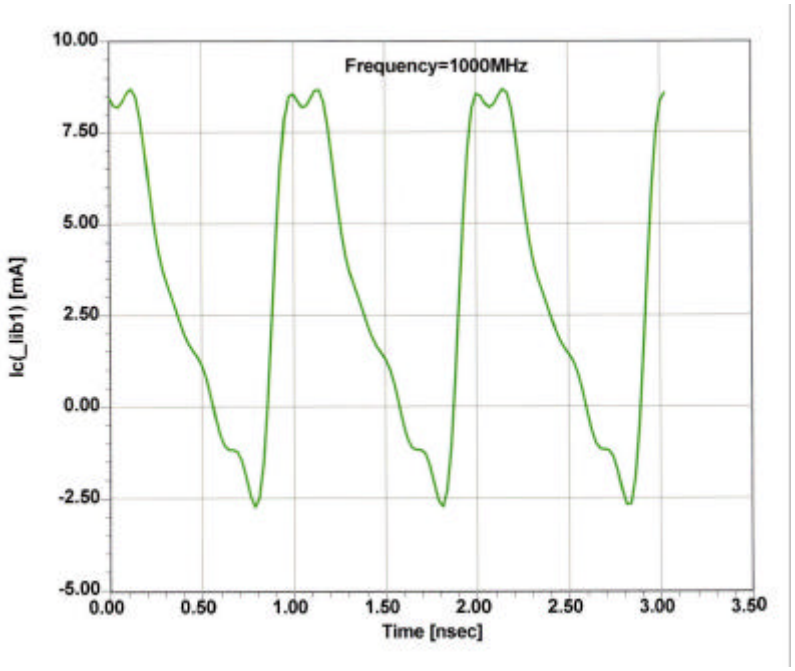

Figure 6-28 Collector current at a normalized drive level x=15. At the peak values, the third harmonic becomes a contributing factor (a dip in the curve) and there is a negative collector current.

7 Noise in Oscillators

Section 6 and Appendix A derive all the necessary equations that are needed to design power-optimized microwave oscillators. While the concept of noise was already mentioned before, oscillator noise theory will be dealt with here and the design for best phase noise will be derived. The noise in an oscillator is determined by the noise (losses) of the resonator and the noise contributions of the active device. The noise of the transistor comes from several sources, and the derivation of the noise theory is found in Appendices B, C, and D. In the English language, frequently, there is no clear difference between the noise figure in logarithm terms and absolute terms. The noise figure is defined as

$$\mathrm{NF} = 10 \times \log(\mathrm{F})$$

The equations in the appendix, therefore, correctly refer to the noise factor, F, instead of the noise figure NF as typically quoted.

The best signal-to-noise ratio a system can have is the available output power (in dBm) divided by the noise floor (also in dBm). The resulting noise figure is a strong function of the source impedance, which differs from the optimal noise impedance. The optimum noise source calculation is also provided in Appendix D. While the oscillator is a nonlinear circuit, noise theory is assumed to be linear. This means that the noise mechanism in an oscillator has to be treated under steady-state conditions, at points of the RF current and voltage waveforms. There will be an average noise figure as a result of this. Computation of the noise in a system such as an oscillator is best done using the noise correlation matrix approach. Since the noise itself consists of small currents and voltages, one can begin to describe the noise of an oscillator using the linear approach.

7.1 Linear Approach to the Calculation of Oscillator Phase Noise

Since an oscillator can be viewed as an amplifier with feedback as shown in Figure 2-1, it is helpful to examine the phase noise added to an amplifier that has a noise factor *F*. With *F* defined as

$$F = \frac{(S/N)_{\mathrm{in}}}{(S/N)_{\mathrm{out}}} = \frac{N_{\mathrm{out}}}{N_{\mathrm{in}} G} = \frac{N_{\mathrm{out}}}{GkTB} \tag{7-1}$$

$$N_{\mathrm{out}} = FGkTB \tag{7-2}$$

$$N_{\mathrm{in}} = kTB \tag{7-3}$$

where N_{in} is the total input noise power to a noise-free amplifier. The input phase noise in a 1 Hz bandwidth at any frequency $f_0 + f_m$ from the carrier produces a phase deviation given by Figure 7-2.

$$\Delta q_{1\text{peak}} = \frac{V_{\text{nRMS1}}}{V_{\text{savRMS}}} = \sqrt{\frac{FkT}{P_{\text{sav}}}} \tag{7-4}$$

$$\Delta q_{\text{RMS}} = \frac{1}{\sqrt{2}}\sqrt{\frac{FkT}{P_{\text{sav}}}} \tag{7-5}$$

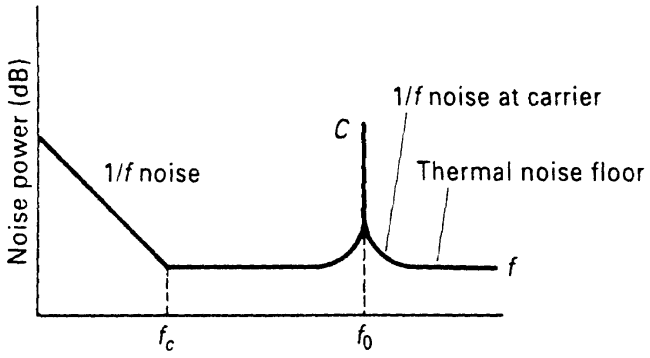

Figure 7-1 Noise power versus frequency of a transistor amplifier with an input signal applied.

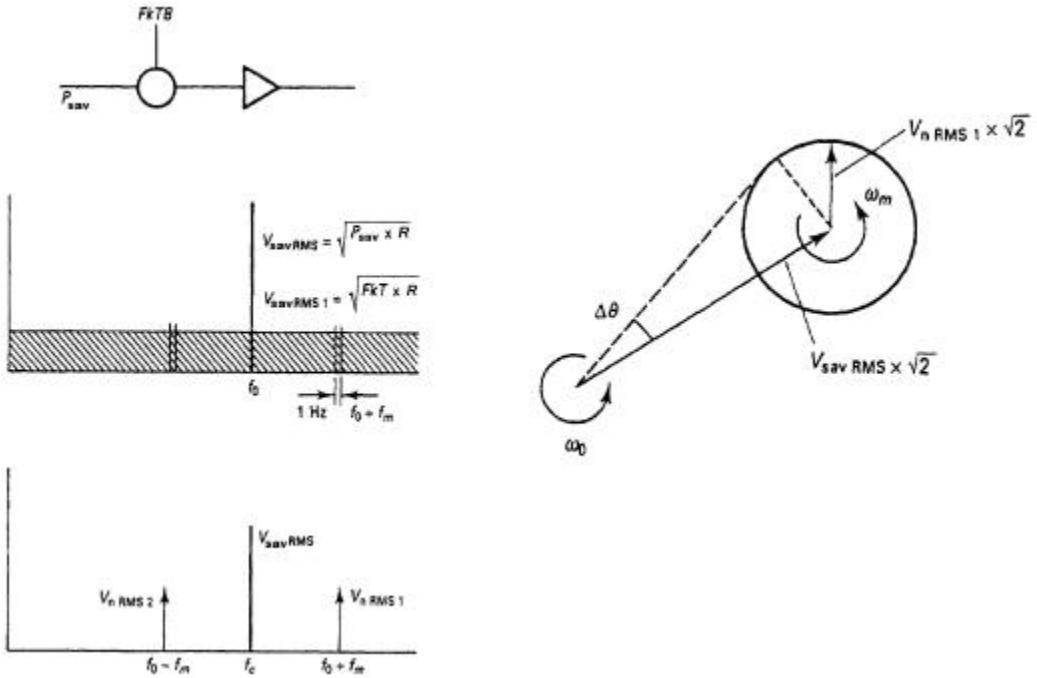

Figure 7-2 Phase noise added to the carrier.

Leeson's Approach

Since a correlated random phase noise relation exists at $f_0 - f_m$, the total phase deviation becomes

$$\Delta q_{\text{RMStotal}} = \sqrt{FkT / P_{sav}} \qquad \text{(SSB)} \tag{7-6}$$

The spectral density of phase noise becomes

$$S_q(f_m) = \Delta q^2_{\text{RMS}} = FkTB / P_{\text{sav}} \tag{7-7}$$

where $B = 1$ for a 1 Hz bandwidth. Using

$$kTB = -174\,\text{dBm} \qquad (B = 1\text{ Hz},\ T = 300\text{K}) \tag{7-8}$$

allows a calculation of the spectral density of phase noise that is far away from the carrier (that is, at large values of f_m). This noise is the theoretical noise floor of the amplifier. For example, an amplifier with +10 dBm power at the input and a noise figure of 6 dB gives

$$S_q(f_m > f_c) = -174\,\text{dBm} + 6\,\text{dB} - 10\,\text{dBm} = -178\,\text{dBm} \tag{7-9}$$

Only if P_{out} is > 0 dBm can we expect $\mathcal{L}$ (signal-to-noise ratio) to be greater than 174 dBc/Hz (1 Hz bandwidth.) For a modulation frequency close to the carrier, S_q (f_m) shows a flicker or 1/f component, which is empirically described by the corner frequency f_c. The phase noise can be modeled by a noise-free amplifier and a phase modulator at the input as shown in Figure 7-3.

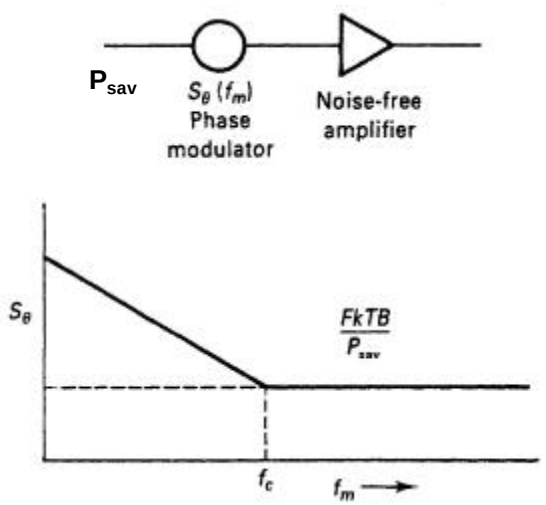

Figure 7-3 Phase noise modeled by a noise free amplifier and phase modulator.

The purity of the signal is degraded by the flicker noise at frequencies close to the carrier. The phase noise can be described by

$$S_q(f_m) = \frac{FkTB}{P_{\text{sav}}}\left(1 + \frac{f_c}{f_m}\right) \qquad (B = 1) \qquad (7\text{-}10)$$

No AM-to-PM conversion is considered in this equation. The oscillator may be modeled as an amplifier with feedback as shown in Figure 7-4.

The phase noise at the input of the amplifier is affected by the bandwidth of the resonator in the oscillator circuit in the following way. The tank circuit or bandpass resonator has a low pass transfer function

$$L(w_m) = \frac{1}{1 + j(2Q_L w_m / w_0)} \qquad (7\text{-}11)$$

where

$$w_0 / 2Q_L = 2p\ B/2 \qquad (7\text{-}12)$$

is the half bandwidth of the resonator. These equations describe the amplitude response of the bandpass resonator; the phase noise is transferred unattenuated through the resonator up to the half bandwidth [70-72].

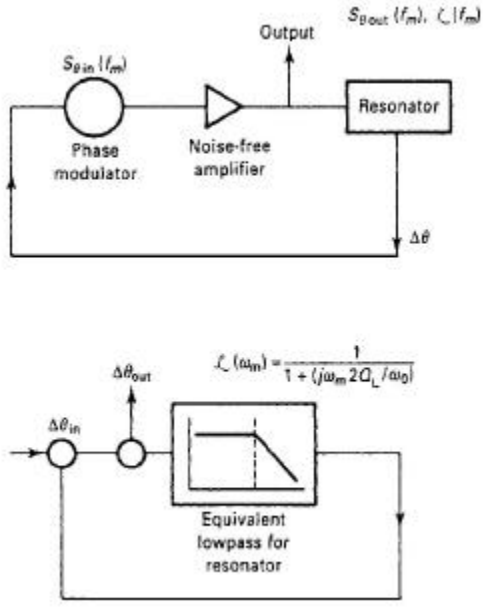

Figure 7-4 Equivalent feedback models of oscillator phase noise.

The closed loop response of the phase feedback loop is given by

$$\Delta q_{\text{out}}(f_m) = \left(1 + \frac{w_0}{j2Q_L w_m}\right)\Delta q_{\text{in}}(f_m) \tag{7-13}$$

The power transfer becomes the phase spectral density

$$S_{q\ \text{out}}(f_m) = \left[1 + \frac{1}{f_m^2}\left(\frac{f_0}{2Q_L}\right)^2\right] S_{q\ \text{in}}(f_m) \tag{7-14}$$

where $S_{q\ \text{in}}$ was given by Eq. (7-10). Finally, £(f_m), which is the single sideband phase noise $\left(\frac{1}{2}\right)$

$$\mathcal{L}(f_m) = \frac{1}{2}\left[1 + \frac{1}{f_m^2}\left(\frac{f_0}{2Q_L}\right)^2\right] S_{\theta\,\text{in}}(f_m) \tag{7-15}$$

This equation describes the phase noise at the output of the amplifier (flicker corner frequency and AM-to-PM conversion are not considered). The phase perturbation $S_{?\text{in}}$ at the input of the amplifier is enhanced by the positive phase feedback within the half bandwidth of the resonator, $f_0/2Q_L$.

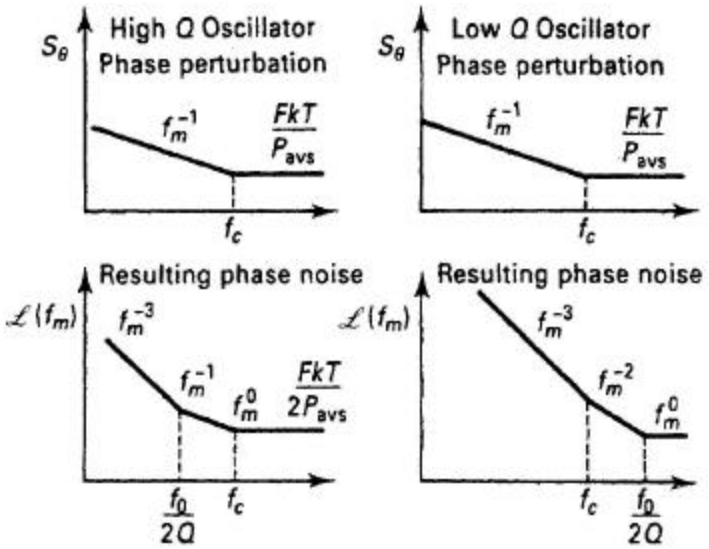

Figure 7-5 Equivalent feedback models of oscillator phase noise.

Depending on the relation between f_c and $f_0/2Q_L$, there are two cases of interest, as shown in Figure 7-5. For the low Q case, the spectral phase noise is unaffected by the Q of the resonator, but the £ (f_m) spectral density will show a $1/f^3$ and $1/f^2$ dependence close to the

carrier. For the high Q case, a region of $1/f^3$ and $1/f$ should be observed near the carrier. Substituting Eq. (7-10) in (7-15) gives an overall noise of

$$\pounds(f_m) = \frac{1}{2}\left[1 + \frac{1}{f_m^2}\left(\frac{f}{2Q_L}\right)^2 \frac{FkT}{P_{sav}}\left(1 + \frac{f_c}{f_m}\right)\right] = \frac{FkT}{2P_{sav}}\left[\frac{1}{f_m^3}\frac{f^2 f_c}{4Q_L^2} + \frac{1}{f_m^2}\left(\frac{f}{2Q_L}\right)^2 + \left(1 + \frac{f_c}{f_m}\right)\right] \text{dBc/Hz} \tag{7-16}$$

Examining Eq. (7-16) gives the four major causes of oscillator noise: the up-converted $1/f$ noise or flicker FM noise, the thermal FM noise, the flicker phase noise, and the thermal noise floor, respectively.

Q_L (loaded Q) can be expressed as

$$Q_L = \frac{w_o W_e}{P_{\text{diss,total}}} = \frac{w_o W_e}{P_{\text{in}} + P_{\text{res}} + P_{\text{sig}}} = \frac{\text{reactive power}}{\text{total dissipated power}} \tag{7-17}$$

where W_e is the reactive energy stored in L and C,

$$W_e = \tfrac{1}{2} C V^2 \tag{7-18}$$

$$P_{\text{res}} = \frac{w_o W_e}{Q_{\text{unl}}} \tag{7-19}$$

$$\mathcal{L}(f_m) = \frac{1}{2}\left[1 + \frac{\omega_o^2}{4\omega_m^2}\left(\frac{P_{\text{in}}}{\omega_o W_e} + \frac{1}{Q_{\text{unl}}} + \frac{P_{\text{sig}}}{\omega_o W_e}\right)^2\right]\left(1 + \frac{\omega_c}{\omega_m}\right)\frac{FkT_o}{P_{\text{sav}}} \tag{7-20}$$

input power over reactive power

resonator Q

signal power over reactive power

flicker effect

phase perturbation

More comments on the Leeson formula are found in [70, 109, 161]. The practical oscillator will experience a frequency shift when the supply voltage, is changed. This is due to the voltage and current dependent capacitances of the transistor. To calculate this effect, we can assume that the fixed tuning capacitor of the oscillator is a semiconductor junction, which is reverse biased. This capacitor becomes a tuning diode. This tuning

diode itself generates a noise voltage and modulates its capacitance by a slight amount, and therefore modulates the frequency of the oscillator by minute amounts. The following calculates the phase noise generated from this mechanism, which needs to be added to the phase noise calculated above.

It is possible to define an equivalent noise R_{aeq} that, inserted in Nyquist's equation,

$$V_n = \sqrt{4kT_o R_{aeq} \Delta f} \tag{7-21}$$

where kT_o = 4.2 × 10^{-21} at 300 K, R is the equivalent noise resistor, and Δf is the bandwidth, determines an open noise voltage across the tuning diode. Practical values of R_{aeq} for carefully selected tuning diodes are in the vicinity of 100Ω, or higher. If we now determine the voltage $V_n = \sqrt{4 \times 4.2 \times 10^{-21} \times 100}$, the resulting voltage value is $1.265 \times 10^{-9}\ \mathrm{V}\sqrt{\mathrm{Hz}}$.

This noise voltage generated from the tuning diode is now multiplied with the VCO gain, resulting in the rms frequency deviation:

$$(\Delta f_{rms}) = K_o \times (1.265 \times 10^{-9} V) \text{ in 1 Hz bandwidth} \tag{7-22}$$

In order to translate this into the equivalent peak phase deviation,

$$q_d = \frac{K_o \sqrt{2}}{f_m} (1.265 \times 10^{-9}\, rad) \text{ in 1 Hz bandwidth} \tag{7-23}$$

or for a typical oscillator gain of 10 MHz/V,

$$q_d = \frac{0.00179}{f_m} \text{ rad in 1 Hz bandwidth} \tag{7-24}$$

For f_m= 25 kHz (typical spacing for adjacent channel measurements for FM mobile radios), the q_d = 7.17 × 10^{-8}. This can be converted into the SSB signal-to-noise ratio

$$\begin{aligned} £(f_m) &= 20 \log_{10} \frac{q_c}{2} \\ &= -149 \text{ dBc/Hz} \end{aligned} \tag{7-25}$$

Figure 7-6 shows a plot with an oscillator sensitivity of 10 kHz/V, 10 MHz/V, and 100 MHz/V. The center frequency is 2.4 GHz. The lowest curve is the contribution of

the Leeson equation. The second curve shows the beginning of the noise contribution from the diode, and the third curve shows that at this tuning sensitivity, the noise from the tuning diode by itself dominates as it modulates the VCO. This is valid regardless of the Q. This effect is called modulation noise (AM-to-PM conversion), while the Leeson equation deals with the conversion noise.

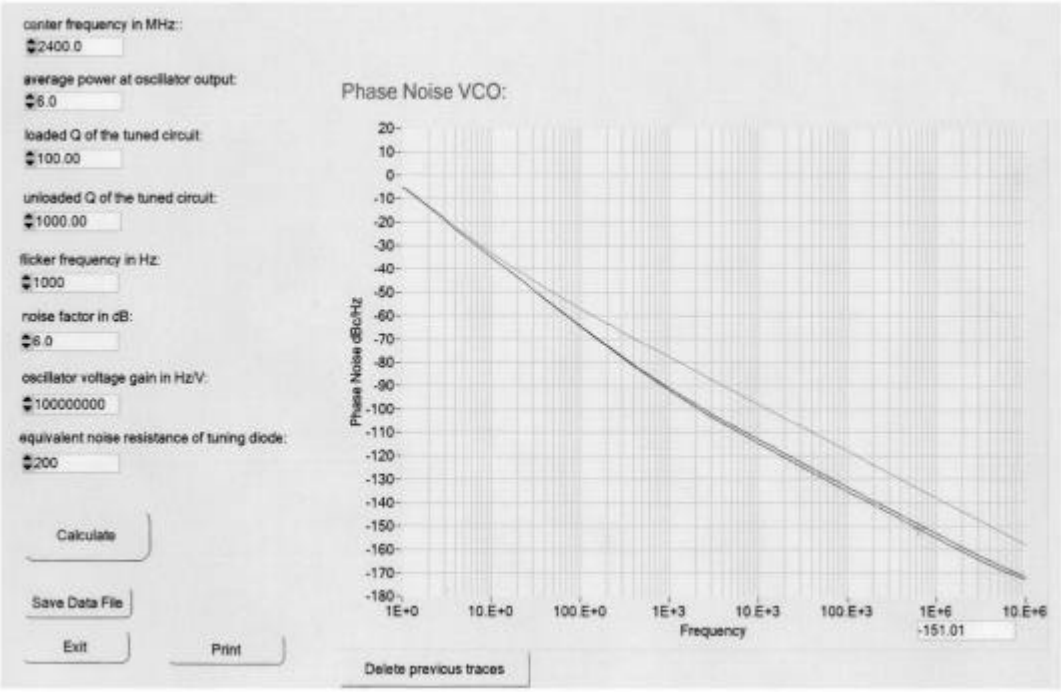

Figure 7-6 Simulated phase noise following Eq. (7-26).

If we combine the Leeson formula with the tuning diode contribution, the following equation allows us to calculate the noise of the oscillator completely.

$$\pounds(f_m) = 10\log\left\{\left[1+\frac{f_0^{\,2}}{(2f_mQ_L)^2}\right]\left(1+\frac{f_c}{f_m}\right)\frac{FkT}{2P_{sav}}+\frac{2kTRK_0^{\,2}}{f_m^{\,2}}\right\} \tag{7-26}$$

where

$\pounds(f_m)$ = ratio of sideband power in a 1 Hz bandwidth at f_m to total power in dB
f_m = frequency offset
f_0 = center frequency
f_c = flicker frequency
Q_L = loaded Q of the tuned circuit
F = noise factor
$kT = 4.1 \times 10^{-21}$ at 300 K_0 (room temperature)
P_{sav} = average power at oscillator output

R = equivalent noise resistance of tuning diode (typically 50 Ω - 10 kΩ)
K_o = oscillator voltage gain

The limitation of this equation is that the loaded Q in most cases has to be estimated and the same applies to the noise factor. The microwave harmonic-balance simulator, which is based on the noise modulation theory (published by Rizzoli), automatically calculates the loaded Q and the resulting noise figure as well as the output power [73]. The following equations, based on this equivalent circuit, are the exact values for P_{sav}, Q_L, and F which are needed for the Leeson equation. This approach shown here is novel. It calculates the output power based on the Eqs. (8-66) to (8-76). The factor of 1000 is needed since the result is expressed in dBm and a function of n and C_1.

$$\left[P_o(n,C_1\right]_{dBm}=10\,Log\left\{\left[\frac{(V_{ce}=-0.7)^2}{4(w_0L)^2}\right]\left[\frac{Q_L^2\left[C_1^2\left(\frac{C_1}{n-1}\right)^2 w_0^4L^2\right]}{Q_L^2\left(C_1+\frac{C_1}{n-1}\right)^2+w_0^4L^2C_1^2\left(\frac{C_1}{n-1}\right)^2}\right]R_L*1000\right\} \quad (7\text{-}27)$$

0.7 = high current saturation voltage, V_{ce} collector emitter voltage $<V_{cc}$

To calculate the loaded Q_L, we have to consider the unloaded Q_0 and the loading effect of the transistor. There we have to consider the influence of $Y_{21}{}^+$. The inverse of this is responsible for the loading and reduction of the Q.

$$Q_L=\frac{Q_0\times Q^*}{Q_0+Q^*};\; Q^*=\frac{w_0\times\left|\frac{1}{Y_{21}{}^+}\right|(C_1+C_2)}{1-w_0{}^2\,C_1\,L(Q=Q_0)} \quad (7\text{-}28)$$

Based on Figure 8-7, which also shows the transformation of the loading of the differential emitter impedance (resistance), we can also calculate the noise factor of the transistor under large-signal conditions. Considering $Y_{21}{}^+$, this noise calculation, while itself uses a totally new approach, is based on the general noise calculations such as the one shown by Hawkins [117] and Hsu and Snapp [118]. An equivalent procedure can be found for FET's rather than bipolar transistors.

$$F=1+\frac{C_2C_c}{(C_1+C_2)C_1r_e}\left[r_b+\frac{1}{2r_eb}\left(r_b+\frac{(C_1+C_2)C_1r_e}{C_2C_c}\right)^2+\frac{r_e}{2}+\frac{1}{2r_e}\left(r_b+\frac{(C_1+C_2)C_1r_e}{C_2C_c}\right)^2\left(\frac{f^2}{f_T^2}\right)\right] \quad (7\text{-}29)$$

When adding an isolating amplifier the noise of an *LC* oscillator system is determined by

$$\begin{aligned} S_f(f_m) = &\left[a_R F_0^4 + a_E (F_0 / (2Q_L))^2\right] / f_m^3 \\ &+ \left[\left(2GFkT / P_0\right)\left(F_0 / \left(2Q_L\right)\right)^2\right] / f_m^2 \\ &+ \left(2a_R Q_L F_0^3\right) / f_m^2 \\ &+ a_E / f_m + 2GFkT / P_0 \end{aligned} \tag{7-30}$$

where

G = compressed power gain of the loop amplifier
F = noise factor of the loop amplifier
k = Boltzmann's constant
T = temperature in Kelvins
P_0 = carrier power level (in watts) at the output of the loop amplifier
F_0 = carrier frequency in Hz
f_m = carrier offset frequency in Hz
$Q_L = (pF_0 t_g)$ = loaded Q of the resonator in the feedback loop
a_R *and* a_E = flicker noise constants for the resonator and loop amplifier, respectively.
[74]

It is important to understand that the Leeson model is the best case since it assumes the tuned circuit filters out all the harmonics. In all practical cases, it is hard to predict the operating Q and the noise figure. When comparing the measured results of oscillators with the assumptions made in Leeson's equation, one frequently obtains a *de facto* noise figure in the vicinity of 20 to 30 dB and an operating Q that is different than the assumed loaded Q. Attempting to match the Leeson calculated curve and measured curve requires totally different values than those assumed. The basic concept of the Leeson equation, however, is correct, and if each of the three unknown terms are inserted properly, the computed results will agree with the measurements. The information that is not known prior to measurement is:

a) the output power,
b) the noise figure under large-signal conditions, and
c) the loaded (operational) noise figure.

Example:

The following is a validation example for this approach.

For an output power of 13 dBm, C_1 = 3.3pF, C_2 = 2.2pF, Y_{21}^+ = 2mS, Q_0 = 1000, Q^+ = 618 loading from the transistor**,** the resulting noise factor is 104 or roughly 20 dB, and the total loaded Q is 380. Figure 7-7 shows the phase noise, including the flicker corner frequency of 10 kHz. This is one way of calculating the phase noise. The result is very close to the CAD simulations and measurements, but is incomplete because many transistor parameters are not considered, which would increase the accuracy. The formula, however, does not allow us to enter more parameters.

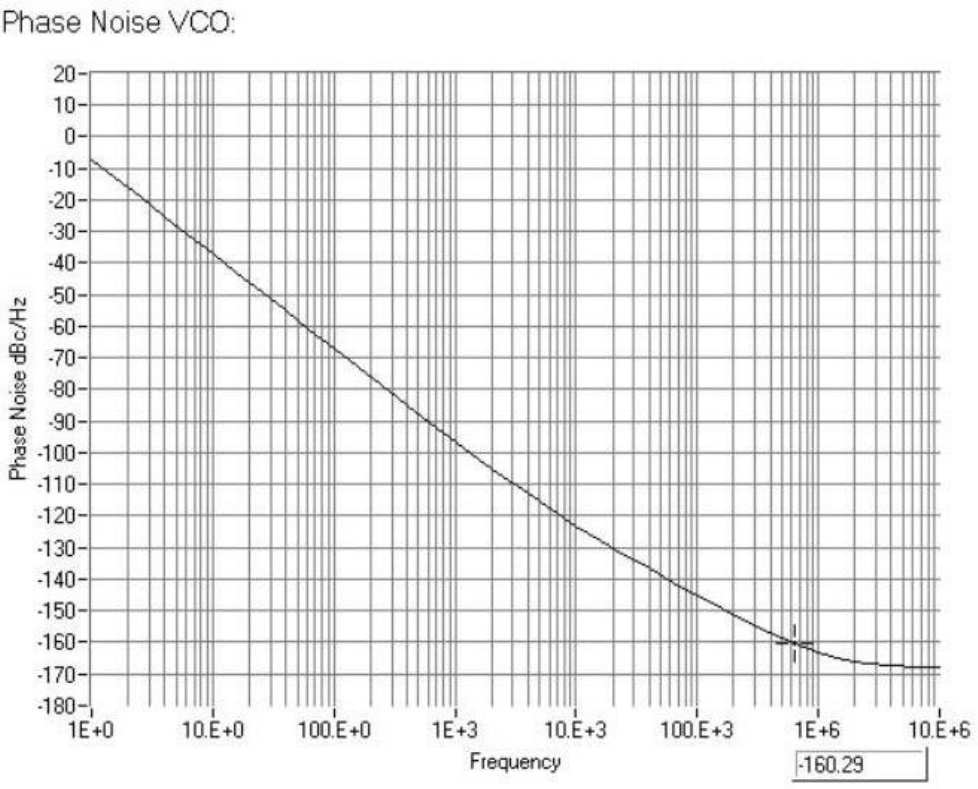

Figure 7-7 Predicted phase noise for an oscillator using the values above. It agrees well with actual measurements.

7.2 Phase Noise Measurements

The single-sideband phase noise of an oscillator has been the subject of many discussions, but how can it be measured?

Spectrum Analyzer

The first and most simple approach is to use a spectrum analyzer which has a sufficiently low phase noise oscillator. The phase noise is measured on the screen as a function of the offset off the carrier. Modern spectrum analyzers, such as the Rohde & Schwarz FSU series, have a carrier phase noise option built-in. The phase noise is measured in a normalized 1 Hz bandwidth. A bandwidth of 1 Hz is at best realizable in a DSP-based IF

stage, but then the measurement time would be huge. A better way to do this is to adjust the bandwidth to be approximately 10% or more off the carrier. As example, when measuring at 100 Hz off the carrier, 10 Hz bandwidth should be used, and at 100 kHz off the carrier, a wider bandwidth, such as 10 kHz, can be used. Most analyzers have an intelligent built-in option (program) which automatically selects the proper sweep speed and bandwidth for this purpose. Since all high performance spectrum analyzers have synthesized local oscillators with wide loop bandwidths, the phase noise of the analyzers at frequencies deviations of about 10 kHz typically exceed the performance of the device under test. High Q oscillators become a problem because they can have better phase noise performance than the spectrum analyzer. Crystal oscillators, ceramic resonator oscillators, SAW oscillators, and dielectric resonator oscillators fall into this category.

Phase Noise Test Setup

There are several phase noise test setups available on the market. The best instruments known are made by Agilent (Hewlett-Packard) and Komstron (EuroTest). Figure 7-8 shows the popular Hewlett-Packard phase noise setup.

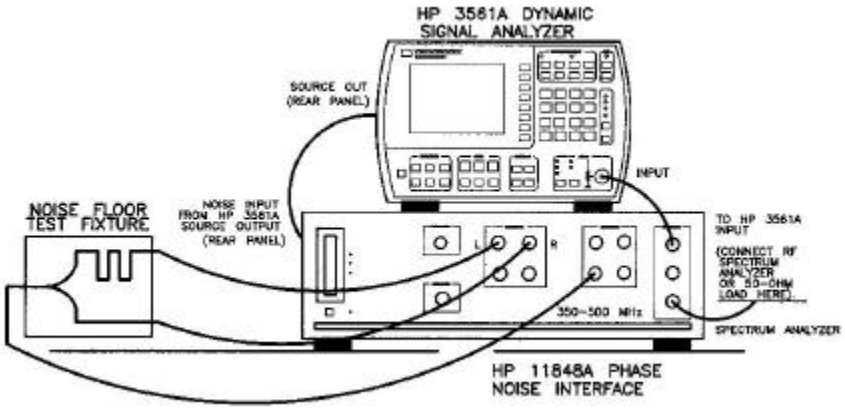

Figure 7-8 Model 3048A -based phase noise test setup.

This system consists of a base unit with a phase detector and amplifier, several signal generators, and a DC output. The test setup shown above is configured to determine the minimum noise floor of the system to make sure there is enough dynamic range. This is accomplished by taking the output of one of the built-in signal sources, splitting the power and feeding the outputs into the built-in high-level double-balanced mixer. One of the outputs is delayed in phase by the delay line shown on the left side of the picture. As a result of this, the double balanced mixer receives the identical frequency into the RF and LO input, and there is a phase difference between both signals. Because there is no difference in frequency between the two signals, the resulting output is a DC voltage with the signal generator's noise on top of it. Because of the conversion to zero IF, the analyzer connected to the output needs to cover DC (10 Hz or less) to 1 - 10 MHz to analyze the noise. Since there are no requirements for linearity for the mixing process, the RF levels, both of the RF and LO input, can be the same.

Using an FFT analyzer, Figure 7-9 shows the noise floor of the system. This is true because the signal source in question is a high performance crystal oscillator with a much better phase noise performance than any practical device under test (DUT).

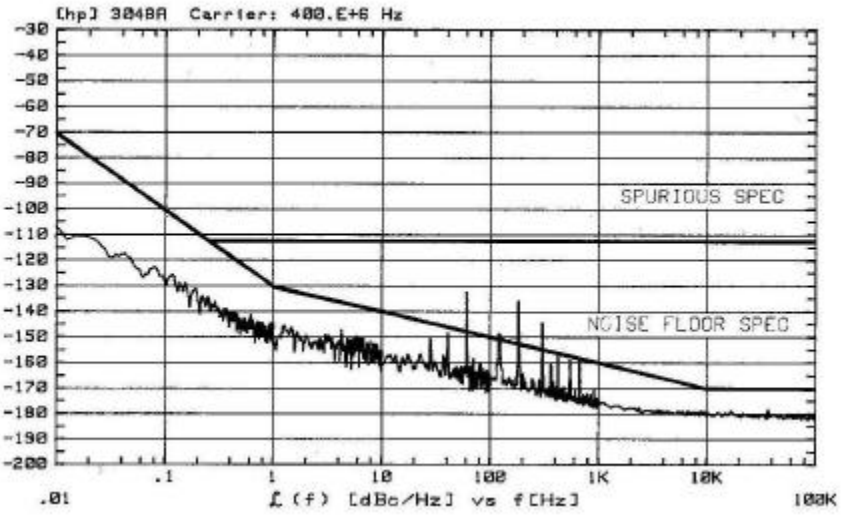

Figure 7-9 HP3048A noise floor performance test results.

Figure 7-10 shows the block diagram of the test setup with a small modification. Instead of having one oscillator with a power splitter and a delay line, it uses two separate oscillators. This is commonly used to measure medium quality oscillators. As long as signal generator 1 is at least 10 dB better than signal generator 2, this approach is valid. If both signal generators are identical, than there would be a 3 dB correction factor. It is good practice to synchronize oscillator 1 against the oscillator 2. The phase noise setup system shown above has several frequency standards built-in. The high quality 10 MHz reference oscillator output can be used to synchronize oscillator 1, if this a synthesized signal generator. This is valid in most cases. If oscillator 2 is a VCO, the test setup provides a DC control voltage, which can phase lock oscillator 2 in the system. Depending on the measurement offset, the system adjusts the loop bandwidth.

Both systems have their plus and minuses. The delay line principle is limited by the delay, which is a sine x/x function that repeats. The delay line measurement system requires several delay lines to cover a wide range of measurements. More details about the limitation of the cable measurement can be found in the system reference manual.

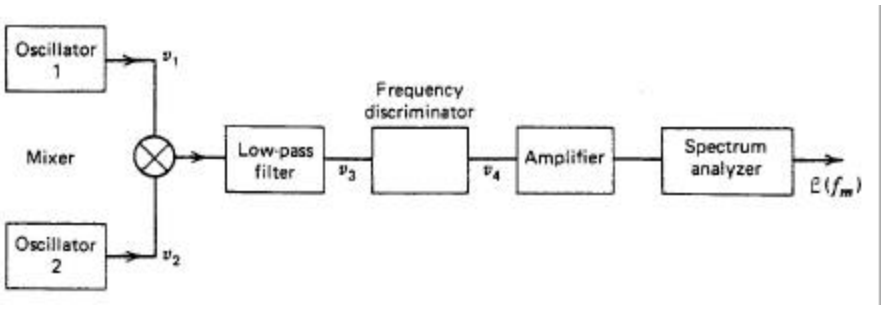

Figure 7-10 Block diagram of the principle of the HP3048A system. There is an additional DC FM feedback loop to phase lock one of the oscillators.

Figure 7-11 shows the area for which the delay line measurements are valid. This is frequency dependent and of course depends on the length of the delay line.

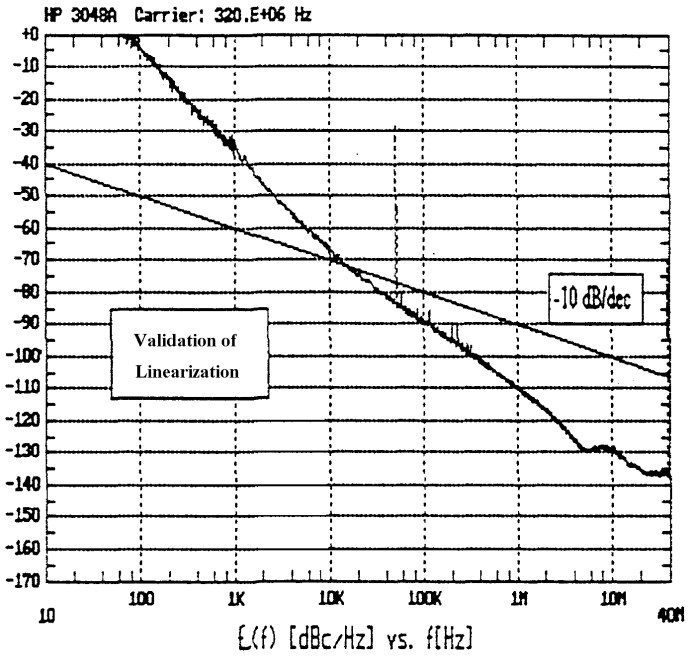

Figure 7-11 Display of a typical phase noise measurement using the delay line principle. This method is only applicable where $x \sim \sin(x)$. The measured values above the solid line violate this relationship, and therefore are not valid.

By choosing the appropriate delay length the dynamic range can be controlled. As an example, the 1*m*S delay line is ideal for most microwave frequencies. The limit of -160 dBc/Hz was due to the system's performance. This can bee seen in Figure 7-12. A longer delay line, which is mechanically very bulky and lossy, allows measurements closer in with better resolution. The delay line ideally is adjustable, which guarantees to make small phase changes since the signal fed to the mixer should be in quadrature compared to the other input. A more detailed description can be found in the system's manual [81].

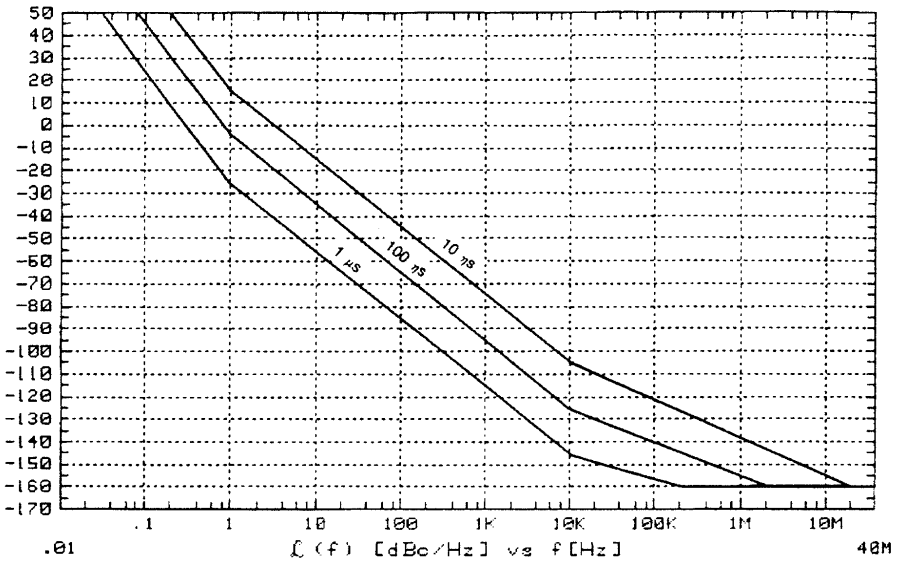

Figure 7-12 Dynamic range as a function of cable delay. 1 *m*s is ideal for microwave frequencies.

In the case of the two-oscillator (signal generator) measurement, the typical problem is that the synthesized signal generator is not always as good as the high Q oscillators under test. While for most cases the setup with one signal generator and the device under test is sufficient, the additional delay line should be available to have a complete system.

The measurements shown in this work were taken with the Hewlett-Packard 3048A and the Euro Test system. Figure 7-13 shows a picture of the test station, which houses both systems.

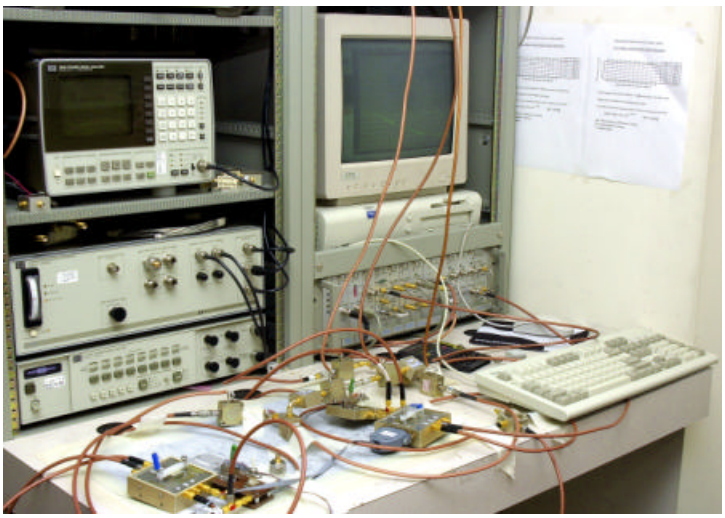

Figure 7-13 Synergy Microwave Corp. in-house automated test system to measure oscillator phase noise.

8 Calculation and Optimization of Phase Noise in Oscillators

8.1 Introduction

This section develops the computation for the noise properties of an oscillator and a design guide for best performance will be given. Two methods will be chosen. One is the calculation of a time-domain dependent negative resistance that is necessary to enable and sustain oscillation. A bias-dependent noise calculation is possible from this approach. The second approach is a loop gain approach in which the oscillator is considered a closed loop. This allows for the calculation of the impact of the various noise sources in the transistor, a bipolar transistor.

8.2 Oscillator Configurations

The most relevant circuit configuration used for microwave applications is the Colpitts oscillator with a parallel tuned circuit operating in an inductive mode as shown in Figure 8-1.

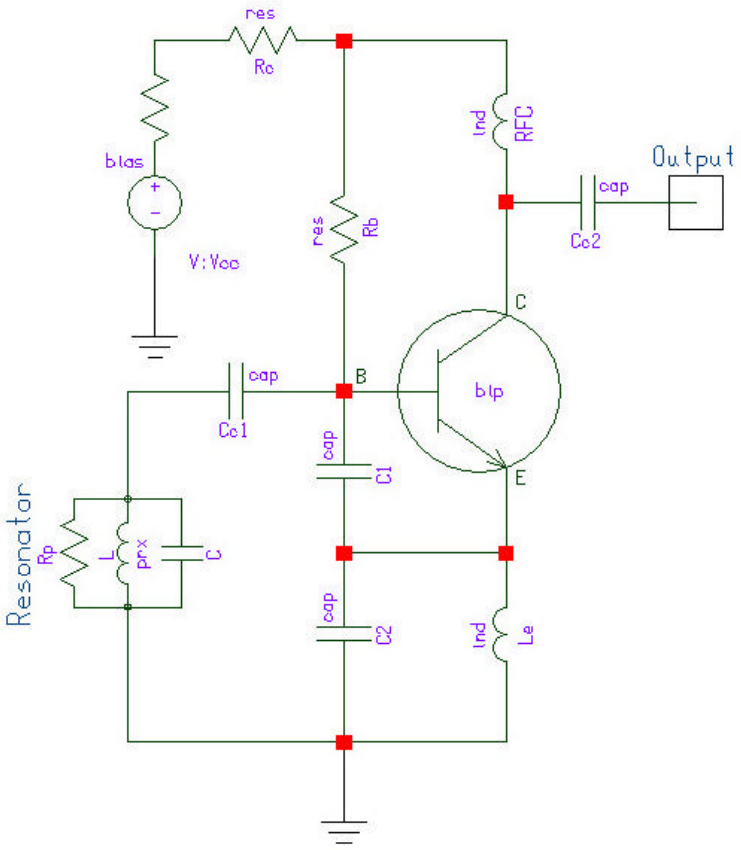

Figure 8-1 Shows a parallel-tuned Colpitts oscillator.

8.3 Oscillator Phase Noise Model for the Synthesis Procedure

Device Phase Noise

Phase noise in an active device is generated by white additive noise as well as by shot noise.

1. For white additive noise, the power spectral density is flat with the frequency. For a device having a noise factor of F, the half sided power spectral density of the phase noise is given as

$$S_{\Delta q}(w) = \frac{FkT}{P_s} \tag{8-1}$$

Where k is a Boltzman's constant, T is absolute temperature and P_s is the signal level at the active device input.

2. For shot noise, the power spectral density of the phase noise representation varies inversely with frequency, and is given by

$$S_{\Delta q}(w) = \frac{K_a}{w} \tag{8-2}$$

where K_α is a constant.

3. The total power spectral density of the input phase error can then be written as

$$S_{\Delta q}(w) = \frac{K_a}{w} + \frac{FkT}{P_s} \tag{8-3}$$

For small phase deviations at a frequency offset less than the resonator half bandwidth $w_0/2Q$, a phase error at the input to the active element of the oscillator results in a frequency error. This frequency error is determined by the phase frequency relationship of the feedback network.

$$\frac{dj}{dt} = \frac{w_0}{2Q_L}\ \Delta q \tag{8-4}$$

Case 1

For noise modulation rates less than the half bandwidth of the feedback loop, the spectrum of the frequency error is identical to the spectrum of the oscillator input phase noise, $S_{\Delta q}(w)$. The spectrum of the phase error can be given as

$$S_j(w) = \left[\frac{w_0}{2Q_L}\right]^2 \frac{S_{\Delta q}(w)}{w^2}; \quad for \quad f < \left[\frac{w_0}{2Q_L}\right] \tag{8-5}$$

Case 2

For noise modulation rates large compared to the half bandwidth of the feedback loop, the series feedback is not effective, and the power spectral density of the output phase, $S_j(w)$ is identical to the spectrum of the oscillator input phase noise, $S_{\Delta q}(w)$.

$$S_j(w) = S_{\Delta q}(w) \tag{8-6}$$

A composite expression for the power spectral density of the output phase is

$$S_j(w) = S_{\Delta q}(w) + \left[\frac{w_0}{2Q_L}\right]^2 \frac{S_{\Delta q}(w)}{w^2} \Rightarrow \left\{1 + \left[\frac{w_0}{2Q_L}\right]^2\right\} \frac{S_{\Delta q}(w)}{w^2} \tag{8-7}$$

$$S_{\Delta q}(w) = \frac{K_a}{w} + \frac{FkT}{P_s} \tag{8-8}$$

$$S_j(w) = \left[\frac{K_a}{w} + \frac{FkT}{P_s}\right]\left\{1 + \left[\frac{w_0}{2Q_L w}\right]^2\right\} \tag{8-9}$$

The phase noise can be described as a short-term random frequency fluctuation of a signal which is measured in the frequency domain, and is expressed as a ratio of signal power to noise ratio measured in a 1 Hz bandwidth at a given offset from the desired signal frequency.

$$£(\Delta w) = 10Log\left[\frac{P_{sideband}(w_0 + \Delta w, 1Hz)}{P_{carrier}}\right] = 10Log[S_j(f)] \tag{8-10}$$

The term $\frac{K_a}{w}$ is typically omitted in the phase noise equations, specifically, derivatives of the Leeson equation.

8.4 Phase Noise Analysis Based on the Negative Resistance Model

The following noise analysis for the oscillator, while based on the approach of Kurokawa [82], is an attempt to introduce the concept of a "noisy" negative resistance, which is time dependent. Kurokawa, addressing the question of synchronized oscillators, provided insight in the general case of a series oscillator. The method introduced here is specific for a real oscillator and real noise sources.

This concept gets started by connecting a parallel-tuned circuit to a transistor in Colpitts configuration. Since, the two capacitors C_1 and C_2 are similar in value, not different by more than a factor of 2 or 3 and connected to a parallel-tuned circuit via a small coupling capacitor C_c, the output impedance of the emitter follower circuit gets transformed to the base. The differential output impedance at the emitter is $1/Y_{21}^{+}$ (large signal), while the input impedance itself is $1/Y_{21}^{+} \times b$. Because of this, the contribution of Y_{11} can be neglected for the basic analysis. This is only valid for this particular case. Consistent with Eq. 6-1, which is based on the same approximation, but includes the parasitics, the transistor circuit now provides a negative resistance (or a negative conductance). This negative conductance cancels the losses concentrated in the loss resistor R_P, which for infinite Q would also be infinite.

Figure 8-2 is a Colpitts oscillator arrangement, simplified for the purpose of showing the circuit components. On the left side we see the resonator tank circuit with the loss resistor R_P, and on the right side we see the negative conductance, which is time dependent. The time dependence comes from the fact that the collector current is a series of pulses and the negative conductance is only present during a small period of time. This explanation is necessary to justify the existence of a loaded Q. If there would be a negative resistance or conductance present all the time, the compensating circuit would reduce the bandwidth to essentially zero or an infinite Q. In reality, however, for most of the time the transistor "loads" the tuned circuit, and therefore, the operating Q is less than the unloaded Q. Another time-domain noise analysis was shown by Anzill [80], but is not useful for HB simulators.

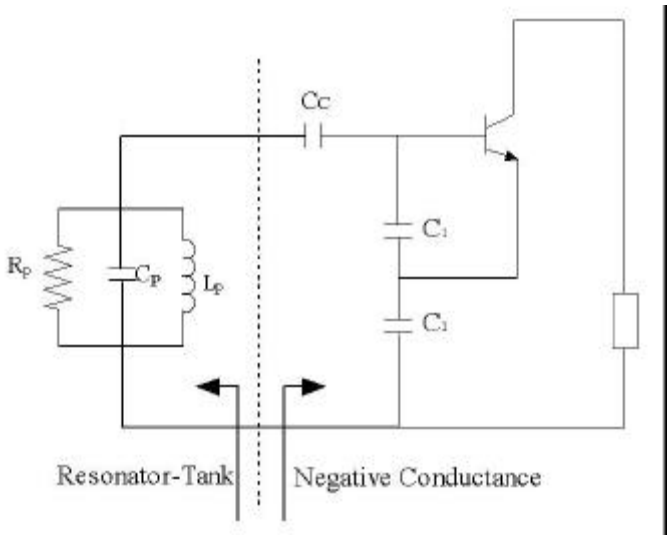

Figure 8-2 Colpitts Oscillator configuration for the intrinsic case, no parasitics assumed, and an ideal transistor considered.

The following two circuits show the transition from a series tuned circuit connected with the series time-dependent negative resistance as outlined in Eq. 6-1 and the resulting input capacitance marked C_{IN}. Translated, the resulting configuration consists of a series circuit with inductance L and the resulting capacitance C'. The noise voltage $e_N(t)$ describes a small perturbation, which is the noise resulting from R_L and $-R_N(t)$.

Figure 8-3 shows the equivalent representation of the oscillator circuit in the presence of noise.

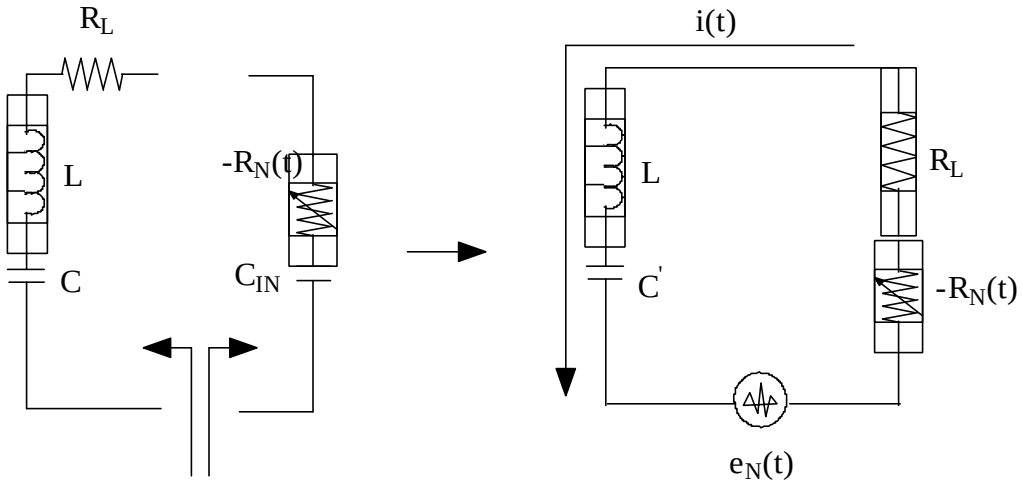

Figure 8-3 Equivalent representation of the oscillator circuit in presence of noise.

The circuit equation of the oscillator circuit of Figure 8-3 can be given as

$$L\frac{di(t)}{dt}+(R_L-R_N(t))i(t)+\frac{1}{C'}\int i(t)dt=e_N(t) \tag{8-11}$$

where i(t) is the time varying resultant current. Due to the noise voltage e_N(t), Eq. 8-11 is a nonhomogeneous differential equation. If the noise voltage is zero, it translates into a homogeneous differential equation.

For a noiseless oscillator, the noise signal $e_N(t)$ is zero and the expression of the free-running oscillator current $i(t)$ can be assumed to be a periodic function of time and can be given as

$$i(t)=I_1\cos(w\,t+j_{\,1})+I_2\cos(2w\,t+j_{\,2})+I_3\cos(3w\,t+j_{\,3})+.....I_n\cos(nw\,t+j_{\,n}) \tag{8-12}$$

where I_1, I_2 …..I_n are peak harmonic amplitudes of the current and j_1, j_2…..j_n are time invariant phases.

In the presence of the noise perturbation $e_N(t)$, the current $i(t)$ may no longer be a periodic function of time and can be expressed as

$$\begin{aligned} i(t)=&I_1(t)\cos[w\,t+j_{\,1}(t)]+I_2(t)\cos[2w\,t+j_{\,2}(t)]+I_3(t)\cos[3w\,t+j_{\,3}(t)]+\\ &....I_{n-2}(t)\cos[(n-2)w\,t+j_{\,n-2}(t)]+I_{n-1}(t)\cos[(n-1)w\,t+j_{\,n-1}(t)]+I_n(t)\cos[nw\,t+j_{\,n}(t)] \end{aligned} \tag{8-13}$$

where $I_1(t)$, $I_2(t)$…..$I_n(t)$ are time variant amplitudes of the current and $j_1(t)$, $j_2(t)$…..$j_n(t)$ are time variant phases.

Considering that $I_n(t)$ and $j_n(t)$ do not change much over the period of $2\pi/nw$; each corresponding harmonic over one period of oscillation cycle remains small and more or less invariant. The solution of the differential equation becomes easy since the harmonics are suppressed due to a Q > 10, which prevents i(t) to flow for the higher terms.

After the substitution of the value of $\frac{di}{dt}$ and $\int i(t)dt$, the complete oscillator circuit equation, as given in Eq. (8-11), can be rewritten as

$$L\{-I_1(t)(w+\frac{dj_1(t)}{dt})\sin[wt+j_1(t)]+\frac{dI_1(t)}{dt}\cos[wt+j_1(t)]+$$

$$-I_2(t)(2w+\frac{dj_2(t)}{dt})\sin[2wt+j_2(t)]+\frac{dI_2(t)}{dt}\cos[2wt+j_2(t)]+$$

$$-I_3(t)(3w+\frac{dj_3(t)}{dt})\sin[3wt+j_3(t)]+\frac{dI_3(t)}{dt}\cos[3wt+j_3(t)]+...$$

$$-I_n(t)(nw+\frac{dj_n(t)}{dt})\sin[nwt+j_n(t)]+\frac{dI_n(t)}{dt}\cos[nwt+j_n(t)]\}+$$

$$[(R_L-R_N(t))i(t)]+$$

$$\frac{1}{C'}\left\{\left[\frac{I_1(t)}{w}-\frac{I_1(t)}{w^2}\left(\frac{dj_1(t)}{dt}\right)\right]\sin[wt+j_1(t)]+\frac{1}{w^2}\left(\frac{dI_1(t)}{dt}\right)\cos[wt+j_1(t)]\right\}+$$

$$\frac{1}{C'}\left\{\left[\frac{I_2(t)}{2w}-\frac{I_2(t)}{4w^2}\left(\frac{dj_2(t)}{dt}\right)\right]\sin(2wt+j_2(t)+\frac{1}{4w^2}\left(\frac{dI_2(t)}{dt}\right)\cos(2wt+j_2(t))\right\}+$$

$$\frac{1}{C'}\left\{\left[\frac{I_3(t)}{3w}-\frac{I_3(t)}{9w^2}\left(\frac{dj_3(t)}{dt}\right)\right]\sin[3wt+j_3(t)]+\frac{1}{9w^2}\left(\frac{dI_3(t)}{dt}\right)\cos[3wt+j_3(t)]\right\}+...$$

$$\frac{1}{C'}\left\{\left[\frac{I_n(t)}{nw}-\frac{I_n(t)}{n^2w^2}\left(\frac{dj_n(t)}{dt}\right)\right]\sin[nwt+j_n(t)]+\frac{1}{n^2w^2}\left(\frac{dI_n(t)}{dt}\right)\cos[nwt+j_n(t)]\right\}=e_N(t) \quad (8\text{-}14)$$

Because Q > 10 we approximate:

$\frac{di(t)}{dt}=-I_1(t)(w+\frac{dj_1(t)}{dt})\sin[wt+j_1(t)]+\frac{dI_1(t)}{dt}\cos[wt+j_1(t)]+$ (slowly varying function at higher order harmonics of a very small amount)

$$\int i(t)dt = \left[\frac{I_1(t)}{w} - \frac{I_1(t)}{w^2}\left(\frac{dj_1(t)}{dt}\right)\right]\sin[w\,t + j_1(t)] + \frac{1}{w^2}\left(\frac{dI_1(t)}{dt}\right)\cos[w\,t + j_1(t)] + \text{ (slowly}$$

varying function at higher order harmonics of a very small amount)

After the substitution of the value of $\frac{di}{dt}$ and $\int i(t)dt$, the oscillator circuit Eq. (8-14) can be rewritten as

$$L\left[-I_1(t)(w + \frac{dj_1(t)}{dt})\sin[w\,t + j_1(t)] + \frac{dI_1(t)}{dt}\cos[w\,t + j_1(t)]\right] + \left[(R_L - R_N(t))I(t)\right] +$$

$$\frac{1}{C}\left\{\left[\frac{I_1(t)}{w} - \frac{I_1(t)}{w^2}\left(\frac{dj_1(t)}{dt}\right)\right]\sin[w\,t + j_1(t)] + \frac{1}{w^2}\left(\frac{dI_1(t)}{dt}\right)\cos[w\,t + j_1(t)]\right\} = e_N(t) \qquad (8\text{-}15)$$

Following [82], and for simplification purposes, the equations above are multiplied with $\sin[w\,t + j_1(t)]$ or $\cos[w\,t + j_1(t)]$ and integrated over one period of the oscillation cycle, which will give an approximate differential equation for phase $j(t)$ and amplitude *i*(t) as

$$\left[\frac{2}{IT_0}\right]\int_{t-T_0}^{t} e_N(t)\sin[w\,t + j(t)]dt = -\frac{dj}{dt}\left[L + \frac{1}{w^2C'}\right] + \left[-w\,L + \frac{1}{w\,C'}\right] \qquad (8\text{-}16)$$

$$\left[\frac{2}{T_0}\right]\int_{t-T_0}^{t} e_N(t)\cos[w\,t + j(t)]dt = \frac{dI(t)}{dt}\left[L + \frac{1}{w^2C'}\right] + \left[R_L - \overline{R_N(t)}\right]I(t) \qquad (8\text{-}17)$$

where $\overline{R_N(t)}$ is the average negative resistance under large signal condition.

$$\overline{R_N(t)} = \left[\frac{2}{T_0 I}\right]\int_{t-T_0}^{t} R_N(t)I(t)\cos^2[w\,t + j)]dt \qquad (8\text{-}18)$$

Since magnitude of the higher harmonics are not significant, the subscript of $j(t)$ and $I(t)$ are dropped. Based on [82], we now determine the negative resistance.

Calculation of the Region of the Nonlinear Negative Resistance

Under steady-state free running oscillation condition,

$$\frac{dI(t)}{dt} \to 0$$

implies steady current, and

$$e_N(t) \to 0$$

with I = fundamental RF current. Solving the now homogeneous differential equation for $R_L - R_N(t)$ and inserting the two terms into 8-17, we obtain

$$\left[\frac{2}{T_0}\right]\int_{t-T_0}^{t} e_N(t)\cos[w\,t + j\,(t)]dt = \frac{dI}{dt}\left[L + \frac{1}{w^2 C'}\right] + \left[R_L - \overline{R_N(t)}\right]I(t) \qquad (8\text{-}19)$$

$$\text{term} \to 0$$

now we introduce γ; $\gamma = \dfrac{\Delta R}{\Delta I}$; for $\Delta \to 0$, $\gamma \to 0$ and

$$[R_L - \overline{R_N(t)}] = g\ \ \Delta I\ ,\ g\ \to 0 \Rightarrow [R_L - \overline{R_N(t)}]I(t) \to 0 \qquad (8\text{-}20)$$

$$R_L - \overline{R_N(t)} = R_{Load} - \left[\frac{2}{T_0}\right]\int_{t-T_0}^{t} R_N(t)\cos^2[w\,t + j\,(t)]dt \to 0 \qquad (8\text{-}21)$$

$[R_L - \overline{R_N(t)}]I(t) \to 0$ gives the intersection of $[\overline{R_N(t)}]$ and $[R_L]$. This value is defined as I_0 which is the minimum value of the current needed for the steady-state sustained oscillation condition.

Figure 8-4 shows the plot of the nonlinear negative resistance, which is a function of the amplitude of the RF current. As the RF amplitude gets larger the conducting angle becomes more narrow.

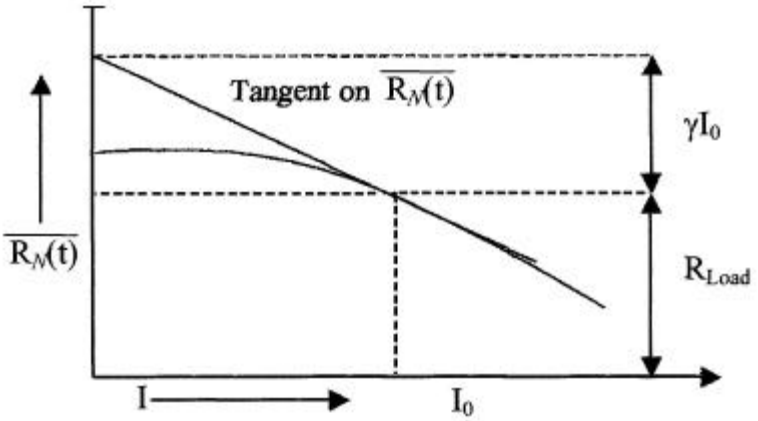

Figure 8-4 Plot of negative resistance of $[\overline{R_N(t)}]$ vs. amplitude of Current I.

For a small variation of the current ΔI from I_0, the relation above is expressed as

$$[R_L - \overline{R_N(t)}] = g\ \Delta I \tag{8-22}$$

$g\ \Delta I$ can be found from the intersection on the vertical axis by drawing the tangential line on $[\overline{R_N(t)}]$ at $I = I_0$. $|\Delta I|$ decreases exponentially with time for $\gamma>0$.

Hence, I_0 represents the stable operating point. On the other hand, if $[\overline{R_N(t)}]$ intersects $[R_L]$ from the other side for $\gamma<0$ then $|\Delta I|$ grows indefinitely with time. Such an operating point does not support stable operation [82].

Calculation of the Noise Signal in Time Domain

From solving the two orthogonal equations, we need to obtain information about current $I(t)$ and $j(t)$.

$$\left[\frac{2}{IT_0}\right]\int_{t-T_0}^{t} e_N(t)\sin[w\,t + j\,(t)]dt = -\frac{dj\,(t)}{dt}\left[L + \frac{1}{w^2 C'}\right] + \left[-w\,L + \frac{1}{w\,C'}\right] \tag{8-23}$$

$$\left[\frac{2}{T_0}\right]\int_{t-T_0}^{t} e_N(t)\cos[w\,t + j\,(t)]dt = \frac{dI(t)}{dt}\left[L + \frac{1}{w^2 C'}\right] + \left[R_L - \overline{R_N(t)}\right]I(t) \tag{8-24}$$

The analysis of the noise signal can be accomplished by decomposing the noise signal $e_N(t)$ to an infinite number of random noise pulses represented by

$$e\,d\,(t - t_0) \tag{8-25}$$

where e is the strength of the pulse at the time instant t_0, and both e and t_0 are independent random variables from one pulse to next pulse!

The time average of the square of the current pulses over a period of time can be shown to be

$$\frac{1}{2T}\int_{-T}^{T}\left[\sum e\,d\,(t - t_0)\right]^2 dt = \overline{e_N^2(t)} \tag{8-26}$$

The mean square noise voltage $\overline{e_N^2(t)}$ is generated in the circuit in Figure 8-3.

Figure 8-5 shows the noise pulse at time instant $t = t_0$

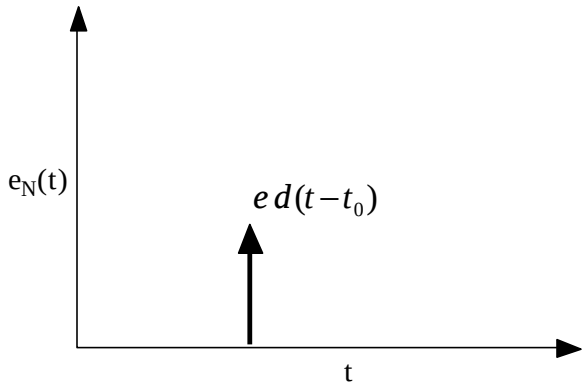

Figure 8-5 The noise pulse at $t = t_0$.

The integral of the single noise pulse above gives the rectangular pulse with the height $\left[\frac{2}{T_0}\right] e \sin[w t + j(t)]$ and the length of T_0 as shown in Figure 8-6.

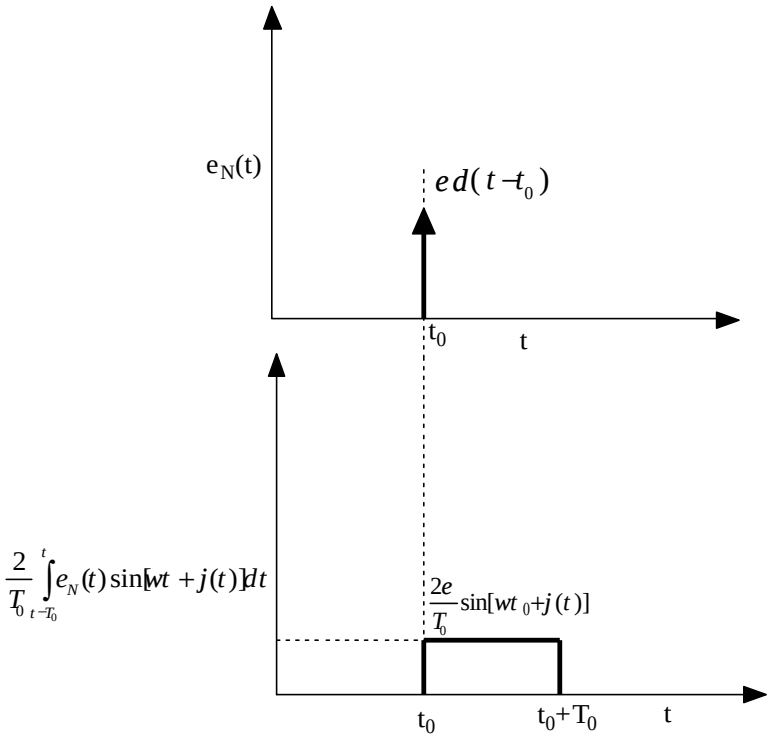

Figure 8-6 The amplitude of the rectangular pulse.

The integration of the single elementary noise pulse, following the Dirac Δ function, results in

$$\left[\frac{2}{T_0}\right]\int_{t-T_0}^{t} e_N(t)\sin[w\,t + j\,(t)]dt \approx \left[\frac{2}{T_0}\right]\int_{t-T_0}^{t} e\,d(t-t_0)\sin[w\,t + j\,(t)]dt] \tag{8-27}$$

$$\left[\frac{2}{T_0}\right]\int_{t-T_0}^{t} e\,d(t-t_0)\sin[w\,t + j\,(t)]dt \approx \left[\frac{2}{T_0}\right] e\sin[w\,t_0 + j\,(t)] \tag{8-28}$$

since the length of time T_0 is considered to be sufficiently small for any variation of $j\ (t)$ and $I(t)$ during the time T_0. The corresponding rectangular pulse of the magnitude $\frac{2}{T_0} e\sin[w\,t_0 + j\,(t)]$ is considered to be another pulse located at $t = t_0$ and can be expressed in the form of an impulse function with the amplitude $2e\sin[w\,t_0 + j\,(t)$ located at $t = t_0$ for calculating the effect using Eqs. (8-23) and (8-24).

The effect of $\left[\frac{2}{T_0}\right]\int_{t-T_0}^{t} e_N(t)\sin[w\,t + j\,(t)]dt$ is given by $[n_1(t)]$ which consists of a number of rectangular pulses. The time average of the square of these pulses, following [82], can be calculated as

$$\frac{1}{2T}\int_{t=-T}^{t=T}\left[\sum 2e\,\sin(w\,t_0 + j\,(t))d(t-t_0)\right]^2 dt = \frac{1}{T}\int_{t=-T}^{t=T}\left[\sum e\,d(t-t_0)\right]^2 dt \tag{8-29}$$

$$\overline{e_N^2(t)} = \frac{1}{2T}\int_{-T}^{T}\left[\sum e\,d(t-t_0)\right]^2 dt \tag{8-30}$$

From the equation above

$$\overline{n_1^2(t)} = 2\overline{e_N^2(t)} \tag{8-31}$$

Similarly, the total response of $\frac{2}{T_0}\int_{t-T_0}^{t} e_N(t)\cos[w\,t + j\,(t)]dt$ can be expressed by $[n_2(t)]$, which consists of a large number of such pulses and the time average of the square of these pulses is

$$\overline{n_2^2(t)} = 2\overline{e_N^2(t)} \tag{8-32}$$

since $\frac{2}{T_0}\int_{t-T_0}^{t} e_N(t)\sin[w\,t + j\,(t)]dt$ and $\frac{2}{T_0}\int_{t-T_0}^{t} e_N(t)\cos[w\,t + j\,(t)]dt$ are orthogonal functions, and in the frequency domain are the upper and lower side bands relative to the carrier, and the correlation of $[n_1(t)]$ and $[n_2(t)]$ is

$$\overline{n_1(t)n_2(t)} = 0 \tag{8-33}$$

Now consider the narrow band noise signal, which is

$$e_N(t) = e_{N1}(t) + e_{N2}(t) \tag{8-34}$$

$$e_{N1}(t) = e_1(t)\sin[w_0\,t + j\,(t)] \tag{8-35}$$

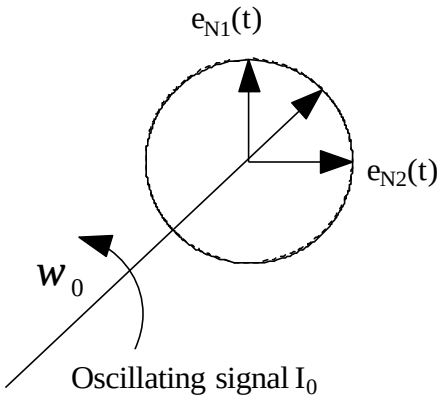

Figure 8-7 Vector presentation of the oscillator signal and its modulation by the voltages e_{N1} and e_{N2}.

$$e_{N2}(t) = -e_2(t)\cos[w_0\,t + j\,(t)] \tag{8-36}$$

where $e_{N1}(t)$ and $e_{N2}(t)$ are orthogonal function, and $e_1(t)$ and $e_2(t)$ are slowly varying function of time.

The calculation of $I_n(t)$ and $j_n(t)$ for the free running oscillator can be derived from Eqs. (8-23) & (8-24) as

$$\left[\frac{2}{IT_0}\right]\int_{t-T_0}^{t} e_N(t)\sin[w\,t + j\,(t)]dt = -\frac{dj\,(t)}{dt}\left[L + \frac{1}{w^2 C'}\right] + \left[-w\,L + \frac{1}{w\,C'}\right] \tag{8-37}$$

$$\left[\frac{2}{IT_0}\right]\int_{t-T_0}^{t} e_N(t)\sin[w\,t + j\,(t)]dt \Rightarrow \left[\frac{1}{I}\right] n_1(t) \tag{8-38}$$

at resonance frequency $w = w_0$,

$$\left\{-\frac{dj\,(t)}{dt}\left[L + \frac{1}{w^2 C'}\right] + \left[-w\,L + \frac{1}{w\,C'}\right]\right\}_{w=w_0} = -2L\frac{dj\,(t)}{dt} \tag{8-39}$$

and

$$\frac{1}{I} n_1(t) = -2L\frac{dj\,(t)}{dt} \tag{8-40}$$

$$\frac{dj\,(t)}{dt} = -\left[\frac{1}{2LI}\right] n_1(t) \tag{8-41}$$

If Eq. (8-41) is transformed in the frequency domain, $j\,(t)$ can be expressed as

$$j\,(f) = \frac{n_1(f)}{2w\,LI} \tag{8-42}$$

Now the spectral density of $[\,j\,(f)\,]$ is

$$\left|j\,(f)\right|^2 = \frac{1}{4w^2 L^2 I^2}\left|n_1(f)\right|^2 \tag{8-43}$$

$$\frac{1}{4w^2 L^2 I^2}\left|n_1(f)\right|^2 = \frac{2\left|e_N(f)\right|^2}{4w^2 L^2 I^2} \Rightarrow \left|j\,(f)\right|^2 = \frac{2\left|e_N(f)\right|^2}{4w^2 L^2 I^2} \tag{8-44}$$

where f varies from -¥ to + ¥ .

The amplitude of the current can be written as $I(t) = I_0 + \Delta I(t)$, where I_0 represents the stable operating point of the free-running oscillator with a loop gain slightly greater than 1.

From Eq. (8-24)

$\frac{2}{T_0}\int_{t-T_0}^{t} e_N(t)\cos[w\,t + j\,(t)]dt = \frac{dI(t)}{dt}\left(L + \frac{1}{w^2 C'}\right) + \left[R_L - \overline{R_N(t)}\right]I(t)$, we can calculate

$$\left[\frac{2}{T_0}\int_{t-T_0}^{t} e_N(t)\cos[w\,t + j\,(t)]dt\right]_{w=w_0} = \left[2L\frac{\partial}{\partial t}[\Delta I(t)] + \Delta I(t) I_0 g + \Delta I^2(t) g\right] \tag{8-45}$$

Since the amplitude of $\Delta I^2(t)$ is negligible, its value can be set to 0;

$$\left[2L\frac{\partial}{\partial t}[\Delta I(t)] + \Delta I(t) I_0 g + \Delta I^2(t) g\right] = 2L\frac{\partial}{\partial t}[\Delta I(t)] + \Delta I(t) I_0 g \tag{8-46}$$

$$n_2(t) = \frac{2}{T_0}\int_{t-T_0}^{t} e_N(t)\cos[w\,t + j\,(t)]dt \tag{8-47}$$

$$n_2(t) = 2L\frac{\partial}{\partial t}[\Delta I(t)] + \Delta I(t) I_0 g \tag{8-48}$$

$$n_2(f) = 2Lw\ \Delta I(f) + \Delta I(f) I_0 g \tag{8-49}$$

The spectral density of $[n_2(f)]$ is

$$\left|n_2(f)\right|^2 = [4L^2 w^2 + (I_0 g)^2]\left|\Delta I(f)\right|^2 \tag{8-50}$$

and the spectral density of $\Delta I(f)$ can be expressed in terms of $\left|n_2(f)\right|^2$ as

$$\left|\Delta I(f)\right|^2 = \frac{1}{[4L^2 w^2 + (I_0 g)^2]}\left|n_2(f)\right|^2 \tag{8-51}$$

$$\left|n_2(f)\right|^2 = 2\left|e_N(f)\right|^2 \Rightarrow \left|\Delta I(f)\right|^2 = \frac{2\left|e_N(f)\right|^2}{[4L^2 w^2 + (I_0 g)^2]} \tag{8-52}$$

since $n_1(t)$ and $n_2(t)$ are orthogonal function and there is no correlation between current and phase

$$\overline{n_1(t) n_2(t)} = 0 \Rightarrow \overline{I(t) j\,(t)} = 0 \tag{8-53}$$

The output power noise spectral density of the current is given as

$$P_{noise}(f) = 2R_L\left|I(f)\right|^2 \tag{8-54}$$

The noise spectral density of the current is given as

$$\left|I(f)\right|^2 = \int_{-\infty}^{\infty} R_I(t)\exp(-jwt)dt \tag{8-55}$$

where $R_I(t)$ is the auto-correlation function of the current and can be written as

$$R_I(t) = \overline{[I(t)I(t+t)\cos[w_0 t + j(t)]\cos[w_0(t+t) + j(t+t)]]} \tag{8-56}$$

Since $I(t)$ and $j(t)$ are uncorrelated, auto-correlation function of the current $R_I(t)$ can be given as

$$R_I(t) = \frac{1}{2}\left[I_0^2 + R_{\Delta I}(t)\right]\cos(w_0 t)\overline{[\cos(j(t+t) - j(t))]} \tag{8-57}$$

From [82], but taking into consideration that both side bands are correlated, we can write

$$R_I(t) = \frac{1}{2}\left[I_0^2 + \frac{2\left|e_N(t)\right|^2}{2Lg\ I_0}\exp\left(-\frac{g\ I_0}{2L}|t|\right)\right]\exp\left(-\frac{\left|e_N(t)\right|^2}{4L^2 I_0^2}|t|\right)\cos(w_0 t) \tag{8-58}$$

Since the publication [82] skipped many stages of the calculation, up to here, a more complete and detailed flow is shown. These results are needed to calculate the noise performance at the component level later. Note, the factor of 2, which results from the correlation.

Considering $\frac{g\ I_0}{2L} >> \frac{2\left|e_N(t)\right|^2}{4L^2 I_0^2}$, the noise spectral density of the current is given by

$$\left|I(f)\right|^2 = \int_{-\infty}^{\infty} R_I(t)\exp(-jwt)dt \tag{8-59}$$

with $I = I_0 + \Delta I(t)$; all RF-currents.

$$|I(f)|^2 = \frac{|e_N(f)|^2}{8L^2}\left[\frac{1}{(w-w_0)^2+\left(\frac{|e_N(f)|^2}{4L^2I_0^2}\right)^2}+\frac{1}{(w+w_0)^2+\left(\frac{|e_N(f)|^2}{4L^2I_0^2}\right)^2}\right]+$$

$$\frac{|e_N(f)|^2}{8L^2}\left[\frac{1}{(w-w_0)^2+\left(\frac{g\ I_0}{2L}\right)^2}+\frac{1}{(w+w_0)^2+\left(\frac{g\ I_0}{2L}\right)^2}\right] \qquad (8\text{-}60)$$

with

$$\frac{|e_N(f)|^2}{8L^2}\left[\frac{1}{(w-w_0)^2+\left(\frac{|e_N(f)|^2}{4L^2I_0^2}\right)^2}+\frac{1}{(w+w_0)^2+\left(\frac{|e_N(f)|^2}{4L^2I_0^2}\right)^2}\right]\rightarrow \text{FM noise} \qquad (8\text{-}61)$$

$$\frac{|e_N(f)|^2}{8L^2}\left[\frac{1}{(w-w_0)^2+\left(\frac{g\ I_0}{2L}\right)^2}+\frac{1}{(w+w_0)^2+\left(\frac{g\ I_0}{2L}\right)^2}\right]\rightarrow \text{ AM noise} \qquad (8\text{-}62)$$

Since $\frac{g\ I_0}{2L} >> \frac{2|e_N(t)|^2}{4L^2I_0^2}$

for $w \rightarrow w_0$, FM noise predominates over the AM noise.

For $w >> w_0$, both the FM noise and AM noise terms give equal contribution.

Considering $\omega+\omega_0 >> \omega-\omega_0$, then

$$\left|I(f)\right|^2 = \frac{\left|e_N(f)\right|^2}{8L^2}\left[\frac{1}{(w-w_0)^2+\left(\frac{\left|e_N(f)\right|^2}{4L^2I_0^2}\right)^2}+\frac{1}{(w-w_0)^2+\left(\frac{g\ I_0}{2L}\right)^2}\right] \tag{8-63}$$

$$P_{noise}(f) = 2R_L\left|I(f)\right|^2 \tag{8-64}$$

$$P_{noise}(f) = 2R_L\left(\frac{\left|e_N(f)\right|^2}{8L^2}\right)\left[\frac{1}{(w-w_0)^2+\left(\frac{\left|e_N(f)\right|^2}{4L^2I_0^2}\right)^2}+\frac{1}{(w-w_0)^2+\left(\frac{g\ I_0}{2L}\right)^2}\right] \tag{8-65}$$

Since $R_{Load} = R_L + R_o$, the effective dynamic resistance of the free running oscillator is given by

$$\sum_{effective}\left|R_{tot}\right| = R_N(t) - R_{Load}] = R_o \tag{8-66}$$

where R_o is the output resistance; $R_0 - R_{\text{tot}} = 0$.

The Q of the resonator circuit is expressed as

$$Q_L = \frac{wL}{R_0} \tag{8-67}$$

The oscillator output noise power in terms of Q is given by

$$P_{noise}(f) = \frac{w_0^2}{2Q_L^2}\frac{\left|e\right|^2}{2\overline{R_N(t)}}\left[\frac{1}{(w-w_0)^2+\left(\frac{w_0^2}{4Q_L^2}\right)^2\left(\frac{\left|e\right|^2}{2\overline{R_N(t)}P_{out}^2}\right)^2}+\frac{1}{(w-w_0)^2+\left(\frac{w_0^2}{Q_L^2}\right)\left(\frac{g\ I_0}{2\overline{R_N(t)}}\right)^2}\right] \tag{8-68}$$

Figure 8-8 shows the Colpitts oscillator with a series resonator and the small signal AC equivalent circuit. From the analytical expression of the noise analysis above, the influence of the circuit components on the phase noise can be explicitly calculated as

$$|j(f)|^2 = \frac{1}{4w^2 L^2 I_0^2(f)} |n_1(f)|^2 \tag{8-69}$$

$$\frac{1}{4w^2 L^2 I_0^2(f)} |n_1(f)|^2 = \frac{2|e_N(f)|^2}{4w^2 L^2 I_0^2(f)} \Rightarrow |j(f)|^2 = \frac{2|e_N(f)|^2}{4w^2 L^2 I_0^2(f)} \tag{8-70}$$

where the frequency f varies from -¥ to +¥ .

The resulting single sideband phase noise is

$$£ = \frac{|e_N(f)|^2}{4w^2 L^2 I_0^2(f)} \tag{8-71}$$

The unknown variables are $|e_N(f)|^2$ and $I_0^2(f)$, which need to be determined next. $I_0^2(f)$ will be transformed into $I_{c0}^2(f)$ by multiplying $I_0^2(t)$ with the effective current gain $Y_{21}^+/Y_{11}^+ = b^+$.

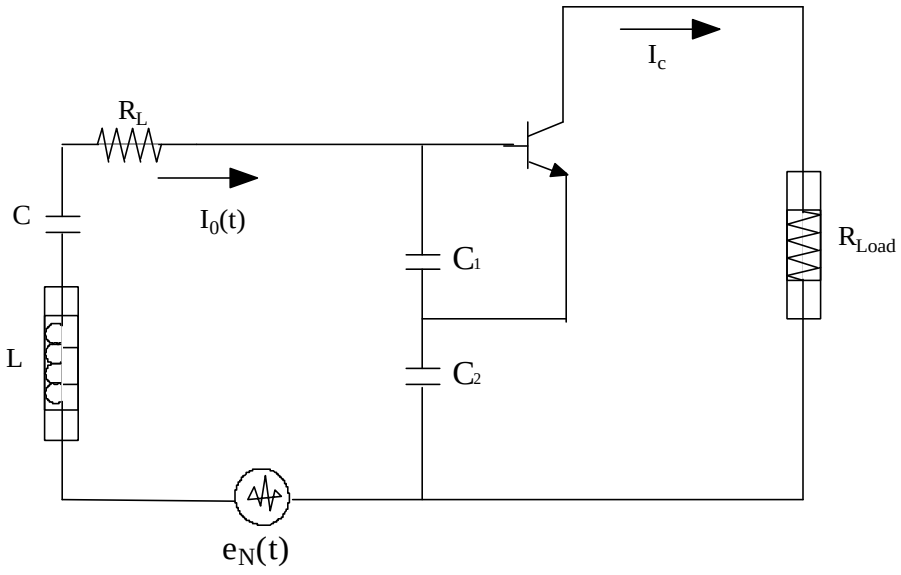

Figure 8-8 Colpitts oscillator with series resonator and small signal AC equivalent circuit.

Calculation of $I_{c0}^2(f)$

From Figure 8-8, the LC-series resonant circuit is in shunt between the base and the emitter with the capacitive negative conductance portion of the transistor. We now introduce a collector load R_{Load} at the output, or better yet, an impedance Z.

The oscillator base current *i*(t) is

$$i(t) = |I_0| \cos(w\,t) = \frac{V_{bc}(t)}{Z} \tag{8-72}$$

and the collector current is

$$|I_{c0}| = \left| \frac{[0.7 - V_{ce}]}{R_{Load} + j\left(w\,L - \dfrac{1}{w\,C_{IN}}\right)} \right| \approx \left| \frac{V_{ce}}{R_{Load} + j\left(w\,L - \dfrac{1}{w\,C_{IN}}\right)} \right|, \text{ or} \tag{8-73}$$

$$\overline{I_{c0}^2(f)} \approx \left\{ \frac{\overline{V_{ce}^2(f)}}{[R_{Load}]^2 + \left(w\,L - \dfrac{1}{w\,C_{IN}}\right)^2} \right\} = \left\{ \frac{\overline{V_{ce}^2(f)}}{\left[\dfrac{w\,L}{Q}\right]^2 + \left(w\,L - \dfrac{1}{w\,C_{IN}}\right)^2} \right\} \tag{8-74}$$

The voltage V_{ce} is the RF voltage across the collector-emitter terminals of the transistor. Considering the steady-state oscillation $w \to w_0$, the total loss resistance is compensated by the negative resistance of the active device as $R_L = \overline{R_N(t)}$. The expression of $\left|\overline{I_{c0}^2(f)}\right|_{w=w_0}$ is

$$\left|\overline{I_{c0}^2(f)}\right|_{w=w_0} = \left| \frac{\overline{V_{ce}^2(f)}}{\left[\dfrac{w_0\,L}{Q}\right]^2 + \left(w_0\,L - \dfrac{1}{w_0\,C_{IN}}\right)^2} \right| = \left| \frac{\overline{V_{ce}^2(f)}}{(w_0\,L)^2 \left[\dfrac{1}{Q^2} + \left(1 - \dfrac{1}{w_0^2\,LC_{IN}}\right)^2\right]} \right| \tag{8-75}$$

$$\left|\overline{I_{c0}^2(f)}\right|_{w=w_0} = \left| \frac{\overline{V_{ce}^2(f)}}{(w_0 L)^2 \left[\frac{1}{Q^2} + \left(1 - \frac{1}{w_0^2 L} \frac{C_1 + C_2}{C_1 C_2} \right)^2 \right]} \right| \tag{8-76}$$

where C_{IN} is the equivalent capacitance of the negative resistor portion of the oscillator circuit.

$$C' = \frac{CC_{IN}}{C + C_{IN}}, \; C_{IN} = \frac{C_1 C_2}{C_1 + C_2} \tag{8-77}$$

$$Q = \frac{w L}{R_L} \tag{8-78}$$

For a reasonably high Q resonator $\left|\overline{I_{c0}^2(f)}\right|_{w=w_0} \propto [C_{IN}]_{w=w_0}$

Calculation of the Noise Voltage $e_N(f)$

The equivalent noise voltage from the negative resistance portion of the oscillator circuit is given an open-circuit noise voltage [EMF] of the circuit as shown in Figure 8-9 below.

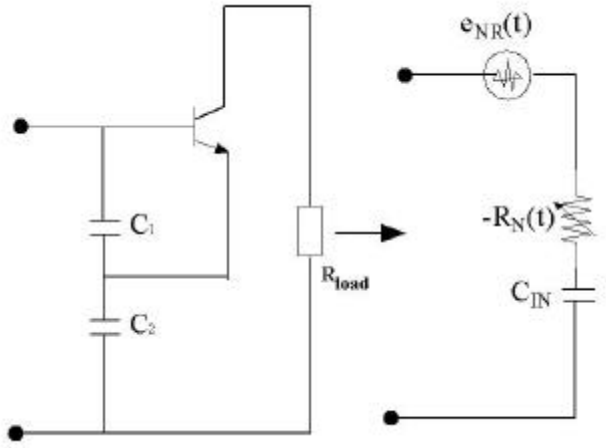

Figure 8-9 Equivalent representation of negative resistance portion of the circuit at the input for the open circuit noise voltage.

The noise voltage associated with the resonator loss resistance R_s is

$$\left|\overline{e_R^2(f)}\right|_{w=w_0} = 4kTBR_s \tag{8-79}$$

R_s denotes the equivalent series loss resistor, which can be calculated from the parallel loading resistor R_{load} , see Figure 8-9.

$$\left|\overline{e_R^2(f)}\right|_{w=w_0} = 4kTR \text{ for B = 1 Hz bandwidth} \tag{8-80}$$

The total noise voltage power within 1 Hz bandwidth can be given as

$$\left|\overline{e_N^2(f)}\right|_{w=w_0} = \overline{e_R^2(f)} + \overline{e_{NR}^2(f)} \tag{8-81}$$

After some lengthy calculations and adding shot noise, flicker noise, the loss resistor, and a drive level dependent current gain, we obtain

$$\left|\overline{e_N^2(f)}\right|_{w=w_0} = [4kTR] + \left[\frac{4qI_{c0}g_m^2 + \frac{K_f I_b^{AF}}{\Delta w} g_m^2}{w_0^2 C_1^2 (w_0^2 (b^+)^2 C_2^2 + g_m^2 \frac{C_2^2}{C_1^2})}\right] \tag{8-82}$$

where

$$b^+ = \left[\frac{Y_{21}^+}{Y_{11}^+}\right]\left[\frac{C_1}{C_2}\right]^p$$

$$g_m = \left[Y_{21}^+\right]\left[\frac{C_1}{C_2}\right]^q, \text{ redefined}$$

The values of p and q depend upon the drive level.

The flicker noise contribution in Eq. (8-82) is introduced by adding term $\frac{K_f I_b^{AF}}{\Delta w}$ in I_{c0}, where K_f is the flicker noise coefficient and *AF* is the flicker noise exponent. This is valid only for the bipolar transistor. For an FET, the equivalent currents have to be used.

The first term in the expression above is related to the thermal noise due to the loss resistance of the resonator tank and the second term is related to the shot noise and flicker noise in the transistor.

Now, the phase noise of the oscillator can be expressed as

$$\left|\overline{j^{2}(w)}\right| = \frac{2\left|\overline{e_N^2(w)}\right|}{4w_0^2 L^2 I_0^2(w)} \tag{8-83}$$

$$\left|\overline{j^{2}(w)}\right|_{SSB} = \frac{1}{2}\left|\overline{j^{2}(w)}\right| = \frac{\left|\overline{e_N^2(w)}\right|}{4w_0^2 L^2 I_0^2(w)} \tag{8-84}$$

$$\left|\overline{j^{2}(w)}\right|_{SSB} = \left\{[4kTR] + \left[\frac{4qI_c g_m^2 + \frac{K_f I_b^{AF}}{w} g_m^2}{w_0^2 C_1^2 (w_0^2 (b^+)^2 C_2^2 + g_m^2 \frac{C_2^2}{C_1^2})}\right]\right\}\left[\frac{(w_0)^2\left[\frac{1}{Q^2} + \left(1 - \frac{1}{w_0^2 L}\frac{C_1 + C_2}{C_1 C_2}\right)^2\right]}{4w^2\left|V_{ce}^2(w)\right|}\right] \tag{8-85}$$

$$\left|\overline{j^{2}(w)}\right|_{SSB} = \left[4kTR + \left[\frac{4qI_c g_m^2 + \frac{K_f I_b^{AF}}{w} g_m^2}{w_0^2 C_1^2 (w_0^2 (b^+)^2 C_2^2 + g_m^2 \frac{C_2^2}{C_1^2})}\right]\right]\left[\frac{w_0^2}{4w^2 V_{ce}^2}\right]\left[\frac{1}{Q^2} + \left(1 - \frac{1}{w_0^2 L}\frac{C_1 + C_2}{C_1 C_2}\right)^2\right] \tag{8-86}$$

Considering $\left(\frac{1}{w_0^2 L}\frac{C_1 + C_2}{C_1 C_2}\right) >> 1$; for $w_0 = 2p\ f = 6.28E9$ Hz, L = 1E-9F, C_1 = 1E-12F, C2 = 1E-12F

$$\left(\frac{1}{w_0^2 L}\frac{C_1 + C_2}{C_1 C_2}\right) = 50.7$$

Since the phase noise is always expressed in dBc/Hz, we now calculate, after simplification of Eq. (8-86),

$$\pounds(w) = 10Log\left\{\left[4kTR + \left[\frac{4qI_c g_m^2 + \frac{K_f I_b^{AF}}{w} g_m^2}{w_0^2 C_1^2 (w_0^2 (b^+)^2 C_2^2 + g_m^2 \frac{C_2^2}{C_1^2})}\right]\right]\left[\frac{w_0^2}{4w^2 V_{cc}^2}\right]\left[\frac{1}{Q^2} + \frac{[C_1 + C_2]^2}{C_1^2 C_2^2 w_0^4 L^2}\right]\right\} \tag{8-87}$$

For the bias condition (which is determined from the output power requirement), the loaded quality factor, and the device parameters [transconductance and b^{+}], the best phase noise can be found by differentiating $\left|\overline{j^{2}(w)}\right|_{SSB}$ with respect to $\frac{C_1}{C_2}$.

Considering that all the parameters of $\left|\overline{j^{2}(w)}\right|_{SSB}$ are constants for a given operating condition (except the feedback capacitor), the minimum value of the phase noise can be determined for any fixed value of C_1 as

$$\left|\overline{j^{2}(w)}\right| = \left[k_0 + \frac{k_1}{k_2 C_1^2 C_2^2 + k_3 C_2^2}\right]\left[\frac{C_1 + C_2}{C_1 C_2}\right]^2 \tag{8-88}$$

$$k_0 = \frac{kTR}{w^2 w_0^2 L^2 V_{ce}^2} \tag{8-89}$$

$$k_1 = \frac{qI_{c0}g_m^2 + \frac{K_f I_b^{AF}}{w} g_m^2}{w^2 w_0^2 L^2 V_{ce}^2} \tag{8-90}$$

$$k_2 = w_0^4 (b^{+})^2 \tag{8-91}$$

$$k_3 = g_m^2 \tag{8-92}$$

Where k_1, k_2, and k_3, are constant only for a particular drive level, with $y = \frac{C_1}{C_2}$. Making k_2 and k_3 also dependent on y, as the drive level changes, the final noise equation is

$$£(w) = 10 \times \log\left[\left[k_0 + \left(\frac{k^3 k_1 \left[\frac{Y_{21}^{+}}{Y_{11}^{+}}\right]^2 [y]^{2p}}{\left[Y_{21}^{+}\right]^3 [y]^{3q}}\right)\left(\frac{1}{(y^2 + k)}\right)\right]\left[\frac{[1+y]^2}{y^2}\right]\right] \tag{8-93}$$

where

$$k_0 = \frac{kTR}{w^2 w_0^2 L^2 V_{cc}^2}$$

$$k_1 = \frac{qI_c g_m^2 + \dfrac{K_f I_b^{AF}}{w} g_m^2}{w^2 w_0^4 L^2 V_{cc}^2} \qquad k_2 = w_0^2 (b^+)^2$$

Figure 8-10 shows the simulated phase noise and its minimum for two values of C_1, 2pF and 5pF. 5pF provides a better phase noise and a flatter response. For larger C_1, the oscillator will cease to oscillate.

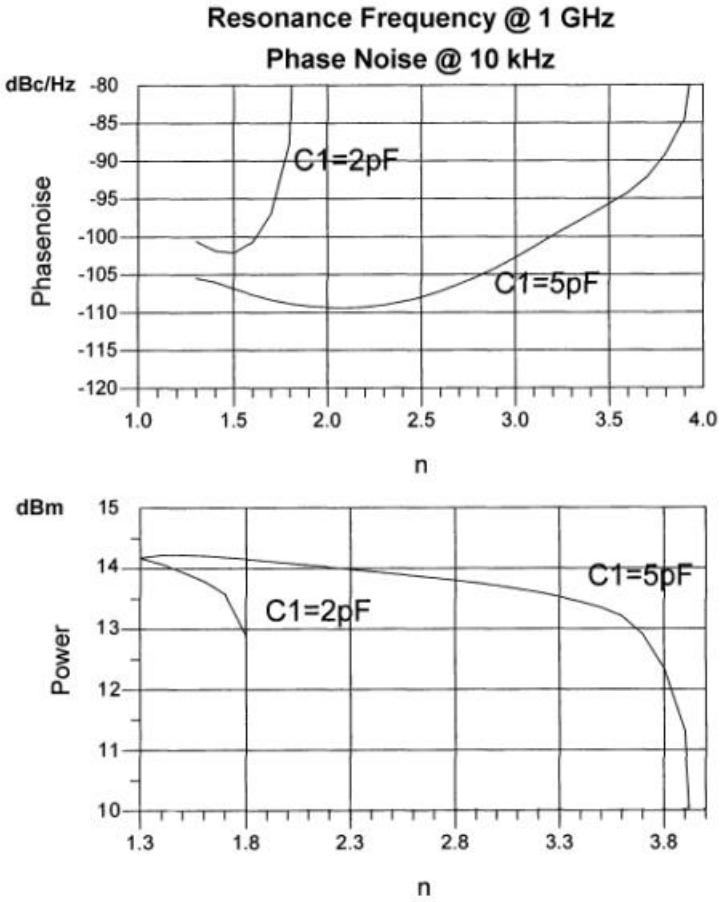

Figure 8-10 Phase noise vs. *n* and output power.

$$\frac{\partial \left| f^2(w, y, k) \right|}{\partial y} \Rightarrow 0$$

$$\frac{\partial}{\partial y}\left\{\left[k_0 + \left(\frac{k^3 k_1 \left[\dfrac{Y_{21}^+}{Y_{11}^+}\right]^2 [y]^{2p}}{\left[Y_{21}^+\right]^3 [y]^{3q}}\right)\left(\frac{1}{(y^2+k)}\right)\right]\left[\frac{[1+y]^2}{y^2}\right]\right\}_{y=m} \Rightarrow 0 \qquad (8\text{-}94)$$

From curve-fitting attempts, the following values for q and p in Eq. 8-94 were determined:

$$q=1 \text{ to } 1.1;\ p = 1.3 \text{ to } 1.6.$$

q and p are a function of the normalized drive level x and need to be determined experimentally.

The transformation factor n is defined as

$$n=1+\frac{C_1}{C_2}\rightarrow 1+y \tag{8-95}$$

The following plot in Figure 8-11 shows the predicted phase noise resulting from Eq. (8-94). For the first time, the flicker corner frequency was properly implemented and gives answers consistent with the measurements. In the following section all the noise sources will be added, but the key contributors are still the resonator noise and the flicker noise. The Shottky noise dominates further out. The break point for the flicker noise can be clearly seen.

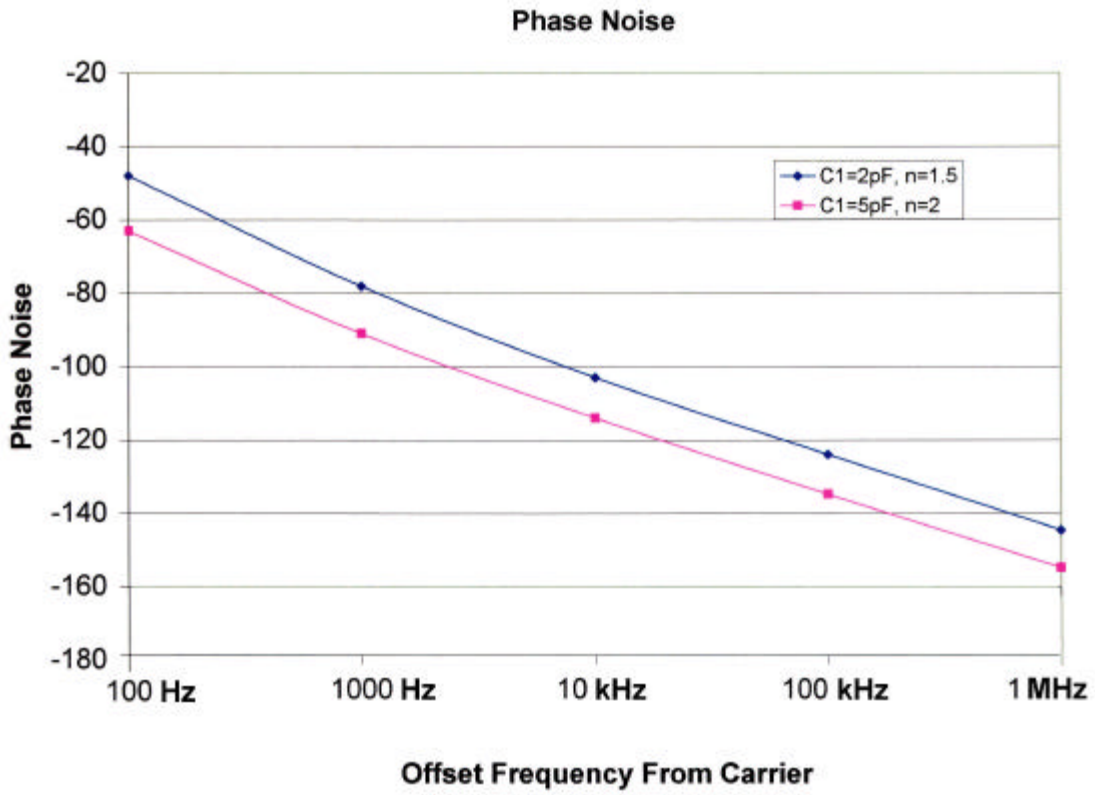

Figure 8-11 Using Eq. (8-94), the phase noise for different values of *n* for constant C_2 can be calculated.

Summary Results

The analysis of the oscillator in the time domain has given us a design criteria to find the optimum value of $y = \frac{C_1}{C_2}$ with values for y + 1 or n ranging from 1.5 to 4. For values above 3.5, the power is reduced significantly.

Consistent with the previous chapters, we note

$$C_1 = C_1^* \pm X(C_P \; or \; L_P) \tag{8-96}$$

$$X(C_{be} \; or \; L_b) \rightarrow C_P \; or \; L_P \tag{8-97}$$

In the case of a large value of C_P (C_P>C_1), X_1 has to be inductive to compensate extra contributions of the device package capacitance to meet the desired value of C_1!

The following is a set of design guides to calculate the parameters of the oscillator.

$$w = \sqrt{\frac{1}{L\left[\frac{C_1 C_2}{C_1 + C_2} + C\right]}} \tag{8-98}$$

$$\left|R_n(L_P = 0)\right| = \frac{Y_{21}}{w^2 C_1 C_2} \tag{8-99}$$

$$C_1 = \frac{1}{w_0} \sqrt{\frac{Y_{11}}{K}} \tag{8-100}$$

C_2 is best be determined graphically from the noise plot.

$$C_C > \left\{\frac{(w^2 C_1 C_2)(1 + w^2 Y_{21}^2 L_P^2)}{[Y_{21}^2 C_2 - w^2 C_1 C_2)(1 + w^2 Y_{21}^2 L_P^2)(C_1 + C_P + C_2)]}\right\} \tag{8-101}$$

$$\frac{C}{10} \geq [C_C]_{L_P=0} > \left[\frac{(w^2 C_1 C_2)}{[Y_{21}^2 C_2 - w^2 C_1 C_2)(C_1 + C_P + C_2)]}\right] \tag{8-102}$$

The phase noise in dBc/Hz is shown as

$$\pounds(w) = 10 \times \log\left[\left[\left[k_0 + \left(\frac{k^3 k_1 \left[\frac{Y_{21}^+}{Y_{11}^+}\right]^2 [y]^{2p}}{\left[Y_{21}^+\right]^3 [y]^{3q}}\right)\left(\frac{1}{(y^2+k)}\right)\right]\left[\frac{[1+y]^2}{y^2}\right]\right]\right] \tag{8-103}$$

The phase noise improves with the square of the loaded Q_L! 10% higher Q $\rightarrow$ 20% better phase noise!

$$L(w) \propto \frac{1}{C_{IN}^2} \tag{8-104}$$

The loaded Q of the resonator determines the minimum possible level of the oscillator phase noise for given bias voltage and oscillator frequency.

To achieve close to this minimum phase noise level set by the loaded Q_L of the resonator, the optimum (rather, how large the value of the C_{IN} can be) value of C_{IN} is to be fixed.

To achieve the best possible phase noise level, the feedback capacitors C_1 and C_2 should be made as large as possible, but still generate sufficient negative resistance for sustaining steady-state oscillation.

$$[-R_N]_{negative\ resistance} \propto \frac{1}{w_0^2}\frac{1}{C_1 C_2}, \text{ (no parasitics)} \tag{8-105}$$

The negative resistance of the oscillator circuit is inversely proportional to the feedback capacitors. Therefore, the limit of the feedback capacitor value is determined by the minimum negative resistance for a loop gain greater than unity.

From the phase noise equation discussed, the feedback capacitor C_2 has more influence compared to C_1. The drive level and conduction angle of the Colpitts oscillator circuit is a strong function of C_2.

The time domain approach has provided us with the design guide for the key components of the oscillator; however, it did not include all the noise sources of the transistor. By using the starting parameters, such as C_1 and C_2 and the bias point, as well as the information about the resonator and the transistor, a complete noise model/analysis will be shown in Section 8.5.

8.5 Phase Noise Analysis Based on the Feedback Model

Up to here we have calculated both the large-signal drive condition, as well as the optimum choice of the feedback capacitance. Now, we are going to consider the oscillator as a feedback loop with a noisy transistor, looking at all typical noise contributions. Based on a fixed set of values of C_1 and C_2, we can now calculate the accurate phase-noise behavior of the oscillator and analyze the various noise contributions.

First, the noisy bipolar transistor will be introduced. Figure 8-12 shows the familiar hybrid-π transistor circuit and Figure 8-13 shows the equivalent circuit with the relevant noise sources included.

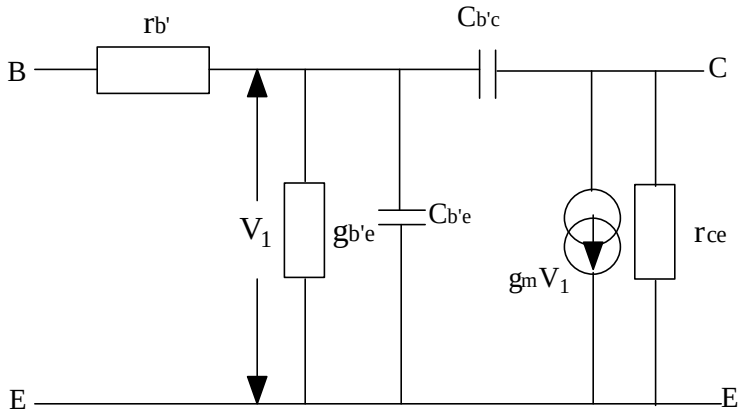

Figure 8-12 Grounded emitter bipolar transistor.

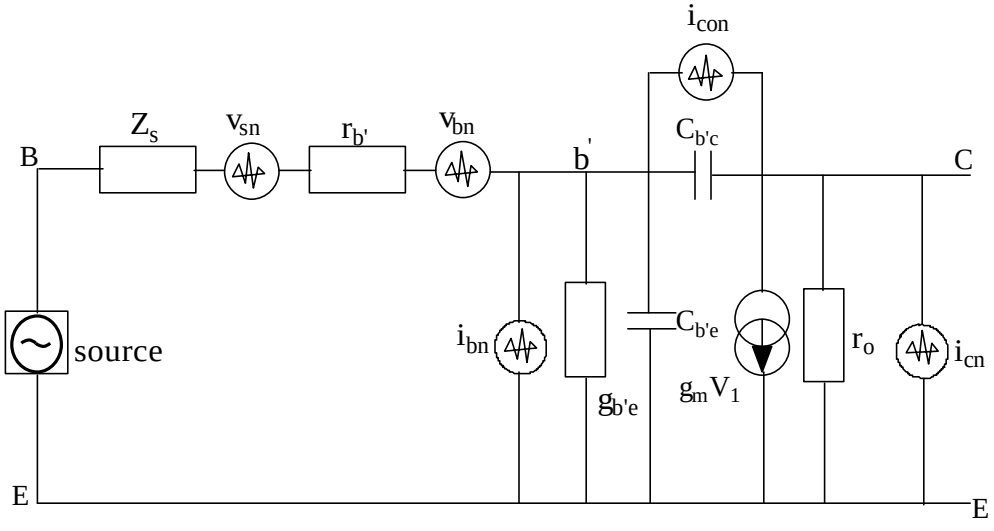

Figure 8-13 Hybrid-π configuration of the grounded bipolar transistor with noise sources.

The mean square value of the noise generators in Figure 8-13, in a narrow frequency offset Δf, are given by

$$\overline{i_{bn}^2} = 2qI_b\Delta f \tag{8-106}$$

$$\overline{i_{cn}^2} = 2qI_c\Delta f \tag{8-107}$$

$$\overline{i_{con}^2} = 2qI_{cob}\Delta f \tag{8-108}$$

$$\overline{v_{bn}^2} = 4kTR_b\Delta f \tag{8-109}$$

$$\overline{v_{sn}^2} = 4kTR_S\Delta f \tag{8-110}$$

where I_b, I_c, and I_{cob} are average DC currents over the Δf noise bandwidth.

The noise power spectral densities due to these noise sources are

$$S(i_{cn}) = \frac{\overline{i_{cn}^2}}{\Delta f} = 2qI_c = 2KTg_m \tag{8-111}$$

$$S(i_{bn}) = \frac{\overline{i_{bn}^2}}{\Delta f} = 2qI_b = \frac{2KTg_m}{b} \tag{8-112}$$

$$S(i_{fn}) = \frac{K_f I_b^{AF}}{f} \tag{8-113}$$

$$S(v_{bn}) = \frac{\overline{v_{bn}^2}}{\Delta f} = 4KTr_b' \tag{8-114}$$

$$S(v_{sn}) = \frac{\overline{v_{sn}^2}}{\Delta f} = 4KTR_s \tag{8-115}$$

where r_b' and R_s are base and source resistance and Z_s is the complex source impedance.

Figure 8-14 shows the feedback arrangement for the Colpitts oscillator with the noise sources.

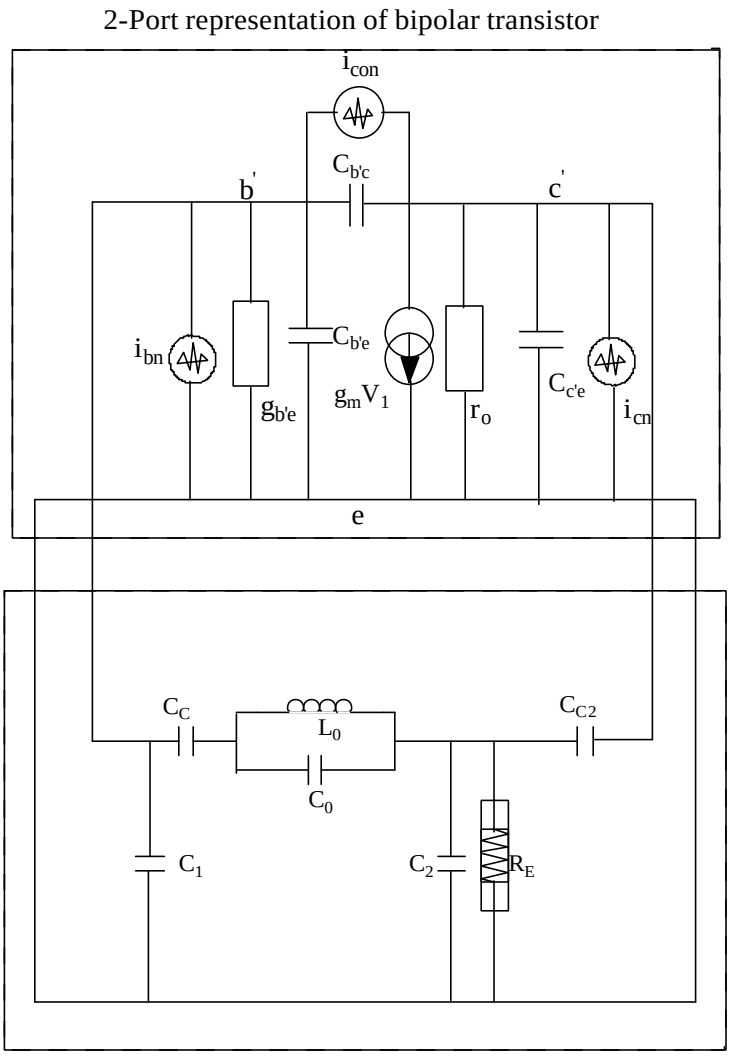

Figure 8-14 Feedback arrangement for the Colpitts oscillator with the noise sources.

The transistor is acting like a gain block. The feedback network includes the load conductance and a small part of the output signal goes to the input of the bipolar transistor through the resonant circuit. The ABCD chain matrix will be used for the analysis.

Figure 8-15 shows the linear representation of the Colpitts oscillator with the input white noise source i_n (w).

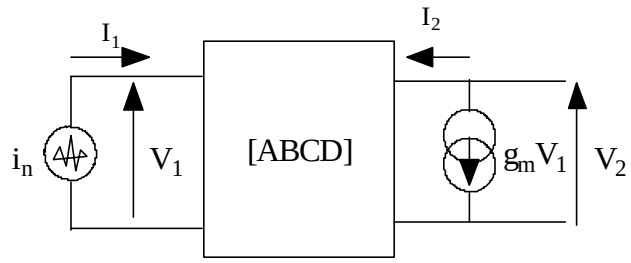

Figure 8-15 Linear representation of feedback Colpitts oscillator with input white noise source i_n (w). This is not consistent with Figure 8-14, but useful because all non-active components are now in the feedback network.

The input noise power spectral density can be given as

$$S_{in} = \frac{\left|\overline{i_n^2}\right|}{\Delta f} \tag{8-116}$$

where

$$\left|\overline{i_n^2}\right| = \sum_{i=1}^{i=N}\left|\overline{i_{ni}^2}\right| = \left|\overline{i_{n1}^2}\right| + \left|\overline{i_{n2}^2}\right| + \left|\overline{i_{n3}^2}\right| ..... + 2C_{ii}[i_{ni}i_{n(i+1)}^{\bullet}] \tag{8-117}$$

and C_{ii} is the noise correlation coefficient.

The [ABCD] matrix of above oscillator circuit can be given as

$$[A] = 1 + \left[\left(\frac{1}{jw\,C_c} + \frac{jw\,L_0}{1 - w^2 L_0 C_0}\right)\left(jw\,C_2 + \frac{1}{R_E}\right)\right]$$

$$[B] = \frac{1}{jw\,Cc_2} + \left(\frac{1}{jw\,C_c} + \frac{jw\,L_0}{1 - w^2 L_0 C_0}\right)\left[1 + \left(jw\,C_2 + \frac{1}{R_E}\right)\left(\frac{1}{jw\,Cc_2}\right)\right]$$

$$[C] = jw\,C_1 + \left(jw\,C_2 + \frac{1}{R_E}\right)\left[1 + jw\,C_1\left(\frac{1}{jw\,C_c} + \frac{jw\,L_0}{1 - w^2 L_0 C_0}\right)\right]$$

$$[D] = \frac{C_1}{Cc_2} + \left[\left(1 + jw\,C_1\left(\frac{1}{jw\,C_c} + \frac{jw\,L_0}{1 - w^2 L_0 C_0}\right)\right)\left(1 + \left(jw\,C_2 + \frac{1}{R_E}\right)\left(\frac{1}{jw\,Cc_2}\right)\right)\right] \tag{8-118A}$$

$$\begin{bmatrix} V_1 \\ I_1 \end{bmatrix} = \begin{bmatrix} A & B \\ C & D \end{bmatrix} = \begin{bmatrix} V_2 \\ -I_2 \end{bmatrix} \tag{8-118B}$$

$$V_1 = AV_2 - BI_2 \tag{8-119}$$

$$I_1 = CV_2 - DI_2 \tag{8-120}$$

$$Z_{in} = \left[\frac{V_1}{I_1}\right]_{I_{2=0}} = \frac{A}{C} \tag{8-121}$$

where

$$I_1 = i_n \tag{8-122}$$

$$I_2 = -g_m V_1 \tag{8-123}$$

The equivalent input noise voltage due to the input noise current, $I_1 = i_n$, is

$$v_n(w) = I_1 Z_{in} = I_1 \left[\frac{V_1}{I_1}\right]_{I_{2=0}} = I_1 \left[\frac{A(w)}{C(w)}\right] = i_n \left[\frac{A(w)}{C(w)}\right] \tag{8-124}$$

The input noise voltage $v_n(w)$ will produce two narrowband (1 Hz) uncorrelated components in the frequency domain located at w-w_0 and w+w_0 as $[v_n(w)]_{w=w_0-\Delta w}$ and $[v_n(w)]_{w=w_0+\Delta w}$.

In presence of the two uncorrelated components of the input noise voltage, $[v_n(w)]_{w=w_0-\Delta w}$ and $[v_n(w)]_{w=w_0+\Delta w}$, the peak carrier signal of amplitude V_c at frequency $\omega = \omega_0$ is modulated with a input phase noise signal $S_{\Delta j_{in}}(w)$.

The input phase noise spectral density at an offset of $\Delta\omega$ is

$$S_{\Delta j_{in}}(\Delta w) = \frac{\left|\overline{[v_n(w)]^2_{w=w_0-\Delta w}}\right| + \left|\overline{[v_n(w)]^2_{w=w_0+\Delta w}}\right|}{\left|\overline{V_c^2(w)}\right|} \tag{8-125}$$

$$S_{\Delta j_{in}}(\Delta w) \cong \frac{2\left|\overline{[v_n(w)]^2}\right|}{\left|\overline{V_c^2(w)}\right|} \tag{8-126}$$

$$S_{\Delta j_{in}}(\Delta w) = \frac{2\left|\overline{[v_n(w)]^2}\right|}{\left|\overline{V_c^2(w)}\right|} = 2\frac{\left|\overline{[i_n(w)]^2}\right|}{\left|\overline{V_c^2(w)}\right|}\frac{\left|\overline{A^2(w)}\right|}{\left|\overline{C^2(w)}\right|} \tag{8-127}$$

$$\left|\overline{i_n^2}\right| = S_{in}\Delta f \tag{8-128}$$

$$\left|\overline{i_n^2}\right|_{\Delta f=1Hz} = S_{in} \tag{8-129}$$

$$S_{\Delta j_{in}}(\Delta w) = 2\frac{S_{in}}{\left|\overline{V_c^2(w)}\right|}\frac{\left|\overline{A^2(w)}\right|}{\left|\overline{C^2(w)}\right|} \tag{8-130}$$

where S_{in} and $S_{\Delta j_{in}}$ are the input noise power and phase noise spectral density.

Based on [70, 83]

$$S_{\Delta j_{out}}(w) = S_{\Delta j_{in}}(w)\left[1+\frac{1}{(w^2)}\left(\frac{w_0}{2Q_L}\right)^2\right] \tag{8-131}$$

$$Q_L(w=w_0) = \frac{w_0}{2}\left|\frac{dj}{dw}\right|_{w=w_0} \tag{8-132}$$

The open loop gain is

$$G_{open}(w=w_0) = -\left[\frac{g_m}{C(w_0)}\right] \tag{8-133}$$

For sustained oscillation $G_{open}(w=w_0)=1.\quad -\left[\frac{g_m}{C(w_0)}\right]=1 \Rightarrow C(w)_{w=w_0}$ is real and negative.

$$C(w_0) = C_{Real}(w_0) + jC_{Imag}(w_0) \tag{8-134}$$

$$C_{Imag}(w_0) = 0 \tag{8-135}$$

$$C_{Real}(w_0) = -g_m \tag{8-136}$$

$$\left[\frac{dj}{dw}\right]_{w=w_0} \approx -\frac{1}{C_{Real}(w_0)}\left[\frac{dC_{Imag}(w)}{dw}\right]_{w=w_0} \tag{8-137}$$

$$Q_L(w = w_0) = \frac{w_0}{2}\left|\frac{dj}{dw}\right|_{w=w_0} \tag{8-138}$$

$$Q_L(w = w_0) = \frac{w_0}{2}\left|\frac{1}{C_{Real}(w_0)}\left[\frac{dC_{Imag}(w)}{dw}\right]\right|_{w=w_0} \tag{8-139}$$

$$S_{\Delta j_{out}}(\Delta w) = S_{\Delta j_{in}}(\Delta w)\left[1 + \frac{1}{(\Delta w^2)}\left[\frac{C_{Real}(w_0)}{\left(\frac{dC_{Imag}(w)}{dw}\right)}\right]^2_{w=w_0}\right] \tag{8-140}$$

$$S_{\Delta j_{in}}(\Delta w) = 2\frac{S_{in}}{\left|\overline{V_c^2(w)}\right|}\frac{\left|\overline{A^2(w)}\right|}{\left|\overline{C^2(w)}\right|} \tag{8-141}$$

$$S_{\Delta j_{out}}(\Delta w) = 2\frac{S_{in}}{\left|\overline{V_c^2(w_0)}\right|}\frac{\left|\overline{A^2(w_0)}\right|}{\left|\overline{C^2(w_0)}\right|}\left[1 + \frac{1}{(\Delta w^2)}\left[\frac{C_{Real}(w_0)}{\left(\frac{dC_{Imag}(w)}{dw}\right)}\right]^2_{w=w_0}\right] \tag{8-142}$$

We now perform the noise analysis of the Colpitts oscillator.

Individual Contribution of all Four Noise Sources

The following contribute to the noise of the oscillator:

- thermal noise associated with the loss resistance of the resonator
- thermal noise associated with the base resistance of the transistor
- shot noise associated with the base bias current, and
- shot noise associated with the collector bias current.

If we now use the oscillator circuit with a noisy resonator, we can calculate the total noise of the oscillator as shown in Figure 8-16.

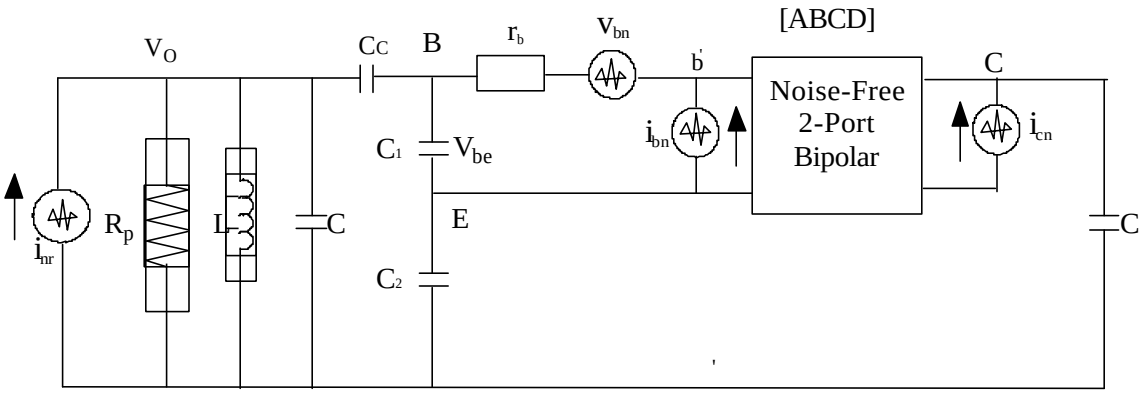

Figure 8-16 The oscillator circuit with 2-port [ABCD] matrix, consistent with the approach of Figure 8-15.

Noise Shaping Function of the Resonator

For phase noise analysis, the oscillator is considered as a feedback system and a noise source is present in the input as shown in the Figure 8-17.

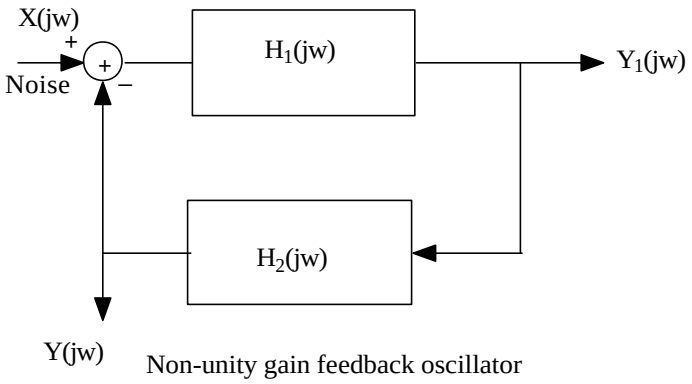

Non-unity gain feedback oscillator

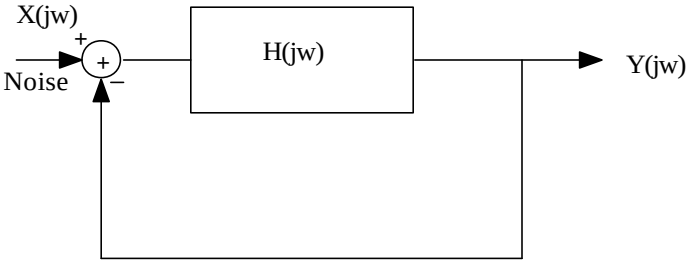

Unity gain feedback oscillator

Figure 8-17 Feedback oscillator with noise source.

Oscillator output phase noise is a function of

- the amount of the source noise present at the input of the oscillator circuit, and
- how much the feedback system rejects or amplifies various noise components.

The unity-gain system closed loop transfer function is

$$[TF(jw)]_{closed-loop} = \frac{Y(jw)}{X(jw)} = \frac{H(jw)}{1+H(jw)} \tag{8-143}$$

$$[H(jw)]_{w=w_0} = -1 \tag{8-144}$$

For frequencies close to $w = \Delta w + w_0$, the open loop transfer function is

$$[H(jw)]_{w=w_0+\Delta w} \approx \left[H(jw_0) + \Delta w \frac{dH(jw)}{dw} \right] \tag{8-145}$$

The noise transfer function is

$$\left[\frac{Y(jw+j\Delta w)}{X(jw+j\Delta w)}\right]=\left[\frac{H(jw_0)+\Delta w\frac{dH(jw)}{dw}}{1+H(jw_0)+\Delta w\frac{dH(jw)}{dw}}\right] \tag{8-146}$$

Since $H(jw_0)$ = -1 and for most practical case $\Delta w\frac{dH(jw)}{dw}$ <<1, we can write

$$\left[\frac{Y(jw+j\Delta w)}{X(jw+j\Delta w)}\right]\approx\left[\frac{-1}{\Delta w\frac{dH(jw)}{dw}}\right] \tag{8-147}$$

From the noise transfer function it appears that the noise component at $w=\Delta w+w_0$ is multiplied by the term $\left[\frac{-1}{\Delta w\frac{dH(jw)}{dw}}\right]$, relative to the output.

The broadband white noise is shaped by the resonator as seen in Figure 8-18.

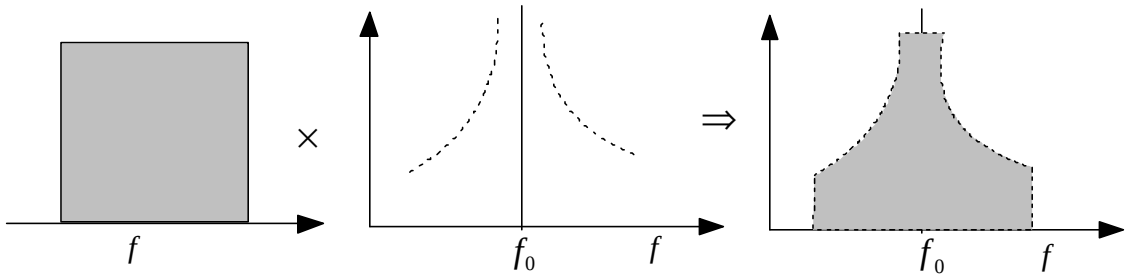

Figure 8-18 Noise shaping in the oscillator.

Therefore, the noise power spectral density can be explained as

$$\left|\frac{Y(jw+j\Delta w)}{X(jw+j\Delta w)}\right|^2=\left|\frac{-1}{\Delta w\frac{dH(jw)}{dw}}\right|^2 \tag{8-148}$$

$$\text{for } H(jw) = A(jw)\exp[jf(jw)] \tag{8-149}$$

$$\frac{dH(jw)}{dw} = \left[\frac{dA(jw)}{dw} + jA(jw)\frac{df(jw)}{dw}\right]\exp[jf(jw)] \tag{8-150}$$

Assume $w = \Delta w + w_0$, $w \to w_0$ and $|A(jw_0)| \to 1$ then the above equation is reduced to

$$\left|\frac{Y(jw + j\Delta w)}{X(jw + j\Delta w)}\right|^2 = \left[\frac{1}{(\Delta w)^2\left\{\left[\frac{dA(jw)}{dw}\right]^2 + \left[\frac{df(jw)}{dw}\right]^2\right\}}\right]_{w=\Delta w + w_0} \tag{8-151}$$

The open loop Q_L becomes

$$Q_L = \frac{w_0}{2}\sqrt{\left[\frac{dA(jw)}{dw}\right]^2 + \left[\frac{df(jw)}{dw}\right]^2} \tag{8-152}$$

and

$$\left|\frac{Y(jw + j\Delta w)}{X(jw + j\Delta w)}\right|^2 = \left[\frac{1}{(\Delta w)^2\left\{\left[\frac{dA(jw)}{dw}\right]^2 + \left[\frac{df(jw)}{dw}\right]^2\right\}}\right]_{w=\Delta w + w_0} = \frac{1}{4Q_L^2}\left[\frac{w_0}{\Delta w}\right]^2 \tag{8-153}$$

For the LC resonator $\left[\frac{dA(jw)}{dw}\right]$ at resonance ($w \to w_0$) becomes zero and $Q_L = \frac{w_0}{2}\frac{dj}{dw}$.

Non-Unity Gain

For the non-unity gain feedback case where

$H(jw) = H_1(jw)H_2(jw)$ (Eq. 8-1)

it follows that

$$\left[\frac{Y(jw+j\Delta w)}{X(jw+j\Delta w)}\right]_{w=\Delta w+w_0} \approx \left[\frac{-1}{\Delta w \dfrac{dH(jw)}{dw}}\right] \tag{8-154}$$

and

$$\frac{Y_1(jw)}{X(jw)} = \frac{H_1(jw_0)}{1+H(jw_0)} \tag{8-155}$$

then the noise power is shaped by the transfer function as

$$\left|\frac{Y_1(jw+j\Delta w)}{X(jw+j\Delta w)}\right|^2 = \frac{\left|H_1(jw)\right|^2}{(\Delta w)^2\left|\dfrac{dH(jw)}{dw}\right|^2} \tag{8-156}$$

For the lossy RLC resonator see Figure 8-19.

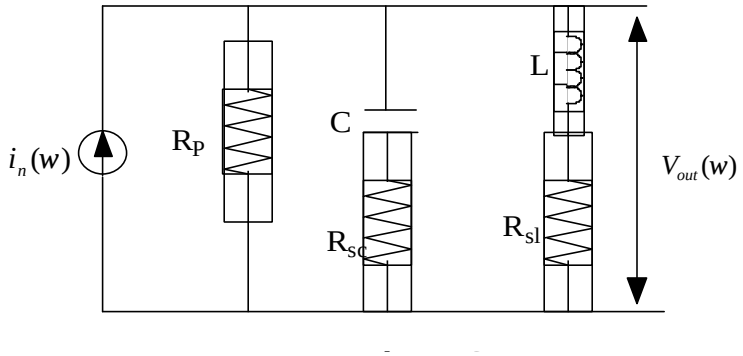

Figure 8-19 Noise response of the RLC resonator.

Then,

$$H(w_0+\Delta w) = \left[\frac{V_{out}(w_0+\Delta w)}{i_n(w_0+\Delta w)}\right]_{w=\Delta w+w_0} = \left[\frac{1}{g_{resonator}}\right]\left[\frac{w_0}{\Delta w}\right]\left[\frac{1}{2Q_L}\right] \tag{8-157}$$

$$g_{resonator} = \frac{1}{R_P} \tag{8-158}$$

where R_P is the equivalent loss resistance of the resonator.

Noise Transfer Function and Spectral Densities

The noise transfer function for the relevant sources is:

$$NFT_{inr}(w_0) = \frac{1}{2}\left[\frac{1}{2jw_0C_{eff}}\right]\left[\frac{w_0}{\Delta w}\right]\rightarrow \tag{8-159}$$

noise transfer function of the thermal loss resistance of the resonator.

$$NFT_{V_{bn}}(w_0) = \frac{1}{2}\left[\frac{C_1 + C_2}{C_2}\right]\left[\frac{1}{2jQ}\right]\left[\frac{w_0}{\Delta w}\right]\rightarrow \tag{8-160}$$

noise transfer function of the transistor's base resistance noise.

$$NFT_{i_{bn}}(w_0) = \frac{1}{2}\left[\frac{C_2}{C_1 + C_2}\right]\left[\frac{1}{2jw_0QC_{eff}}\right]\left[\frac{w_0}{\Delta w}\right]\rightarrow \tag{8-161}$$

noise transfer function of the transistor's base current flicker noise.

$$NFT_{ifn}(w_0) = \frac{1}{2}\left[\frac{C_2}{C_1 + C_2}\right]\left[\frac{1}{2jw_0QC_{eff}}\right]\left[\frac{w_0}{\Delta w}\right]\rightarrow \tag{8-162}$$

noise transfer function of the transistor's flicker noise.

$$NFT_{i_{Cn}}(w_0) = \frac{1}{2}\left[\frac{C_1}{C_1 + C_2}\right]\left[\frac{1}{2jw_0QC_{eff}}\right]\left[\frac{w_0}{\Delta w}\right]\rightarrow \tag{8-163}$$

noise transfer function of the collector current shot noise.

where

$$C_{eff} = C + \frac{C_1C_2}{C_1 + C_2} \tag{8-164}$$

and

$$V_o(w_0) = nV_{be}(w_0) \tag{8-165}$$

$NFT_{in}(w_0)$, $NFT_{V_{bn}}(w_0)$, $NFT_{i_{bn}}(w_0)$ and $NFT_{i_{Cn}}(w_0)$ are the noise transfer functions as explained.

Figure 8-16 showed the four noise sources of the oscillator circuit whereby the flicker noise current is added to the base current and their noise spectral density is $\frac{K_f I_b^{AF}}{f_m}$.

$[NSD]_{inr} = \frac{4KT}{R_P} \rightarrow$ noise spectral density of the thermal noise current from the loss resistance of the resonator.

$[NSD]_{Vbn} = 4KTr_b \rightarrow$ noise spectral density of the thermal noise voltage from the base resistance.

$[NSD]_{ibn} = 2qI_b \rightarrow$ noise spectral density of the shot noise current from the base current.

$[NSD]_{ifn} = \frac{K_f I_b^{AF}}{f_m} \rightarrow$ Noise spectral density due to 1/f- flicker noise.

$[NSD]_{icn} = 2qI_c \rightarrow$ noise spectral density of the shot noise current from the collector current.

The phase noise contribution now is:

$$PN(w_0 + \Delta w) = [NSD]_{noise-source}\left[NFT_{noise-source}(w_0)\right]^2 \quad (8\text{-}166)$$

$$PN_{inr}(w_0 + \Delta w) = \frac{4KT}{R_P}\left[NF_{inr}(w_0)\right]^2 \quad (8\text{-}167)$$

$$PN_{Vbn}(w_0 + \Delta w) = 4KTr_b\left[NF_{Vbn}(w_0)\right]^2 \quad (8\text{-}168)$$

$$PN_{ibn}(w_0 + \Delta w) = 2qI_B\left[NF_{ibn}(w_0)\right]^2 \quad (8\text{-}169)$$

$$PN_{ifn}(w_0 + \Delta w) = \frac{K_f I_b^{AF}}{f_m}\left[NF_{ibn}(w_0)\right]^2 \quad (8\text{-}170)$$

$$PN_{icn}(w_0 + \Delta w) = 2qI_c\left[NF_{icn}(w_0)\right]^2 \quad (8\text{-}171)$$

where $PN(w_0 + \Delta w)$ is the phase noise at the offset frequency Δw from the carrier frequency w_0 and $[NSD]_{noise-source}$ is the noise spectral density of the noise sources. The phase noise contribution is

$$PN_{inr}(w_0 + \Delta w) = \frac{4KT}{R_P}\left[NFT_{inr}(w_0)\right]^2 = \frac{4KT}{R_P}\left\{\frac{1}{2}\left[\frac{1}{2jw_0C_{eff}}\right]\left[\frac{w_0}{\Delta w}\right]\right\}^2 \rightarrow \text{phase noise}$$

contribution from the resonator tank.

$$PN_{Vbn}(w_0 + \Delta w) = 4KTr_b\left[NFT_{Vbn}(w_0)\right]^2 = 4KTr_b\left\{\frac{1}{2}\left[\frac{C_1 + C_2}{C_2}\right]\left[\frac{1}{2jQ}\right]\left[\frac{w_0}{\Delta w}\right]\right\}^2 \rightarrow \text{phase noise}$$

contribution from the base resistance.

$$PN_{ibn}(w_0 + \Delta w) = 2qI_b\left[NFT_{ibn}(w_0)\right]^2 = 2qI_b\left\{\frac{1}{2}\left[\frac{C_2}{C_1 + C_2}\right]\left[\frac{1}{jw_0QC_{eff}}\right]\left[\frac{w_0}{\Delta w}\right]\right\}^2 \rightarrow \text{phase noise}$$

contribution from the base current.

$$PN_{ifn}(w_0 + \Delta w) = \frac{K_f I_b^{AF}}{f_m}\left[NF_{ibn}(w_0)\right]^2 = \frac{K_f I_b^{AF}}{f_m}\left\{\frac{1}{2}\left[\frac{C_2}{C_1 + C_2}\right]\left[\frac{1}{j2w_0QC_{eff}}\right]\left[\frac{w_0}{\Delta w}\right]\right\}^2 \rightarrow \text{phase}$$

noise contribution from the flicker noise of the transistor.

$$PN_{icn}(w_0 + \Delta w) = 2qI_c\left[NFT_{icn}(w_0)\right]^2 = 2qI_c\left\{\frac{1}{2}\left[\frac{C_1}{C_1 + C_2}\right]\left[\frac{1}{2jw_0QC_{eff}}\right]\left[\frac{w_0}{\Delta w}\right]\right\}^2 \rightarrow \text{phase}$$

noise contribution from the collector current.

The total effect of all the four noise sources can be expressed as

$$PN(w_0 + \Delta w) = [PN_{inr}(w_0 + w)] + [PN_{Vbn}(w_0 + w)] + [PN_{ibn}(w_0 + w)] + [PN_{icn}(w_0 + w) \tag{8-172}$$

$$PN(w_0 + \Delta w) = \frac{4KT}{R_P}\left\{\frac{1}{2}\left[\frac{1}{2jw_0C_{eff}}\right]\left[\frac{w_0}{\Delta w}\right]\right\}^2 + 4KTr_b\left\{\frac{1}{2}\left[\frac{C_1 + C_2}{C_2}\right]\left[\frac{1}{2jQ}\right]\left[\frac{w_0}{\Delta w}\right]\right\}^2$$

$$+\left[2qI_b + \frac{2pK_f I_b^{AF}}{\Delta w}\right]\left\{\frac{1}{2}\left[\frac{C_2}{C_1 + C_2}\right]\left[\frac{1}{j2Qw_0C_{eff}}\right]\left[\frac{w_0}{\Delta w}\right]\right\}^2 + 2qI_c\left\{\frac{1}{2}\left[\frac{C_1}{C_1 + C_2}\right]\left[\frac{1}{2jw_0QC_{eff}}\right]\left[\frac{w_0}{\Delta w}\right]\right\}^2 \tag{8-173}$$

where

K_f = Flicker noise constant

AF = Flicker noise exponent.

$$C_{eff} = C + \frac{C_1 C_2}{C_1 + C_2} \tag{8-174}$$

Note: The effect of the loading of the Q of the resonator is calculated by the noise transfer function multiplied with the noise sources.

The phase noise contribution from the different noise sources for the parallel tuned Colpitts oscillator circuit at $\Delta w = 10$ kHz $.2\pi$ from the oscillator frequency $w_0 = 1000$ MHz $.2\pi$ will now be computed:

Circuit parameters:

Base resistance of transistor $r_b = 6.14$ ohm.

Parallel loss resistance of the resonator $R_P = 12000$ ohm.

Q of the resonator = 380

Resonator inductance = 5nH

Resonator capacitance = 4.7pF

Collector current of the transistor I_c = 28mA

Base current of the transistor I_b = 250uA.

Flicker noise exponent AF = 2

Flicker noise constant K_f = 1E-7

Feedback factor n = 2.5.

Phase noise @ 10 KHz:

$$PN_{inr}(w_0 + 10KHz) \approx -125dBc/Hz$$

$$PN_{Vbn}(w_0 + 10KHz) \approx -148dBc/Hz$$

$$PN_{(ibn+ifn)}(w_0 + 10KHz) \approx -125dBc/Hz$$

$$PN_{icn}(w_0 + 10KHz) \approx -142dBc/Hz$$

Note: The noise contribution from the resonator at this offset is the same as the flicker noise contribution from the transistor. For low-Q cases, this can be identified as the flicker corner frequency.

Phase noise @ 100Hz:

$$PN_{inr}(w_0 + 100Hz) \approx -85dBc/Hz$$

$$PN_{Vbn}(w_0 + 100Hz) \approx -108dBc/Hz$$

$$PN_{(ibn+ifn)}(w_0 + 100Hz) \approx -68dBc/Hz$$

$$PN_{icn}(w_0 + 100Hz) \approx -102dBc/Hz$$

It appears that the flicker noise and the noise from the resonator are the limiting factors for the overall phase noise performance of the oscillator circuit.

The dependence of the phase noise performance due to different noise sources present in the oscillator circuits are

$$PN_{imr}(w_0 + \Delta w) \propto \frac{1}{R_P} \tag{8-175}$$

$$PN_{Vbn}(w_0 + \Delta w) \propto= r_b \left\{ \frac{1}{Q} \left[1 + \frac{C_1}{C_2} \right] \right\}^2 \tag{8-176}$$

$$PN_{ibn}(w_0 + \Delta w) \propto I_b \left\{ \frac{1}{QC_{eff}} \left[\frac{C_2}{C_1 + C_2} \right] \right\}^2 \tag{8-177}$$

$$PN_{icn}(w_0 + \Delta w) \propto= I_c \left\{ \frac{1}{QC_{eff}} \left[\frac{C_1}{C_1 + C_2} \right] \right\}^2 \tag{8-178}$$

Once the resonator Q is known (parallel loss resistance is fixed) then the only option left is to select a device having a low flicker noise. The base resistance, current, and collector current add little to the performance! Finally, optimization of the phase noise can be done by proper selection of the feedback capacitor under the constraints of the loop gain so that it maintains oscillation.

The combined phase noise, a result of all the noise contributions, depends on the semiconductor, the resonator losses, and the feedback capacitors. Figure 8-20 shows the simulated phase noise for a given set of semiconductor parameters and various levels of *n*. While the values for *n* = 1.5 and 2 provide similar results and converge for frequencies more than 1 MHz off the carrier, the results for *n* = 3 also provides a much noisier condition, even at far-out frequencies. The reason is the reduced output power and a heavier loading of the resonator.

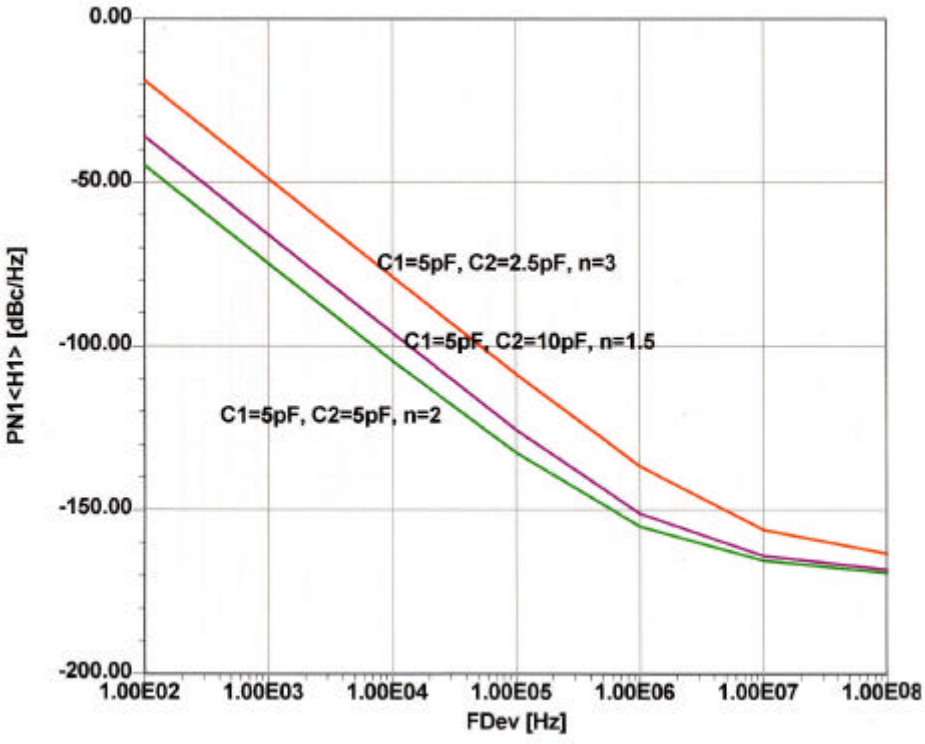

Figure 8-20 Phase noise as a function of feedback factor n.

The next section shows a variety of test circuits, which were built and measured to validate the theory shown here.

9 Validation Circuits

Section 7 developed the mathematical background for optimizing microwave oscillators. The next step is to validate the synthesis of the circuits. The following circuits have been chosen for validation:

- 1000 MHz bipolar transistor-based oscillator with ceramic resonator.
- 4100 MHz bipolar transistor-based oscillator with transmission line resonators.
- 2000 MHz GaAs FET-based oscillator with transmission line resonators.

9.1 1000 MHz CRO

Many applications require a very low noise microwave oscillator in the 1000 MHz region, and this is best accomplished with a ceramic resonator. An operating Q in the vicinity of 500 is available in this material. An oscillator using an NEC NE68830 transistor has been selected because of its superior flicker noise. The Colpitts oscillator uses an 8.2 Ω resistor between the emitter and the capacitive feedback. Rather than take the RF signal at the collector, it is taken from a tap of the emitter inductor. The collector circuit, using PNP transistors, has been designed to set the DC current. The necessary equations for this DC bias are found in [88].

Class-A common-emitter amplifiers are usually very sensitive to stray impedance in the emitter circuit. Any small inductance in series with the emitter will cause instability; for this reason, the emitter needs to be grounded as directly as possible, and bias components in the emitter are generally undesirable. In the schematic in Figure 9-1, Q_1 is the RF amplifier, and Q_2 provides its base current required for constant voltage difference across R_c. This constant voltage difference then ensures constant collector current.

Diode D_1 provides some measure of temperature compensation. R_b should be high in order not to affect base impedance, but not so high to cause Q_2 to saturate over temperature and b_1 variations. Neglecting the base current of Q_2, the design equations are

$$I_c = \frac{R_1(A^+ - V_d)}{R_c(R_1 + R_2)} \tag{9-1}$$

$$V_c = A^+ - I_c R_c \tag{9-2}$$

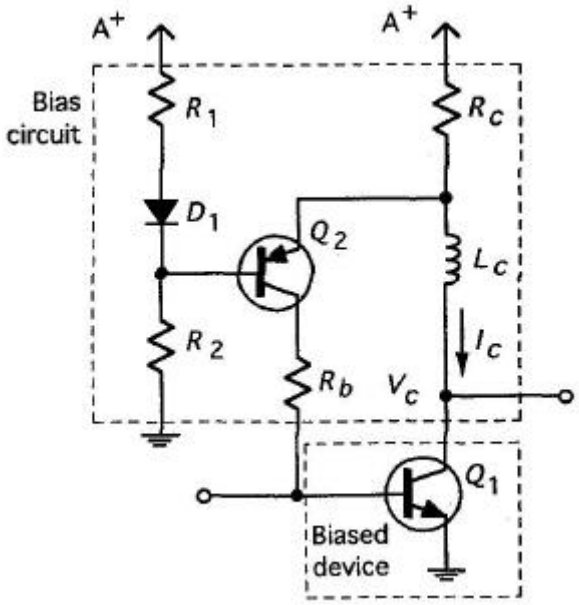

Figure 9-1 Active bias network for a common-emitter RF amplifier stage.

Assuming that we are designing the bias circuit to provide a certain device bias current I_c and collector voltage V_c, select a convenient supply voltage $A^+ > V_c$. The component values are then supplied by the following equations:

$$R_c = \frac{A^+ - V_c}{I_c} \tag{9-3}$$

$$R_1 = \frac{A^+ - V_c}{I_d} \tag{9-4}$$

$$R_2 = \frac{V_c - V_d}{I_d} \tag{9-5}$$

$$R_b < b_{\min} \frac{V_c - V_d - 0.2}{I_c} \tag{9-6}$$

I_c = desired collector current of Q_1 (A)

V_c= desired collector voltage of Q_1 (V)

V_d = diode, or base-emitter voltage drop, nominally 0.7 (V)

A^+ = chosen supply voltage (V)

R_i = resistor values as shown in Figure 9-1 (Ω)

I_d = bias current through R_1, R_2, and D_1 (A)

b_{min} – minimum beta of Q_1

The bias circuit shown has to be carefully bypassed at both high and low frequencies. There is one inversion from base to collector of Q_1, and another inversion may be introduced by L_c matching components and stray capacitances, resulting in positive feedback around the loop at low frequencies. Low ESR electrolytic or tantalum capacitors from the collector of Q_2 to ground is usually adequate to ensure stability.

The ceramic resonator is coupled loosely to the transistor with a capacitor of 0.9pF. The resonator has a parallel capacitor of 0.6pF, which reduces the manufacturing tolerances of the resonator. The tuning diode assembly, two diodes in parallel, is coupled to the resonator with 0.8pF. The reason for using two diodes was that there was not one single diode available with the necessary capacitance and Q. Figure 9-2 shows the schematic of the oscillator.

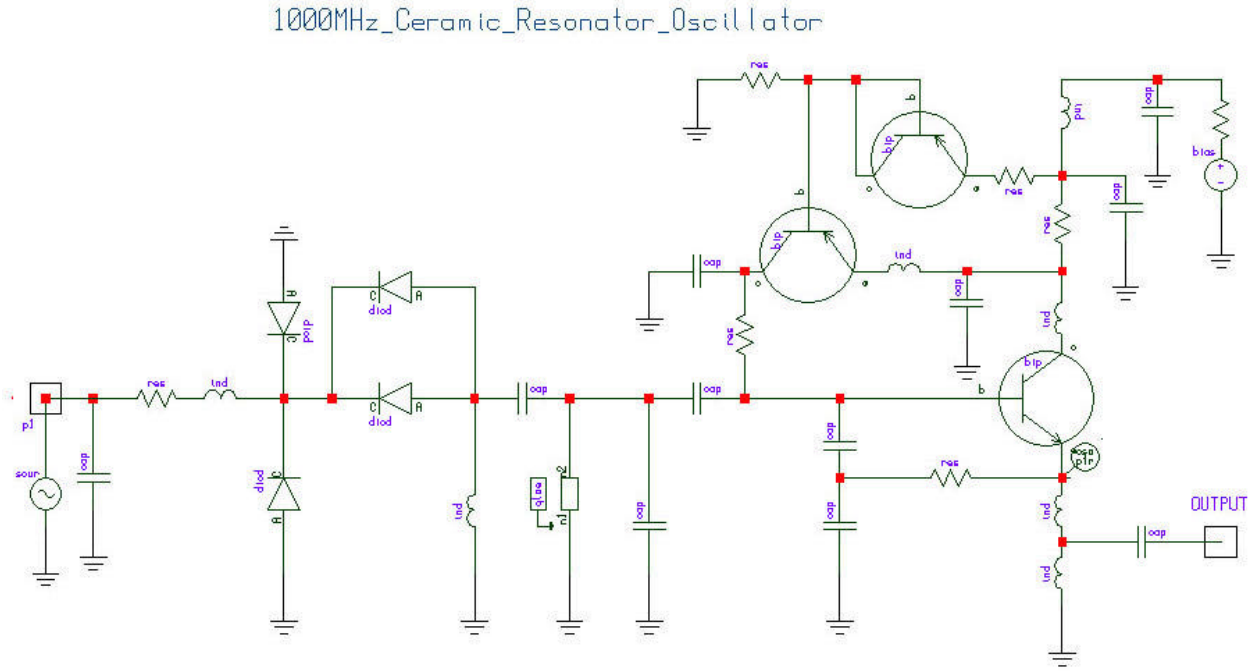

Figure 9-2 1000 MHz ceramic resonator oscillator.

It has been pointed out that the best operating condition will be the case where the most negative resistance occurs at the point of resonance to achieve the best phase noise. This is shown in Figure 9-3. The purple-colored curve starting below zero shows the imaginary current which resonates at 1000 MHz, while the green-colored curve shows the negative resistance. Its maximum negative peak occurs at exactly 1000 MHz, as it should be.

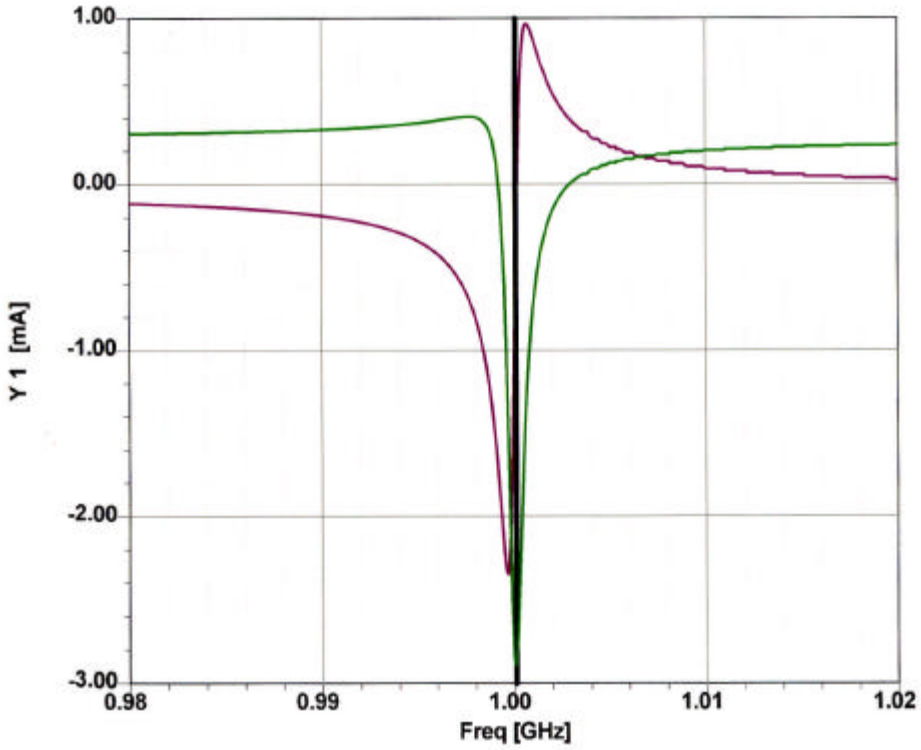

Figure 9-3 Plot of the real and imaginary oscillator currents as a function of frequency.

Figure 9-4 shows the measured phase noise of this oscillator. The measurements were performed with the Aeroflex Euro Test system. At 1 kHz the phase noise is approximately 95 dBc/Hz and at 10 kHz it is approximately 124 dBc/Hz. This is a 30 dB/decade slope, which is triggered by the flicker corner frequency of the transistor. From 10 kHz to 100 kHz, the slope is 20 dB/decade with a phase noise of –145.2 dBc/Hz at 100 kHz. At 1 MHz off the carrier, it is –160 dBc/Hz.

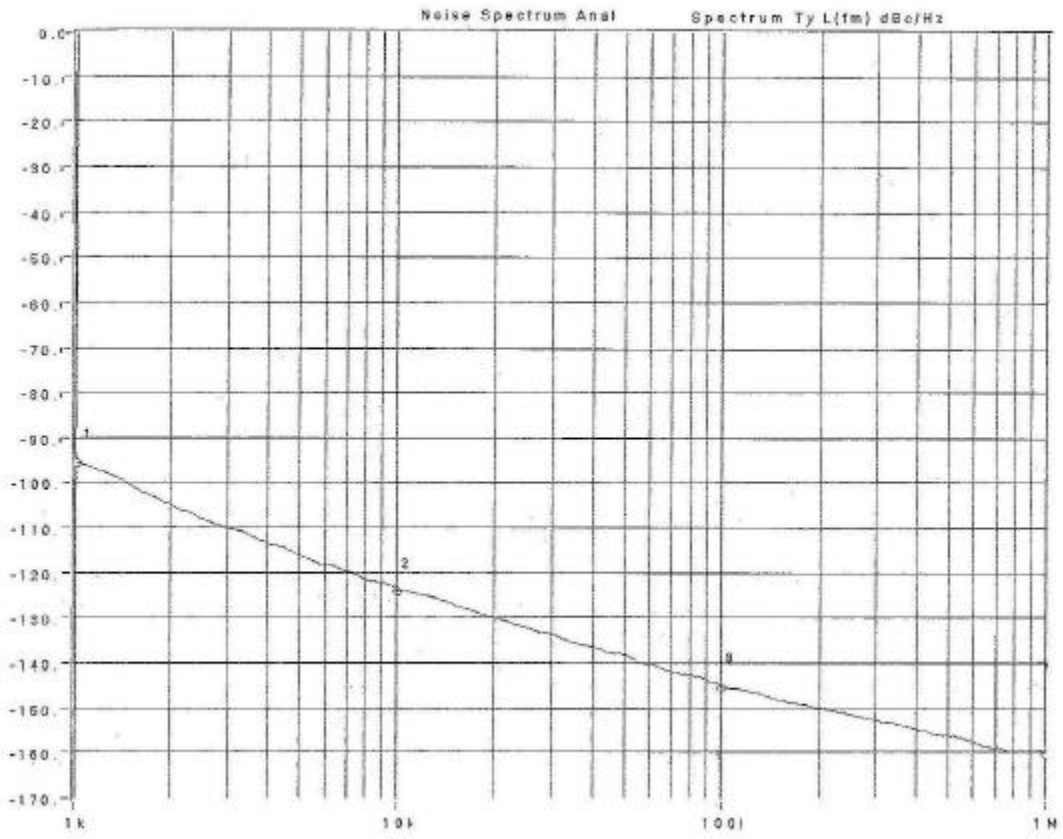

Figure 9-4 Measured phase noise of the 1000 MHz ceramic resonator oscillator.

Because of the narrow tuning range and the loose coupling of the tuning diode, the noise contribution of the diode is negligible.

This circuit has been designed using the synthesis procedure and also has been analyzed with the harmonic-balance simulator *Microwave Harmonica* from Ansoft Corporation. Figure 9-5 shows the predicted performance of the phase noise. The actual circuit arrangement is shown in Figure 9-6. The ceramic resonator can be spotted easily.

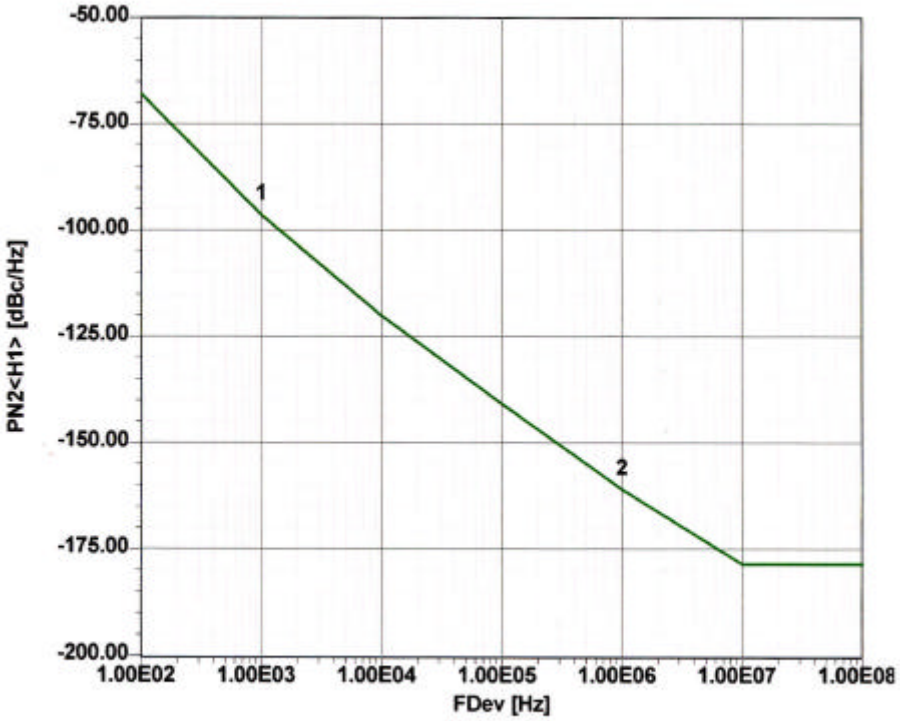

Figure 9-5 Predicted phase noise of the CRO at 1 GHz shown in Figure 9-2.

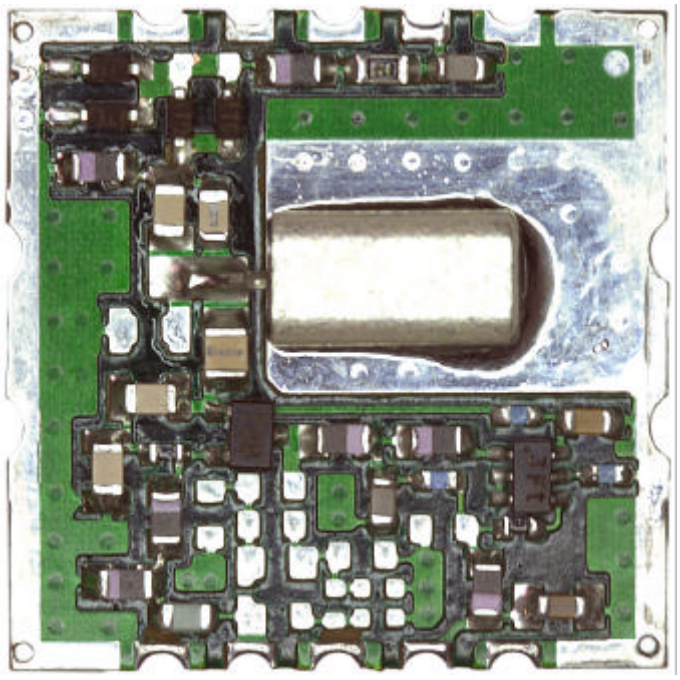

Figure 9-6 Photograph of the 1 GHZ CRO of the schematic shown in Figure 9-2.

9.2 4100 MHz Oscillator with Transmission Line Resonators

For less demanding applications, it is possible to design oscillators using transmission line resonators. Transmission line resonators were discussed in Section 5. Their Q depends on the material and implementation of the resonator. Figure 9-7 shows the circuit of the oscillator. While the previous example was a Colpitts parallel resonant circuit, this circuit operates in series resonant mode. The NPN transistor NE68830 has parasitic inductance in the emitter, base, and collector lines. For the purpose of accurate modeling, TEE and cross-junction models were used, as well as transmission lines where applicable. The DC stabilization circuit uses the same technique as shown in Figure 9-2. This time the RF power is taken from the collector and uses a 10 dB attenuator to minimize frequency pulling. The ground connections for the capacitors are done using via holes. A via hole is the electrical equivalent of a small inductor.

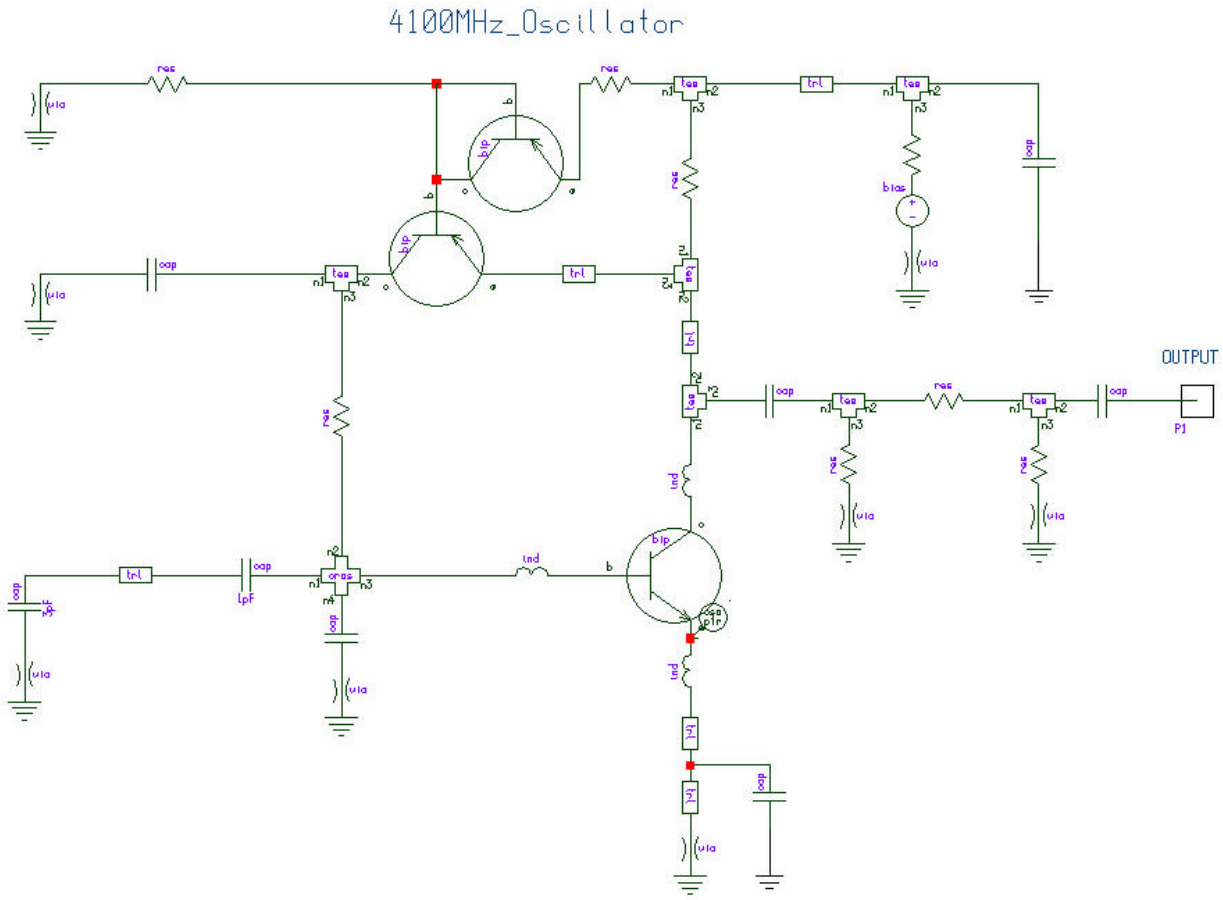

Figure 9-7 Circuit diagram of the 4.1 GHz oscillator.

The phase noise of this oscillator was simulated using the values of the synthesis program. Figure 9-8 shows the predicted phase noise.

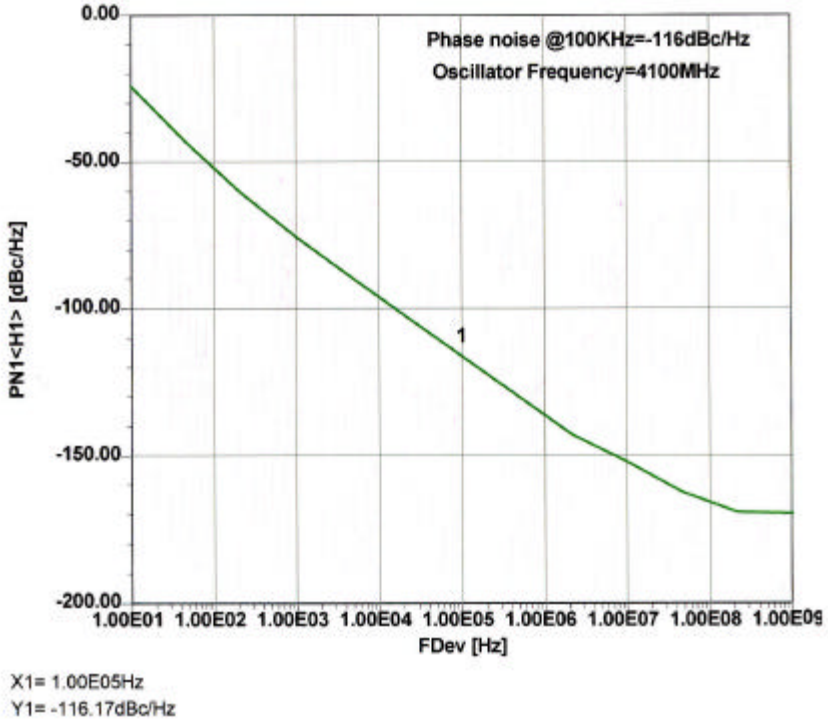

Figure 9-8 Predicted phase noise of the 4.1 GHz oscillator.

The output power of this oscillator is 6.8 dBm. This oscillator was built and measured. Figure 9-9 shows the printed circuit board of the oscillator.

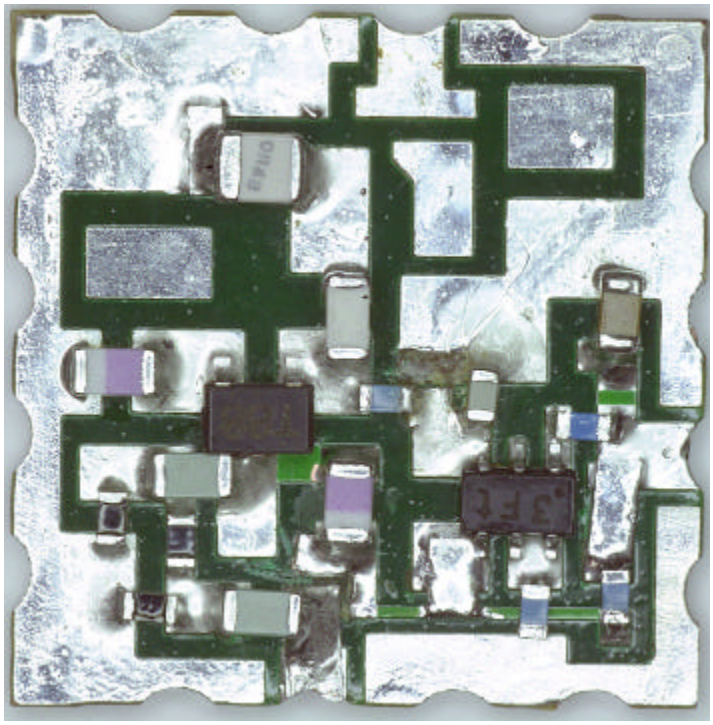

Figure 9-9 Printed circuit board of the 4.1 GHz oscillator shown in Figure 9-8.

Because of the pad-like microstrips, the simulation needs to be done very carefully, and the soldering of the component is also very critical. This frequency range makes the assembly very difficult because it is not high enough for an RFIC and still needs to be done on a printed circuit board. The measured phase noise is shown in Figure 9-10. It agrees well with the predicted phase noise. At 100 kHz the difference is about 3 dB. The same is valid at 10 kHz. At 1 kHz there is a larger difference. The flicker corner frequency of the actual device is different than the simulation.

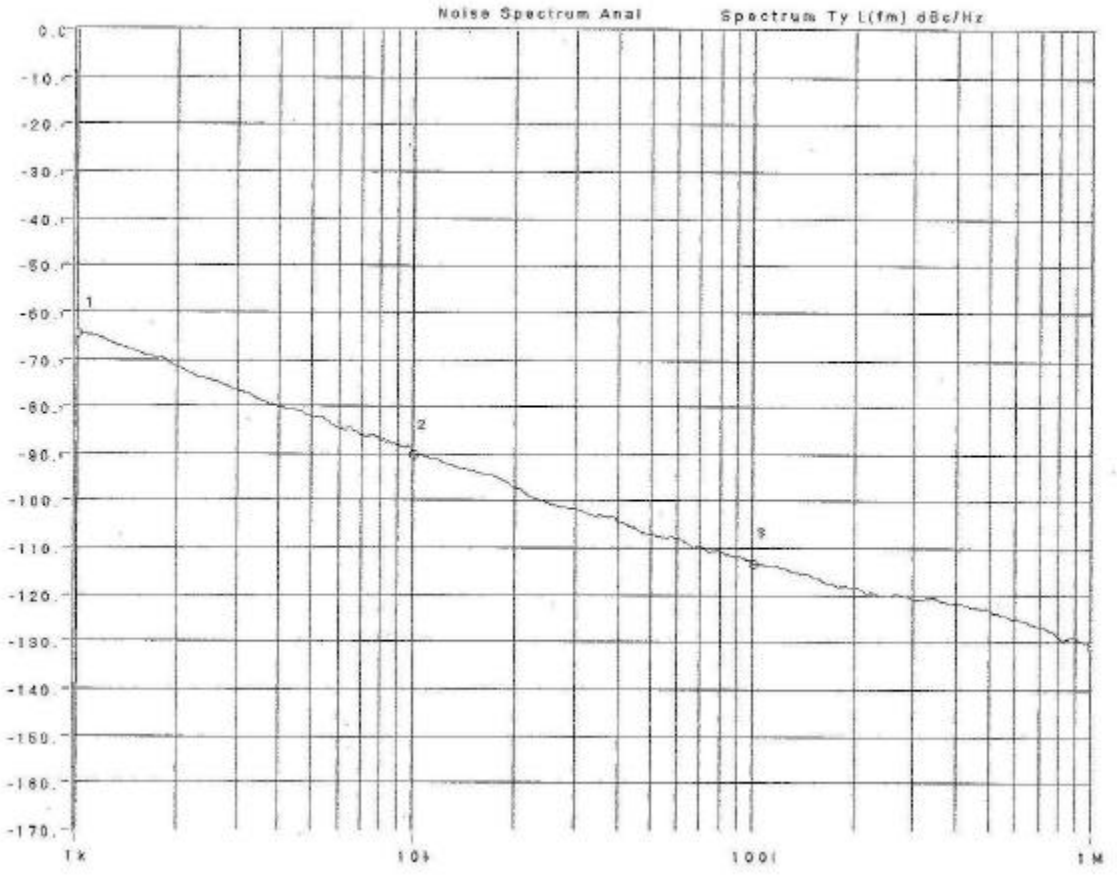

Figure 9-10 Measured phase noise of the 4.1 GHz oscillator.

9.3 2000 MHz GaAs FET-Based Oscillator

Low cost applications are frequently implemented as an RFIC. For further validation, a GaAs FET-based 2000 MHz Colpitts oscillator was designed and built. Figure 9-11 shows the circuit diagram of the oscillator. It uses a combination of transmission lines and rectangular inductors as resonators. The inductor in the middle of the schematic in Figure 9-11, connected to a via hole, is needed as a DC return. If a tuning diode is connected to the capacitor on the left of the schematic in Figure 9-11, then a DC control voltage can be applied, and the center inductor becomes and RF choke. The output is taken from the source. An additional external DC decoupling capacitor will be needed because of the DC coupling. The transistor and the circuit were constructed using the TriQuint GaAs Foundry and the transistor was optimized for the DC current. Figure 9-12 shows the predicted phase noise of this oscillator.

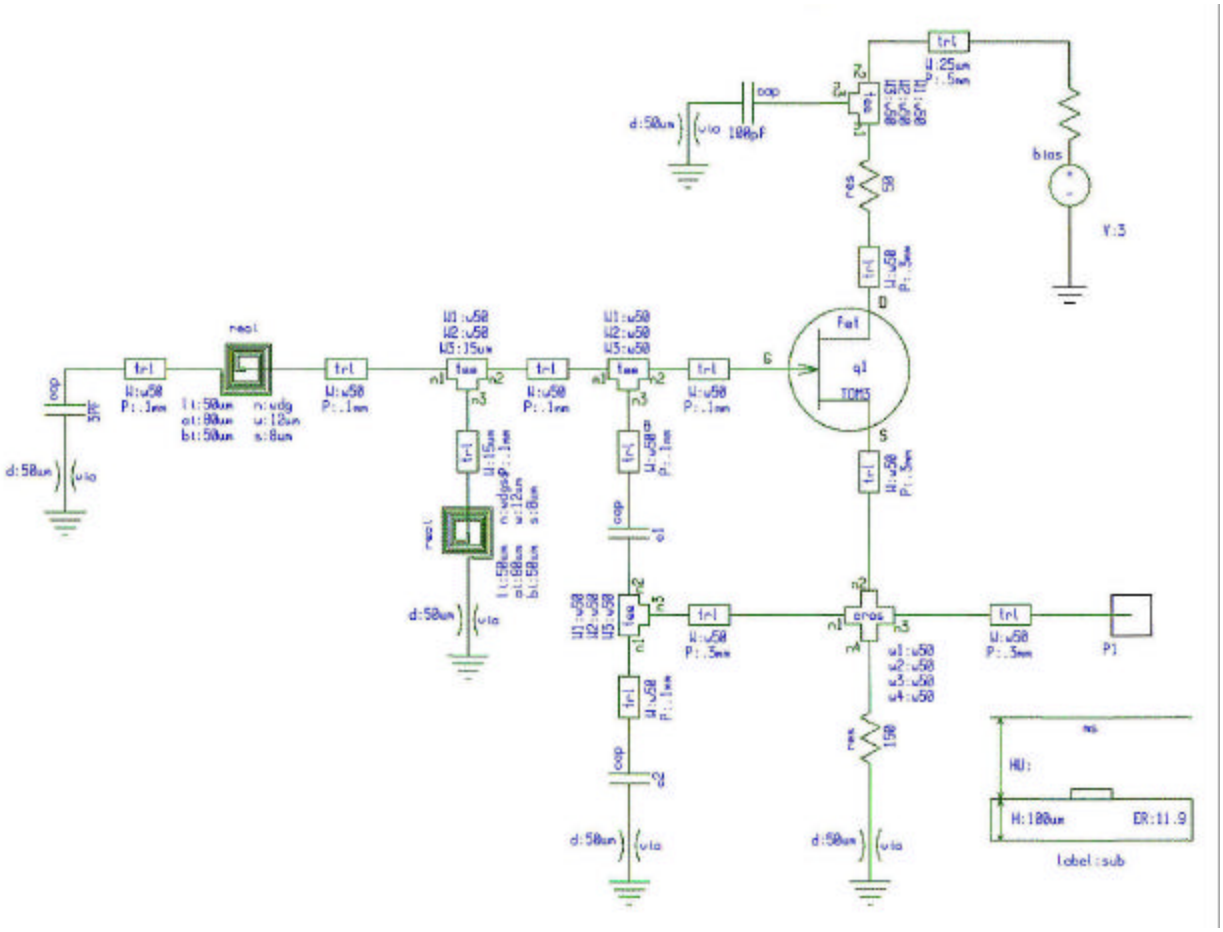

Figure 9-11 Circuit diagram of the 2 GHz GaAs FET oscillator.

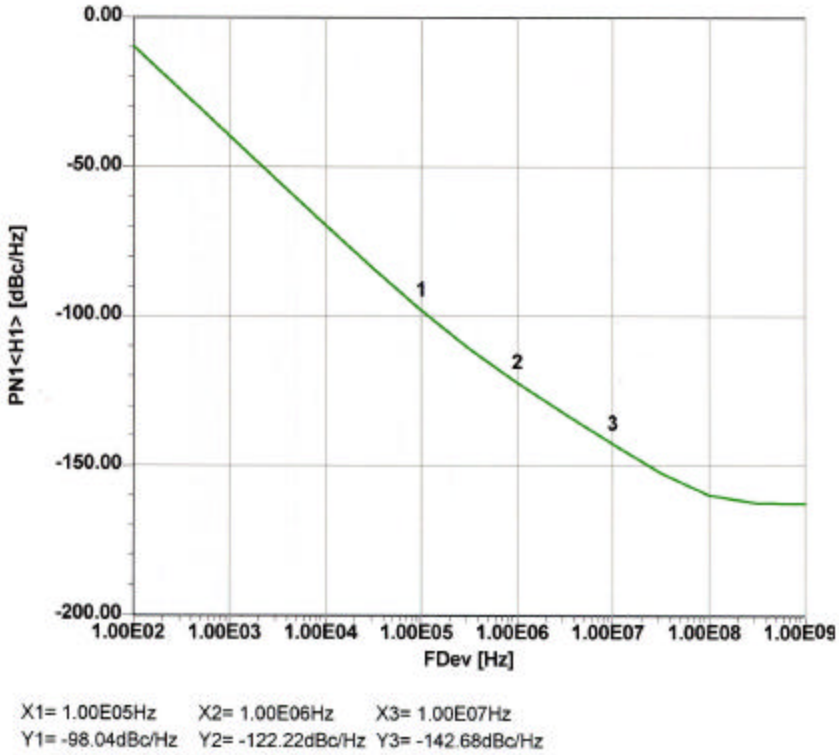

Figure 9-12 Predicted phase noise of the oscillator shown in Figure 9-11. The measured values were 100 dBc/Hz at 100 kHz and 120 dBc/Hz at 1 MHz. There is a deviation of about 2 dB compared to simulation.

It is interesting to examine the load line of this oscillator, which is shown in Figure 9-13. This circuit is operated in a fairly linear range.

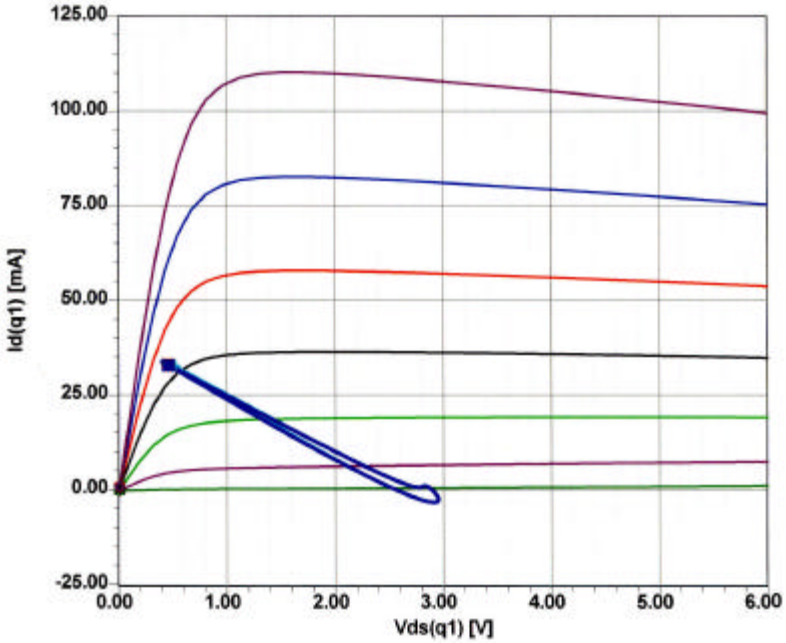

Figure 9-13 Shows the DC-IV and the load line for the GaAs FET oscillator.

Figure 9-14 shows the layout of the 2 GHz GaAs FET oscillator. Its output power is 1.8 dBm.

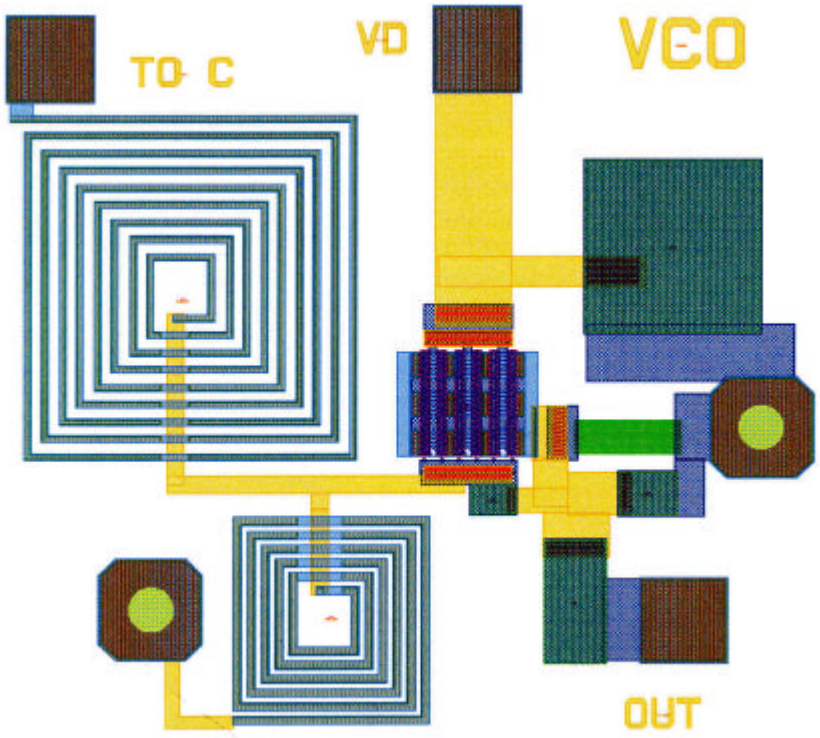

Figure 9-14 Layout of the 2 GHz GaAs FET oscillator.

10 Conclusions and Future Possibilities

Conclusions

The purpose of this work was to determine how to design optimal microwave oscillators. In doing so, some basic oscillator circuits were used rather than voltage controlled oscillators, as the phase noise of the tuning diode then masks the oscillation noise. As a result of this work, a set of good design guides and accurate equations were found. They cover the large-signal operation of the transistor, particularly the drive level for best output power. It was found that the output power remains constant over a fairly wide range of drive levels, which shortens the conducting angle of the transistor. A further reduction of the conducting angle results in large voltage swings and makes the oscillator very noisy. The following is specific for the Colpitts oscillator, but similar relationships can be found for all other oscillator configurations. The normalized drive level can be between 8 to 20 depending upon the application. It was further confirmed that the Q largely determines the best phase noise for a given device. For medium to low Q values $n = (1 + \frac{C_1}{C_2})$ varies between 2 and 4. The absolute value of C_1 is determined by the loop gain and for safety reasons, a loop gain reserve factor of 2 is recommended.

The Colpitts oscillator shows good phase noise performance up to very high frequencies. When a wide tuning range is required, the series resonant circuit is typically favored at the expense of lower phase noise. This is due to the fact that transistor parasitics no longer allow for obtaining the optimum C_1 and C_2 values. Because of these parasitics, it also may be necessary to replace C_2 with an inductor to adjust to the needed values.

For wireless applications, push-pull CMOS oscillators are state-of-the-art. Here the flicker corner frequency and the loaded Q strongly determine the performance. Based on the push-pull arrangement of a non-Colpitts oscillator, C_1 and C_2 are automatically equal. This means that n=2, and this is not the best phase noise condition. However, recently published push-pull Colpitts oscillators avoid this problem [119].

Besides finding a repeatable synthesis procedure, a set of analytical equations were derived that predict the phase noise of the oscillators even in the presence of parasitics. These equations also consider the loading of the Q based on the oscillator circuit and the flicker noise. The selection of a transistor for best performance needs to be divided into two areas. If the parasitics do not play a large role, then it is a good choice to take the largest device possible. Because of flicker noise, it should be operated at low current and should have a low flicker-noise contribution. If the device is too high in its operating frequency, there is typically a penalty in the flicker noise, and parasitics (fingers of the transistor layout) degrade the noise performance. All the important circuits were built, measured, and analyzed in Microwave Harmonica. Their design was based on these

analytic equations. All three approaches showed excellent agreement. At 10 kHz a phase noise of –124 dBc/Hz were both measured and predicted. The Leeson equation set, the time-domain approach, and the loop-gain approach, as well as the harmonic-balance calculation, all agreed within 1 dB of accuracy.

Future Possibilities

As indicated, the areas of most concern in oscillators are the flicker frequency effects, the Q, and the phase noise, which is a function of both, as well as the supply voltage. As the industry migrates to lower voltages, better devices need to be developed which show good performance at these low voltages. Since most designs are not used as an oscillator at a fixed frequency, but as a voltage-controlled oscillator with a wide tuning range, this topic needs to be thoroughly analyzed and good solutions need to be found. My extension to the Leeson formula clearly shows that after a certain tuning sensitivity, the tuning diode dominates the noise regardless of Q and flicker effects. Possible solutions here are multi-resonator oscillators, binary-switched capacitances, and inductors to minimize the influence of the tuning diode. This will be an important area of research.

11 Abbreviations and Symbols

Symbol	Description
LTV	Linear time variant
NLTV	Nonlinear time variant
LTIV	Linear time invariant
G_m	Large-signal transconductance
g_m	Small-signal transconductance
$a_n(x)$	Fourier coefficient
$I_n(x)$	Modified Bessel function of order n
$I_e(t)$	Emitter current
$I_c(t)$	Collector current
I_{cob}	Collector reverse current
$V_{n(total)}$	Total noise voltage
V_{sn}	Noise due to source
$V_{n(network)}$	Noise due to network
Y_g	Generator admittance
Y_{opt}	Optimum noise admittance
F_{min}	Minimum achievable noise figure
R_n	Noise resistance
$[C_y]$	Y-parameter noise correlation matrix
$[C_A]$	ABCD Correlation Matrix
Y_{cor}	Correlation factor

$\overline{i_{bn}^2} = 2qI_b\Delta f$	Mean square value of noise due to base current
$\overline{i_{cn}^2} = 2qI_c\Delta f$	Mean square value of noise due to collector current
$\overline{i_{con}^2} = 2qI_{cob}\Delta f$	Mean square value of noise due to reverse collector current
$\overline{v_{bn}^2} = 4kTR_b\Delta f$	Mean square value of noise voltage due to base resistance
$S(i_{cn}) = 2KTg_m$	Noise power spectral densities due to collector current
$S(i_{bn}) = \frac{2KTg_m}{b}$	Noise power spectral densities due to base current
$S(v_{bn}) = 4KTR_b$	Noise power spectral densities due to base resistance
$S(v_{sn}) = 4KTR_s$	Noise power spectral densities due to source resistance
$\overline{i_d^2} = 4kTg_mP\Delta f$	Mean square value of noise due to drain current
$\overline{i_g^2} = \frac{4kT(wC_{gs})^2R}{g_m}\Delta f$	Mean square value of noise due to gate current
$P = \left[\frac{1}{4kTg_m}\right]\overline{i_d^2} / Hz$	FET noise coefficient
$R = \left[\frac{g_m}{4kTw^2C_{gs}{}^2}\right]\overline{i_g^2} / Hz$	FET noise coefficient
$C = -j\left[\frac{\overline{i_g i_d^{\bullet}}}{\sqrt{[\overline{i_d^2}\,\overline{i_g^2}]}}\right]$	FET noise coefficient
P	0.67 for JFETs and 1.2 for MESFETs
R	0.2 for JFETs and 0.4 for MESFETs
C	0.4 for JFETs and 0.6-0.9 for MESFETs

Z_s	Complex source impedance
$a = \left[1 + \frac{f^2}{f_b^2} - a_0\right]\frac{1}{a_0}$	Modified factor
X	Drive-Level
(kT/q)x	Drive-Voltage
$2[I_1(x)/I_0(x)]$	Fundamental component of current
$[I_2(x)/I_1(x)]$	Second harmonic component of current
φ	Conduction angle
n	Transformation factor
n_{opt}	Optimum transformation ratio
R_P	Parallel loss resistance
Q_L	Loaded quality factor
f_0	Center frequency
f_c	Flicker corner frequency
f_m	Frequency offset
P_{sav}	Average power at oscillator output
K_0	Oscillator voltage gain
$F = \frac{\overline{i_L^2}}{\overline{i_{LO}^2}}$	Noise factor
NF	Noise Figure
$£(f_m)$	Ratio of sideband power in a 1 Hz bandwidth at f_m

E_B, E_H	Vector of harmonic-balance (HB) errors
E	Vector of real and imaginary parts of all HB errors
X_B, X_H	Vector of state variable (SV) harmonics
J_B, J_H	Vector of forcing terms
δX_B, δX_H	Perturbation of the circuit state
M	Jacobian matrix of the HB errors
$\delta\omega_0(\omega)$	Phasor of the pseudo-sinusoidal components
$N_k(\omega)$	Noise power spectral density
$C_k(\omega)$	Normalized correlation coefficient
$J_p(w)$	Side-band noise sources
$U_p(w)$	Side-band noise sources
I_k^{ss}	Noise power spectral density
$S_{\Delta\theta}(\omega)$	Power spectral density of the input phase error
θ_d	Peak phase deviation
$e_N(t)$	Noise signal voltage
$R_N(t)$	Time variant negative resistance
k	Boltzman's constant (1.38E-23 J/K)
kT	4.1×10^{-21} at 300 K_0 (room temperature)
R	Equivalent noise resistance of tuning diode
G	Compressed power gain of the loop amplifier
TF(jω)	Closed loop transfer function

H(jω)	Open loop transfer function
$\left\langle \left\| dj_{ck}(w) \right\|^2 \right\rangle$	PM noise at k^{th} harmonic
$\left\langle \left\| dj_{mk}(w) \right\|^2 \right\rangle$	PM noise due to contribution of modulation
$\left\langle \left\| dA_{ck}(w) \right\|^2 \right\rangle$	AM noise to carrier ratio at k^{th} harmonic
$\left\langle d\Phi_{ck}(w) dA_k(w)^* \right\rangle$	PM-AM correlation coefficient for the k^{th} harmonic
$\left\langle \left\| J_H(w) J_H^{\otimes}(w) \right\| \right\rangle$	Correlation matrix
$T_F^{\otimes}$	Conjugate-transpose
T_{Ak}	Row-matrix
T_F	Frequency transfer matrix
$Y_R(kw_0)$	Transadmittance matrix
$\left\| I_k^{SS} \right\| \exp(j2j_k^{ss})$	k^{th} harmonic of the steady-state current through the load
$C_{k,-k}^{\bullet}(w)$	Correlation coefficient of the upper and lower sidebands
m(t)	Modulating signal
K_p	Phase sensitivity
$b = \frac{\Delta f}{f_m}$	Modulation index of the modulating signal
SNR	Signal to noise ratio
A_{SSB}	Sideband amplitude of a phase modulation
C_0	Coefficient of Fourier series, 0^{th} order of the ISF
Δf	Noise bandwidth

$w_{1/f}$	1/f noise corner frequency of the device/transistor
q_{max}	Maximum charge on the capacitors in the resonator
$NFT_{inr}(\omega)$	Noise transfer function due to resonator loss resistance
$NFT_{vbn}(\omega)$	Noise transfer function due to transistor base resistance
$NFT_{ibn(}\omega)$	Noise transfer function due to the transistor base current
$NFT_{ifn}(\omega)$	Noise transfer function due to flicker noise
$NFT_{icn}\omega)$	Noise transfer function due to collector current
K_f	Flicker noise constant
AF	Flicker noise exponent
$\sigma(t)$	Complex envelope of the frequency modulated signal
Γ(rms)	Impulse sensitivity function
EMF	Electromotive force
b^+	Large-signal current gain
Y_{11}^+	Large-signal input admittance
Y_{21}^+	Large-signal transconductance

12 References

1. The references used in the Introduction in Section 1 for the early oscillators were found in the book by H.E. Hollmann, Physik und Technik der ultrakurzen Wellen, Erster Band, Erzeugung ultrakurzwelliger, Schwingungen; Verlag von Julius Springer, 1936, and by themselves are probably no longer obtainable.
2. G.R. Basawapatna, R. B. Stancliff, "A Unified Approach to the Design of Wide-Band Microwave Solid-State Oscillators," IEEE Trans. Microwave Theory Tech., Vol. 27, pp. 379-385, May 1979.
3. M. Sebastein, N. Jean-Christophe, Q. Raymond, P. Savary, J. Obregon.," A Unified Approach for the Linear and Nonlinear Stability Analysis of Microwave Circuits Using Commercially Available Tolls," IEEE Trans. Microwave Theory Tech., Vol. 47 , pp. 2403-2409, Dec 1999.
4. M. Prigent, M. Camiade, J.C. Nallatamby, J. Guittard, J. Obregon, "An Efficient Design Method of Microwave Oscillator Circuits for Minimum Phase Noise," IEEE Trans. Microwave Theory Tech., Vol. 47, pp. 1122-1125, July 1999.
5. P. Bolcato, J.C. Nallatamby, R. Larcheveque, M. Prigent, J. Obregon, "A Unified Approach of PM Noise Calculation in Large RF Multitude Autonomous Circuits," IEEE MTT-S Symp. Digest, 2000.
6. S. Mons, M.A. Perez, R. Quere, J. Obregon, “A Unified Approach for the Linear and Nonlinear Stability Analysis of Microwave Circuits Using Commercially Available Tools,” IEEE MTT-S Symp. Digest, Vol .3, pp. 993-996, 1999.
7. Alper Demir, Amit Mehotra, and Jaijeet Roychowdhury, “Phase Noise in Oscillators: A Unifying Theory and Numerical Methods for Characterization,” IEEE Transactions on Circuits and Systems, Vol. 47, pp.655-674, May 2000.
8. A. Grebennikov, “ Microwave Transistor Oscillators: An Analytic Approach to Simplify Computer-Aided Design,” Microwave Journal, pp 292-299, May 1999.
9. T. Hajder, “Higher Order Loops Improve Phase Noise of Feedback Oscillators,” Applied Microwave & Wireless, pp. 24-31, October 2002.
10. R.J. Gilmore, M.B. Steer, “Nonlinear Circuit Analysis Using the Method of Harmonic Balance – A Review of the Art. Part I. Introductory Concepts,” International Journal of Microwave and Millimeter-Wave Computer-Aided Engineering, Volume 1/Number 1, pp. 22-37, January 1991.
11. R.J. Gilmore, M.B. Steer, “Nonlinear Circuit Analysis Using the Method of Harmonic Balance – A Review of the Art. Part II. Advanced Concepts,” International Journal of Microwave and Millimeter-Wave Computer-Aided Engineering, Volume 1/Number 2, pp. 159-180, April 1991.
12. J.G. Proakis, Editor – U.L. Rohde: “Frequency Synthesizers,” *The Wiley Encyclopedia of Telecommunications*, John Wiley & Sons, December 2002, ISBN 0-471-36972-1.
13. U.L. Rohde, *Microwave and Wireless Synthesizers: Theory and Design*, John Wiley & Sons, August 1997, ISBN 0-471-52019-5

14. U.L. Rohde, D.P. Newkirk, *RF/Microwave Circuit Design for Wireless Applications*, John Wiley & Sons, April 2000, ISBN 0-471-29818-2.
15. U.L. Rohde, J. Whitaker, *Communications Receivers, Third Edition*, McGraw-Hill, December 2000, ISBN 0-07-136121-9.
16. G. Vendelin, A.M. Pavio, U.L. Rohde, *Microwave Circuit Design Using Linear and Nonlinear Techniques*, John Wiley & Sons, January 1990, ISBN 0-471-58060-0.
17. K. Kurokawa, "Some Basic Characteristics of Broadband Negative Resistance Oscillator Circuits," Bell Syst. Tech. Journal, pp. 1937-1955, July-August 1969.
18. User's Manual for Berkley-SPICE.
19. User's Manual for H-SPICE.
20. User's Manual for P-SPICE
21. User's Manual for RF Spectre.
22. H.C. de Graaff, W.J. Kloosterman, IEEE Trans. Electr. Dev. ED-32, 2415, 1986.
23. H.C. de Graaff, W.J. Kloosterman, T.N. Jansen, Ext. Abstr. Solid State Dev. Mat. Conf. Tokyo, paper B-5-3, 1986.
24. H.C. de Graaff, W.J. Kloosterman, J.A.M. Geelen, M.C.A.M. Koolen, "Experience with the New Compact MEXTRAM Model for Bipolar Transistors," Phillips Research Laboratories, 1989.
25. U.L. Rohde, "New Nonlinear Noise Model for MESFETS Including MM-Wave Application," First International Workshop of the West German IEEE MTT/AP Joint Chapter on Integrated Nonlinear Microwave and Millimeterwave Circuits (INMMC'90) Digest, October 3-5, 1990, Duisburg University, Duisburg, Germany.
26. U.L. Rohde, "Improved Noise Modeling of GaAs FETS: Using an Enhanced Equivalent Circuit Technique," Microwave Journal, pp. 87-101 - November 1991, pp. 87-95 - December 1991.
27. R.A. Pucel, W. Struble, R Hallgren, U.L. Rohde, "A General Noise De-embedding Procedure for Packaged Two-Port Linear Active Devices," IEEE Transactions on Microwave Theory and Techniques, Vol. 40, No. 11, pp. 2013-2024, November 1992.
28. U.L. Rohde, "Parameter Extraction for Large Signal Noise Models and Simulation of Noise in Large Signal Circuits Like Mixers and Oscillators," 23rd European Microwave Conference, Madrid, Spain, September 6-9, 1993.
29. P.R. Gray and R.G. Meyer, *Analysis and Design of Analog Integrated Circuits, Third Edition*, ISBN 0-47157495-3, 1993.
30. R.A. Pucel and U.L. Rohde, "An Exact Expression for the Noise Resistance R_n of a Bipolar Transistor for Use with the Hawkins Noise Model," IEEE Microwave and Guided Wave Letters, Vol. 3, No. 2, February, 1993, pp. 35-37. 1993.
31. H.K. Gummel, H. C. Poon, "An Integral Charge Control Model of Bipolar Transistors," Bell Syst. Tech. Journal, pp. 827-852, May-June 1970.

32. G. M. Kull, L.W. Nagel, S. Lee, P. Lloyd, E.J. Prendergast, H. Dirks, “A Unified Circuit Model for Bipolar Transistors Including Quasi-Saturation Effects,” IEEE Transactions on Electron Devices, Vol. 32, No. 6, June 1985.
33. H.C. de Graff, W.J. Koostermann, “Modeling of the Collector Epilayer of a Bipolar Transistor in the Mextram Model,” IEEE Transactions on Electron Devices, Vol. 36, No. 7, pp. 274-282, February 1995.
34. M. Schroeter, H. M. Rein, “Investigation of Very Fast and High-Current Transients in Digital Bipolar IC’s Using Both a New Model and a Device Simulator,” IEEE Journal of Solid-State Circuits, Vol. 30, pp. 551-562, May 1995.
35. M. Rudolph, R. Doerner, K. Beilenhoff, P. Heymann, “Scalable GaIn/GaAs HBT Large-Signal Model,” IEEE Transactions on Microwave Theory and Techniques, Vol. 48, pp. 2370-2376, December 1990.
36. C.C. McAndrew, J.A. Seitchik, D.F. Bowers, M. Dunn, M. Foisy, I. Getreu, M. McSwain, S. Moinian, J. Parker, D.J. Roulston, M. Schroeter, P. van Wijnen, L.F. Wagner, “VBIC95, The Vertical Bipolar Inter-Company Model,” IEEE Journal of Solid-State Circuits, Vol. 31, No. 10, pp. 1476-1483, October 1996.
37. Xiaochong Cao, J. McMacken, K. Stiles, P. Layman, J.J. Liou, A. Ortiz-Conde, S. Moinian, “Comparison of The New VBIC and conventional Gummel-Poon Bipolar Transistor Models,” IEEE Transactions on Electron Devices, Vol. 47, No. 2, pp. 427-433, February 2000.
38. R.A. Pucel, H.A. Haus, and H. Statz, “Signal and Noise Properties of Gallium Arsenide Microwave Field-Effect Transistors, In Advances in Electronics and Electron Physics,” Vol. 38, New York: Academic Press, 1975.
39. A. Cappy, “Noise Modeling and Measurement Techniques,” in IEEE Trans., Microwave Theory and Tech., Vol. 36, pp. 1-10, January 1988.
40. M.W. Pospieszalski, “Modeling of Noise Parameters of MESFET’s and MODFET’s and Their Frequency and Temperature Dependence,” IEEE Trans., Microwave Theory and Tech., Vol. 37, pp.1340-1350, September 1989.
41. V. Rizzoli, F. Mastri, C. Cecchetti, “Computer-Aided Noise Analysis of MESFET and HEMT Mixers,” IEEE Trans. on Microwave Theory and Tech., Vol. 37, pp. 1401-1411, September 1989.
42. A. Riddle, “Extraction of FET Model Noise Parameters from Measurement,” IEEE MTT-S, Int. Microwave Symposium Digest, pp. 1113-1116, 1991.
43. R.A. Pucel, W. Struble, R. Hallgren, U.L. Rohde, “A General Noise De-Embedding Procedure for Packaged Two-Port Linear Active Devices,” IEEE Trans., Microwave Theory and Tech., Vol. 40, pp. 2013-2024, November 1992.
44. J. Portilla, R. Quere, J. Obregon, “An Improved CAD Oriented FET Model for Large-Signal and Noise Applications,” IEEE-MTT-S Digest, pp. 849-852, 1994.
45. T. Felgentreff, G. Olbrich, P. Russer, “Noise Parameter Modeling of HEMTs with Resistor Temperature Noise Sources,” IEEE MTT-S, Int. Microwave Symposium Digest, pp. 853-856, 1994.

46. J. Stenarson, M. Garcia, I. Angelov, H. Zirath, "A General Parameter-Extraction Method for Transistor Noise Models," in IEEE Trans., Microwave Theory and Tech., Vol.47, pp.2358-2363, December 1999.
47. D. Lee, Y. Kwon, Hong-Shick Min, "Physical-Based FET Noise Model Applicable to Millimeter-Wave Frequencies," IEEE MTT-S, Int. Microwave Symposium Digest, pp.01-04, 1999.
48. M.R. Murti, J .Laskar, S. Nuttinck, S. Yoo, A. Raghavan, J.I. Bergman, J. Bautista, R. Lai, R. Grundbacher, M. Barsky, P. Chin, P. H. Liu," Temperature-Dependent Small-Signal and Noise Parameters Measurement and Modeling on InP HEMTs," IEEE Trans., Microwave Theory and Tech., Vol. 48, pp. 2579-2586, December 2000.
49. A. Pascht, G. Markus, D. Wiegner, M. Berroth," Small-signal and Temperature Noise Model for MOSFETs," IEEE Trans., Microwave Theory and Tech., Vol. 50, pp.927-1934, August 2002.
50. Y.P. Tsividis, *Operation and Modeling of the MOS Transistor*, McGraw Hill, 1987.
51. BISIM3v3 Manual, Department of Electrical Engineering and Computer Sciences, University of California, Berkeley.
52. Z. Liu, C. Hu, J. Huang, T. Chan, M. Jeng, P. K. Ko, Y. C. Cheng, "Threshold Voltage Model for Deep-Submicronmeter MOSFET's," IEEE Trans. Electron Devices, Vol. 40, No. 1, pp. 86-95, January 1993.
53. Y. Cheng, M. Jeng, Z. Liu, J. Juang, M. Chan, K. Chen, P. K. Ko, C. Ho, "A Physical and Scalable *I-V* Model in BISIM3v3 for Analog/Digital Circuit Simulation," IEEE Trans. Electron Devices, Vol. 44, No. 2, pp. 277-287, February 1997.
54. Rohde & Schwarz, "Introduction Manual for *Z*-G Diagraph, Models ZGU and ZDU," 1963.
55. "*S*-Parameters, Circuit Analysis and Design," Hewlett-Packard Application Note 95, September 1968.
56. P. Bodharamik, L. Besser, R.W. Newcomb, "Two Scattering Matrix Programs for Active Circuit Analysis," IEEEE Transactions on Circuit Theory, Vol. CT-18, pp. 610-619, November 1971.
57. Integrated Circuits (RFIC) Symposium "*S*-Parameter Design," Hewlett-Packard Application Note 154, April 1972.
58. C. Arnaud, D. Basataud, J. Nebus, J. Teyssier, J. Villotte, D. Floriot, "An Active Pulsed RF and Pulsed DC Load-Pull System for the Characterization of HBT Power Amplifiers Used in Coherent Radar and Communication Systems," IEEE Transactions on Microwave Theory and Techniques, Vol. 48, No. 12 , pp. 2625 –2629, December 2000.
59. F.M. Ghannouchi, R. Larose, R.G. Bosisio, "A New Multiharmonic Loading Method for Large-Signal Microwave and Millimeter-Wave Transistor Characterization," IEEE Transactions on Microwave Theory and Techniques, Vol.39, No. 6, pp. 986 –992, June 1991.

60. H. Abe, Y. Aono, "11 GHz GaAs Power MESFET Load-Pull Measurements Utilizing a New Method of Determining Tuner *Y*-Parameters, IEEE Transactions on Microwave Theory and Techniques, Vol. 27, No. 5, pp. 394 –399, May 1979.
61. Q. Cai, J. Gerber, S. Peng, "A Systematic Scheme for Power Amplifier Design Using a Multi-Harmonic Load-Pull Simulation Technique," Microwave Symposium Digest, 1998 IEEE MTT-S International, Vol. 1, pp. 161 -165, June 7-12, 1998.
62. P. Berini, M. Desgagne, F.M. Ghannouchi, R.G. Bosisio, "An Experimental Study of the Effects of Harmonic Loading on Microwave MESFET Oscillators and Amplifiers," IEEE Transactions on Microwave Theory and Techniques, Vol. 42, No. 6 , pp. 943 –950, June 1994.
63. K.K. Clarke, D.T. Hess, *Communication Circuits: Analysis and Design*, Chapter 4: Nonlinear Controlled Sources, Addison Wesley, 1971.
64. M. Odyniec, Editor, *RF and Microwave Oscillator Design*, Chapter 3: Linearity, Time Variation, and Oscillator Phase Noise, by T. Lee and A. Hajimiri, Artech House, 2002.
65. A. Hajimiri, T. Lee, "A General Theory of Phase Noise in Electrical Oscillators," IEEE Journal of Solid-State Circuits, Vol. 33, No. 2, pp. 179-194, February 1998.
66. D. Ham, A. Hajimiri, "Concepts and Methods in Optimization of Integrated LC VCOs," IEEE Journal of Solid-State Circuits, June 2001.
67. A. Hajimiri, S. Limotyrakis, T. Lee, " Jitter and Phase Noise in Ring Oscillators," IEEE Journal of Solid-State Circuits, Vol. 34, No. 6, pp. 790-804, June 1999.
68. W.H. Haywood, Introduction to Radio Frequency Design, Prentice Hall, 1982.
69. Chris O' Connor, " Develop a trimless voltage-controlled oscillator," Microwave & RF, January 2000.
70. D.B. Leeson, A Simple Model of Feedback Oscillator Noise Spectrum," Proc. IEEE, 54, 329-330, 1966.
71. T. Hajder, "Higher Order Loops Improve Phase Noise of Feedback Oscillators," Applied Microwave & Wireless, October 2002.
72. M. Vidmar, "A Wideband, Varactor-Tuned Microstrip VCO," Microwave Journal, June 1999.
73. M. Odyniec, Editor, *RF and Microwave Oscillator Design*, Chapter 5: Modern Harmonic-Balance Techniques for Oscillator Analysis and Optimization, by V. Rizzoli, A. Neri, A. Costanzo, F. Mastri, Artech House, 2002.
74. U.L. Rohde, G. Klage, "Analyze VCOs and Fractional-N Synthesizers," Microwaves & RF, pp. 57-78, August 2000.
75. U.L. Rohde, C.R Chang, J. Gerber, "Design and Optimization of Low-Noise Oscillators Using Nonlinear CAD Tools," IEEE Frequency Control Symp. Proc., pp 548-554, 1994.
76. U. L. Rohde, C. R. Chang, J. Gerber, "Parameter Extraction for Large Signal Noise Models and Simulation of Noise in Large Signal Circuits Like Mixers and Oscillators," Proceedings of the 23rd European Microwave conference, Madrid, Spain, Sept. 6-9, 1993.

77. V. Rizzoli, F. Mastri, C. Cecchefti, "Computer-Aided Noise Analysis of MESFET and HEMT Mixers," IEEE Trans. Microwave Theory and Techniques, Vol. MTT-37, pp 1401-1410, Sept. 1989.
78. V. Rizzoli, A. Lippadni, "Computer-Aided Noise Analysis of Linear Multiport Networks of Arbitrary Topology," IEEE Trans. Microwave Theory and Techniques, Vol. MTT-33, pp 1507-1512, Dec. 1985.
79. V. Rizzoli, F. Mastri, D. Masotti, "General-Purpose Noise Analysis of Forced Nonlinear Microwave Circuits," Military Microwave, 1992.
80. W. Anzill, F. X. Kärtner, P. Russer, "Simulation of the Single-Sideband Phase Noise of Oscillators," Second International Workshop of Integrated Nonlinear Microwave and Millimeterwave Circuits, 1992.
81. Hewlett-Packard, 3048A Operating Manual.
82. K. Kurokawa, " Noise in Synchronized Oscillators," IEEE Trans. on MTT, Vol. 16, pp. 234-240, April 1968.
83. J..C. Nallatamby, M. Prigent, M. Camiade, J. Obregon, "Phase Noise in Oscillators-Leeson Formula Revisted," IEEE Transactions on Microwave Theory and Techniques, Vol. 51, No. 4 , pp. 1386 –1394, April 2003.
84. U.L. Rohde, "A Novel RFIC for UHF Oscillators (Invited)," 2000 IEEE Radio Frequency m, Boston, MA, June 11-13, 2000.
85. D. J. Healy III, "Flicker of Frequency and Phase and White Frequency and Phase Fluctuations in Frequency Sources," *Proceedings of the 26th Annual Symposium on Frequency Control*, Fort Monmouth, NJ, June 1972, pp. 43-49.
86. Michael M. Driscoll, "Low Noise Oscillator Design Using Acoustic and Other High Q Resonators," *44th Annual Symposium on Frequency Control*, Baltimore, MD, May 1990.
87. U.L. Rohde, K. Danzeisen, Feedback Oscillators, Patent No. DE10033741A1 (Germany, United States, Japan).
88. P. Vizmuller, RF Design Guide: Systems, Circuits, and Equations, Artech House, p. 76, 1995.
89. C. Rheinfelder, Ein Gross-signal-Modell des SiGe-Hetero-Bipolar-Transistors fuer den Entwurf monolithisch intergrierter Mikrowellen-Schaltungen, Fortschritt-Berichte VDI, 1998. Also, personal communication with the author.
90. C. Rheinfelder, M. Rudolph, F. Beißwanger, W. Heinrich, "Nonlinear Modeling of SiGe HBTs up to 50 GHz," 1997 IEEE Int. Microwave Symposium Digest, Vol. 2, pp. 877-880.
91. C.N. Rheinfelder, K.M. Strohm, L. Metzger, J.-F. Luy, W. Heinrich, "A SiGe-MMIC Oscillator at 47 GHz," 1999 Int. Microwave Symp. Digest, Vol. 1, pp. 5-8.
92. F. Lenk, M. Schott, J. Hilsenbeck, J. Würfl, W. Heinrich," Low Phase-Noise Monolithic GaInP/GaAs-HBT VCO for 77 GHz," accepted for presentation at 2003 IMS.

93. F. Lenk, J. Hilsenbeck, H. Kuhnert, M. Schott, J. Würfl, W. Heinrich, "GaAs-HBT MMIC-Oscillators for Frequencies up to 40 GHz," 2nd Symposium on Opto- and Microelectronic Devices and Circuits (SODC 2002), Stuttgart, Germany, March 17-23, 2002.
94. H. Kuhnert, W. Heinrich, W. Schwerzel, and A. Schüppen, "25 GHz MMIC Oscillator on Commercial SiGe-HBT Process," IEE Electronics Letters, Vol. 36, No.3, pp. 218-220, February 2000.
95. H. Kuhnert, F. Lenk, J. Hilsenbeck, J. Würfl, and W. Heinrich, "Low Phase-Noise GaInP/GaAs-HBT MMIC Oscillators up to 36 GHz," 2001 Int. Microwave Symposium Digest, Vol. 3, pp. 1551-1554.
96. H. Kuhnert, W. Heinrich, "5 to 25 GHz SiGe MMIC Oscillators on a Commercial Process," Proc. 2nd Topical Meeting on Silicon Monolithic Integrated Circuits in RF Systems, pp. 60-63, April 2000.
97. H. Kuhnert, W. Heinrich, "Coplanar SiGe VCO MMICs Beyond 20 GHz," 2001 IEEE Topical Meeting on Silicon Monolithic Integrated Circuits in RF Systems, Ann Arbor, Digest, pp. 231-233, September 12-14, 2001.
98. F. Lenk, M. Schott, W. Heinrich, "Modeling and Measurement of Phase Noise in GaAs HBT Ka-band Oscillators," 2001 European Microwave Conference Digest, Vol. 1, pp. 181-184.
99. M. Nemes, "Entwicklung eins UHF-Transceivers fuer das ISM-Frequenzband 868-870 MHz in einer 0,8 *m*m-CMOS-Technologie," Ph.D. Dissertation, University of Cottbus, 2003.
100. A. Roufougaran, J. Rael, M. Rofougaran, and A. Abidi, "A 900MHz CMOS LC-Oscillator with Quadrature Outputs, "ISSCC Dig. Tech. Papers, pp. 392-393, February 1996.
101. B. Razvi, " Study of Phase Noise in CMOS Oscillators," IEEE J. Solid-State Circuits, Vol. 31, pp. 331-343, March 1996.
102. J. Craninckx and M. Steyaert, " A Fully Integrated Spiral-LC CMOS VCO Set with Prescaler for GSM and DCS-1800 Systems," Proc. Custom Integrated Circuits Conf., pp. 403-406, May 1997.
103. M. Thanmsirianunt and T. A. Kwasniewski, "CMOS VCO's for PLL Frequency Synthesis in GHz Digital Mobile Radio Communications," IEEE J. Solid-State Circuits, Vol. 32, pp. 1511-1518, October 1997.
104. Frank Herzel, Michael Pierschel, Peter Weger, and Marc Tiebout, "Phase Noise in Differential CMOS Voltage-Controlled Oscillator for RF Applications," IEEE Trans. on circuits and systems, Vol.47, No.1, pp 11-15, January 2000.
105. F. Herzel, H. Erzgraber and P. Weger, " Integrated CMOS Wideband Oscillator for RF Applications, Electronics Letters, Vol. 37, March 2001.
106. A. Hajimiri, T. Lee, " Design Issues in CMOS Differential LC Oscillators," IEEE Journal of Solid-State Circuits, May 1999.
107. T.H. Lee, *The Design of CMOS Radio-Frequency Integrated Circuits*, Cambridge University Press, 1998.

108. K. Cheng, K. Chan, “Power Optimization of High-Efficiency Microwave MESFET Oscillators,” IEEE Transactions on Microwave Theory and Techniques, Vol. 48, No. 5, pp. 787 –790, May 2000.
109. G. Sauvage, “Phase Noise in Oscillators: A Mathematical Analysis of Leeson’s Model,” IEEE Transactions on Instrumentation and Measurement, Vol. IM-26, No. 4, December 1977.
110. G. Böck, P.W. v. Basse, J.E. Müller, W. Kellner, “Accurate SPICE Modeling of GaAs-MESFETs for Use in GaAs-IC Design,” Proc. On 11th Workshop of Compound Semiconductor Devices and Integr. Circuits, S. 66 - 69, 04. - 06. May 87, Grainau (Garmisch-Partenkirchen).
111. W. Stiebler, M. Matthes, G. Böck, T. Koppel, A. Schäfer, “Bias Dependent Cold - (H)FET Modeling,” IEEE MTT—S 1996 International Microwave Symposium, Digest of technical papers, San Francisco, pp. 1313-1316, June 1996.
112. L. Klapproth, G. Böck, A. Schäfer, W. Stiebler, “On the Determination of HFET Noise Parameters from 50Ohm Noise Figure Measurements,” MIOP ’97, Sindelfingen, Kongreßunterlagen, S., pp.348-352.
113. P. Heymann, M. Rudolph, H. Prinzler, R. Doerner, L. Klapproth, G. Böck “Experimental Evaluation of Microwave Field-Effect-Transistor Noise Models,” IEEE Trans. on MTT, February 1999.
114. N. H. W. Fong, J. O. Plouchart, N. Zamdmer, D. Liu, L. F. Wagner, C. Plett, and N. G. Tarr,” A 1-V 3.8-5.7-GHz Wide-Band VCO with Differentially Tuned Accumulation MOS Varactors for Common-Mode Noise Rejection in CMOS SOI Technology,” IEEE Trans. on MTT, February 2003.
115. Application Notes, Temperature Stable Microwave Ceramics, Products for RF/Microwave Application, Trans-Tech, pp. 6-85.
116. D. Kajfez, “ Q Factor Measurement with a Scalar Network Analyzer,” IEE Proc. Microwave Antennas Propag., Vo. 142, pp. 389-372, October 1995.
117. R.J. Hawkins, “Limitations of Nielsen’s and Related Noise Equations Applied to Microwave Bipolar Transistors and a New Expression for the Frequency and Current Dependent Noise Figure,” Solid-State Electron., Vol. 20 pp. 191-196, March 1977.
118. T.H. Hsu, C.P. Snapp, “Low-Noise Microwave Bipolar Transistor with Sub-Half-Micrometer Emitter Width,” IEEE Trans. Electron Devices, Vol. ED-25, pp. 723-730, June 1978.
119. R. Aparicio, A. Hajimiri, “A CMOS Noise Shifting Colpitts VCO," 2002 Digest of Technical Papers ISSCC, Session 17.2, pp. 288-299.

13 Appendices

Appendix A - Design of an Oscillator Using Large Signal S-Parameters

Figure A-1 is a numerical calculation of a 3000 MHz oscillator based on the parallel feedback case using large-signal *S*-parameters. This example is of particular interest because it requires an inductor instead of the familiar capacitor, C_2, between base and emitter. The circuit as such is a Colpitts oscillator.

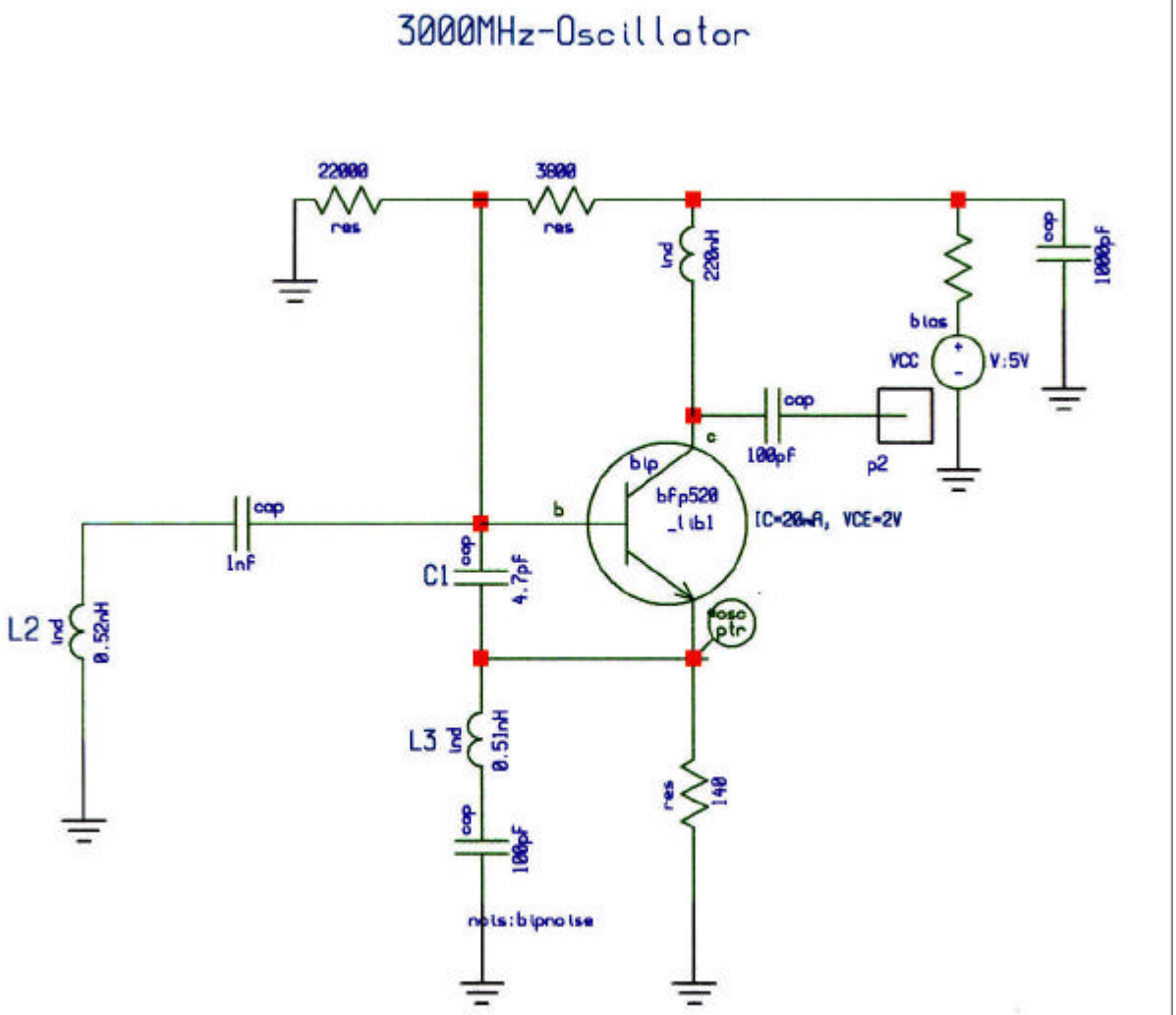

Figure A-1 A 3000 MHz oscillator using a BFP520 transistor operating at 2V and 20mA. In this case, the capacitor C_2 needs to be replaced by an inductor L_3 which tunes out the collector emitter capacitance to achieve the optimum value. The 1nF on the left is a DC separation capacitor. This case is optimized for output power.

The measured large-signal *Y*-parameter data (I_c=20mA, V_{ce}=2V) @ 3000MHz are:

$$Y_{11} = G_{11} + jB_{11} = (11.42 + j8.96)\ mS \tag{A-1}$$

$$Y_{21} = G_{21} + jB_{21} = (4.35 - j196.64)\,mS \tag{A-2}$$

$$Y_{12} = G_{12} + jB_{12} = (-433.09 - j1.5643\ mS \tag{A-3}$$

$$Y_{22} = G_{22} + jB_{22} = (4.41 + j9.10)\ mS \tag{A-4}$$

The optimum values of feedback element are calculated from the given expression of B_1^* and B_2^* are

$$B_1^* = -\left\{B_{11} + \left[\frac{B_{12} + B_{21}}{2}\right] + \left[\frac{G_{21} - G_{12}}{B_{21} - B_{12}}\right]\left[\frac{G_{12} + G_{21}}{2} + G_{11}\right]\right\} \tag{A-5}$$

$$jB_1^* = 89.8E - 3 \tag{A-6}$$

$$jB_1^* = jwC_1 \tag{A-7}$$

$$C_1 = \frac{89.8E - 3}{2pf} = 4.77\,pF \tag{A-8}$$

$$B_2^* = \left[\frac{B_{12} + B_{21}}{2}\right] + \left[\frac{(G_{12} + G_{21})(G_{21} - G_{12})}{2(B_{21} - B_{12})}\right] \tag{A-9}$$

$$jB_2^* = -103.5E - 3 \tag{A-10}$$

$$jB_2^* = \frac{1}{jwL_2} \tag{A-11}$$

$$L_2 = \frac{1}{(2pf) \times 103.5E - 3L_2} 0.515nH \tag{A-12}$$

The optimum values of the real and imaginary part of the output admittance are

$$Y_{out}^* = [G_{out}^* + jB_{out}^*] \tag{A-13}$$

where G_{out}^{*} and B_{out}^{*} is given as

$$G_{out}^{*} = G_{22} - \left[\frac{(G_{12}+G_{21})^2 (B_{21}-B_{12})^2}{4G_{11}}\right] \tag{A-14}$$

$$G_{out}^{*} = -823.53E-3 \tag{A-15}$$

$$B_{out}^{*} = B_{22} + \left[\frac{G_{21}-G_{12}}{B_{21}-B_{12}}\right] - \left[\frac{(G_{12}+G_{21})}{2} + G_{22} - G_{out}^{*}\right] + \left[\frac{B_{21}+B_{12}}{2}\right] \tag{A-16}$$

$$B_{out}^{*} = -105.63E-3 \tag{A-17}$$

$$jB_{out}^{*} = \frac{1}{jwL_3} \tag{A-18}$$

$$L_3 = 0.502nH \tag{A-19}$$

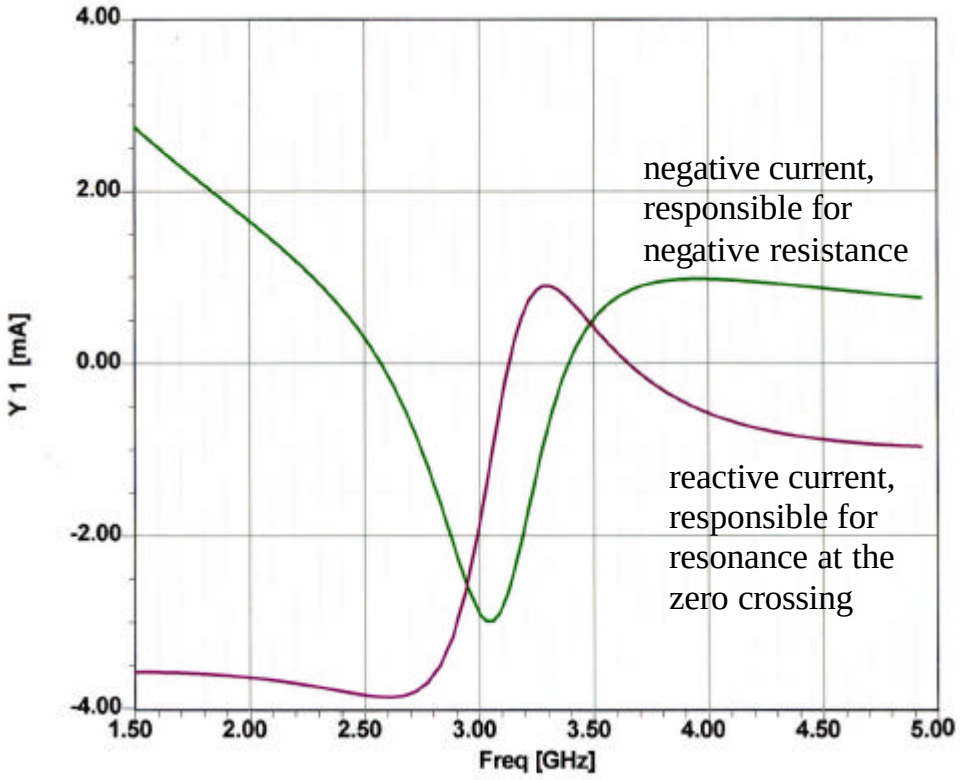

Figure A-2 Shows the real and imaginary currents for oscillation. The reactive current crosses the zero line at 3120 MHz. This is close, but not exactly at the point of most negative resistance current. The reason for the shift of 120 MHz is due to the use of small-signal analysis rather than the large-signal analysis.

Figure A-2 shows the simulated response of the oscillator circuit having resonance at 3120 MHz or 5% error. The little variation in resonant frequency may be due to the frequency dependent packaged parameters, but it is a good starting value for tuning and optimization for the best phase noise and output power. The best phase noise at a given power output is basically dependent upon the ratio and absolute value of the feedback capacitors, which in turn depends upon the optimum drive-level.

Appendix B - Design Example for Large Signal Design Based on Bessel Functions

Frequency = 1000 MHz.
Power output = 5 mW
Load = 500Ω

Figure B-1 shows the schematic of the 1 GHz oscillator as described in Section 9. The output termination is 500Ω.

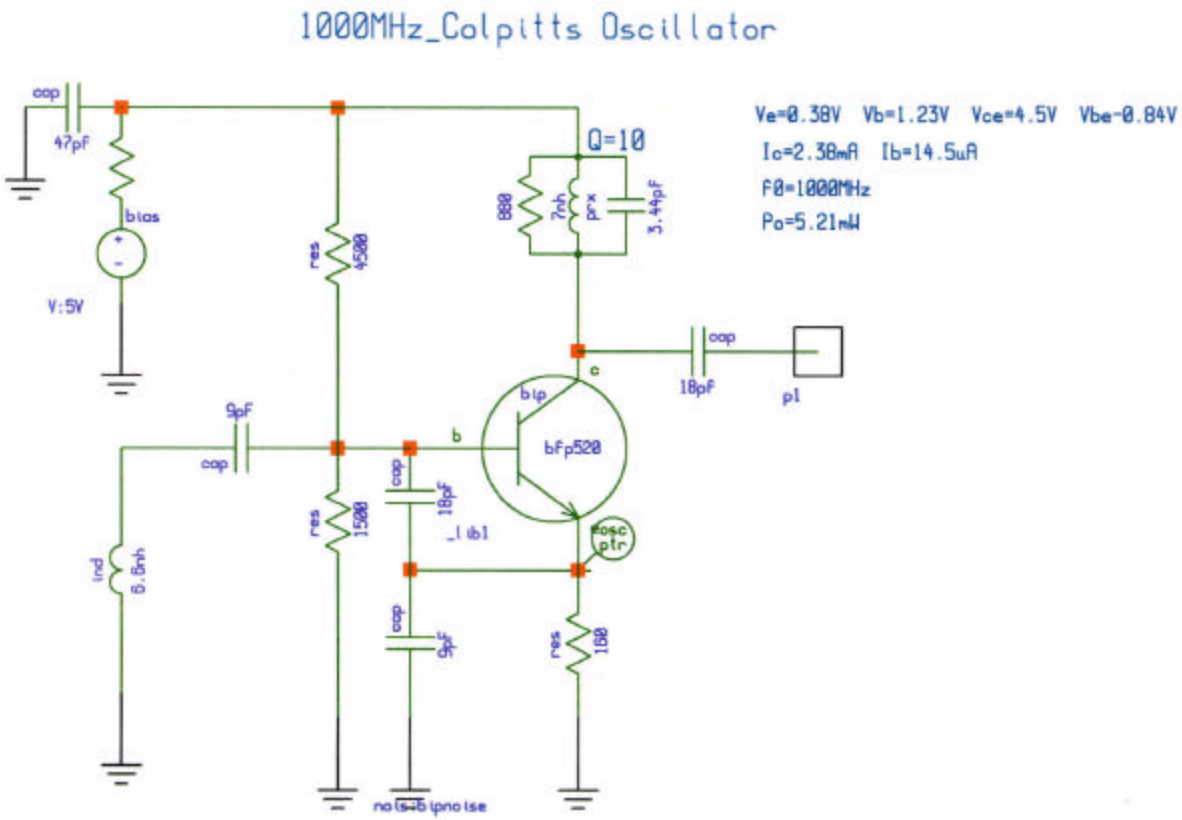

Figure B-1 The 1000 MHz oscillator chosen for the design example.

Step 1:

The 1000 MHz oscillator, using the bipolar transistor BFP520 (Infineon), is designed based on analytical equations and is later verified with results. Based on the output power requirement and harmonics at a given load, the drive level is fixed.

The normalized drive level of x = 15 is chosen to allow adequate drive level to sustain oscillation and yet, not to produce excessive harmonic content. For drive level x = 15, the fundamental peak current is given from a graph/table as

$$I_1(\,fundamental) = 1.932 I_{dc} \tag{B-1}$$

I_1 is the fundamental current specified by the output power needed for the designated load.

$$R_L = 500\Omega \tag{B-2}$$

$$V_{out} = \sqrt{P_{out}(mW) \times 2R_L} = \sqrt{5E-3 \times 2 \times 500} = 2.236V \quad \text{(no saturation voltage assumed!)} \tag{B-3}$$

$$I_1 = \frac{V_{out}}{500} = \frac{2.236}{500} = 4.472mA \tag{B-4}$$

$$I_e = I_{dc} = \frac{I_1}{1.932} = \frac{4.472}{1.932} = 2.314mA \tag{B-5}$$

Step 2:

To avoid saturation in the transistor, select an emitter resistor R_e to maintain a sufficiently small emitter signal voltage of approximately half the base-emitter drop. The DC emitter voltage also provides a reasonable offset to the variations in the base-emitter bias voltage. R_e is set to 160Ω. Using the common equation for biasing, the expression for the voltage at the base is given as

$$V_b = I_e\left[R_e + \frac{R_e}{b+1}\right] + V_{be} = 1.23V \tag{B-6}$$

b is assumed to be around 100 and V_{be} is approximately 0.8V.Bias resistor R_1 and R_2 is given as

$$V_b = \frac{R_2}{R_1 + R_2} V_{cc} = 1.23V \Rightarrow \frac{R_1}{R_2} \approx 3 \tag{B-7}$$

$$R_1 = 1500\Omega \tag{B-8}$$

$$R_2 = 4500\Omega \tag{B-9}$$

$$V_{cc} = 5V \tag{B-10}$$

Step 3:

The large-signal transconductance is determined as

$$Y_{21} = \left.\frac{I_1}{V_1}\right|_{fundamental-freq} = \frac{1.932 I_{dc}}{260mV} = \frac{4.472mA}{260mV} = 17.2mS \quad \text{(B-11)}$$

Step 4:

The value of n-factor is calculated from the equation above as

$$n^2(G_2 + G_3) - n(2G_3 + Y_{21}a) + (G_1 + G_3 + Y_{21}) = 0 \quad \text{(B-12)}$$

$$G_1 = 0 \quad \text{(B-13)}$$

$$G_2 = \frac{1}{R_1 \| R_2} = .88mS \quad \text{(B-14)}$$

$$G_3 = \frac{1}{R_e} = \frac{1}{160} = 6.25mS \quad \text{(B-15)}$$

$$Y_{21} = 17.2mS \quad \text{(B-16)}$$

where $$a = 0.99 \quad \text{(B-17)}$$

The quadratic equation above is reduced to

$$n^2(G_2 + G_3) - n(2G_3 + Y_{21}a) + (G_1 + G_3 + Y_{21}) = 0 \quad \text{(B-18)}$$

$$n^2(0.88 + 6.25) - n(2 \times 6.25 + 17.2 \times 0.99) + (0 + 6.25 + 17.2) = 0 \quad \text{(B-19)}$$

$$7.13n^2 - 29.528n + 23.45 = 0 \quad \text{(B-20)}$$

$$n = \frac{29.528 \pm \sqrt{(29.528)^2 - 4 \times 7.13 \times 23.45}}{2 \times 7.13} = \frac{29.528 \pm \sqrt{871.9 - 668.794}}{2 \times 7.13} \quad \text{(B-21)}$$

$$n = \frac{29.528 \pm 14.25}{14.26} \Rightarrow n_1 = 3.06 \text{ and } n_2 = 1.071 \quad \text{(B-22)}$$

The higher value of the transformation factor, n, is selected as $n = 3$.

The values of $C1$ and C_2 are calculated as

$$\frac{C_2}{C_1 + C_2} = \frac{1}{n} \Rightarrow C_2 = \frac{C_1}{n-1} \tag{B-23}$$

$$C_2 = \frac{C_1}{n-1} = \frac{C_1}{2} \Rightarrow \frac{C_1}{C_2} = 2 \tag{B-24}$$

The ratio of the capacitor C_1 to C_2 is 2. The absolute values of the capacitors are determined from the loop-gain condition of the oscillator as

$$Y_{21}\Big|_{l\arg e-signal} = G_m(x) = \frac{qI_{dc}}{kTx}\left[\frac{2I_1(x)}{I_0(x)}\right]_{n=1} = \frac{g_m}{x}\left[\frac{2I_1(x)}{I_0(x)}\right]_{n=1} \tag{B-25}$$

$$G_m(x) = \frac{1}{R_P}\frac{[C_1 + C_2]^2}{C_1 C_2} \tag{B-26}$$

$$\frac{g_m}{x}\left[\frac{2I_1(x)}{I_0(x)}\right]_{n=1} = \frac{1}{R_P}\frac{[C_1 + C_2]^2}{C_1 C_2} = \frac{1}{R_P}\frac{C_1}{C_2}\left[1 + \frac{C_2}{C_1}\right]^2 \tag{B-27}$$

$$\frac{88mS}{10} \times 1.932 = \frac{1}{R_P}\frac{C_1}{C_2}\left[1 + \frac{C_2}{C_1}\right]^2 \tag{B-28}$$

$$17.01E-3 = \frac{4.50}{R_P} \tag{B-29}$$

$$R_P = \frac{4.50}{17.01E-3} = 264.5\Omega \tag{B-30}$$

The quality factor of the inductor is assumed 10 at 1000 MHz, a low Q case.

The value of inductor is obtained as

$$Q_T = \frac{R_P}{w_0 L} \Rightarrow L = \frac{264.5}{10 \times w_0} \tag{B-31}$$

$$L = \frac{264.5}{10 \times 2p \times 1000E6} = 4.2nH \tag{B-32}$$

$$w = \sqrt{\frac{1}{L}\left[\frac{1}{C_1} + \frac{1}{C_2}\right]} \tag{B-33}$$

$$w^2 = \frac{1}{L}\left[\frac{1}{C_1} + \frac{1}{C_2}\right] = \frac{C_1 + C_2}{LC_1C_2} \tag{B-34}$$

The value of the capacitor is determined as

$$C_2 = \frac{3}{w^2 \times 8.4E - 9} \Rightarrow C_2 = \frac{3}{331.5E - 9} = 9pF \tag{B-35}$$

$$C_1 = 2C_2 = 18pF \tag{B-36}$$

Step 5:

The value of the coupling capacitor, C_s, is assumed to be 10pF and the effect of C_s on the series reactance of the inductor L must be is considered. Therefore, the inductor value is adjusted to

$$jw_0 \times L = jw_0(L' - \frac{1}{w_0^2 C_s}) \tag{B-37}$$

$$jw_0 \times 4.2nH = jw_0(L' - \frac{1}{w_0^2 \times 10E - 12}) \tag{B-38}$$

$$L' = 6.6nH \tag{B-39}$$

The base–lead inductance of the BFP520 is approximately 0.4nh, and after correcting this, the effective value of the inductor is 6.2nH.

Step 6:

The harmonic content can be calculated from the table of Bessel functions as

$$x = 15 \Rightarrow I_1 = 1.932 I_{dc}; I_2 = 1.742 I_{dc}; I_3 = 1.272 I_{dc}; I_4 = 0.887 I_{dc} \quad \text{(B-40)}$$

The parallel tank circuit at the output of the oscillator is designed to filter out higher harmonics.

$$Q = \frac{R}{wL} \quad \text{(B-41)}$$

$$Q = 20 \quad \text{(B-42)}$$

$$R = 880 \quad \text{(B-43)}$$

$$L = 7nH \quad \text{(B-44)}$$

$$C = 3.60pF \quad \text{(B-45)}$$

The analytically calculated values are in good agreement with the simulated and published results. Figure B-2 shows both the base-emitter voltage, which looks sinusoidal, and the collector current under the given operating condition. As previously shown, due to the harmonic contents, there is a certain amount of ringing as well as negative collector current. This is due with the tuned collector circuit.

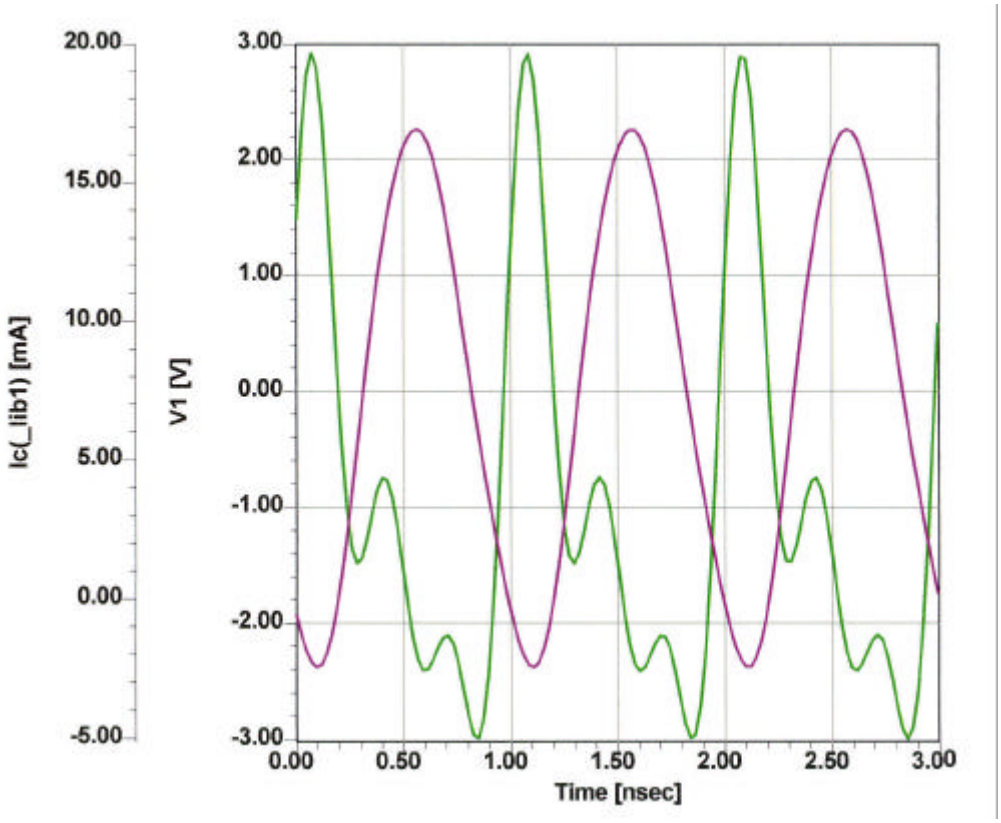

Figure B-2 Shows the base voltage and collector current of the oscillator in Figure B-1.

Figure B-3 shows the predicted phase noise as a function of the normalized drive level using values of x between the levels of 4 and 18. The phase noise is not the optimized phase noise for this configuration because the best phase noise can be achieved by adjusting the proper ratio and absolute values of the feedback capacitors at a given drive level and required output power.

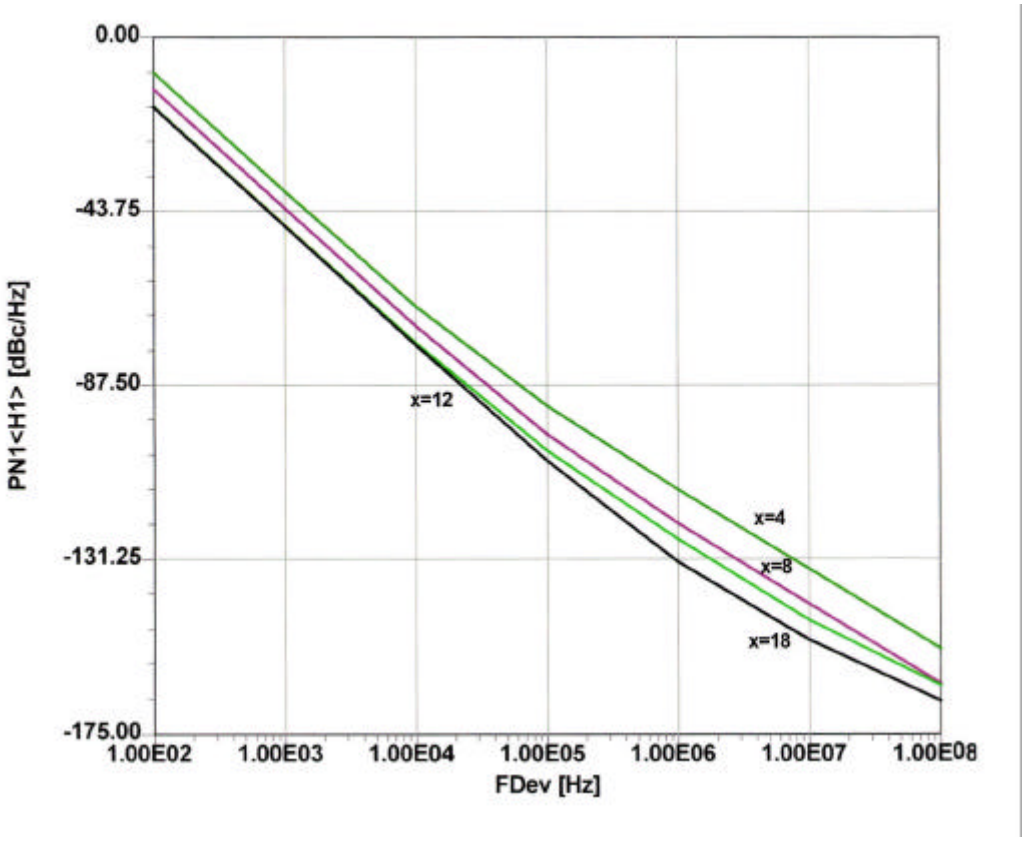

Figure B-3 Shows the predicted phase noise of the circuit shown in Figure B-1 with different normalized drive levels.

Appendix C - Design Example for Best Phase Noise and Good Output Power

Figure C-1 shows the parallel-tuned Colpitts oscillator circuit, which has to be designed with the following specifications. The unit was also built and measured. It uses a ceramic resonator and its equivalent circuit is shown.

Requirements:

- output power requirement: 13 dBm
- operating frequency: 1000 MHz
- load: 50 Ω
- phase noise –124 dBc/Hz @10KHz

Design Steps

Step 1:

Calculation of the operating point for a fixed, normalized drive of x = 20 (high output power).

Based on output power requirement, the following is calculated.

The oscillator output voltage at the fundamental frequency is

$$V_{out}(w_0) = \sqrt{P_{out}(w_0) * 2R_L} = \sqrt{20E-3 * 2 * 50} \approx 1.414V \qquad \text{(C-1)}$$

The fundamental current is

$$I_{out}(w_0) = \frac{V_{out}(w_0)}{50} = \frac{1.414}{50} = 28.3mA \qquad \text{(C-2)}$$

The DC operating point is calculated based on the normalized drive level x = 20. The expression for the emitter dc current can be given in terms of the Bessel function with respect to the drive level is

$$[I_E(w_0)] = 2I_{DC}\left[\frac{I_1(x)}{I_0(x)}\right]_{x=Normalized-Drive-Level} \qquad \text{(C-3)}$$

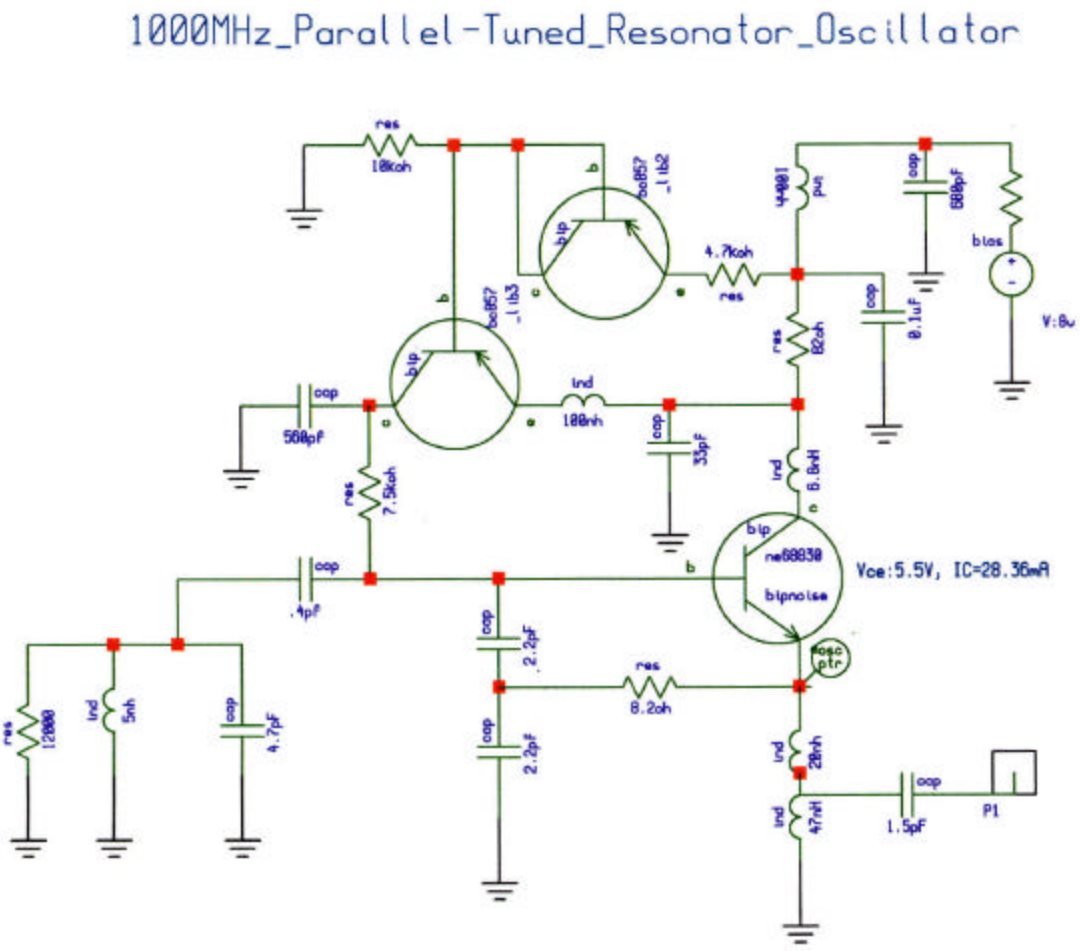

Figure C-1 Schematic of the 1000 MHz oscillator.

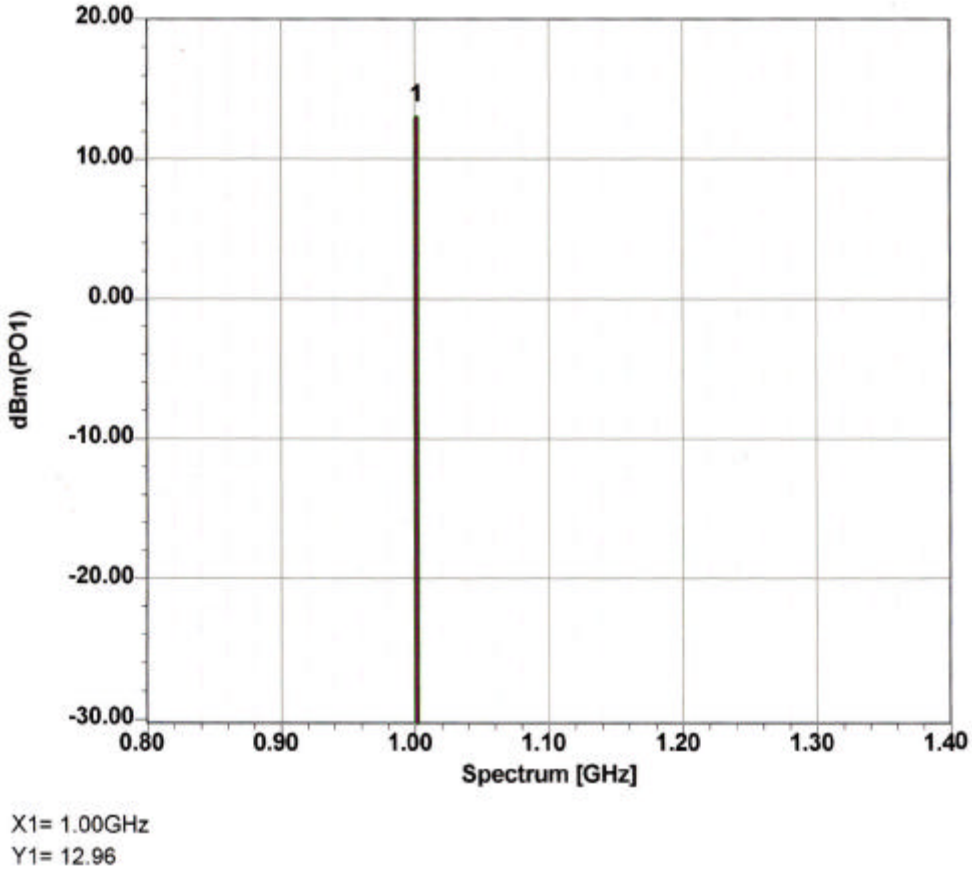

Figure C-2 Predicted output power of the oscillator.

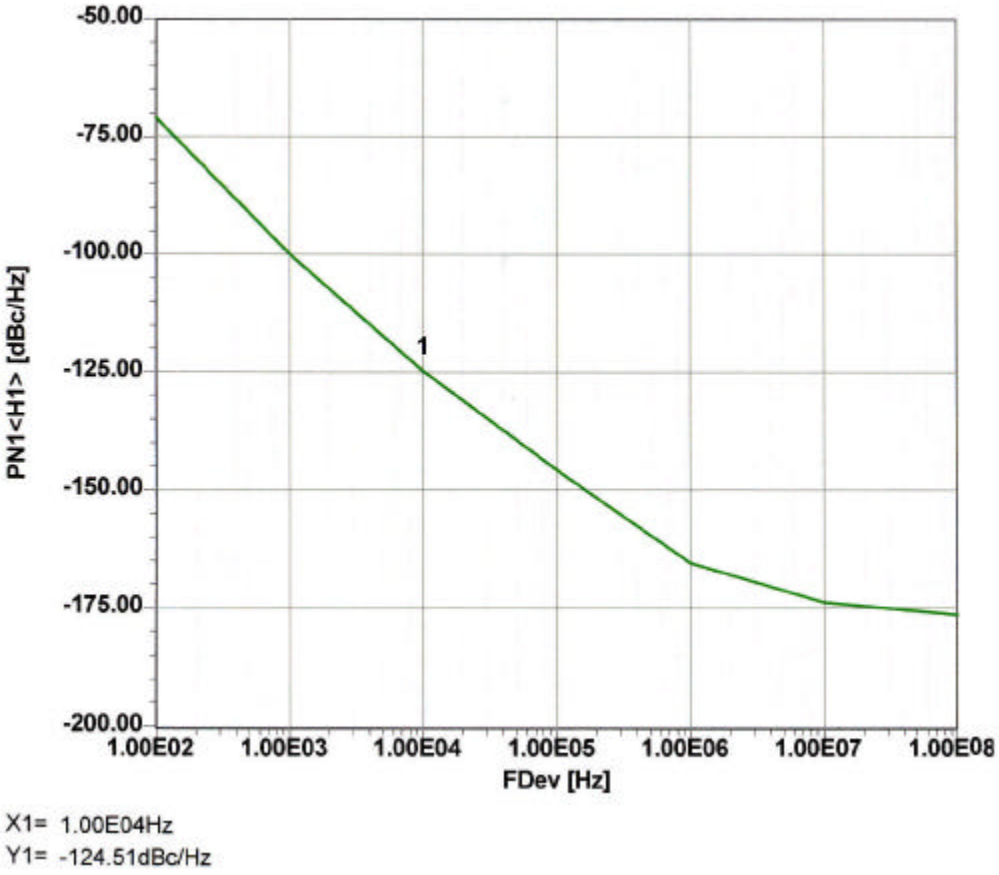

Figure C-3 Predicted phase noise of the oscillator.

For the normalized drive level x = 20, the output emitter current at the fundamental frequency can be given as

$$[I_E(w_0)]_{x=20} = [I_{E1}(w_0)]_{x=20} + [I_{E2}(w_0)]_{x=20} = 2I_{DC}\left[\frac{I_1(x)}{I_0(x)}\right]_{x=20} \approx 56mA \qquad \text{(C-4)}$$

$$[I_{E1}(w_0)]_{x=20} = I_{out}(w_0) = 28.3mA \text{ (output current to the load)} \qquad \text{(C-5)}$$

Figure C-4 shows the oscillator circuit configuration in which DC and RF current distribution is shown and divided into its components.

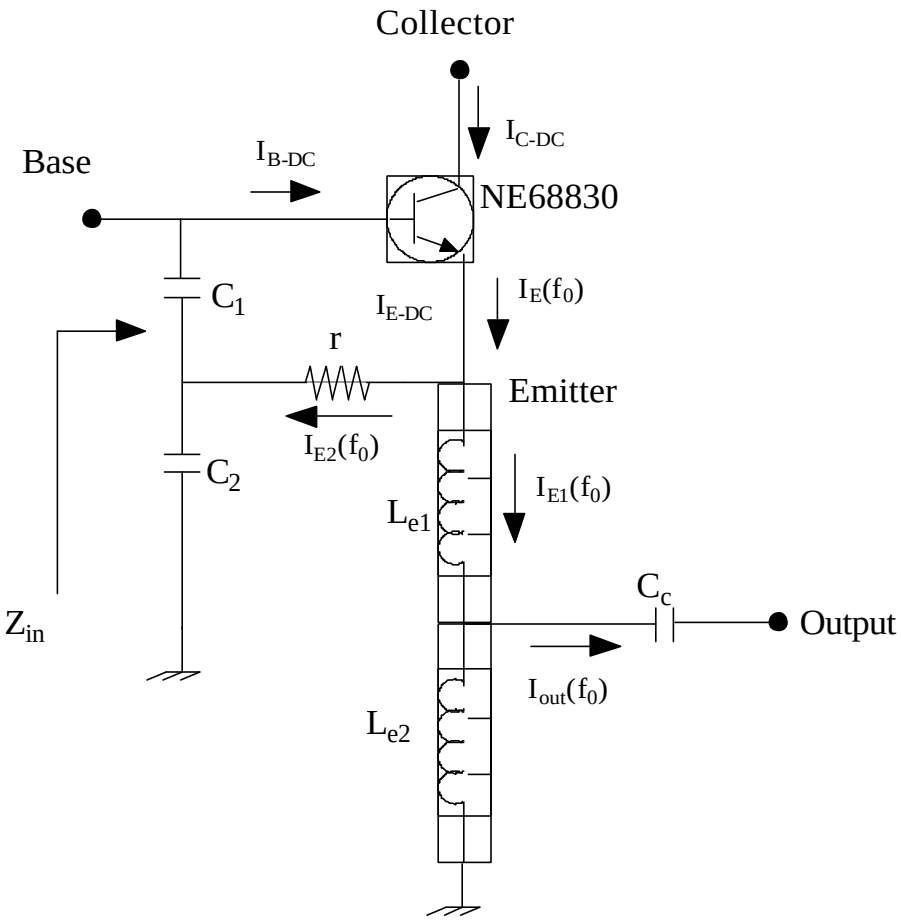

Figure C-4 Current distribution in the oscillator circuit.

$$\left[I_{E2}(w_0)\right]_{x=20} = \left[I_E(w_0)\right]_{x=20} - \left[I_{E1}(w_0)\right]_{x=20} = 27.3mA \tag{C-6}$$

$$I_{E-DC} = \frac{\left[I_E(w_0)\right]_{x=20}}{2\left[\frac{I_1(x)}{I_0(x)}\right]_{x=20}} = 28.3mA \tag{C-7}$$

For this application, the NE68830 was selected.

Step 2:

Biasing circuit

For the best phase noise close-in, a DC/AC feedback circuit is incorporated which provides the desired operating DC condition [84]:

I_E=28.3mA

V_{CE}=5.5V, Supply Voltage V_{cc}=8V

b=120

I_B≈0.23mA

Step 3:

Calculation of the large-signal transconductance.

$$Y_{21}\Big|_{large-signal} = G_m(x) = \frac{qI_{dc}}{kTx}\left[\frac{2I_1(x)}{I_0(x)}\right]_{fundamental} \quad \text{(C-8)}$$

$$\left[Y_{21}\right]_{w=w_0} = \left[\frac{1.949 I_{E-DC}}{520mV}\right] = 0.107 \quad \text{(C-9)}$$

Step 4:

Loop Gain.

The loop gain is

$$Loop-Gain = [LG]_{sustained-condition} = \left[\frac{R_P Y_{21}(x)}{n}\right] = \left[\frac{R_P g_m}{x}\right]\left[\frac{2I_1(x)}{I_0(x)}\right]\left[\frac{1}{n}\right] > 1 \quad \text{(C-10)}$$

$$R_{PEQ}(f_0) = R_P \parallel Bias-circuit \Rightarrow 50.73\Omega \quad \text{(C-11)}$$

As earlier derived, the loop gain should be 2.1 to have good starting conditions!

$$n = \left[\frac{R_{PEQ} Y_{21}(x)}{2.1}\right] = \frac{0.107 * 50.73}{2.1} \approx 2.523 \quad \text{(C-12)}$$

Step 5:

Calculation of the feedback capacitor ratio.

$$n = 1 + \left[\frac{C_1}{C_2}\right] = 2.523 \Rightarrow \left[\frac{C_1}{C_2}\right]_{x=20} = 1.523 \ (2.523 - 1) \tag{C-13}$$

Step 6:

Calculation of absolute values of feedback capacitor.

The expression of Z_{in} (Looking in to the base of the transistor) can be given as

$$Z_{in} \cong -\left[\left(\frac{Y_{21}}{w^2(C_1^* + C_p)C_2}\right)\left(\frac{1}{(1+w^2Y_{21}^2L_p^2)}\right)\right] - j\left[\left(\frac{(C_1^* + C_P + C_2)}{w(C_1^* + C_P)C_2}\right) - \left(\frac{wY_{21}L_P}{(1+w^2Y_{21}^2L_p^2)}\right)\left(\frac{Y_{21}}{w(C_1^* + C_P)C_2}\right)\right] \tag{C-14}$$

where

C_P = (C_{BEPKG} +Contribution from layout)=1.1pF

L_P=(L_B + L_{BX} +Contribution from layout)=2.2nH.

The expression for the negative resistance R_n is

$$R_{neq} = \frac{R_n}{(1+w^2Y_{21}^2L_P^2)} = \frac{R_n}{[1+(2p*1E9)^2*(0.107)^2*(2.2nH)^2]} \tag{C-15}$$

$$R_{neq} \approx \frac{R_n}{3.65} \tag{C-16}$$

$$R_n = -\left[\frac{Y_{21}^{+}}{w^2 C_1 C_2}\right]_{x=20} = \frac{0.107}{(2p * 1E9)^2 C_1 C_2} \quad \text{(C-17)}$$

R_n is the negative resistance without parasitics (C_P, L_P).

For sustained oscillation $\rightarrow R_{neq} \geq 2R_{PEQ} \cong 101.4$ Ohm

$$R_n = 3.65 * 101.4 \approx 371 Ohm \quad \text{(C-18)}$$

$$C_1 C_2 = \left[\frac{1}{w^2}\right]\left[\frac{0.107}{371}\right] \approx 7.26 \quad \text{(C-19)}$$

$$\left[\frac{C_1}{C_2}\right]_{x=20} \approx 1.52 \quad \text{(C-20)}$$

$$C_1 = 3.3 pF \quad \text{(C-21)}$$

$$C_2 = 2.2 pF \quad \text{(C-22)}$$

Step 7:

Calculation of the coupling capacitor r_e.

The expression for the coupling capacitor is

$$\frac{C}{10} > C_C > \left\{\frac{(w^2 C_1 C_2)(1 + w^2 Y_{21}^2 L_P^2)}{[Y_{21}^2 C_2 - w^2 C_1 C_2)(1 + w^2 Y_{21}^2 L_P^2)(C_1 + C_P + C_2)]}\right\} \quad \text{(C-23)}$$

$$C_c \rightarrow 0.4 pF \quad \text{(C-24)}$$

Figure C-5 shows the transistor in the package parameters for the calculation of the oscillator frequency and loop gain.

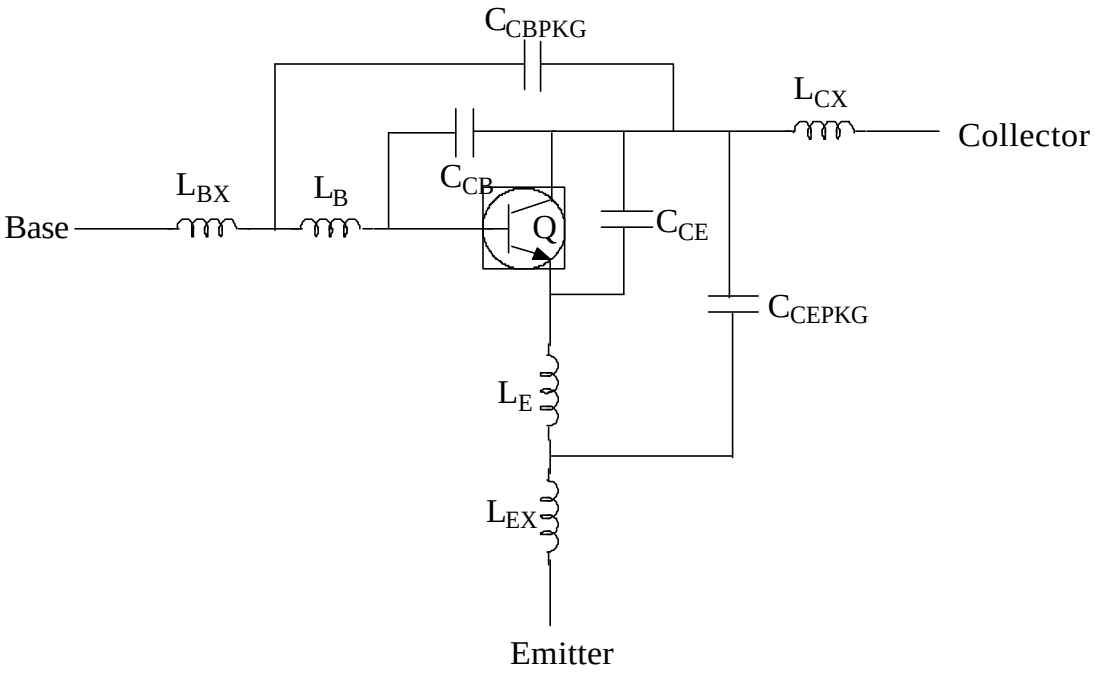

Figure C-5 NE68830 with package parasitics. Q is the intrinsic bipolar transistor.

Tables C-1a and C-1b show NE68830 nonlinear parameters and package parameters which were taken from the NEC data sheets.

Table C-1a Nonlinear parameters

Parameters	Q	Parameters	Q
IS	3.8E-16	MJC	0.48
BF	135.7	XCJC	0.56
NF	1	CJS	0
VAF	28	VJS	0.75
IKF	0.6	MJS	0
NE	1.49	TF	11E-12
BR	12.3	XTF	0.36
NR	1.1	VTF	0.65
VAR	3.5	ITF	0.61
IKR	0.06	PTF	50
ISC	3.5E-16	TR	32E-12
NC	1.62	EG	1.11
RE	0.4	XTB	0
RB	6.14	XTI	3
RBM	3.5	KF	0
IRB	0.001	AF	1
RC	4.2	VJE	0.71
CJE	0.79E-12	MJE	0.38
CJC	0.549E-12	VJC	0.65

Table C-1b Package parameters of NE68830

Parameters	NE68830
C_{CB}	0.24E-12
C_{CE}	0.27E-12
L_B	0.5E-9
L_E	0.86E-9
C_{CBPKG}	0.08E-12
C_{CEPKG}	0.04E-12
C_{BEPKG}	0.04E-12
L_{BX}	0.2E-9
L_{CX}	0.1E-9
L_{EX}	0.2E-9

Design Calculations

1. Frequency of Oscillation

Frequency of the oscillation is

$$w_0 = \sqrt{\frac{1}{L\left[\frac{\left[\frac{(C_1^* + C_P)C_2C_c}{(C_1^* + C_P + C_2)}\right]}{\left[\frac{(C_1^* + C_P)C_2}{(C_1^* + C_P + C_2)} + C_c\right]} + C\right]}} \approx 1000\,MHz \qquad \text{(C-25)}$$

with

L = 5nH (Inductance of the parallel resonator circuit)

C_1^*= 2.2pF

$C_1 = C_1^* + C_P$

C_P=1.1Pf (C_{BEPKG} + Contribution from layout)

C_2 = 2.2pF

C_c = 0.4pF

C =4.7pF

R_P=12000 (Measured)

$$Q_{unloaded} = \left[\frac{R_P}{w\,L}\right] = 380$$

2. Calculation of the Phase Noise

The noise equation which was determined in Section 8.4, Eq. (8-94), and which contains resonator noise, shot noise, and flicker noise, can now be used to graphically determine the best phase noise as a function of *n*. Figure C-6 shows a plot of this curve. It gives the best number of *n* to be 2.5, which is consistent with the calculation done for the large-signal condition. Eq. (C-12) gives the same result.

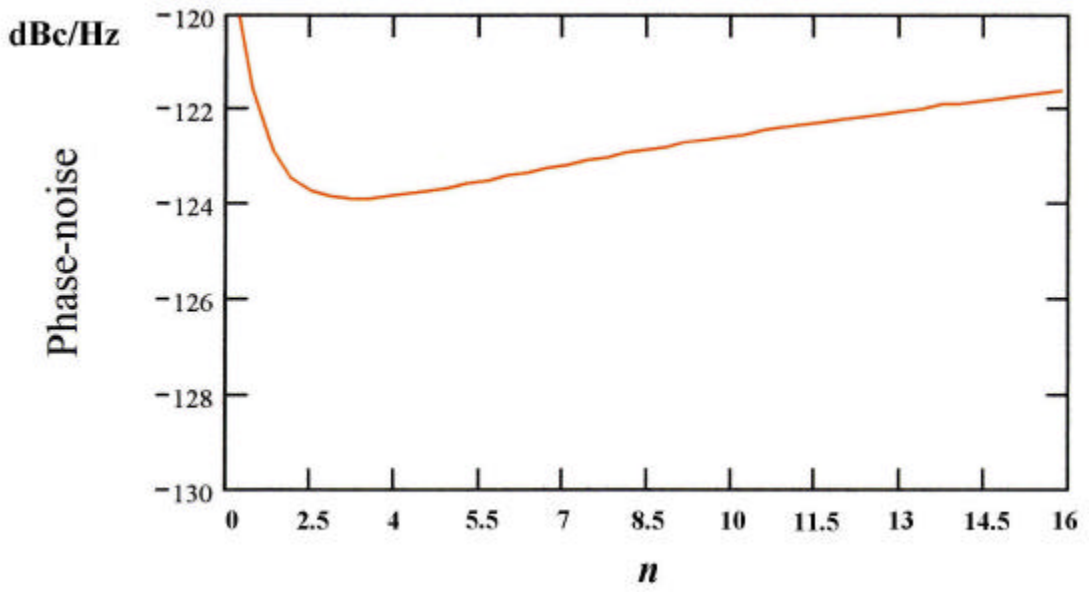

Figure C-6 The phase noise contribution of the lossy resonator at 10KHz offset.

The calculated phase noise at 10 KHz off the carrier is –124 dBc/Hz, which agrees with the measurements within 1 dB. The other values are –140 dBc/Hz at 100 kHz offset and –160 dBc/Hz at 1 MHz offset.

This circuit is shown in Section 9.1, Figure 9-2. The actual measured phase noise is shown in Figure 9-4, and the simulation is shown in Figure 9-5. Considering that Eq. (8-94) only contains shot and flicker noise, as well as resonator noise, it has been proven that this by itself is a very accurate formula for practical use. Figure 9-5 has been generated from using Ansoft Designer, which includes all noise sources and is based on the harmonic balance principle.

The important conclusion found in Section 8 is that for the first time we have a complete mathematical synthesis procedure for best phase noise that covers both flicker noise and white noise for the oscillator. In the past, most publications have referenced an oscillator built with many shortcuts and then the author found that the measured results agree with the expectations. A complete synthesis approach has not appeared previously.